Novel Methods for Estimating Extreme Design Rainfalls at Gauged and Ungauged Locations in a Changing Climate

Truong-Huy Nguyen

Doctor of Philosophy

Department of Civil Engineering and Applied Mechanics
McGill University
Montreal, Quebec
2020-04-27

A thesis submitted to McGill University in partial fulfillment
of the requirements for the degree of Doctor of Philosophy

Dedication

To my family.

Acknowledgements

I would like to express my special thanks to my supervisor, Professor Van-Thanh-Van Nguyen, for all his time, encouragement and patience with me in both my PhD study and research.

Many thanks to my wife, little daughter, and parents, whose support and encouragement helped me to overcome difficulties during my studies and research. Without their support, my work would have been impossible.

My sincere thanks also go to the professors of the Water Resources Group, Department of Civil Engineering and Applied Mechanics at McGill University for all the knowledge I gained in their graduate courses.

My sincere thanks also extend to my colleagues and friends in my research team, especially, Myeong-Ho Yeo, Alireza Zareie, Malika Khalili, Sarah Outayek, Sunny Lim, and Hoang-Lam Nguyen.

Finally, I am grateful for the financial support provided by the Faculty of Engineering at McGill University and the Natural Science and Engineering Research Council (NSERC) Canadian FloodNet (Grant number: NETGP 451456) for this research.

Abstract

Information on the variability of extreme rainfalls in time and in space is of critical importance for many types of extreme hydrologic studies related to the estimation of runoff characteristics for planning, design, and management of various water resources systems. In particular, for urban watersheds that are generally characterized by a fast response, the design of different urban infrastructures (such as small dams, culverts, storm sewers, detention basins, and so on) require hence an accurate and robust estimation of extreme design rainfalls for very high temporal resolutions (ranging from a few minutes to one day) in order to provide an accurate and reliable description of runoff properties for urban inundation management. In addition, in recent years, climate change has been recognized as having a profound impact on the hydrologic cycle at different temporal and spatial scales. Consequently, the intensity and frequency of extreme storm events in most regions will be likely increased in the future. The present study is therefore was carried out to develop appropriate methods for improving the accuracy of design rainfall estimation at gauged and ungauged locations in the current climate as well as in the context of climate variability and climate change. This study can be divided into five primary parts.

The first part presents a general procedure for assessing systematically the performance of different commonly used probability distributions in extreme rainfall frequency analyses based on their descriptive as well as predictive abilities. This assessment procedure relies on an extensive set of graphical and numerical performance criteria to identify the most suitable models that could provide the most accurate and most robust extreme rainfall estimates. The proposed systematic

assessment approach has been shown to be more efficient and more robust than the traditional model selection method based on only limited goodness-of-fit criteria. To test the feasibility of the proposed procedure, an illustrative application was carried out using 5-minute, 1-hour, and 24-hour annual maximum rainfall data from a network of 21 raingages located in the Ontario region in Canada. Results have indicated that the Generalized Extreme Values (GEV), Generalized Normal (GNO), and Pearson Type 3 (PE3) models were the best models for describing the distribution of daily and sub-daily annual maximum rainfalls in this region. The GEV distribution, however, was preferred to the GNO and PE3 because it was based on a more solid theoretical basis for representing the distribution of extreme random variables.

The second part introduces a new probability-weighted-moment-based scaling Generalized Extreme Value (GEV/PWM) distribution model for modeling rainfall extremes across a wide range of time scales (e.g., from several minutes to one day). The GEV distribution has been recommended in the national guidelines of many countries. The mathematical framework and the scaling properties of the proposed GEV/PWM model were derived. The relations between the GEV/PWM model and three existing scaling models such as the non-central-moment-based GEV (GEV/NCM) and the NCM- and PWM-based Gumbel models (GUM/NCM and GUM/PWM) were described. A comparative study was then carried out to asses the performance of these models using the available extreme rainfall data from a network of 74 raingages located across Canada. The scaling behaviours of extreme rainfall processes were also analyzed using both NCM and PWM estimation methods. Results of this comparative study have indicated the superior performance of the proposed GEV/PWM model as compared to the existing GEV/NCM, GUM/NCM, and GUM/PWM based on an extensive set of graphical and numerical comparison criteria. In particular, the PWM method can provide a more accurate and more robust identification of the scaling behaviour of extreme rainfall processes than the NCM procedure for different rainfall scaling regimes and for higher order statistical moments.

The third part proposes an innovative spatio-temporal statistical downscaling approach for establishing the linkage between daily extreme rainfalls at regional scales and daily and sub-daily extreme rainfalls at a given local site. The spatial downscaling was relied on the scaling factor method while the temporal downscaling was based on the proposed GEV/PWM model. The feasibility and accuracy of the proposed method were assessed for a case study in Ontario (Canada) using observed extreme rainfall data from seven raingages and climate simulation outputs from 21 different Global Climate Models (GCMs) that have been downscaled by NASA to a regional 25-km scale for the RCP 4.5 scenario. Results based on various graphical and numerical comparison criteria have indicated the feasibility and accuracy of the proposed downscaling approach. In addition, a robust assessment of the climate change impacts on the extreme rainfalls for urban drainage system design was performed using a series of statistical tests in sequence to evaluate the significant changes of rainfalls among different time periods. It was found that significant increases by 8% to 18% in extreme design rainfalls for return periods up to T = 25 years, and insignificant increases by 3% to 8% for the 50-year and 100-year design rainfalls for many locations, except for one location with a significant increase of 18%. The confidence intervals were also computed for these estimated design rainfalls with a range of uncertainty varying from 5% to 22%.

The fourth part introduces new scale-invariancce models for modeling rainfall extremes across a wide range of time scales. The spatial downscaling approaches have been extensively developed to link the regional projected climate change simulations to the local daily extreme rainfalls in many studies. However, very few models have been proposed for describing the linkages between the daily and sub-daily extreme rainfalls. The present study presented hence some general mathematical frameworks for three commonly-used probability distributions in hydrologic frequency analyses such as the Generalized Logistic (GLO), Generalized Normal (GNO), and Pearson Type 3 (PE3) using both NCM and PWM estimation methods. Results of an illustrative application using the observed IDF data from a network of 74 raingages located across Canada have indicated the feasibility and accuracy of these new scale-invariance models. Furthermore, it was found that the PWM method can provide more accurate extreme rainfall estimates than those given by the NCM procedure. In particular, the GNO/PWM and GEV/PWM were found as the two best models, among the eight candidates considered, that could be recommended for the estimation of extreme design rainfalls in practice for the current climate as well as for future climate change scenarios.

Finally, the fifth part consists of developing a convenient decision-support tool (referred herein as SMExRain) for the construction of robust rainfall IDF relations in consideration of model uncertainty and potential climate change impacts for the design and management of urban water systems at a given location of interest. More specifically, this tool can readily be used to identify in an objective and systematic manner the most suitable probability models for accurate and robust estimation of design rainfalls. In addition, in the context of a changing climate, the proposed tool was able to establish the linkage between large-scale climate predictors given by GCMs and the daily and sub-daily extreme rainfalls at a given site. The SMExRain represents therefore an efficient and practical tool for establishing reliable IDF relations at a given site and for assessing the potential impacts of climate change on the estimated design rainfalls. An illustrative application of the SMExRain was presented to demonstrate the efficiency and usefulness of the proposed tool in engineering practice using climate simulations from 21 different GCMs and extreme rainfall data available from a network of 15 raingages located in Ontario (Canada).

Résumé

L'information sur la variabilité des précipitations extrêmes dans le temps et dans l'espace est très importante pour plusieurs études hydrologiques extrêmes concernant le calcul du ruissellement pour la planification, la conception, et la gestion des réseaux de ressources hydriques. En particulier, pour les bassins versants urbains ayant généralement une réponse rapide, la conception de diverses infrastructures urbaines (par exemples, petites barrages, ponceaux, réseau d'égouts, bassins de rétention, etc.) requiert alors une estimation précise et robuste des pluies extrêmes de conception aux échelles de temps très fines (de quelques minutes jusqu'un jour) afin de fournir une estimation précise et fiable du ruissellement pour la gestion de l'inondation dans une région urbaine. De plus, plus récemment, on avait reconnu que le changement climatique avait causé des impacts significatifs sur le cycle hydrologique aux diverses échelles de temps et de l'espace. Par conséquent, l'intensité et la fréquence des événements de pluies extrêmes dans plusieurs régions pourraient être augmentés dans le futur. La présente étude était alors réalisée pour élaborer des méthodes plus appropriées pour améliorer la précision de l'estimation de pluie de conception pour des sites jaugés et non-jaugés pout le présent climat et également dans un contexte du changement et de la variabilité du climat. Cette étude se divise en cinq parties principales.

La première partie présente une méthodologie générale pour évaluer d'une façon systématique la performance des divers modèles de probabilité qui ont été fréquemment utilisés dans l'analyse fréquentielle des pluies extrêmes en considérant leur capacités descriptive et

prédictive. Cette procédure d'évaluation est basée sur un ensemble des critères graphiques et numériques pour identifier les modèles les plus appropriés qui sont capable de fournir une estimation le plus précise et le plus robuste des pluies extrêmes. On avait démontré que la méthode d'évaluation systématique proposée était plus efficace et plus fiable que la méthode traditionnelle qui était basée simplement sur les critères concernant la capacité descriptive de ces modèles. Pour démontrer la faisabilité de la méthode proposée, on avait effectué une application de cette méthode aux données des pluies annuelles maximales de durées de 5 minutes, 1 heure et 24 heures du réseau pluviométrique de 21 stations en Ontario, Canada. Les résultats de cette application ont indiqué que la loi des valeurs extrêmes généralisée (VEG), la loi normale généralisée (NOG), et la loi Pearson de type 3 (PE3) sont les meilleurs modèles pour représenter les distributions des pluies maximales journalières et aux plus courtes durées pour cette région. Toutefois, parmi ces trois modèles, la loi VEG était la plus appropriée parce qu'elle possède une base théorique plus solide pour représenter la distribution des variables aléatoires extrêmes.

La deuxième partie de cette étude propose un nouveau modèle de distribution d'invariance d'échelle basé sur la loi VEG et les moments de probabilité pondérés (VEG/MPP) pour la modélisation des processus de pluies extrêmes pour une large gamme d'intervalles de temps (de quelques minutes à un jour). La loi VEG a été recommandée comme la meilleure loi dans les guides techniques de plusieurs pays. On a présenté en détail dans ce chapitre la méthodologie mathématique et les propriétés d'invariance d'échelle du modèle VEG/MPP. On a également expliqué la relation entre le modèle VEG/MPP et les trois modèles d'invariance d'échelle existants : modèle VEG basé sur les moments non-centrés (VEG/MNC), modèle Gumbel basé sur MNC (GUM/MNC), et modèle Gumbel basé sur MPP (GUM/MPP). Une étude comparative a été effectuée pour évaluer la performance de ces modèles en utilisant les données des pluies annuelles maximales disponibles d'un réseau de 74 stations à travers le Canada. On a également effectué une analyse des propriétés d'invariance d'échelle de ces données en considérant les deux méthodes d'estimation basées sur MNC et MPP. Les résultats de cette étude comparative ont indiqué la meilleure performance du modèle VEG/MPP par rapport aux modèles existants VEG/MNC, GUM/MNC, et GUM/MPP en se basant sur un nombre de critères de comparaison graphiques et numériques. En particulier, la méthode d'estimation basée sur MPP est capable de fournir une identification plus précise et plus robuste des propriétés d'invariance d'échelle du processus de pluies extrêmes que celle par la méthode basée sur MNC pour des régimes de pluie différents et pour des moments statistiques d'ordres supérieures.

La troisième partie de l'étude propose une procédure innovatrice de mise à l'échelle statistique dans le temps et dans l'espace pour établir le lien entre les pluies extrêmes journalières à l'échelle régionale et les pluies extrêmes journalières et plus courtes durées en un point donné. La méthode de mise à l'échelle spatiale était basée sur un facteur de changement d'échelles tandis que la procédure de mise à l'échelle temporelle était basée sur le modèle VEG/MPP. Une application numérique avait été effectuée pour évaluer la faisabilité et la précision de la méthode proposée en utilisant les données de pluies extrêmes disponibles à sept stations pluviométriques en Ontario (Canada) et les données de simulation de 21 modèles du climat à l'échelle de 25 km fournies par le NASA pour le scénario RCP4.5. Les résultats de cette application ont indiqué la faisabilité et la précision de la méthode de mise à l'échelle spatio-temporelle proposée en se basant sur un nombre de critères de comparaison graphiques et numériques. De plus, une évaluation détaillée des impacts du changement climatique sur les pluies extrêmes pour la conception des réseaux de drainage urbain avait été effectuée en utilisant un nombre de tests statistiques pour identifier des changements significatifs des précipitations en des périodes de temps différentes. On a observé une augmentation significative de 8% à 18% pour la pluie de conception pour des périodes de retour jusqu'à T = 25 ans, et un changement moins important de 3% à 8% pour des pluies de 50 ans et 100 ans à plusieurs endroits, sauf à une place avec une augmentation significative de 18%. Les intervalles de confiance ont été également calculées pour ces pluies de conception avec une variabilité entre 5% et 22%.

La quatrième partie de l'étude présente de nouveaux modèles d'invariance d'échelle pour la modélisation des processus de pluies pour une large gamme d'échelles temporelles. Plusieurs méthodes de mise à l'échelle spatiale sont disponibles dans des études précédentes pour établir le lien entre les projections du changement climatique à l'échelle régionale et les pluies extrêmes journalières en un site. Toutefois, il existe seulement quelques études qui examinent le lien entre les pluies extrêmes journalières et celles à courtes durées. Pour résoudre ce problème, la présente étude propose alors une formulation mathématique générale pour trois modèles de probabilité qui sont fréquemment utilisées en analyse fréquentielle hydrologique : la loi Logistique généralisée (LOG), la loi Normale généralisée (NOG) et la loi de Pearson type 3 (PE3) en utilisant les deux méthodes d'estimation basées sur MNC et MPP. Les résultats d'une application en utilisant les données des pluies extrêmes disponibles aux 74 stations à travers le Canada ont indiqué la faisabilité et la précision de ces nouveaux modèles. De plus, on a trouvé que la méthode d'estimation basée sur MPP est plus précise que la méthode basée sur MNC. En particulier, les modèles NG/MPP et EVG/MPP sont les meilleurs parmi 8 modèles considérés. On peut recommander ces deux modèles pour l'estimation des pluies de conception en pratique pour le présent climat ou pour les scénarios de changement climatique dans le futur.

Finalement, la cinquième partie de cette recherche consiste à développer un outil pratique de l'aide à la décision (appelé SMExRain) pour la dérivation des relations intensité-durée-fréquence (IDF) en un site donné en considérant l'incertitude des modèles choisis et les impacts potentiels par le changement climatique pour la conception et la gestion des réseaux de ressources hydriques. Plus spécifiquement, cet outil peut être utilisé pour identifier d'une façon systématique et objective le modèle de probabilité le plus appropriée pour une estimation précise et robuste de la pluie de conception. En plus, dans le contexte de changement climatique, l'outil proposé permet d'établir les liens entre les prédicteurs climatiques à l'échelle globale fournis par les modèles globaux du climat et les pluies extrêmes journalières et à courtes durées en un site donné. L'outil SMExRain représente alors un outil efficace et pratique pour l'estimation des relations IDF et pour l'évaluation les impacts potentiels du changement climatique sur la pluie de conception. Une application numérique a été effectuée pour démontrer l'efficacité et l'avantage en pratique de cet outil en utilisant les données de simulation fournies par 21 modèles globaux du climat et les données des pluies extrêmes disponibles d'un réseau de 15 stations pluviométriques en Ontario (Canada).

Preface

This thesis is an original work by Truong-Huy Nguyen. Professor V.-T.-V. Nguyen was the supervisory author and was involved with concept formation and manuscript composition of all chapters. S. Outayek and S. Lim contributed to part of the data collection and part of the literature review in Chapter 2. H.-L. Nguyen contributed to part of the data collection in Chapter 3 and Chapter 6.

Table of Content

List of Figures

List of Tables

List of Symbols

Roman Symbols

a	Coefficient of an IDF regression model in real space
AIC	Akaike information criterion
$AICc$	Adjusted Akaike information criterion
b	Coefficient of an IDF regression model in real space
BIC	Schwarz Bayesian Criterion
c	Coefficient of an IDF regression model in real space
c_i	Coefficients of the $e(F)$ function (i = 0, 1, 2)
CC	Correlation coefficient
C_k	Coefficients of an IDF regression model in log-space
D	Rainfall duration
$e(F)$	Bias correction function associated with $\hat{X}(F)$;
exp (.)	Exponential function
$f(x)$	Probability density function
F^*	Critical value for the ANOVA F-test
$F(x)$	Cumulative distribution function
$g(t)$	Skewness of a data sample at the time scale t
p_i	Non-exceedance probability
p	Polynomial order
q^*	Critical value for the Tukey test
r^{th}	Moment order
m	Number of distribution parameters
MAD	Mean absolute deviation
$MADr$	Mean absolute relative deviation
MAE	Maximum absolute error

n	Sample size
R^2	Coefficient of determination
R^2_{adj}	Adjusted coefficient of determination
RI	Average rainfall intensity
$RMSE$	Root mean square error
$RMSEr$	Root mean square relative error
T	Return period
$\bar{x}$	Average value of the observations
$x(F)$	Quantile function
x_i	Observed values
$\hat{X}(F)$	Daily regional extreme rainfall at the grid level
X_T	Design quantile value corresponding to the design period T
$X_i(F)$	Adjusted daily extreme rainfall at the local site of interest i
$\bar{y}$	Average value of the estimated quantiles
y_i	Estimated values

<u>Greek Symbols</u>

α	Scale parameter
β_r	Probability weighted moment order r^{th}
γ	Shape parameter
ε	Error term
δ_i	Scaling factor at site i
η	Scaling exponent
κ	Shape parameter
λ	Scaling ratio
μ	Location parameter
$\hat{\mu}$	Mean of the regional values at the grid level
μ_i	Mean of the daily ERs at the local site i
μ_r	Non-central moment order r^{th}

ξ	Location parameter
σ	Scale parameter
τ_3	Sample L-skewness
Γ	Gamma function

List of Abbreviations

AIC	Akaike Information Criterion
AMS	Annual Maximum Series
ANOVA	Analysis of Variance
ASFA	At-Site Frequency Analysis
BC	Bias Correction
BEK	Beta-K Distribution
BEP	Beta-P Distribution
BIC	Schwarz Bayesian Criterion
CC	Correlation Coefficient
CDF	Cumulative Distribution Function
CMIP5	Coupled Model Inter-Comparison Project Phase 5
CSA	Canadian Standard Association
DD	Dynamical Downscaling
ECDF	Empirical Cumulative Distribution Function
ER	Extreme Rainfall
GCM	Global Climate Models
GEV	Generalized Extreme Values
GLO	Generalized Logistics
GNO	Generalized Normal
GOF	Goodness-of-Fit
GPA	Generalized Pareto
GUM	Gumbel
IDF	Intensity-Duration-Frequency
LIO	Land Information Ontario
L-MOM	Method of L-Moment
LN3	Log-Normal Three Parameters

LP3	Log-Pearson Type 3
MAD	Mean Absolute Deviation
MADr	Mean Absolute Relative Deviation
MAE	Maximum Absolute Error
MEAN	Mean
MOM	Method of Moment
NCM	Non-Central Moments
PDF	Probability Density Function
PE3	Pearson Type 3
PPCC	Probability Plot Correlation Coefficient
PWM	Probability Weighted Moments
Q-Q	Quantile-Quantile Plot
RCM	Regional Climate Models
RCP	Representative Concentration Pathways
RFA	Regional Frequency Analysis
RMSE	Root Mean Square Error
RMSEr	Root Mean Square Relative Error
RRMSE	Relative Root Mean Square Error
SD	Statistical Downscaling
STSD	Spatio-Temporal Statistical Downscaling
WAK	Wakeby Distribution
WMO	World Meteorological Organization

Chapter 1. General Introduction

1.1 Problem Statement

Canada and many nations over the world have significant investments in urban water infrastructures (urban drainage systems, water supply systems, wastewater treatment plants, etc.). Every day, residents rely on these infrastructures to protect lives, property, and to reduce the pollution effects on natural systems such as creeks, rivers, and lakes. The installation of the urban water infrastructures, however, could make the cities more vulnerable to extreme rainfall events which are a major contributor to many severe flooding events in urban areas (CSA, 2012; Lemmen et al., 2016; Zhang et al., 2019). Infrastructure failure and loss are often associated with these flooding events as infrastructure design criteria are exceeded (CSA, 2012). More recently, it has been observed that there is a notable increase in damages caused by extreme storms in many urban municipalities across Canada (IBC, 2018). Some typical examples of the impacts of these extreme weather events in Canada include the extreme storm in Toronto on July 8, 2013 - roughly 126 mm of rain fell over a two-hour duration- causing a severe loss of $982 million to the Canadian insurance industry; the severe storm in Toronto on August 19, 2005 - resulting in $762 million in losses (IBC, 2018); and other extreme rainfalls over the past years that have caused severe damages to several urban municipalities across the country such as Calgary, Saskatoon, Winnipeg, London, Burlington, Ottawa, Montreal and Moncton (Sandink, 2015). Hence, an accurate estimation of the design storm (that is, the rainfall intensity of an extreme storm event for a given duration and for a given probability of occurrence) is of critical importance for sustainable design and management of the urban water infrastructures (see Figure 1-1). Furthermore, for most cities it is expected that these increasing trends will continue over the coming decades due to the increasing climate variability and climate change in addition to other non-climatic effects such as population growth and urban land-use change. Consequently, the design of urban water infrastructures needs urgently to incorporate more sustainable approaches to account for these climate and environmental changes.

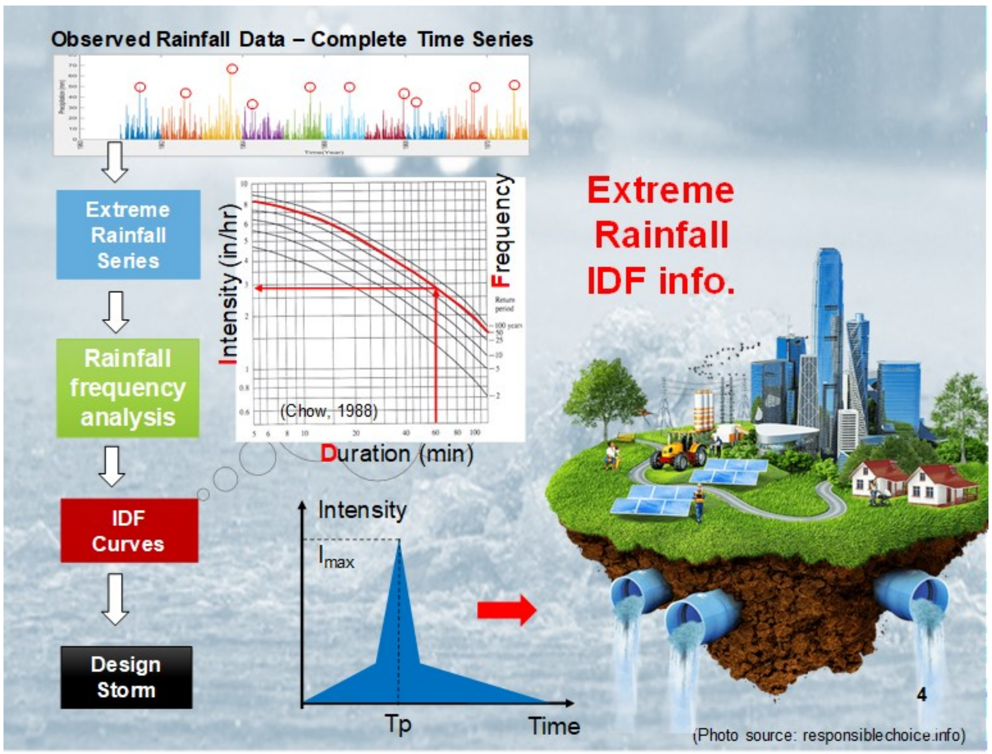

Figure 1-1. Design storm and extreme rainfall intensity-duration-frequency (IDF) relations

In current engineering practice, for estimating the "design storm" the extreme rainfall intensity-duration-frequency (IDF) relations at a location of interest is required. These IDF relations represent hence a critical design tool that is commonly used by hydraulic engineers and water resource professionals for sustainable design and management of the urban drainage networks (Chow, 1964; WMO, 2009a). However, there are many challenging issues in the existing methods for constructing IDF relations in practice, especially in the context of a changing climate.

These include: (i) the lack of a suitable procedure for selecting an appropriate probability distribution model for rainfall frequency analysis; (ii) the unavailability of sub-daily extreme rainfall series at a given location of interest; (iii) the lack of a suitable downscaling procedure for establishing the linkages between the climate projections given by Global Climate Models (GCMs) at global scales and the observed extreme rainfalls at a given local site; and (iv) the lack of a decision-support tool that can be used for constructing robust rainfall IDF relations in consideration of model uncertainty and climate change information.

First of all, to construct the IDF curves, different observed annual maximum rainfall series (AMS) from a few minutes to one day are required at the given location of interest (Chow, 1964; WMO, 2009a). The historical records of the “gauged” site must be sufficiently long, normally more than 20 years (WMO, 2009a), in order to have a reliable extreme rainfall frequency analysis result. The at-site frequency analysis (ASFA) can be then performed for the “gauged” site by fitting an appropriate probability distribution model to the AMS (see Figure 1-2) and then computing the model parameters and design rainfall quantiles (Stedinger et. al., 1993; WMO, 2009a). Currently, there are many probability models available in the literature for modelling the distribution of extreme hydrologic variables at a single site. However, there is no general agreement as to which distribution(s) should be used (WMO, 2009a; Nguyen et al., 2017). Furthermore, in current practice, the performances of several distributions were compared and assessed based on different graphical and statistical assessment criteria, such as quantile-quantile plots and goodness-of-fit tests. A probability distribution is then considered as the most suitable among many plausible candidates if it can provide the best fit to the observed data (Chow, 1964; Kite, 1977; Hosking and Wallis, 1997; Rao and Hamed, 2000). Consequently, the best-fit selection technique depends strongly on the characteristics of the existing rainfall records at a given site. However, this approach cannot be used to assess the performance of the selected models for extreme events that occur outside the observed rainfall record; that is, based on the best "predictive" ability of a given probability model. This model performance assessment criterion (i.e., the model predictive ability) is considered critical in the selection of the most suitable probability model for estimating the extreme design rainfall for design purposes because the design rainfall usually requires a long return period (e.g., more than 100 years) that is much longer than the available historical rainfall records. Hence, when comparing the performance of different probability models for extreme design rainfall estimation, it is necessary to assess the performance of a probability model based on both its descriptive and predictive abilities. The present study proposed therefore a general procedure for assessing systematically the performance of different probability distributions for rainfall frequency analyses based on both their descriptive as well as predictive abilities. So far, very few studies have been able to provide a similar model assessment (Wilks, 1993; Oztekin, 2007).

In many circumstances, the short-duration (sub-daily or sub-hourly) extreme rainfall data are often unavailable or very limited (e.g. less than 10 years) at the location of interest while the daily data are widely available due to the cost of measurement and maintenance (Nguyen et al., 2002b; Mekis et al., 2018). These sites are referred to as "partially gauged" sites (see Figure 1-2). In this case, the short-duration extreme rainfalls or their distributions must be estimated in order to be able to construct the IDF relations for extreme rainfalls at sub-daily time scales. Scale-invariance (or scaling) models that relate the statistical properties of extreme hydrologic variables over a wide range of time scales have received increasing attention as a promising tool for dealing with this issue (Nguyen et al., 1998; Sposito, 1998; Hubert, 2001; Bernardara et al., 2007). In other words, the scale-invariance technique could be used to infer the sub-daily extreme rainfalls from daily extreme rainfalls available at the site of interest. In the present study, scale-invariance models based on the probability weighted moments (PWMs) will be developed for modeling extreme rainfall processes over a wide range of time scales (i.e., from several minutes to one day). The PWMs have been known to be more robust against outliers and hence more suitable for use with short rainfall records as compared to the ordinary statistical moments that have been commonly used in some previous studies (Nguyen et al., 2002b).

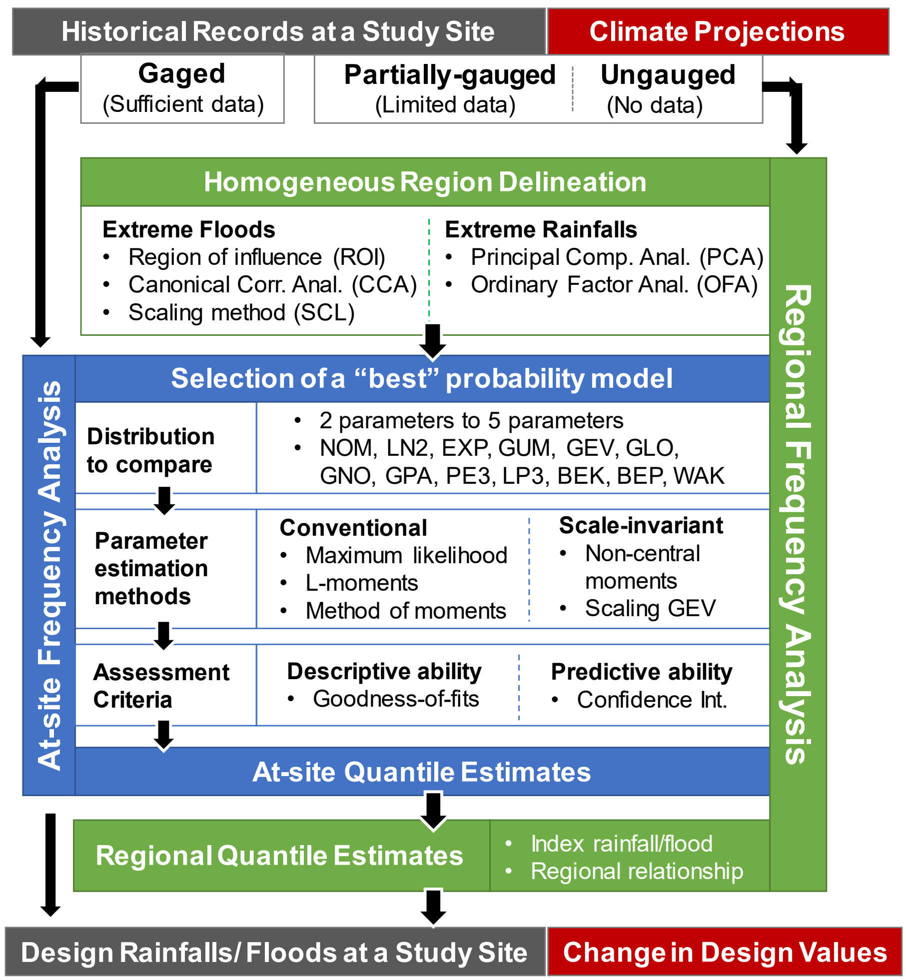

Figure 1-2. At-site and regional frequency analysis of extreme hydrologic variables

In addition, for the completely "ungauged" sites; that is, where no daily or sub-daily extreme rainfall data are available, it is necessary to develop a method for transferring the estimated design rainfall quantiles from the neighboring sites to the given location of interest (Hosking and Wallis, 1997; Nguyen et al., 2002b). Such a technique is referred to as the regional frequency analysis approach that consists of three basic tasks: (i) the identification of regional rainfall homogeneity or similarity; (ii) the selections of an underlying regional rainfall distribution as well as a proper parameter-estimation method; and (iii) the transfer of the estimated regional values to the at-site values at the location of interest (Hosking and Wallis, 1997). In the first step, the scaling approach has been used to identify rainfall regional homogeneity (Nguyen and Pandey, 1994; Nguyen et al., 1998). In the second step, the selection of a suitable regional rainfall distribution could be based on a similar procedure as being used for the at-site frequency analysis. In the last step, the current practice is relied on the index flood (or index rainfall) method to estimate the regional value and then to transfer this estimated value to the study location where data are unavailable (Dalrymple, 1960; Ojha et al., 2008). The index flood/rainfall method is, however, considered as a special case of the scaling approach (Smith, 1992). In particular, Nguyen et al. (2002b) used the scaling GEV distribution to estimate extreme rainfalls at ungauged sites by transferring the rainfall NCMs from neighboring sites to the site of interest located within the rainfall homogeneous region. Therefore, in the present study a special procedure was developed for constructing the IDF curves for an ungauged location.

In addition to the above-mentioned issues related to partially-gauged and ungauged sites, the climate change has been recently recognized as having a profound impact on the hydrologic cycle, especially for urban areas (Willems et al. 2012; Kharin et al., 2013; Lemmen et al., 2016; Zhang et al., 2019). However, the existing traditional methods for constructing IDF relations were not able to account for the possible climate change impacts. Consequently, given the current context of a changing climate there is an urgent need to develop improved methods for estimating IDF curves for different possible climate change scenarios in order to improve the design and management of urban water infrastructures (CSA, 2012; Simonovic et al., 2016). The main challenge is how to develop the linkages between daily rainfalls at global/regional scales given by global climate models (GCMs) and daily and sub-daily extreme rainfalls at a local site of interest. Downscaling approaches have been proposed in many previous studies to downscale these global/regional-scale GCM daily information to daily rainfall projections at a local scale. However, these daily downscaled data are still considered too coarse in both spatial and temporal resolutions and hence they are not suitable for climate change impact studies for small urban watersheds (Nguyen and Nguyen, 2007; 2008). Therefore, in the present study, a novel spatio-temporal statistical downscaling approach was developed for establishing the linkages between daily rainfall projections by GCMs and daily and sub-daily extreme rainfalls at a local site of interest.

Finally, IDF relations are essential for estimating extreme rainfalls for design of various hydraulic structures (CSA, 2012; Simonovic et al., 2016). However, in current engineering practice, the construction of these relations represents a challenging and tedious task since it involves the uncertainty analysis of different probability models and the frequency analyses of a large amount of extreme rainfall data for different durations at a given site or over many different locations (Nguyen and Nguyen, 2019b). In particular, the selection of the best probability model for extreme rainfalls is the most difficult decision since it requires two main challenging tasks: (i) a detailed evaluation of the descriptive and predictive abilities of each selected distribution as well as the analysis of its uncertainty; and (ii) a systematic comparison of the accuracy and robustness of all candidate models based on a number of graphical and numerical performance criteria (Nguyen et al., 2017). Furthermore, to assess the climate change impacts on the IDF relations, there are many different sources of downscaled climate projections available from a large number of different organizations in Canada and in many other countries (Nguyen and Nguyen, 2019a, 2020). Each data source itself contains a very large amount of data from several different climate models. It is therefore necessary to develop a decision-support tool that could facilitate the construction of robust rainfall IDF relations at a given site or at many sites of interest in consideration of the available large data sets and the different sources of uncertainty from different probability and climate models. The proposed tool will be a convenient and effective means for improving the estimation of the design rainfall for design and management of urban water systems.

1.2 Objectives of the Study

In view of the afore mentioned issues, the overall objective of the proposed research is to develop innovative methods for modelling extreme rainfall processes over a wide range of spatial and temporal scales in the context of a changing climate and for cases where rainfall records are limited or unavailable. Results of this research could provide new procedures and tools for improving the accuracy of design rainfall estimation for water infrastructure design. These procedures and tools could also be used for high-quality climate change impact assessment studies in water-related areas such as agriculture, irrigation and drainage, transportation, public health, and so on. More specifically, the proposed research is aiming at the following objectives:

(1) Development of a systematic approach for selecting the best probability model(s) that could accurately describe the distributions of rainfall extremes.

(2) Development of an original scale-invariance mathematical framework for the Generalized Extreme Value (GEV) distribution based on the probability weighted moment (PWM) concept to represent the distributions of rainfall extremes over a wide range of time scales.

(3) Development of an innovative approach to establishing the linkages between daily climate change information provided by large scale climate models to sub-daily extreme rainfall processes at a given local site.

(4) Development of original scale-invariance mathematical frameworks for commonly-used probability distributions for modelling of extreme rainfall processes over different time scales: Generalized Logistic (GLO), Generalized Normal (GNO), and Pearson Type 3 (PE3) probability distributions.

(5) Development of a decision-support tool for constructing robust extreme rainfalls IDF relations for gauged and ungauged sites, and for assessing the climate change impacts on extreme design rainfalls.

1.3 Organization of the Thesis and Chapter Overview

The thesis consists of eight chapters and the coherent links between the five main chapters (Chapters 2 to 6) are indicated in Figure 1-3. Chapter 1 provides a general introduction of the main research topic related to the estimation of extreme design rainfall. This chapter also presents an overview of the limitations of existing methods, the key challenging issues related to this rainfall estimation, especially in the context of climate variability and climate change, and the description of the specific objectives of this research to address these issues. Chapter 2 introduces an original systematic procedure for evaluating the performance of different popular probability distributions for rainfall frequency analyses in order to determine the best probability models that could provide the most accurate and most robust extreme design rainfall estimates. Chapter 3 proposes a novel scale-invariant Generalized Extreme Value (GEV) distribution model based on the Probability-Weighted Moment (PWM) concept. This GEV/PWM model can be used for modeling extreme rainfall processes in consideration of the scaling properties of rainfalls over a wide range of time scales. For assessing the climate change impacts on extreme rainfalls at a given location , Chapter 4 presents an innovative spatio-temporal statistical downscaling approach for establishing the linkage between daily extreme rainfalls given by climate models at regional scales and daily and sub-daily extreme rainfalls at a local (point) scale using the proposed GEV/PWM model. Chapter 5 introduces a more general original mathematical framework for modeling extreme rainfall processes over different time scales using the Generalized Logistic (GLO), Generalized Normal (GNO), and Pearson Type 3 (PE3) probability distributions. These probability models have been recommended in the technical design guidelines in several countries. Chapter 6 presents an effective and practical decision-support tool to assist in the evaluation of the performance of the different procedures as described in Chapters 2 to 5 for constructing robust rainfall IDF relations in consideration of the model uncertainty and climate change information for the design and management of urban water systems. The major findings and recommendations for further studies are summarized in Chapter 7. Finally, Chapter 8 provides a summary of the original contributions of the present research as well as the list of peer-reviewed journals and refereed conference papers based on the results of this doctoral thesis work.

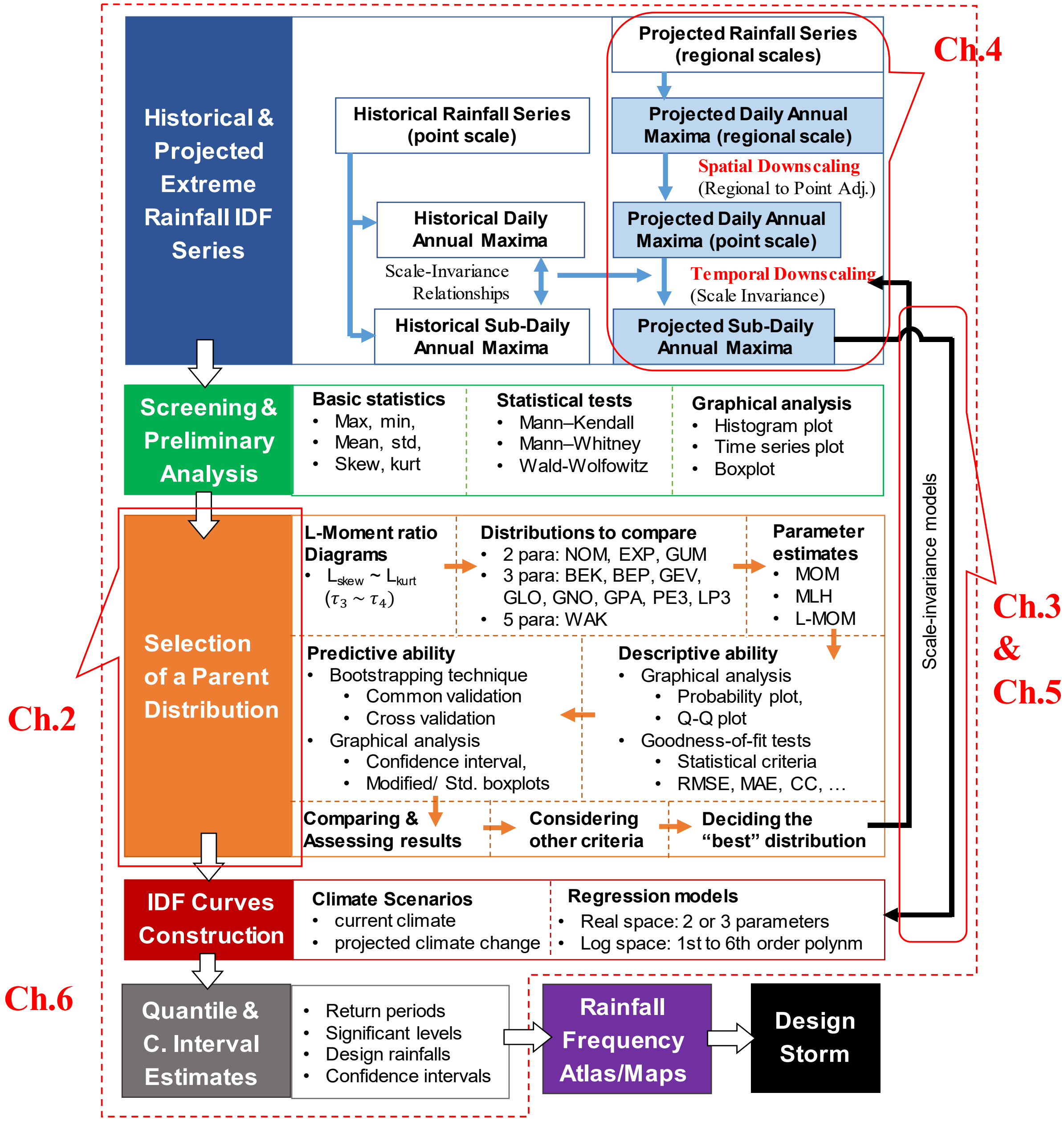

Figure 1-3. The big picture and the five main chapters of the thesis

Chapter 2. A Systematic Approach to Selecting the Best Probability Models for Annual Maximum Rainfalls – A case study using data in Ontario (Canada)

2.1 Introduction

Design and management of various hydraulic structures, particularly urban drainage systems, require information on the probability of annual maximum rainfall occurrence and amount of durations from several minutes to days. This information is often presented in the form of extreme rainfall intensity-duration-frequency (IDF) relations (Chow, 1964). In order to construct IDF curves, first, annual maximum rainfall series (AMS) are generally required to perform rainfall frequency analyses due to its much simpler structure comparing to the peak over threshold series (Lang et al., 1999; WMO, 2009a; WMO, 2009b). The next step is to select a suitable distribution that could describe well the distribution of the annual maximum rainfall data. This task, however, is not easy and remains as one of the major challenges in engineering practice due to significant spatial and temporal variability of rainfall maxima.

In fact, many probability models have been proposed for representing the distribution of annual hydrologic extremes at a single site (Chow, 1964; Kite, 1977; Stedinger et. al., 1993; Hosking and Wallis, 1997; Rao and Hamed, 2000; Nguyen et al., 2002a; WMO, 2009a; Salinas et al., 2014a, 2014b); however, there is still no general agreement as to which distribution(s) should be used due to the lack of a suitable evaluation procedure. The national guidelines of different countries recommend the use of different distributions. For instance, Log-Pearson 3 has been recommended in the US in Bulletin 17B (Griffis and Stedinger, 2007). The generalized extreme value (GEV) distribution and LP3 are recommended in Australia (Ball et al., 2016). GEV distribution is also a recommended choice in many other countries in Europe, including Austria, Germany, Italy, and Spain (Salinas et al., 2014b). However, many other distributions have also been used popularly, including the Gumbel (GUM) distribution in Finland and Spain, the generalized Pareto (GPA) distribution in Belgium, the generalized logistic (GLO) distribution in the UK (Salinas et al., 2014b). In Canada, the use of a specific distribution is not compulsory, however, LP3, Log-normal three parameters (LN3), GEV, and GUM have been used popularly (Chow and Watt, 1991; Adamowski et al. 1996; Alila, 1999; Hansen, 2015). Environment Canada currently uses GUM to construct at-site IDF curves for all stations in Canada (Environment Canada, 2014). This distribution is also recommended for the development of rainfall IDF relations by the Canadian Standard Association (CSA, 2012).

In general, the common method for selecting a proper probability model is mainly based on the best fit of the model to the observed data; that is, the model with its best descriptive ability (Mielke and Johnson, 1974; Wilks, 1993; Laio et al., 2009; Haddad and Rahman, 2011). Consequently, the best-fit selection approach depends strongly on the characteristics of the existing rainfall record at a given site. However, this approach cannot be used to assess the performance of the selected models for extreme events that occur outside the considered rainfall record; that is, based on the best model predictive ability. This characteristic (i.e. model extrapolation or prediction) is considered vital when comparing the performance of different probability models for annual extreme rainfall series, however, there are only a few studies concerning this point

(Wilks, 1993; Oztekin, 2007). Nevertheless, none of these publications have addressed the comparison of a large number of popular probability models for a wide range of short-to-long duration AMS data based on both the descriptive and predictive performance.

In view of the above-mentioned issues, the present study proposes therefore a systematic procedure for assessing and comparing the performance of different probability models in terms of both their descriptive and predictive abilities in order to determine the “best” model that could provide the most accurate extreme rainfall estimates. More specifically, ten common probability distributions for extreme rainfalls were considered in this comparative study (WMO 2009a): Beta-K (BEK), Beta-P (BEP), GEV, GLO, LN3 or Generalized Normal (GNO), GPA, GUM, LP3, Pearson Type III (PE3), and Wakeby (WAK). Graphical and numerical comparison criteria were utilized to evaluate the performance of the selected probability models based on their degree of overall fit to the data, their degree of fit at the right-tails, the accuracy of their right-tail extrapolations, which is of particular importance for engineering design purposes (El Adlouni et al., 2008), and their overall computational facility. The feasibility of the suggested procedure was tested using a total of 63 available AMS data for 5-minute, 1-hour, and 24-hour durations from a network of 21 raingauges located in the Ontario region in Canada. These data are provided in Section 2.2, while the methodology – the systematic approach, is described in detail in Section 2.3. Section 2.4 presents the results and Section 2.5 provides the conclusions.

2.2 Study Sites and Data

A total of 63 annual maximum rainfall series for three different durations from a network of 21 stations located in the Ontario province in Canada were selected for this study as shown in Figure 2-1. Details of the 21 study stations are presented in Table 2-1. The record lengths for these datasets vary from 40 years to 75 years. These data were obtained from the website of the Government of Canada (Environment Canada, 2014). Selection of the stations relied on the quality of the data, the adequate length of available historical extreme rainfall records, and the representative spatial distribution of raingauges.

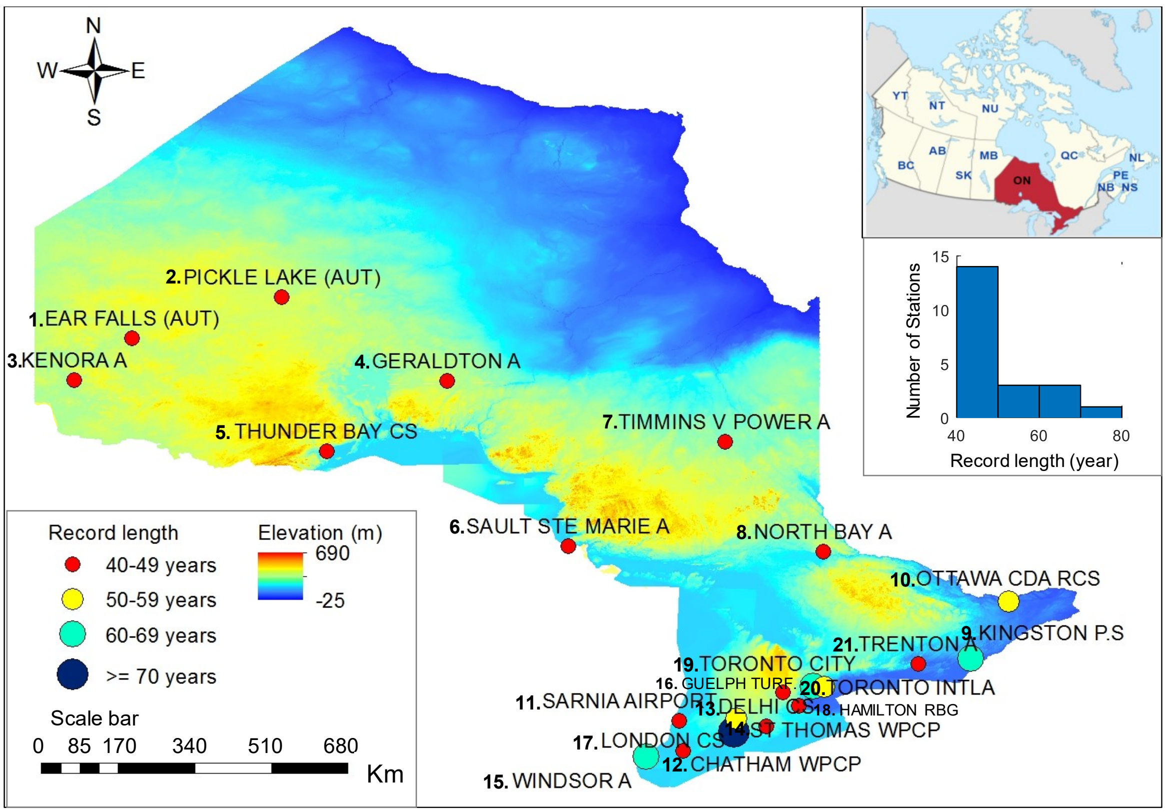

Figure 2-1. Locations of 21 study raingauges in Ontario. The provincial digital elevation model was obtained from LIO (2016).

In order to ensure the quality of data, only data from recording raingauges under the supervision of the Atmospheric Environmental Service of Environment Canada were used. At least 40 years of historical records is required in order to provide reliable estimates of rainfall quantiles for the descriptive ability test. Furthermore, half of the sample have at least 20 years of record for the purpose of distribution fitting and then extrapolating for reliable predictive ability evaluation. The raingauges were selected from different geography locations across West to East to probably represent different climatic conditions of Ontario. Finally, for illustrative application purposes, three rainfall intensity durations (5-minute, 1-hour, and 24-hour) were chosen based on their popular applications in practice such as for urban drainage system design.

Table 2-1. Details of the 21 study stations used in this research, including identification number (ID), station name, latitude (Lat, degree), longitude (Lon, degree), elevation (Elev, meter), record year (Start-End), and record length (RCL, year)

No	ID	Station name	Lat	Lon	Elev	Start	End	RCL
1	6012199	Ear Falls (AUT)	50.63	-93.22	362	1952	2006	49
2	6016525	Pickle Lake (AUT)	51.45	-90.22	390	1953	2004	41
3	6034075	Kenora A.	49.79	-94.37	409	1966	2007	40
4	6042716	Geraldton A.	49.78	-86.93	348	1952	2006	48
5	6048268	Thunder Bay CS	48.37	-89.33	199	1952	2006	47
6	6057592	Sault Ste Marie A.	46.48	-84.51	192	1962	2006	45
7	6078285	Timmins Vic. Power A.	48.57	-81.38	294	1952	2006	47
8	6085700	North Bay A.	46.36	-79.42	370	1964	2006	41
9	6104175	Kingston Pumping Stn	44.24	-76.48	76	1914	2007	63
10	6105978	Ottawa CDA RCS	45.38	-75.72	79	1905	2007	50
11	6127514	Sarnia Airport	42.99	-82.3	180	1962	2006	40
12	6131415	Chatham WPCP	42.39	-82.22	180	1966	2007	40
13	6131983	Delhi CS	42.87	-80.55	231	1962	2007	42
14	6137362	St Thomas WPCP	42.77	-81.21	209	1926	2007	75
15	6139525	Windsor A.	42.28	-82.96	189	1946	2007	60
16	6143090	Guelph Turf Grass CS	43.55	-80.22	325	1954	2003	42
17	6144478	London CS	43.03	-81.15	278	1943	2007	57
18	6153301	Hamilton RBG CS	43.29	-79.91	102	1962	2007	44
19	6158355	Toronto City	43.67	-79.4	112	1940	2007	59
20	6158731	Toronto Intl. A.	43.68	-79.63	173	1950	2013	60
21	6158875	Trenton A.	44.12	-77.53	86	1965	2013	41

The L-moment ratio diagram of all 63 AMS is presented in Figure 2-2. The wide spread of data points from one cloud or one group of the same duration in particular and from all three clouds or three groups of different durations in general on L-diagram show that no distribution can be served at the best distribution for all these datasets. The majority of the 5-min data points seem to fall close to the PE3, GNO, and GEV distributions, while those of 1-hour and 24-hour durations are close to the GEV, GNO, and GLO distributions.

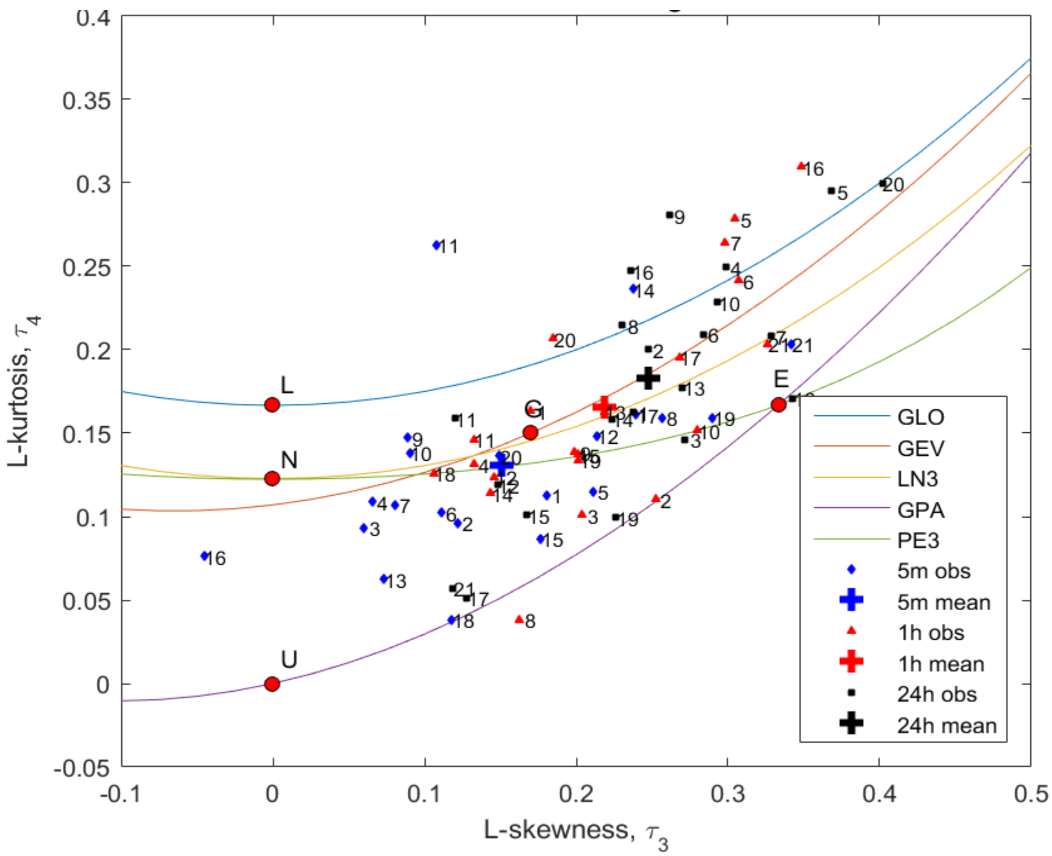

Figure 2-2. L-moment ratio diagram of 63 AMS from 21 raingauges. The blue diamond and '+', red triangle and '+', and black rectangle and '+' markers denote 5-min, 1-hour, and 24-hour dataset L-skewness and L-kurtosis and their corresponding group average values respectively.

It is acknowledged that one can go further by conducting the discordancy measure to group stations within homogeneous regions and then taking the distribution(s) which the average points fall close to as the representative distribution(s) for those distinct delineated homogeneous regions. However, using this approach, some distributions including BEK, BEP, and WAK, could not be investigated. In addition, the performances of the predictive ability of different distributions in predicting quantiles, could not be investigated. This section presents the application of a systematic procedure to identify the most appropriate distribution(s) for Ontario daily and sub-daily AMS. The proposed procedure is presented in Section 2.3.

2.3 Methodology: A Systematic Approach to Determining the 'Best' Distribution for Modeling Annual Maximum Rainfall Processes

This section presents a systematic evaluation procedure for examining and comparing different popular probability distributions in order to determine the most appropriate probability model(s) for depicting the distribution of annual maximum rainfalls. Ten probability models commonly used in hydrologic frequency analyses and their corresponding parameter estimation methods are first presented in Section 2.3.1. The graphical and numerical comparisons of model performance in terms of both descriptive and predictive abilities are then described in Section 2.3.2.

2.3.1 Probability distributions and parameter estimation methods

Ten probability models of two to five parameters commonly used in hydrologic frequency analyses were examined, including BEK, BEP, GEV, GLO, GNO, GPA, GUM, LP3, PE3, and WAK (Chow, 1964; Kite, 1977; Wilks, 1993; Stedinger et. al., 1993; Hosking and Wallis, 1997; Rao and Hamed, 2000; WMO, 2009a). Among them, only GUM and WAK contain two and five parameters respectively, the remaining models contain three parameters. These distributions are chosen based on their popularity in practice and their potential suitability for application in the study region. A summary of the ten models including their probability density functions, quantile functions, and their parameters is provided in Table 2-2. A brief explanation of all 10 distributions are presented as follows.

The GNO distribution is the re-parameterized version of the three-parameter log-normal (LN3) distribution (Hosking and Wallis, 1997). The LN3 distribution has its limit on fitting expectations in real situations where many times the data could show different trend (Martin and Perez, 2009). Still the fitting methods of the log-normal distribution is found robust and reliable, especially when the distribution of the logarithms departs from normality (Stedinger, 1980). The modified version has several advantages over the LN3 since it includes both LN3 distribution with positive and negative skewness and the normal distribution as the special case of zero skewness (Hosking and Wallis, 1997).

The PE3 and LP3 distributions are the most popular models in the Gamma family frequently used for hydrological frequency analysis (Bobée and Ashkar, 1991). If the log of rainfall data follows a PE3 distribution, then the rainfall data is said to follow a LP3 distribution. The LP3 has been extensively used as the base method of flood frequency analysis in the US (WMO, 2009a). The performance of LP3 can widely vary according to the parameter estimation applied. The estimation procedure for the LP3 recommended by the U.S. Water Resources Council in 1967 and subsequently updated in 1975, 1977 and 1981 was found unreliable after many investigations (Arora and Singh, 1989). LP3 has a tendency to give low upper bounds of the precipitation magnitude, which is undesirable for analyzing maximum events (Cunnane, 1989).

The GUM and GEV are from the family of extreme value distributions. GEV is an incorporated general mathematical form of the type I, II and III extreme value distributions for maxima and GUM is a special case of GEV when the shape parameter is equal to zero. GUM can be used when an independent set of daily rainfall with the exponential like upper tail (WMO, 2009a). The GEV distribution has been commonly used to describe the probability distribution of annual extreme rainfalls and for the construction of the IDF curves (Schaefer, 1990).

The GLO distribution used in this paper is introduced by Hosking and Wallis (1997). When the skewness is equal to zero, the GLO becomes the logistic distribution. GLO is a re-parameterized form of the log-logistic distribution proposed by Ahmad et al. (1988). The parameterization and behaviour on tails with large values of GLO are similar to the GEV distribution (WMO, 2009a). The distribution has been used for flood frequency analysis in the United Kingdom as suggested by Robson and Reed (1999).

The WAK distribution is first introduced by Houghton (1978) to be used for the flood frequency analysis. However, the associated parameter estimates often have large standard errors which result in wide confidence intervals for the quantile estimates (Ahmad et al., 1988). The GPA distribution is a special case of the WAK and exponential distribution with three parameters. It is useful for modelling extreme rainfalls or floods that exceed a specified lower bound (Öztekin 2005; WMO, 2009a).

The BEK and BEP distributions are two distinct special cases of the generalized beta distribution. These distributions appear to provide reasonable descriptions of commonly encountered types of measurements and, possess very desirable computational properties. BEK was found providing an excellent computational facility with order statistic distributions (Mielke and Johnson, 1974; Murshed et al., 2011).

Regarding the estimation of the distribution parameters, some common procedures include the method of moments, the maximum likelihood method, the method of probability weighted moments and L-moments (Chow, 1964; Kite, 1977; Hosking, 1990; Stedinger et. al., 1993; Hosking and Wallis, 1997; and Rao and Hamed, 2000), and the method of non-central moments (NCMs) (Nguyen et al., 2002b). These approaches differ in the weights they give to different elements in the selected data set. The maximum likelihood method yields asymptotically optimal estimators of the parameters for some distributions; however, it often involves tedious computation, and it is very sensitive to the computational techniques considered. The probability weighted moments and L-moments estimators are more robust than conventional moments to outliers in the data and sometimes yield more efficient parameter estimates than the maximum likelihood estimates (Stedinger et al., 1993; Hosking and Wallis, 1997). The method of NCMs has been shown to be able to consider some scale-invariance property of the NCMs of extreme rainfall data for different durations (Nguyen et al., 2002b; Nguyen and Nguyen, 2008; Nguyen et al., 2007).

Hence, in the present study, the method of L-moments is used for all distributions (Hosking and Wallis, 1997) except the BEK and BEP models estimated by the method of maximum likelihood (Mielke and Johnson, 1974). The method of L-moments is also available for BEK (Murshed et al., 2011), however, it is not preferable since the estimation procedure is more complicated and tedious than the method of maximum likelihood, but results are approximate. GEV parameter is estimated by both the L-moment (denotes as GEV) and non-central moment (denotes as GEV*) methods.

In general, it is expected that models with more parameters could fit better to the observed data; however, their parameter estimates would be more complex; and more importantly, their prediction abilities may not be better than those models with fewer parameters. The performance assessment of a distribution, hence, should rely on both its descriptive and predictive abilities.

Table 2-2. Probability distributions and their parameters

Model	PDF $f(x)$ and Quantile function $x(F)$	Parameters	Ref.
BEK	$f(x) = \left(\frac{\alpha\theta}{\beta}\right)\left(\frac{x}{\beta}\right)^{\alpha\theta-1}\left[1+\left(\frac{x}{\beta}\right)^{\theta}\right]^{-(\alpha+1)}$; $x(F) = \beta\left[\frac{F^{1/\alpha}}{(1-F^{1/\alpha})}\right]^{1/\theta}$; $(x>0, \alpha>0, \beta>0, \theta>0)$;	$\alpha, \theta > 0$: shape $\beta > 0$: scale	Mielke & Johnson (1974)
BEP	$f(x) = \left(\frac{\alpha\theta}{\beta}\right)\left(\frac{x}{\beta}\right)^{\theta-1}\left[1+\left(\frac{x}{\beta}\right)^{\theta}\right]^{-(\alpha+1)}$; $x > 0$ $x(F) = \beta\left[(1-F)^{-\frac{1}{\alpha}}-1\right]^{1/\theta}$;	$\alpha, \theta > 0$: shape $\beta > 0$: scale	Mielke & Johnson (1974)
GEV, GUM[a]	$f(x) = \frac{1}{\alpha}e^{-(1-k)y-e^{-y}}$; $y = \begin{cases} -k^{-1}\log\left[1-\frac{k(x-\xi)}{\alpha}\right] & ; k \neq 0 \\ (x-\xi)/\alpha & ; k = 0 \end{cases}$ $x(F) = \begin{cases} \xi + \frac{\alpha[1-(-\log F)^{k}]}{k} & ; k \neq 0 \\ \xi - \alpha\log(-\log F) & ; k = 0 \end{cases}$	ξ: location α: scale κ: shape	Jenkinson (1955); Von Mises (1954); Gumbel (1958)
GLO	$f(x) = \frac{\alpha^{-1}e^{-(1-k)y}}{(1+e^{-y})^2}, y = \begin{cases} -k^{-1}log\left\{1-\frac{k(x-\xi)}{\alpha}\right\}, k \neq 0 \\ (x-\xi)/\alpha \quad , k = 0 \end{cases}$ $x(F)) = \begin{cases} \xi + \alpha\frac{\left\{\frac{1-F}{F}\right\}^{k}}{k}, & k \neq 0 \\ \xi - \alpha log\left\{\frac{(1-F)}{F}\right\}, & k = 0 \end{cases}$	ξ: location α: scale κ: shape	Hosking & Wallis (1997)
GNO	$f(x) = \frac{e^{ky-\frac{y^2}{2}}}{\alpha\sqrt{2\pi}}$; $y = \begin{cases} -k^{-1}\log\left[1-\frac{k(x-\xi)}{\alpha}\right]; k \neq 0 \\ (x-\xi)/\alpha \quad ; \quad k = 0 \end{cases}$	ξ: location α: scale κ: shape	Hosking & Wallis (1997)
GPA	$f(x) = \frac{1}{\alpha}e^{-(1-k)y}$, $y = \begin{cases} -k^{-1}\log\left(1-\frac{k(x-\xi)}{\alpha}\right); k \neq 0 \\ (x-\xi)/\alpha \quad ; k = 0 \end{cases}$ $x(F) = \begin{cases} \xi + \frac{\alpha[1-(1-F)^{k}}{k} ; & k \neq 0 \\ \xi - \alpha\log(1-F); & k = 0 \end{cases}$ Range: $\xi \leq x \leq \xi + \frac{\alpha}{k}$ if $k > 0$; $\xi \leq x < \infty$ if $k \leq 0$	ξ: location α: scale κ: shape	Pickands (1975); Hosking & Wallis (1987)
PE3, LP3[b]	$\gamma = 0: f(x) = \phi\left(\frac{x-\mu}{\sigma}\right)$; $-\infty < x < \infty$; $\gamma > 0: f(x) = \frac{(x-\xi)^{\alpha-1}e^{-\frac{x-\xi}{\beta}}}{\beta^{\alpha}\Gamma(\alpha)}$; $\xi \leq x < \infty$; $\gamma < 0: f(x) = \frac{(\xi-x)^{\alpha-1}e^{-\frac{\xi-x}{\beta}}}{\beta^{\alpha}\Gamma(\alpha)}$; $-\infty < x \leq \xi$ $\alpha = \frac{4}{\gamma^2}$, $\beta = \frac{\sigma\lvert\gamma\rvert}{2}$, $\xi = \mu - \frac{2\sigma}{\gamma}$	μ: location σ: scale γ: shape	Pearson (1893); Bobée & Ashkar (1991)
WAK	$x(F) = \xi + \frac{\alpha}{\beta}\{1-(1-F)^{\beta}\} - \frac{\gamma}{\beta}\{1-(1-F)^{-\delta}\}$ $\begin{cases} \xi \leq x < \infty; \ if\ \delta \geq 0\ and\ \gamma > 0 \\ \xi \leq x \leq \xi + \alpha/\beta - \gamma/\delta; \ if\ \delta < 0\ or\ \gamma = 0 \end{cases}$	ξ: location α, γ: scale β, δ: shape	Houghton (1978)

[a] The GUM distribution is a special case of the GEV distribution and is obtained by setting $k = 0$

[b] The LP3 distribution is obtained by changing x in the equations to $y = \ln(x)$

2.3.2 Selection of the best probability distributions

This section presents the use of various graphical and numerical comparisons to compare the performance of different distributions in describing the distribution of AMS and in extrapolating quantiles that lie beyond the available record length in order to identify the best distribution(s).

2.3.2.1 Descriptive ability test

Graphical display is a simple yet effective way to compare the observed to the estimated values. The quantile-quantile (Q-Q) plots is adopted to visualize the adequacy of fitted distributions. To estimate the non-exceedance probability p_i, the Cunnane (1978) plotting position formula shown in Eqn. (2-1) is implemented for its ability to yield approximately unbiased quantiles for a wide range of distributions.

$$p_{i:n} = \frac{i - 0.4}{n + 0.2} \tag{2-1}$$

The Q-Q plots are helpful for visual judgement. However, it is subjective and cannot precisely depict the statistical significance of the fit, particularly with a large number of statistical models to compare. Various test statistics have been developed to justify whether a sample is actually drawn from an assumed distribution, such as Chi-square, likelihood ratio, Kolmogorov-Smirnov, Anderson-Darling, and so on. In the present study, for the ease of computation of a large number of distributions, six test criteria are used. They are: root mean square error (RMSE), relative root mean square error (RRMSE), maximum absolute error (MAE), correlation coefficient (CC), Akaike Information Criterion (AIC) and Schwarz Bayesian Criterion (BIC) as follows:

$$RMSE = \left\{ \sum \frac{(x_i - y_i)^2}{(n-m)} \right\}^{\frac{1}{2}} \tag{2-2}$$

$$RRMSE = \left[\frac{1}{(n-m)} \sum \left\{ \frac{(x_i - y_i)}{x_i} \right\}^2 \right]^{\frac{1}{2}} \tag{2-3}$$

$$MAE = \max(|x_i - y_i|) \tag{2-4}$$

$$CC = \frac{\sum\{(x_i - \bar{x})(y_i - \bar{y})\}}{\{\sum(x_i - \bar{x})^2 \sum(y_i - \bar{y})^2\}^{\frac{1}{2}}} \tag{2-5}$$

$$AIC = 2m + n \cdot \ln(RSS) \tag{2-6}$$

$$AICc = AIC + \frac{2(m+1)(m+2)}{n-m-2} \tag{2-7}$$

$$BIC = \ln(n) \cdot m + n \cdot \ln(RSS) \tag{2-8}$$

where n = sample size; m = number of distribution parameters; $i = 1, 2, \dots, n$; x_i = observed values; y_i = values estimated from an assumed probability distribution for the same probability level; $\bar{x}$ = average value of the observations; and $\bar{y}$ average value of the estimated quantiles; RSS = residual sum of square. AIC_c is AIC with a correction for finite sample sizes. Since AIC_c converges to AIC as n gets large (Burnham and Anderson, 2004), AIC_c is employed in the paper rather than AIC.

RMSE is a popular method to measure residuals – the differences between observed and theoretical values and is expressed in Eqn. (2-2). It is also a good indicator for comparing errors of different models of particular variables (Hyndman and Koehler, 2006). However, since RMSE is computed based on the absolute errors, it gives heavy weighting to large errors that might cover the true image of the fit of a distribution.

In the presence of outliers, which is common in annual extreme rainfalls, a distribution may yield a high RMSE even many other data points are well fitted. Thus, RRMSE as expressed in Eqn. (2-3), based on the proportion of errors and the length of the observation, are used along with RMSE to reduce the impact of outliers and to provide a better image of the overall fit of a distribution. The magnitude of RRMSE tends to decrease with the increase in the sample size (Yu et al., 1994).

MAE represents the largest absolute difference between the observed and computed values. Unlike the relative error, the absolute error describes how large the error is, not the relative to the observed value. The formula of MAE is closely related to the Kolmogorov – Smirnov statistics test and is shown in Eqn. (2-4).

The correlation coefficient (CC) indicates the linearity of the Q-Q plot. It has a range between -1 and 1; where values near -1 and +1 indicates a perfect positive and negative linear relationship respectively; values close to 0 indicates no linear relationship. The CC is defined as in Eqn. (2-5).

Regarding AIC and BIC criteria, the use of the log-likelihood functions is required to estimate the values of AIC and BIC. These functions are available for all distributions, except the Wakeby distribution (WAK) since only the quantile function is available for WAK while the probability density function is unavailable. However, since only the differences in AIC and BIC are meaningful to analyze distribution fit, another way to look at these criteria is to use the residual sum of square (RSS) for the goodness-of-fit term and to keep the same penalty term (Burnham and Anderson, 2002) for these criteria as shown in Eqn. (2-6) to (2-8).

After computing the six statistical tests, a ranking scheme is utilized to rank all the selected distributions. Ranking scores is assigned to each distribution according to the value computed for each criterion. A distribution with the lowest RMSE, RRMSE, MAE, AIC_c, BIC or highest CC is given a rank of 1 for this assessment category. In case of a tie, average ranks are given to those corresponding distributions. Furthermore, for each numerical criterion, the overall rank associated with each distribution is computed by summing the individual rank obtained for each of the study stations.

2.3.2.2 Predictive ability test

The predictive ability of a distribution is a vital characteristic to be evaluated after the descriptive ability as the accuracy of rainfall quantile prediction depends on it. Often it is known as the more parameters a distribution has, the better it will fit to the data. However, estimation of parameter could be challenging with a distribution with parameters more than three, like WAK. In addition, the extrapolation could result critically inaccurate prediction, as the distribution maybe too rigid (Vogel, 1995).

To evaluate the predictive ability of distributions, the bootstrapping method which yields multiple synthetic samples having the same size as the existing record is used in this research (Efron and Tibshirani, 1994). The most attractive feature of the bootstrapping procedure is that it is a powerful tool to describe the behavior of distribution only with the obtained sample values, even when the information about the true distribution is lacking. Moreover, this procedure could be conveniently used to assess the sampling uncertainty. The distribution of sample statistics computed from the bootstrap samples is thus a good representation of the respective distribution of the observed statistics (Vogel, 1995).

To carry out the assessment of distribution extrapolation ability using the bootstrapping method, one thousand bootstrap samples of size equal to half of the actual sample size are first generated. Each candidate distribution is then fitted to the bootstrap samples and is extrapolated to estimate the right-tail quantiles corresponding to the four largest observed rainfall amounts in the full data set. The variability in the estimation of these extrapolated quantiles are presented in the form of modified box plots (Helsel and Hirsch, 2002). The middle line of a modified box is the sample mean, the box height is twice standard deviation, the upper and lower whisker extend to the maximum and minimum value of the sample respectively. Large box widths or long whiskers imply high uncertainty in the estimation of these extreme values. If the observed values fall outside the box, then the distribution fitted to the bootstrap samples has overestimated or underestimated the true values and is therefore not commendable.

2.4 Results

2.4.1 Descriptive ability test results

The Q-Q plots of all 63 AMS shows that all distributions closely described the left-tail and central parts. The right-tail parts, however, are less well described and there are no obvious trends. These values can be well estimated, over-estimated, or under-estimated by any of the ten models. Nonetheless, it is found that the WAK model consistently performs superior to the remaining models at fitting all regions of the data sample. This can be expected since WAK is a flexible model with 5 parameters and that helps it mimic the shape of many other distributions. For purposes of illustration, only results for 1-hour AMS from the longest record station – St-Thomas station, is presented here as shown in Figure 2-3.

From the visual standpoint, all distributions seem to perform well in this case, except the BEK and GPA models. However, the significance of the differences between the remaining models is difficult to judge solely based on the graphical display. A more objective evaluation using numerical comparison criteria is thus necessary.

The ranking scheme described in Section 2.3 was then applied to assess the overall goodness-of-fit of each distribution using the six numerical assessment criteria. Results of the 5-min AMS of the 21 stations are shown in Figure 2-4 as an example. The results reveal that no unique distribution ranks consistently best at all locations and for all three rainfall durations. This agrees well with the preliminary investigation using L-moment ratio diagram presented in Section 3.1 above. However, the rank sum results of the 21 stations of three durations, presented in Figure 2-5, show that WAK model outperforms the others in describing the distribution of daily and sub-daily AMS.

The GEV, GNO, and PE3 models also performed well overall and their scores are close to each other (see Figure 2-5). This can be expected since these models are advocated for use in frequency analyses of hydrologic extreme variables by many researchers (see Section 2.1). It is also noticed that PE3 model performed slightly better than GEV and GNO models for 5-min duration data. However, for data set of longer durations – 1-hour and 24-hour, GEV and GNO are slightly better.

The GUM, GPA, and BEK models rank consistently poorly compared to the others. It could be explained that GUM, naturally, has a weaker descriptive ability than GEV or other distributions with three or more parameters, because it lacks a shape parameter. GPA contains three parameters and this distribution is commonly used with POT rather than with AMS data. Regarding BEK distribution, simulation results of many stations show that it tends to over-estimate the right-tail part, and this leads to a poor result in statistical test results. A similar behaviour was found for the

BEP distribution. However, the over-estimation by the BEP is smaller than the estimation by the BEK model; indicating that the BEP model has a better performance.

The GEV*, LP3, and GLO models performed adequately and they stand in the middle positions (see Figure 2-5). It is also interesting to notice that if only RRMSE is considered, LP3 is even better than WAK for 5-min and 1-hour AMS and stands after the WAK for 24-hour AMS.

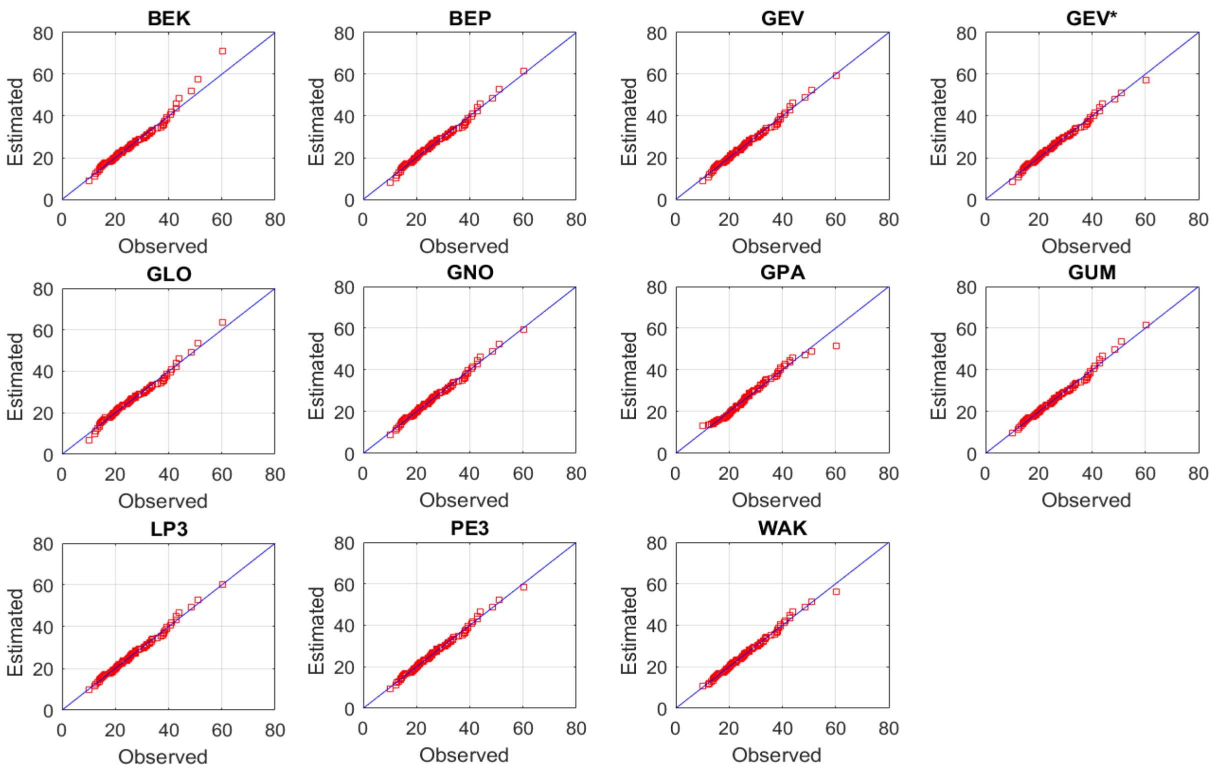

Figure 2-3. Q-Q plots between observed (x-axis) and estimated (y-axis) 1-hr AMS (mm) at St-Thomas station using all eleven candidate models

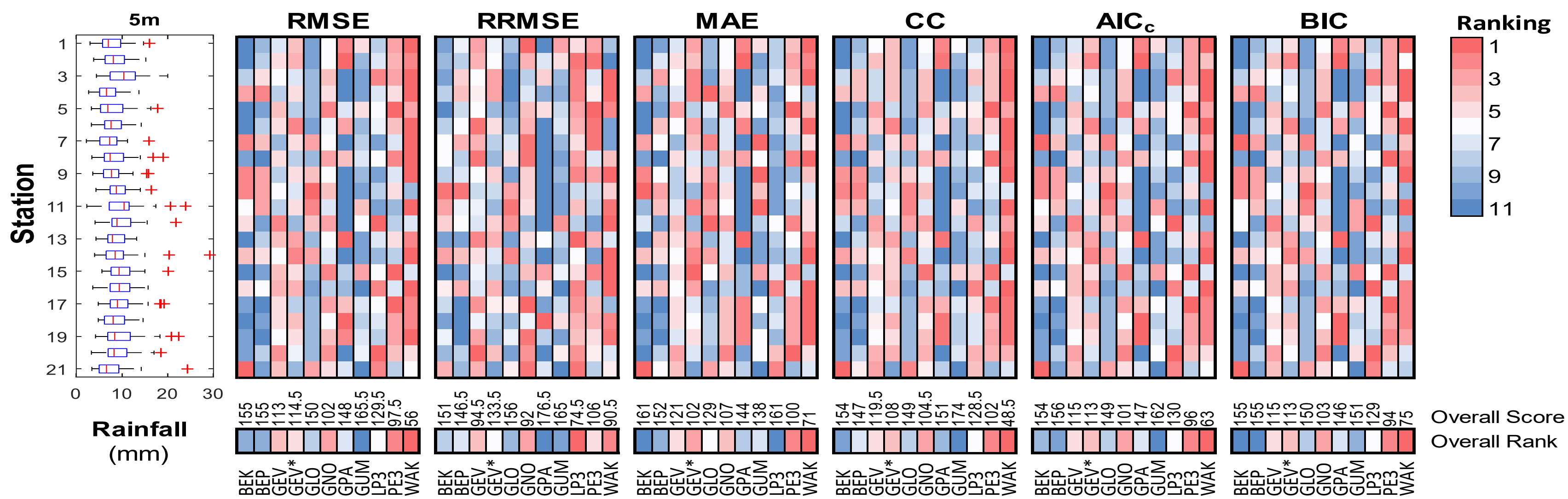

Figure 2-4. The ranking of 11 candidates for 5-min AMS for each station individually and the overall rank for 21 stations based on the six statistical criteria. Rank = 1 (or close to 1) indicates the best model(s) and rank = 11 (or close to 11) indicates the worst model(s).

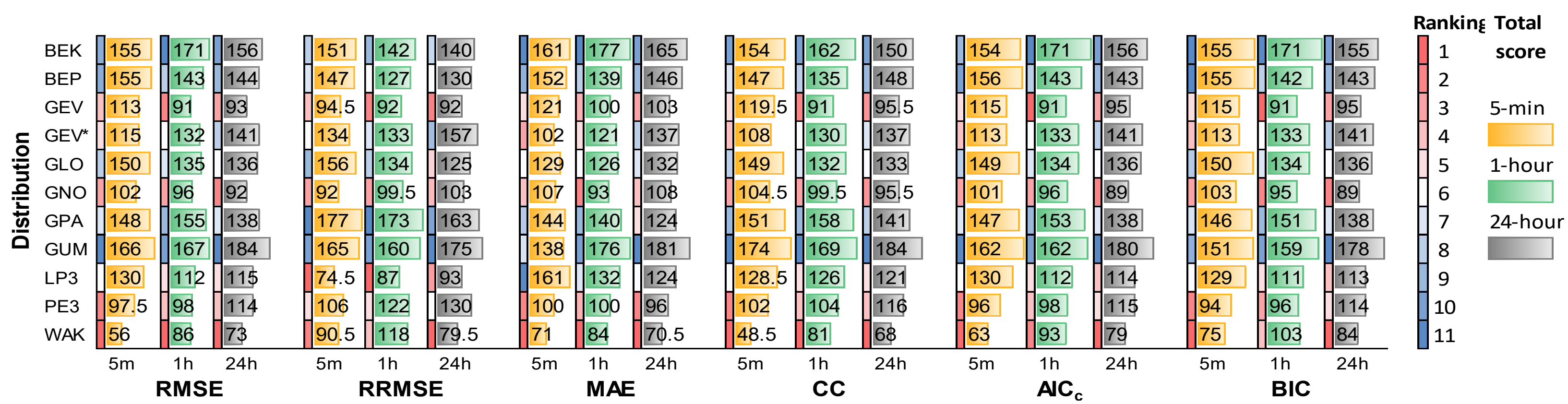

Figure 2-5. The overall rank for all 21 stations based on the four statistical tests for all three durations of 5-min, 1-hour, and 24-hour AMS (The lowest scores or the shortest bar indicates the best model).

2.4.2 Predictive Ability Test Results

The modified boxplots of 63 AMS show that, generally, the BEK and BEP models consistently performed extremely poor with high sampling variation and bias (large box widths and very long whiskers) for all three rainfall durations. For instance, Figure 2-6 shows the modified boxplots of extrapolated right-tail bootstrap data for 1-hour AMS at St-Thomas station. This can be expected since the BEK and BEP models share last positions in the ranking table for the descriptive ability; as they produced much higher values of RMSE, RRMSE, and MAE and much lower values of CC compare to the other models.

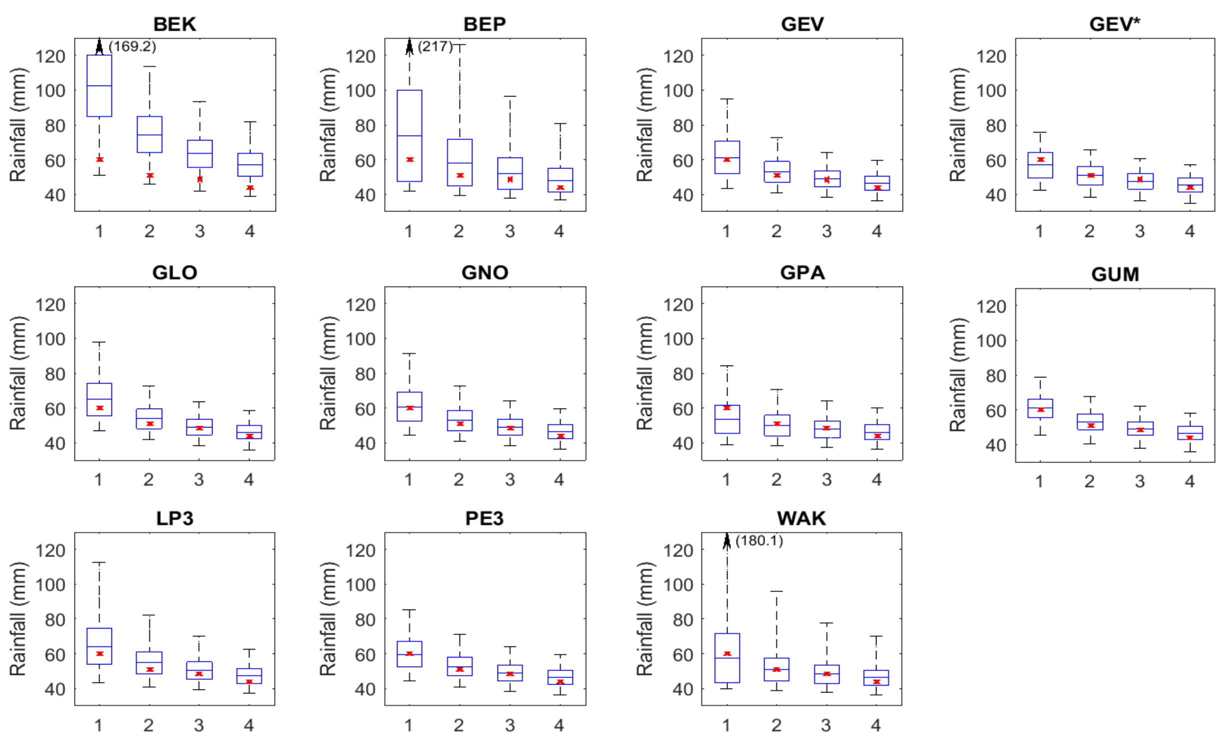

Figure 2-6. Boxplots of extrapolated right-tail bootstrap data for 1-hr AMS at St-Thomas station. The X-axis shows the four-largest values of the observed and simulated data set.

Unlike the BEK and BEP models, the modified boxplots for the WAK model do not show large box widths, however, they reveal long upper whiskers. This can be explained as the WAK model, with five parameters, can mimic many distributions and can fit close to any observed data set and this makes WAK becoming the best distribution in describing the AMS with best goodness-of-fit test scores as investigated in Section 2.4.1 above. However, the disadvantage is that WAK can be a very rigid model with its large number of parameters, and it cannot provide good predictive values as presented by the whisker length of its modified boxplot.

Results of modified boxplots reveal that, the LP3 model produced larger box widths than other distributions, yet it was not as poorly performed as BEK, BEP or WAK. Furthermore, the result shows that the GUM model exhibited the lowest sample variation in most cases, but it tends to overestimate or underestimate the observed values most frequently.

The GEV, GEV*, GLO, GNO, GPA, and PE3 distributions produced satisfactory results at most stations, where the box enclosed the observed right-tail values with a reasonable whisker spread and correlation with the observed values. In particular, both GEV and GNO distributions produced almost identical results. The PE3 distribution produced slightly shorter boxes, upper whiskers, and slightly lower means compared to those of GEV and GNO distributions. Occurrences of over- and under-estimation of several largest rainfall amounts however did occur for all distributions at several stations.

2.5 Selection of the most suitable probability distribution(s)

In general, it is observed that no unique distribution performed consistently best at all stations for each category and for all three rainfall durations. This could be due to the strong spatial variation of rainfall characteristics within this study region. While it is difficult to provide a clear physical interpretation of the regional variability of the probability distribution parameters, one is still able to rely on the proposed approach to identify the GEV, GNO, and PE3 as the best distributions for a large number of cases considered. Furthermore, it is easy to recognize the distributions that did not perform satisfactory, but it is more difficult to identify the best distribution. These three models can be thus used alternately for the frequency analysis of annual extreme rainfalls as shown in Figure 2-7.

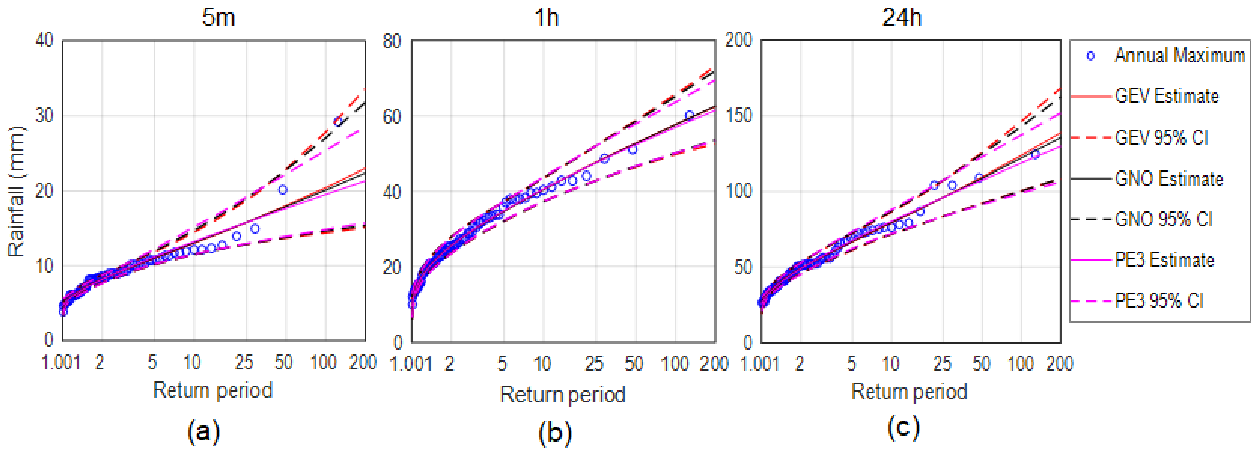

Figure 2-7. Frequency curves (solid lines) and 90% confidence limits (90% CI, dashed lines) of (a) 5-minute, (b) 1-hour, and (c) 24-hour AMS (blue circle markers) at St-Thomas station using the top three distributions – GEV, GNO, and PE3. Note that 5-min duration data of this station is extremely skew and none of the three distributions is able to capture the two largest extreme values. Even the WAK distribution performing better than the GEV, GNO, and PE3 distributions in this case, it still could not capture those extreme values.

The difference in extreme design rainfall estimates produced by the three distributions is also further investigated for all stations and is shown in Figure 2-8. Results reveal that the estimated values for return periods within twice of sample lengths (that is, up to 100-year return periods) are almost identical for the three distributions. However, the GEV model tends to provide slightly higher values for high return periods, while the PE3 model tends to give slightly higher values for low return periods. The three models, therefore, could be used interchangeably in constructing IDF relations and estimating extreme design rainfalls for Ontario region. Nonetheless, if only one probability model is preferred for the entire region, other criteria should be thus considered in the choice of an appropriate distribution. For instance, the GEV model is based on a more solid theoretical basis than the other two distributions because it was derived from the statistical theory of extreme random variables. Therefore, the GEV could be considered as the most suitable distribution for describing the distribution of annual maximum rainfalls in Ontario.

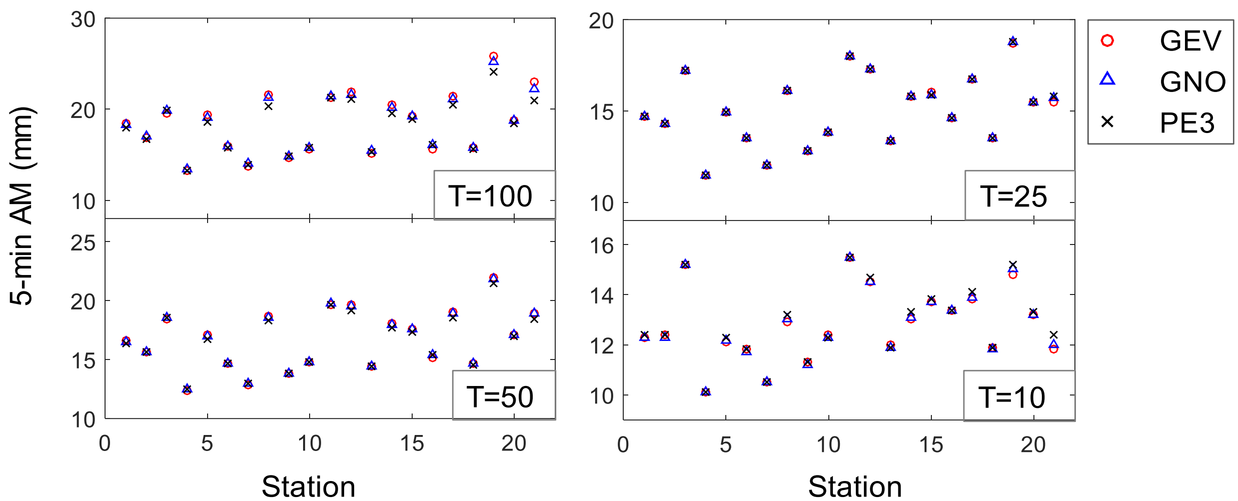

Figure 2-8. Comparing extreme design rainfalls estimates for different return periods (T=10, 25, 50, and 100 years) using 5-min AMS of all 21 stations and the top three distributions GEV, GNO, and PE3

2.6 Summary and Conclusion

The present study proposes a general procedure for assessing systematically the performance of different probability distributions that have been commonly used in hydrologic frequency analysis in order to identify the most appropriate probability model(s) for representing the distribution of annual extreme rainfalls. The proposed procedure relies on a number of graphical and numerical performance criteria to evaluate both the descriptive and predictive abilities of each model. More specifically, the assessment of the model goodness-of-fit was performed through the visual inspection of the quantile-quantile plots as well as the results of six numerical criteria – RMSE, RRMSE, MAE, CC, AICc, and BIC. In addition, the evaluation of model predictive ability was conducted through the utilization of resampling-with-replacement bootstrap technique and the visual inspection of the modified boxplots of the four largest values.

Following a review of various probability distributions available in the literature, ten popular probability models were selected for this study. These models include the BEK, BEP, GEV, GLO, GNO, GPA, GUM, LP3, PE3, and WAK distributions. Results of an illustrative application using AMS data for 5-min, 1-hour, and 24-hour from a network of 21 raingauges located in Ontario have indicated the feasibility of the proposed model evaluation method. In particular, it was found that, among the ten distributions considered, the GEV, GNO, and PE3 are the top three distributions that provided the greatest goodness-of-fit and robust quantile extrapolations for different rainfall durations and for a number of locations in the study region. These distributions can be thus alternately used for the frequency analysis of daily and sub-daily annual extreme rainfalls in this area. The GEV and GNO produced almost identical quantiles and confidence interval estimations, while those of PE3 were slightly lower.

Finally, for practical application purposes, the GEV is preferable to the GNO and PE3 due to its more solid theoretical basis (Coles, 2001; Smith, 2003), and the inherent scale-invariance property of its non-central moments over different time scales, which is useful for the modelling of sub-daily extreme rainfall processes in the context of climate change (Nguyen and Nguyen, 2008; Nguyen et al., 2007). Therefore, the GEV could be considered as the most suitable probability model for representing the distribution of daily and sub-daily annual maximum rainfalls for the Ontario region in Canada.

Chapter 3. A Novel Scale-Invariance Probability-Weighted-Moment-Based Generalized Extreme Value Distribution for Modeling Rainfall Extremes Across A Wide Range of Time Scales

3.1 Introduction

Information on the spatio-temporal variability of rainfall characteristics is of critical importance for many types of hydrologic studies related to the estimation of runoffs for planning, design, and management of various water resources systems (CSA, 2012; WMO, 2009). In particular, for urban and small rural watersheds that are generally characterized by fast response, the designs of various hydraulic structures such as small dams, culverts, storm sewers, detention basins and so on require extreme rainfall input with short temporal time scales (e.g., few minutes or hours) for runoff simulation models (CSA, 2012). This high-resolution extreme rainfall information is necessary for the construction of the "design storm" – that is the extreme rainfall intensity of a given storm duration for a given return period at a given location (Chow, 1964; WMO, 2009a). More specifically, the required extreme rainfall information is often extracted from the available extreme rainfall intensity-duration-frequency (IDF) relations at the location of interest.

To construct the IDF curves at a given location, annual maximum rainfall series (AMS) of different rainfall durations ranging from a few minutes to one day are required. However, such short-duration extreme rainfall records are often unavailable or very limited (e.g., less than 10 years) because of the high measurement costs involved while daily extreme rainfall data are widely available For instance, in Canada, Environment Canada provides short-duration extreme rainfall data for nine rainfall durations (D = 5, 10, 15, 30, 60, 120, 360, 720, and 1440 minutes) for constructing IDF relations for only 596 stations across Canada (Environment Canada, 2019), while the daily rainfall or hourly rainfall records are available for 1735 raingage stations (Mekis et al., 2018). Hence there exists an urgent need to develop new methods for modeling extreme rainfall processes over a wide range of time scales (i.e., from several minutes to days) such that information related to sub-hourly or sub-daily extreme rainfalls could be inferred from the daily extreme rainfalls available at the site of interest.

More recently, climate change has been recognized as having a profound impact on the hydrologic cycle at more vulnerable urban areas (Willems et al. 2012; Kharin et al. 2013). Consequently, the development of IDF relations in consideration of the potential impacts of the climate change has become critical for the design and management of urban water infrastructures. However, the projections of sub-daily extreme rainfalls under different climate change scenarios are often not available at the location of interest since climate simulation outputs given by global/regional climate models are often limited to the daily scale because of their current modeling and computational limitations. Therefore, it is critical to develop an improved rainfall modeling approach that can be used to determine the distributions of sub-daily AMS from the distributions of available daily AMS.

In recent years, the scale-invariance (or scaling) concept has increasingly become a promising methodology for modeling of various hydrological processes across a wide range of time scales (Sposito, 1998; Hubert, 2001; Schertzer et al., 2010; Lovejoy and Schertzer, 2012). This scaling concept implies that the statistical properties of extreme rainfalls over different time scales are related to each other by an operator involving only the scale ratio and the scaling exponent (Gupta and Waymire, 1990; Bernardara et al., 2007). The scale invariance is based on the fractal and multi-fractal concepts. Historically, at the beginning of the 90s, fractal science provided a more theoretical framework to address the scaling issues in geosciences through the concept of scale invariance (Schertzer and Lovejoy, 1991). Lovejoy (1982) first studied the single fractal dimension of rainfall phenomena using radar rainfall data. Later on, Schertzer and Lovejoy (1987) have proposed the multifractal dimension concept for describing these physical phenomena due to the underlying physically complex rainfall process. The scale invariance properties of rainfall processes based on fractal and multifractal modeling and analysis approaches have been reported in previous studies for different climatic regions (Veneziano et al., 2006; Bernardara et al., 2007). In particular, many empirical studies have suggested that rainfalls, in time and space, show a scale invariant behaviour within a certain range of rainfall durations (Schertzer and Lovejoy, 1987; Gupta and Waymire, 1993; Menabde et al., 1999; Veneziano and Furcolo, 2002; Veneziano and Lepore, 2012).

Pioneering works in the application of the scaling method for deriving short-duration from longer-duration AMS and for constructing IDF relations have begun since the last decade of the 20th century. These studies were primarily relied on the empirical relationships between different ordinary statistical moments (or non-central moments, NCMs) of observed rainfall data over different rainfall durations and the scale-invariance relations between the parameters of the distributions of extreme rainfalls at different durations (Gupta and Waymire, 1990; Nguyen and Pandey, 1994; Nguyen and Wang, 1996; Burlando and Rosso, 1996; Nguyen et al., 1998; and Menabde et al., 1999).

More specifically, Gupta and Waymire (1990) described two common properties of empirical moments shared by spatial rainfall and river flow data as well as provided some general mathematical frameworks for the simple scaling processes. Nguyen and Pandey (1994) proposed a scale-independent mathematical model to represent the probability distribution of rainfalls at various time scales on the basis of the theory of multifractal multiplicative cascades. In addition, Nguyen and Wang (1996) introduced a time resolution independent mathematical models based on the multifractal multiplicative cascade mechanism for transferring rain fluxes from large time scales (e.g., one day or longer) to smaller time intervals (e.g., one hour or shorter). Burlando and Rosso (1996) analyzed the scaling and multi-scaling properties of the statistical empirical moments of rainfall depths of different durations and then developed a scaling two-parameter log-normal (LN2) probability distribution to construct depth-duration-frequency relations. Menabde et al. (1999) proposed the NCM-based scaling Gumbel (GUM/NCM) distribution rather than the LN2 as suggested by Burlando and Rosso (1996) for deriving the maximum rainfall IDF relations. However, Nguyen et al. (1998) has developed a more general mathematical framework using the NCM-based scaling Generalized Extreme Value (GEV/NCM) distribution. The scaling properties of the GEV model are also presented in detail in Nguyen et al. (2002). It can be seen that the scaling GUM/NCM as proposed by Menabde et al. (1999) is a special case of the GEV/NCM since the two-parameter GUM is a special case of the three-parameter GEV distribution when the shape parameter is equal to zero.

Since then, the application of the scaling method based on the scale-invariance of empirical statistical moments of rainfall amounts over different rainfall durations has become popular and has been applied extensively to the estimation of short-duration extreme rainfalls at gauged and ungauged sites based on both at-site and regional frequency analyses (Nguyen et al., 2002b; Yu et al. 2004; Bougadis and Adamowski, 2006; Blanchet et al., 2016; Ghanmi et al., 2016; Soltani et al., 2017; Van de Vyver, 2018; Mélèse et al., 2018). It has also been applied to updating the IDF curves considering climate impacts (Nguyen et al., 2007, 2008; Vu et al., 2016; Herath et al., 2016).

Compared to the raw statistical moments (also known as conventional moments or ordinary moments), the applications of the probability weighted moments (PWMs) and its linear combination forms (L-moments) to assess rainfall scaling processes have been found very limited in literature (Kumar et al., 1994; Yu et al., 2004; Bairwa et al., 2016). The PWMs, however, have been generally known to be more robust and against outliers when applying to small size samples which are quite common for the study of extreme hydrologic variables (Greenwood et al., 1979; Hosking and Wallis, 1997). In particular, Kumar et al. (1994) have indicated the scale-invariance properties of rainfalls over different durations based on the empirical estimates of the more robust PWMs. The use of PWMs for assessing the simple scaling behaviour of rainfall processes was further examined at a regional scale using rainfall series from Taiwan in a study by Yu et al. (2004), in which the PWMs clearly exhibited the scale-invariance behaviour over different rainfall durations and the scaling exponents can be used for the delineation of the study area into different homogeneous regions. Furthermore, the scaling GUM/PWM distribution was used in this study for constructing the regional IDF curves. A similar approach based on the GUM/PWM was also used for deriving the IDF curves by Bairwa et al. (2016) using rainfall data in India.

In summary, based on the best of our knowledge from this literature review, no study has been able to provide a general theoretical framework for assessing the scale-invariance properties of extreme rainfall processes using the GEV model and the PWMs. In addition, no previous work has developed a generalized mathematical framework for describing the scaling properties of the

GEV distribution for different statistical moment categories. Furthermore, most previous studies investigated the scaling behaviour of extreme rainfall processes using only limited available IDF data and for a limited number of existing raingage stations.

In view of the above-mentioned issues, the present study proposes a novel PWM-based scaling GEV distribution model (hereafter referred to as the GEV/PWM model) for modeling extreme rainfall processes over a wide range of temporal scales (i.e., from several minutes to one day). An extensive set of long records of IDF data from a network of 74 stations located across Canada were used in this study to assess the performance of the proposed model as well as to compare with other existing scaling models. The study sites and data are described in Section 3.2. The mathematical frameworks and scaling properties of the GEV distribution model based on both NCM and PWM systems are provided in Section 3.3. The feasibility and accuracy of the GEV/PWM model was assessed and compared with the three existing popular models (GEV/NCM, GUM/NCM, and GUM/PWM models) in Section 3.4. Research findings and conclusions are provided in Section 3.5.

3.2 Study Sites and Data

In Canada, rainfall data are collected by Environment Canada, provincial and territorial ministries, municipalities, and other organizations. They are collected through a variety of measuring devices and to a variety of standards. Environment Canada's networks and individual monitoring stations are generally designed, located, and operated in accordance with the two WMO guidelines: the guide to Meteorological Instruments and Methods of Observations (WMO, 2008) and the Guide to Hydrological Practices (WMO, 2009a). In addition, before data are added to the archive, Environment Canada conducts further automated and manual quality control checks to mainly verify that the collected values are within realistic physical limits and that there is internal consistency amongst all the amounts abstracted from the daily chart. Environment Canada currently provides observed short-duration extreme rainfall series of nine different rainfall durations ranging from 5 minutes to 1440 minutes (i.e., 24 hours) and their statistics as well as extreme rainfall quantiles (using the Gumbel distribution model) for 596 locations across Canada in electronic file formats (Environment Canada, 2019). These statistics and values are primarily used for the designs of various hydraulic structures, especially in urban areas such as road culverts, and municipal storm sewer and drainage systems.

Among approximately 600 stations across Canada, a total of 74 stations with an adequate record length of at least 40 years were selected for this study. These stations are located in different regions from the west to the east coast and from the north to the south representing the diverse climatic conditions of Canada. To ensure the quality of the selected data, only the data from the recording raingages under the management of the Atmospheric Environmental Service of Environment Canada were used. Furthermore, the data at these stations are available for all nine durations and must successfully pass three statistical tests for independence, homogeneity, and stationarity at the 5% significant level. These tests include the Mann-Whitney test for homogeneity and stationarity (jumps), the Mann–Kendall test for trend detection, and the Wald-Wolfowitz test for independence and stationarity (Rao and Hamed, 2000; WMO, 2009a). The test results are shown in the Appendix B. The station information and locations are presented in Table 3-1 and Figure 3-1.

Table 3-1. Details of the 74 study stations used in this research, including territory and province (TP), identification number (ID), station name, latitude (Lat, degree), longitude (Lon, degree), elevation (Elev, meter), record year (Year), and record length (RCL, year)

No	TP	ID	Station name	Lat	Lon	Elev	Year	RCL
1	YT	2101310	Whitehorse Auto	60.73	135.10	707	1960-2016	44
2	NT	2202102	Fort Simpson Climate	61.77	121.23	168	1969-2017	42
3	BC	1018611	Victoria Gonzales CS	48.42	123.32	61	1925-2017	65
4	BC	1018621	Victoria Intl A	48.65	123.43	19	1965-2017	50
5	BC	1021830	Comox A	49.72	124.90	25	1963-2006	40
6	BC	1038205	Tofino A	49.08	125.77	24	1970-2017	45
7	BC	1068131	Terrace PCC	54.50	128.62	67	1968-2017	47
8	BC	1096450	Prince George A	53.88	122.68	691	1960-2002	41
9	BC	1105192	Mission West Abbey	49.15	122.27	197	1963-2017	54
10	BC	1106180	Pitt Polder	49.27	122.63	5	1965-2007	40
11	BC	1108395	Vancouver Intl A	49.18	123.18	4	1953-2017	63
12	BC	1126150	Penticton A	49.47	119.60	344	1953-2002	45
13	BC	1166R45	Salmon Arm A	50.68	119.23	527	1964-2016	44
14	BC	1160899	Blue River A	52.13	119.28	690	1970-2016	44
15	AB	3012206	Edmonton Intl CS	53.32	113.62	715	1961-2017	52
16	AB	3012209	Edmonton Blatchford	53.57	113.52	671	1914-2015	69
17	AB	3025481	Red Deer Regional A	52.18	113.88	904	1959-2014	49
18	AB	3031094	Calgary Int L CS	51.12	114.00	1081	1947-2015	61
19	AB	3033890	Lethbridge CDA	49.70	112.77	910	1960-2017	47
20	AB	3034485	Medicine Hat RCS	50.03	110.72	715	1971-2017	42
21	AB	3081680	Cold Lake A	54.42	110.28	541	1966-2017	49
22	SK	401HP5R	Weyburn	49.70	103.80	588	1962-2017	43
23	SK	4012410	Estevan	49.22	102.97	580	1964-2016	52
24	SK	4015322	Moose Jaw CS	50.33	105.53	577	1960-2014	49
25	SK	4016560	Regina Int L A	50.43	104.67	577	1941-1995	52
26	SK	4043901	Kindersley A	51.52	109.18	693	1966-2016	50
27	SK	4057165	Saskatoon RCS	52.17	106.72	504	1960-2017	40
28	SK	4060983	Buffalo Narrows (AUT)	55.83	108.42	440	1968-2017	41
29	MB	5012324	Portage Southport	49.90	98.28	272	1964-2017	40
30	MB	502S001	Winnipeg A CS	49.92	97.25	238	1944-2016	57
31	MB	5040681	Dauphin CS	51.10	100.07	304	1954-2016	40
32	MB	5050919	Flin Flon	54.68	101.68	303	1970-2017	42
33	MB	5062921	Thompson A	55.80	97.87	224	1971-2017	43
34	ON	6012199	Ear Falls (AUT)	50.63	93.22	362	1952-2007	50
35	ON	6016525	Pickle Lake (AUT)	51.45	90.22	390	1953-2007	42
36	ON	6034073	Kenora RCS	49.78	94.38	412	1966-2011	44
37	ON	6037775	Sioux Lookout A	50.12	91.90	383	1963-2007	40
38	ON	6042716	Geraldton A	49.78	86.93	348	1952-2007	50
39	ON	6048268	Thunder Bay CS	48.37	89.33	199	1952-2012	53
40	ON	6057592	Sault Ste Marie A	46.48	84.52	192	1962-2007	46

No	TP	ID	Station name	Lat	Lon	Elev	Year	RCL
41	ON	6073980	Kapuskasing CDA ON	49.42	82.43	218	1966-2013	42
42	ON	6078285	Timmins V. Power A	48.57	81.38	294	1952-2007	48
43	ON	6085700	North Bay A	46.37	79.42	370	1964-2006	41
44	ON	6104175	Kingston Pumping Stn	44.23	76.48	76	1914-2007	63
45	ON	6105978	Ottawa CDA RCS	45.38	75.72	79	1905-2011	54
46	ON	6127519	Sarnia Climate	43.00	82.30	181	1962-2016	49
47	ON	6131415	Chatham WPCP	42.38	82.22	180	1966-2007	40
48	ON	6131983	Delhi CS	42.87	80.55	231	1962-2015	50
49	ON	6137362	St Thomas WPCP	42.77	81.22	209	1926-2007	75
50	ON	6139525	Windsor A	42.28	82.97	189	1946-2007	60
51	ON	6143089	Guelph Turfgrass	43.55	80.22	325	1954-2017	52
52	ON	6144478	London CS	43.03	81.15	278	1943-2016	65
53	ON	6153301	Hamilton RBG CS	43.28	79.92	102	1962-2016	52
54	ON	6158355	Toronto City	43.67	79.40	112	1940-2017	67
55	ON	6158731	Toronto Intl A	43.68	79.63	173	1950-2017	64
56	ON	6158875	Trenton A	44.12	77.53	86	1965-2017	46
57	QC	701S001	QC Jean Lesage Intl	46.80	71.38	60	1961-2015	46
58	QC	7014160	L Assomption	45.82	73.43	21	1963-2017	45
59	QC	7018001	Shawinigan	46.57	72.73	110	1968-2017	41
60	QC	702S006	Montreal P.E.T. Intl	45.47	73.73	32	1943-2014	61
61	QC	7024280	Lennoxville	45.37	71.82	181	1960-2017	45
62	QC	7060400	Bagotville A	48.33	71.00	159	1961-2017	45
63	NB	8100885	Charlo Auto	47.98	66.33	42	1959-2013	51
64	NB	8101605	Fredericton CDA CS	45.92	66.62	35	1959-2015	47
65	NB	8103201	Moncton Intl A	46.12	64.68	70	1946-2016	67
66	NB	8104900	Saint John A	45.32	65.88	108	1958-2002	40
67	NS	8202000	Greenwood A	44.98	64.92	28	1964-2016	44
68	NS	8204700	Sable Island	43.93	60.02	5	1962-2013	51
69	NS	8205092	Shearwater RCS	44.63	63.52	24	1955-2016	59
70	NS	8205702	Sydney CS	46.17	60.03	62	1961-2016	53
71	NS	8206495	Yarmouth A	43.83	66.08	42	1971-2016	43
72	NF	8401705	Gander Airport CS	48.95	54.57	151	1939-2017	70
73	NF	8403820	Stephenville RCS	48.57	58.57	58	1967-2017	48
74	NF	8501900	Goose A	53.32	60.42	48	1961-2016	53

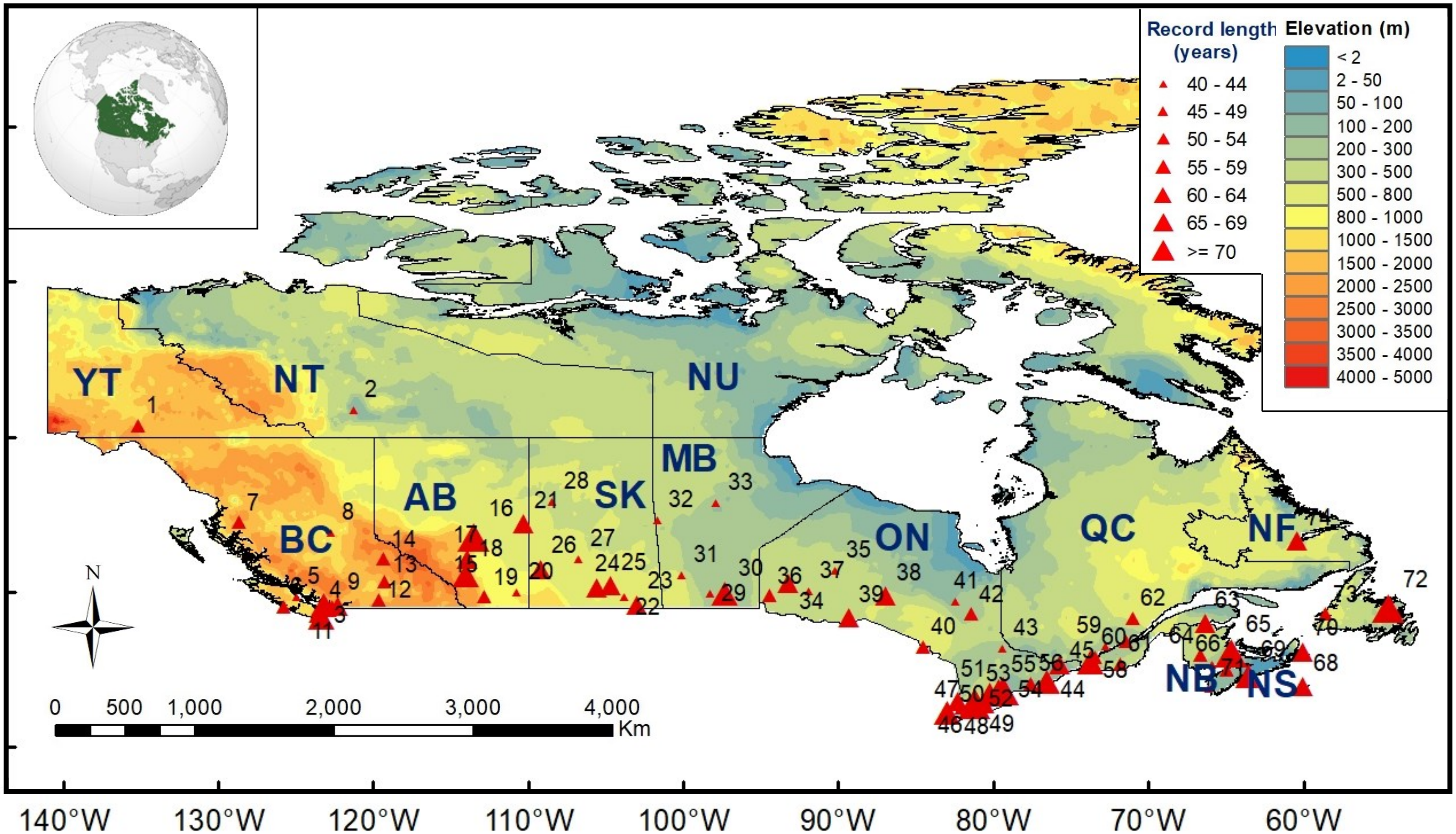

Figure 3-1. Locations and record lengths of the 74 selected raingages. The digital elevation model is generated based on data from the Government of Canada (2018). Territorial names: YT = Yukon, NT = Northwest Territories, NU = Nunavut. Provincial names: BC = British Columbia, AB = Alberta, SK = Saskatchewan, MB = Manitoba, ON = Ontario, QC = Quebec, NB = New Brunswick, NS = Nova Scotia, PE = Prince Edward Island, and NF = Newfoundland and Labrador

Table 3-2 provides some basic statistics of the 666 time series of annual maximum rainfalls for all nine selected rainfall durations and for all selected 74 stations. These basic statistics include the maximum rainfall amount, the mean, the standard deviation, and the skewness coefficient. In addition, three values were computed for each statistic to represent the range of variability from the minimum value to the mean and to the maximum value. Due to the space constraint, only the analysis of the maximum rainfall statistic was described in depth in this chapter (see, e.g., Figure 3-2). For the other statistics (i.e., the standard deviation and the skewness), similar analyses could be carried out to obtain a representative picture of the variability of extreme rainfall statistics across Canada.

Table 3-2. Sample statistics of AMS data for 74 selected stations. (Note: the three values given in each column represent the interval starting from the minimum to the mean to the maximum)

Dur	Max (mm)	Mean (mm)	SD (mm)	Cv	Skewness
5-min	5 – 16 – 31	2 – 7 – 10	1 – 3 – 5	0.3 – 0.4 – 0.7	0.0 – 1.2 – 3.0
10-min	7 – 22 – 43	3 – 10 – 15	1 – 4 – 7	0.3 – 0.4 – 0.6	0.2 – 1.1 – 2.9
15-min	8 – 28 – 57	4 – 12 – 18	1 – 5 – 9	0.3 – 0.4 – 0.6	0.3 – 1.2 – 3.4
30-min	10 – 37 – 83	5 – 16 – 24	2 – 6 – 13	0.2 – 0.4 – 0.7	-0.2 – 1.3 – 3.5
1-hour	15 – 48 – 87	6 – 19 – 29	2 – 8 – 14	0.2 – 0.4 – 0.8	0.4 – 1.5 – 3.4
2-hour	21 – 59 – 114	9 – 24 – 36	4 – 10 – 20	0.2 – 0.4 – 0.7	0.5 – 1.6 – 4.6
6-hour	31 – 78 – 149	13 – 35 – 64	4 – 12 – 25	0.2 – 0.4 – 0.6	0.1 – 1.5 – 3.8
12-hour	43 – 91 – 162	17 – 43 – 94	6 – 15 – 29	0.2 – 0.3 – 0.5	0.4 – 1.3 – 2.9
24-hour	48 – 112 – 228	21 – 52 – 133	7 – 18 – 31	0.2 – 0.4 – 0.6	0.2 – 1.3 – 3.0

Based on Figure 3-2, it can be easily seen that the largest extreme storms of different rainfall durations happened in different parts of Canada. Firstly, the largest extreme storms of rainfall durations equal to or longer than 12 hours occurred in both the British Columbia Coast and the Maritime Provinces. In particular, the Tofino Airport station, located in British Columbia province, recorded the largest value of the 24-hour storm event of 228 mm, while the Sydney CS station, located in Nova Scotia province, observed the largest value of the 12-hour storm event of 162 mm. The heavy storms of 6-hour duration (i.e., 125 mm) and 24-hour duration (i.e., 161 mm) with rainfall depths greater than or equal to the 95 percentiles were also measured in Saint John Airport station in New Brunswick. Secondly, the largest extreme storms of rainfall duration equal to or less than 1 hour happened in the Prairies of Canada. In particular, the Regina International Airport station, located in Saskatchewan, recorded the largest values of 31 mm, 43 mm, and 57 mm for 5-minute, 10-minute, and 15-minute durations, respectively, while the largest values for 30-minute and 60-minute durations (83 mm and 87 mm) were observed at the Dauphin CS station in Manitoba. The heavy storm events with rainfall depths greater than or equal to the 95 percentiles were also observed in Lethbridge CDA station in Alberta. Finally, the largest extreme storms of rainfall duration between 1 hour and 12 hours are mostly observed in Ontario. In particular, the Kenora RCS station recorded the largest values of 114 mm and 149 mm for the 2-hour and 6-hour storms, respectively.

A preliminary analysis using the L-moment ratio diagram was carried out to identify the potential candidate distributions for extreme rainfalls in the study area as shown in Figure 3-3 for all computed values of L-skewness, τ_3, and L-kurtosis, τ_4, from all 666 AMS data for nine different rainfall durations (from 5 minutes to 1440 minutes) and for all 74 stations. In other words, there are nine groups of data representing nine different rainfall durations, and each group contains 74 pairs for the 74 selected stations. These groups are plotted on the L-moment ratio diagram using different colors and markers, including also the mean value of each group.

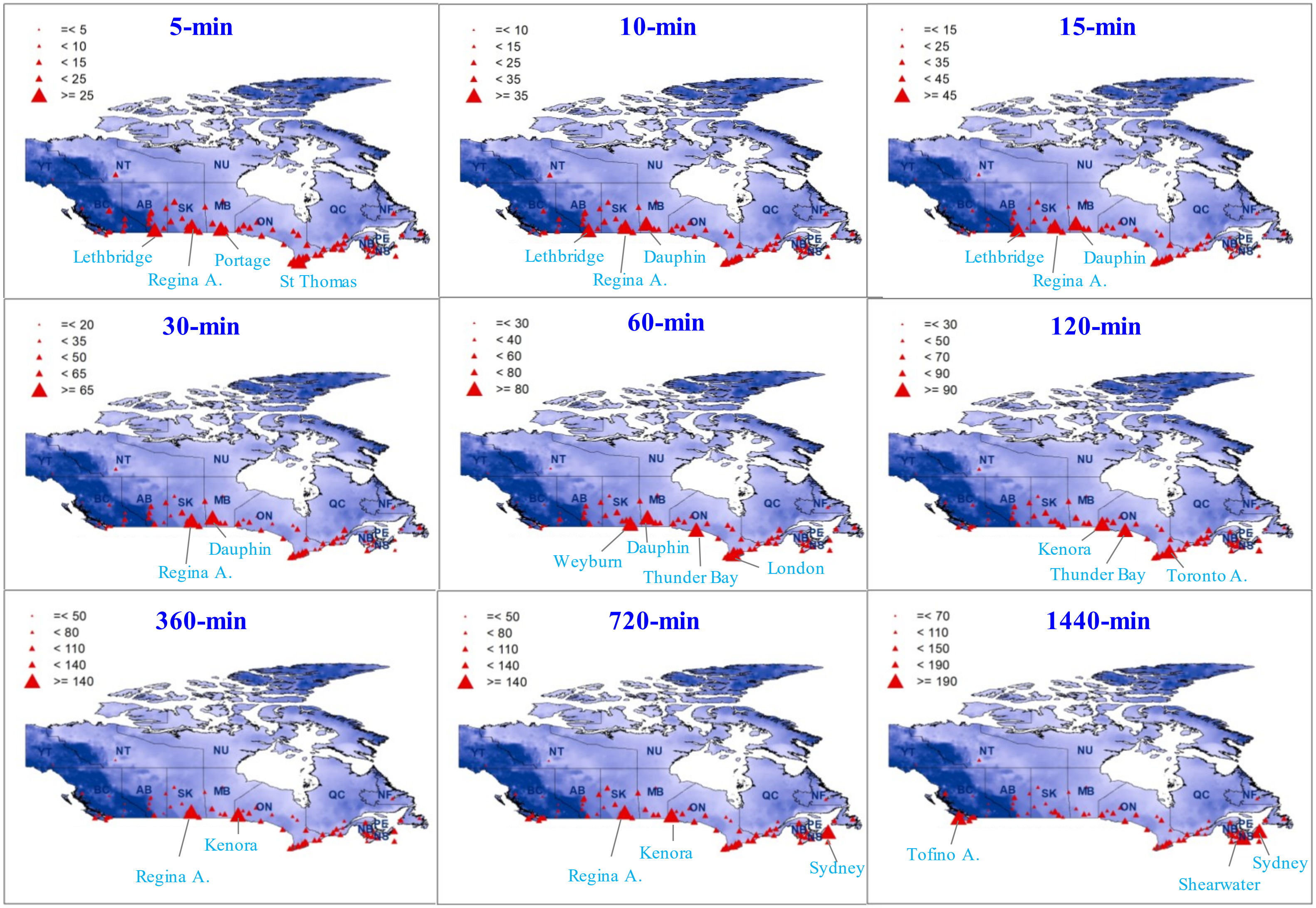

Figure 3-2. Spatial representation of the maximum rainfall values of different rainfall durations for 74 selected stations across Canada

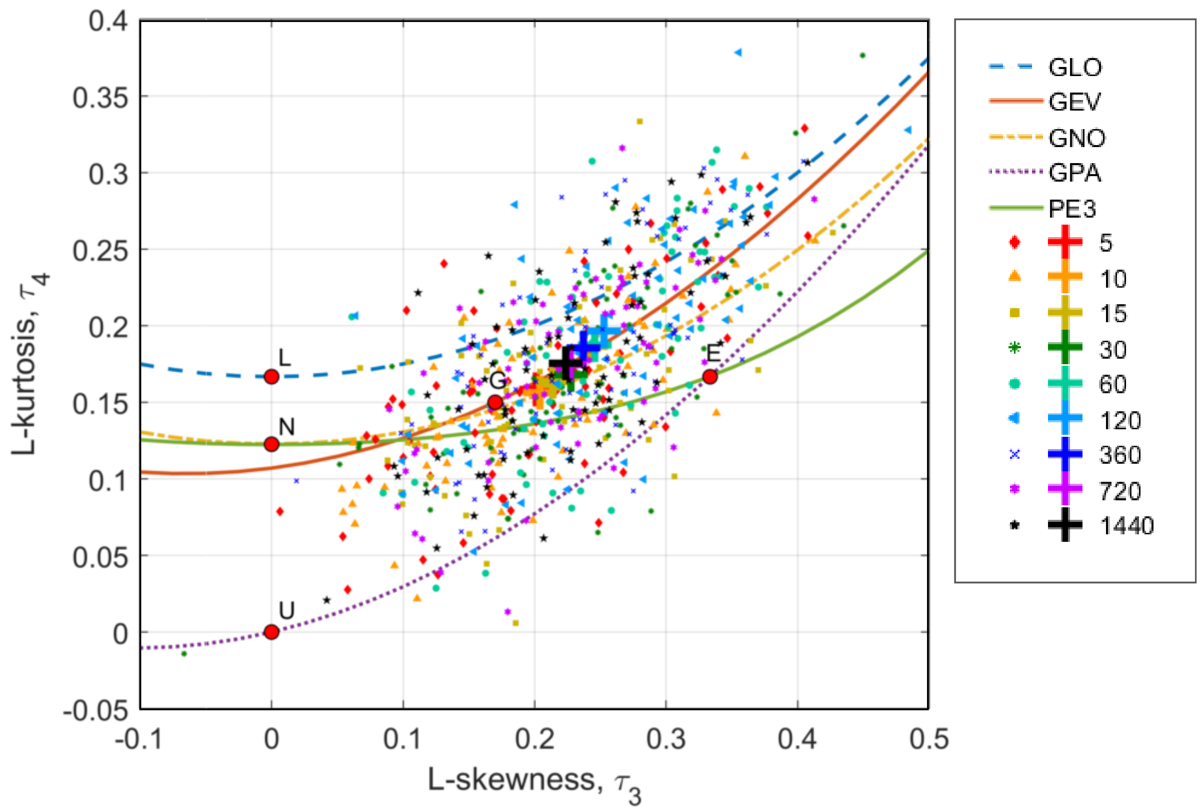

Figure 3-3. L-moment ratio diagram of 666 annual maximum rainfall series for nine groups representing nine different rainfall durations from 5 minutes to 1440 minutes. Each group contains 74 points for the 74 selected stations. The average value of each group is also plotted with a big '+' sign with the same color. Three-parameter distributions (represented as lines): GLO = generalized logistic, GEV = generalized extreme values, GNO = generalized normal (or three-parameter log-normal), GPA = generalized pareto, PE3 = Pearson type III. Two-parameter distributions (represented as red circle markers): L = logistic, N = normal, U = uniform, G = Gumbel, E = exponential

The wide spread of data points for each group of data for the same rainfall duration as well as for all nine groups of different durations on the L-diagram has indicated that no particular distribution can be selected as the best distribution to represent all these extreme rainfall data. However, it can be observed that the average values of all nine groups were located close to the Generalized Extreme Value (GEV) distribution than any other distributions. Beside this, the L-diagram also shows that the Generalized Normal (GNO) distribution is also a good candidate for all these extreme rainfall series, especially, for rainfall durations less than 1 hour or more than 6 hours. Furthermore, the large dispersion of data points on the L-moment ratio diagram as obtained in this study have also indicated the major limitation of this popular L-diagram approach for identifying the best distributions for extreme rainfalls for a given region due to the high spatial variability of extreme rainfalls at different locations as observed in this study region. The proposed method for selecting the best distributions for extreme rainfalls as described in Chapter 2 could be the preferred approach to the L-moment ration diagram. However, as indicated above the GEV was found to be a reasonable probability model for describing the distributions of extreme rainfalls for the selected AMS datasets as indicated by the L-moment ration diagram as well as by the selection approach proposed in Chapter 2. The GEV distribution was hence selected for further development to account for the scaling properties of the underlying extreme rainfall processes as presented in Section 3.3.

3.3 Methodology

3.3.1 The Generalized Extreme Values (GEV) distribution

On the theoretical basis of extreme value theory, the GEV distribution has been recognized as being the most appropriate distribution for representing the distribution of the extremes of random variables (Coles, 2001; Katz et al., 2002; Smith, 2003). Hence, this distribution has been widely used for describing the probability distribution of annual rainfall maxima and for constructing the rainfall IDF relations as recommended in a number of technical guidelines for hydrological practices by the World Meteorological Organization (WMO, 2009a) as well as by many other countries such as Australia, Austria, Germany, Italy, and Spain (Salinas et al., 2014; Ball et al., 2016; Nguyen et al., 2017, 2019). The cumulative distribution function (CDF), $F(x)$, of the GEV distribution is given as follows:

$$F(x) = exp\left[-\left(1-\frac{\kappa(x-\xi)}{\alpha}\right)^{\frac{1}{\kappa}}\right] \quad ; \quad (\kappa \neq 0) \qquad (3\text{-}1)$$

in which $\xi, \alpha,$ and κ are the location, scale, and shape parameters, respectively.

The quantile, X_T, corresponding to certain return periods, $T = \frac{1}{1-F(x)}$, can be obtained using the following expression:

$$X_T = \xi + \frac{\alpha}{\kappa}\{1 - [-\ln(F(x))]^{\kappa}\} \qquad (3\text{-}2)$$

where $F(x)$ is the cumulative probability of interest.

For the particular case when the shape parameter $\kappa = 0$, the GEV distribution becomes the two-parameter Gumbel distribution with the CDF and quantile function as follows:

$$F(x) = \exp\left[-exp\left(-\frac{x-\xi}{\alpha}\right)\right] \quad ; \quad (\kappa = 0) \qquad (3\text{-}3)$$

$$X_T = \xi - \alpha \cdot \ln(-\ln F) \qquad (3\text{-}4)$$

Based on Eqn. (3-2), if the three parameters of the GEV distribution are known, then extreme rainfall quantiles can be easily computed. Since daily extreme rainfall data are widely available for many locations, estimation of these parameters for the distribution of daily extreme rainfalls and the coresponding design daily rainfall quantiles are thus straightforward. However, for sub-daily rainfall durations, data are commonly unavailable, hence the estimation of these parameters from the missing data is impossible. Therefore, to deal with this difficult missing data issue, it is necessary to examine the scale-invariance behaviour of the extreme rainfall processes in order to be able to establish some relationships between the daily and sub-daily statistical properties of these processes as described in the folowing sections. Firstly, Section 3.3.2 presents the details regarding the scaling GEV/NCM model based on the NCMs of extreme rainfalls as suggested in the previous work by Nguyen et al. (1998); and secondly, Section 3.3.3 introduces a new scaling GEV/PWM model based on the probability weighted moments (PWMs).

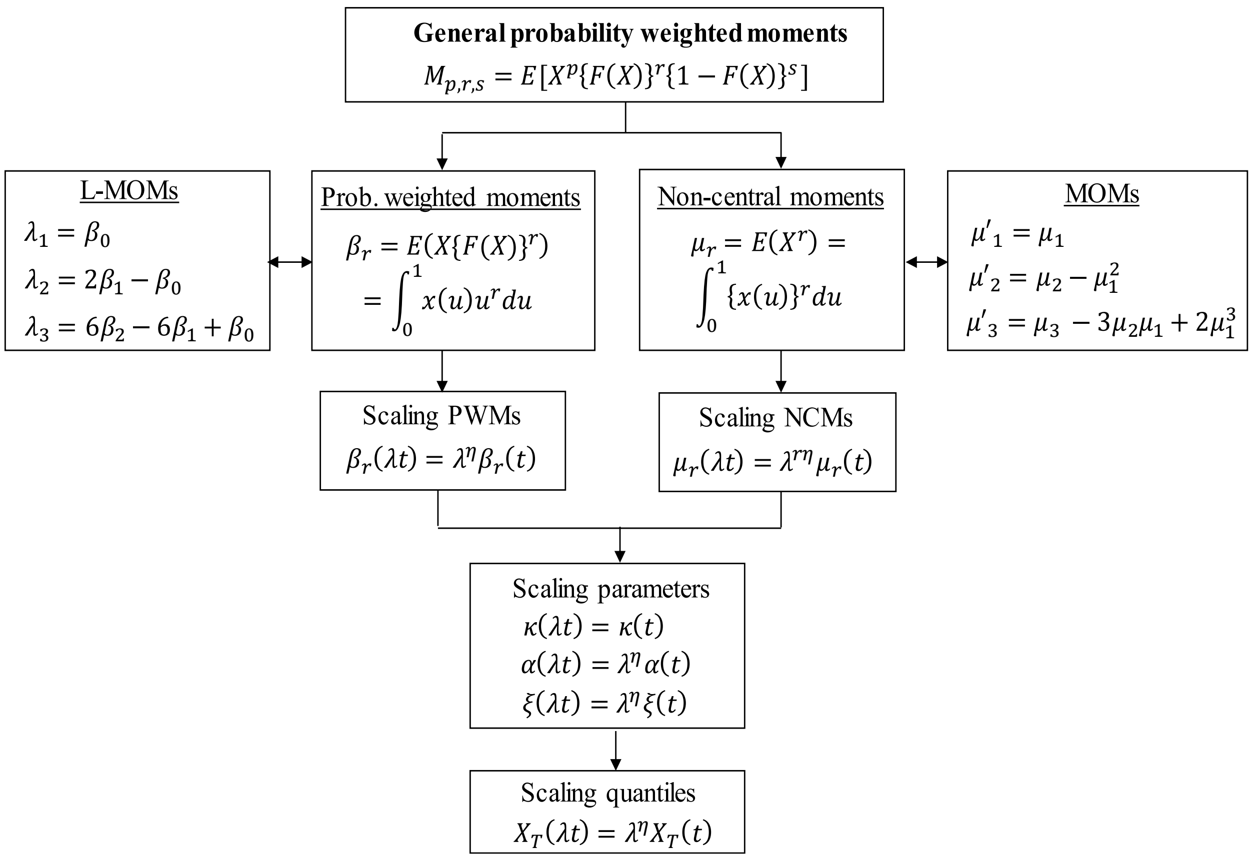

Figure 3-4. Mathematical frameworks and scaling properties of the GEV distribution based on the PWMs and the NCMs

It is necessary to note that both the PWMs and NCMs are particular cases of the general PWMs depending upon whether the weight is placed on the data *X* or on its probability *F(X)* (see Figure 3-4). Hence, the scaling exponents, η, are determined by two different mathematical expressions using these two different categories of statistical moments. For the NCM category, the scaling exponents of the higher-order NCMs are expected to be approximately equal to a multiple of the exponent of the first-order moment (i.e., the mean); while for the PWM catregory, the scaling exponents of the higher-order PWMs are approximately constant for all higher orders and equal to the exponent of the zero-order PWM (i.e. the mean). Note that if the scaling exponents are a linear function of the statistical moment orders, then in such cases the process is said to be simple scaling. Otherwise, the process is said to be multiscaling. Nevertheless, the scaling properties of the GEV parameters, which are computed using these two different NCM and PWM methods, are expected to be the same as described in detail in the following sections.

3.3.2 A NCM-based scaling GEV model

3.3.2.1 Scaling properties

The non-central moment (NCM) method (similar to the popular method of moment, MOM) can be used for estimating the GEV parameters and can also account for the scaling property of the extreme rainfall process over different rainfall durations.

For a distribution of a random variable X with a probability density function $f(x)$ and a cumulative distribution function $F(x)$, the r^{th}-order non-central moment (NCM) is given by:

$$\mu_r = \mathrm{E}(\mathrm{X}^\mathrm{r}) = \int_{-\infty}^{+\infty} x^r f(x)dx = \int_{-\infty}^{\infty} x^r dF(x) \tag{3-5}$$

Applying the transformation $u = F(x)$ and provided that the integral in the Eqn. (3-5) exists, the r^{th}-order NCM, μ_r, can be expressed as in Eqn. (3-6) (Hosking and Wallis, 1997):

$$\mu_r = \mathrm{E}(\mathrm{X}^\mathrm{r}) = \int_{0}^{1} \{x(u)\}^r du \tag{3-6}$$

where $0 < u < 1$ and $x(u)$ is a unique value satisfying $F(x(u)) = u$.

The NCMs of r^{th}-order, μ_r, of the GEV distribution are given by Nguyen et al. (2002b):

$$\mu_r = \left(\xi + \frac{\alpha}{\kappa}\right)^r + (-1)^r \left(\frac{\alpha}{\kappa}\right)^r \Gamma(1 + r\kappa) + r \sum_{i=1}^{r-1} (-1)^i \left(\frac{\alpha}{\kappa}\right)^i \left(\xi + \frac{\alpha}{\kappa}\right)^{r-\mathrm{i}} \Gamma(1 + i\kappa) \tag{3-7}$$

in which $\Gamma(.)$ is the gamma function.

For a simple scaling process, it can be shown that the NCMs of two different time scales, t and (λt), are related as follows (Nguyen et al., 2002b):

$$\mu_r(\lambda t) = \lambda^{\eta_r} \mu_r(t) = \lambda^{r\eta} \mu_r(t) \tag{3-8}$$

where $\eta_r = r\eta$, and $\eta = \eta_1$ is the scaling exponent of the NCM order $r = 1$ (i.e. the mean) and λ is the scaling ratio.

Furthermore, let $g(t)$ and $g(\lambda t)$ denote the skewness of the data samples for two different time scales t and (λt) respectively. The skewness is the dimensionless version of the third order moment. It is obtained by dividing the third-order moment by the second-order moment. Hence, for a simple scaling process it can be shown that:

$$\begin{aligned} g(\lambda t) &= \frac{[\mu_3(\lambda t) - 3\mu_2(\lambda t)\mu_1(\lambda t) + 2\mu_1^3(\lambda t)]}{[\mu_2(\lambda t) - \mu_1^2(\lambda t)]^{\frac{3}{2}}} = \frac{\lambda^{3\eta}}{\lambda^{3\eta}} \frac{[\mu_3(t) - 3\mu_2(t)\mu_1(t) + 2\mu_1^3(t)]}{[\mu_2(t) - \mu_1^2(t)]^{\frac{3}{2}}} \\ &= g(t) \end{aligned} \tag{3-9}$$

Equation (3-9) indicates that the skewness is constant over different time scales. Consequently, for the simple scaling process, the shape parameter of the GEV distribution κ, which is a function of the skewness, is also constant over the time scale, that is,

$$\kappa(\lambda t) = \kappa(t) \tag{3-10}$$

From Eqn. (3-7) and after some mathematical manipulations, the first- and second-order NCMs can be written as follows:

$$\mu_1 = \xi + \frac{\alpha}{\kappa}\{1 - \Gamma(1+\kappa)\} \tag{3-11}$$

$$\mu_2 = \mu_1^2 + \left[\frac{\alpha}{\kappa}\right]^2 [\Gamma(1+2k) - \Gamma^2(1+k)] \tag{3-12}$$

On the basis of Eqns. (3-8), (3-10)-(3-12) the location and scale parameters of the GEV distribution for different time scales can be related as follows:

$$\alpha(\lambda t) = \lambda^{\eta}\alpha(t) \tag{3-13}$$

$$\xi(\lambda t) = \lambda^{\eta}\xi(t) \tag{3-14}$$

and the quantiles for different time scales can also be expressed as:

$$X_T(\lambda t) = \lambda^{\eta} X_T(t) \tag{3-15}$$

Hence, on the basis of these equations, for the same scaling regime, it is possible to derive the distributions and the quantiles of sub-daily AMSs from those of the daily AMS as presented in the next Section.

3.3.2.2 Quantile estimates

For estimating sub-daily extreme rainfall quantiles, Figure 3-4 indicates that there are two methods: the direct and indirect methods.

The direct method derives the quantiles for rainfall duration (λt) from those for duration t directly using Eqn. (3-15). Therefore, the parameters of the distributions of sub-daily rainfalls are not required by this direct method. However, if necessary, the GEV parameters can be estimated using all three equations (3-10), (3-13), and (3-14). Then, the extreme rainfall quantiles can be computed using Eqn. (3-2). The results are exactly identical to those given by the direct method using the quantile scaling Eqn. (3-14). Note that from Eqn. (3-8), with $r = 1$, it can be easily shown that λ^{η} equals the ratio between the mean of sub-daily AMS and the mean of daily AMS.

For the indirect method, the first three NCMs of sub-daily AMSs are computed from those of the daily AMS based on the scaling relationships of NCMs over different rainfall durations (see Figure 3-5a, for example). Once the three NCMs are known, Eqn. (3-7) is then used for estimating the three GEV parameters based on the first-, second-, and third-order NCMs. Substitute these estimated parameters back into the quantile function to obtain the extreme rainfall quantiles or the distributions of the sub-daily AMSs.

The direct and indirect methods can be therefore thought as the simple scaling and multi scaling method, respectively. They can also be referred to as one-moment-based and three-moment-based scaling methods, respectively. Nguyen (2003) compared the two approaches in estimating 5-min and 1-hour AMS from 1-day AMS using data from 88 raingauges located in Quebec. His work showed that the three-moment-based method performed better than the one-moment method since it can extract more information from the observed data.

3.3.2.3 A special case

For the special case when the shape parameter $\kappa = 0$, the scaling relationships between the scaling parameters (or location parameters) of the sub-daily and daily AMSs indicated by Eqn. (3-13) or (3-14) continue to hold true. The quantile scaling relationship provided by Eqn. (3-15) also holds true. These properties are referred to as the scaling properties of the GUM distribution model (a special case of the GEV model with $\kappa = 0$) based on the NCMs as described in the work by Menabde et al. (1999).

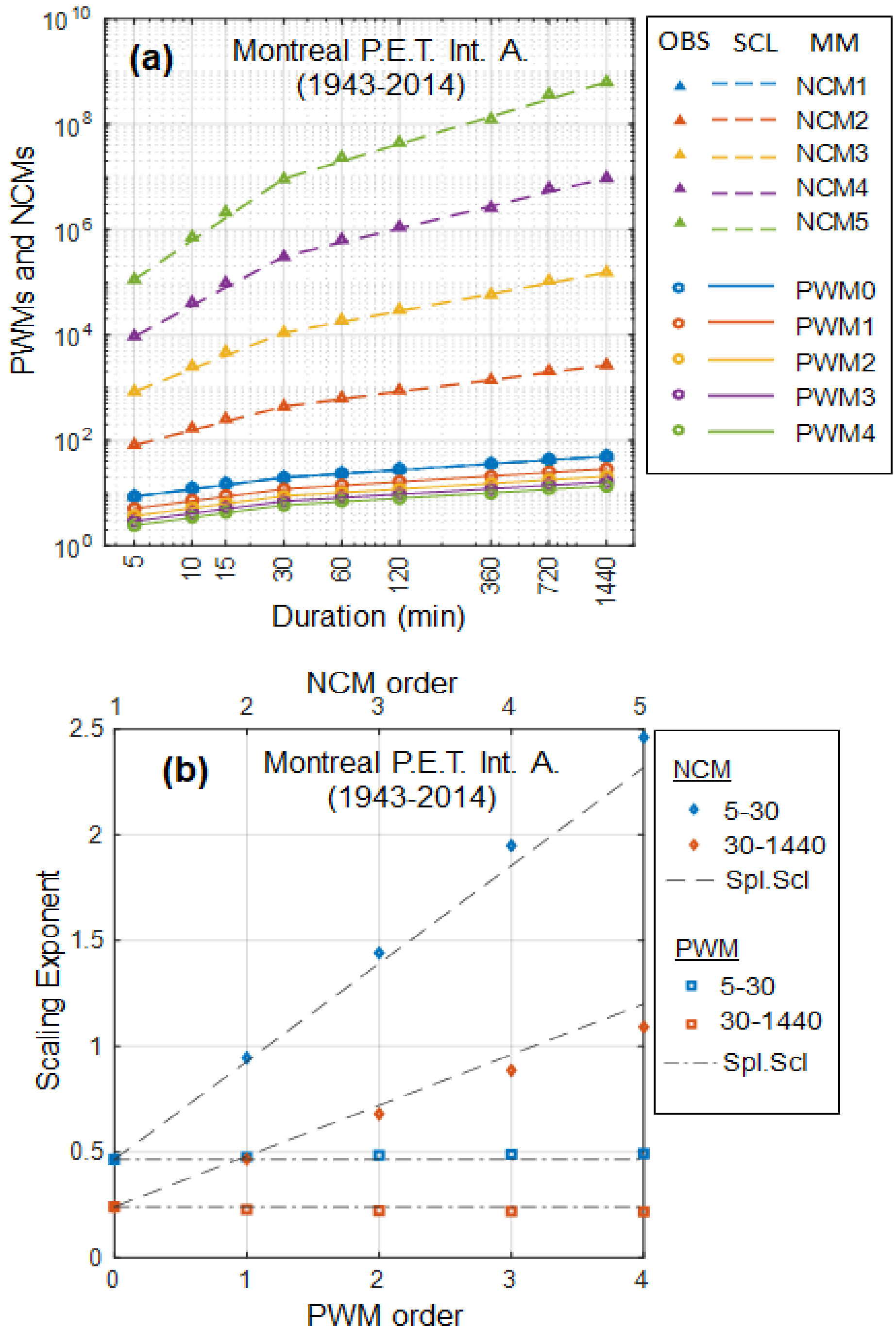

Figure 3-5. (a) Log-log plot of the first five NCMs (triangle markers) and PWMs (circle markers) over different rainfall durations (D = 5 to 1440 minutes). The dash and continuous lines show the regression models for the NCM and PWM systems: the first scaling regime from 1440 to 30 minutes and the second scaling regime from 30 to 5 minute; (b) Plot of the scaling exponents estimated based on NCMs (diamond markers) and PWMs (square markers). The dash and discontinuous lines show the theoretical simple scaling exponents for the NCMs and PWMs

3.3.3 A novel PWM-based scaling GEV model

3.3.3.1 Scaling properties

The probability weighted moment (PWM) method (or method of L-moment, L-MOM) can be used for estimating the GEV parameters in consideration of the scaling property of the extreme rainfall processes over different rainfall durations. For a distribution of a random variable X that has a quantile function, $x(u)$, the PWM of r^{th}-order can be expressed as (Hosking and Wallis, 1997):

$$\beta_r = \mathrm{E}(\mathrm{X}\{F(X)\}^r) = \int_0^1 x(u)u^r du \tag{3-16}$$

The PWMs of r^{th}-order, β_r, of the GEV distribution are given by Hosking et al. (1985):

$$\beta_r = M_{1,r,0} = E[X\,\{F(X)\}^r] = (r+1)^{-1}\left(\xi + \frac{\alpha}{\kappa}\{1-(r+1)^{-\kappa}\,\Gamma(1+\kappa)\}\right) \tag{3-17}$$

in which $\xi, \alpha,$ and κ are the location, scale, and shape parameters respectively; $F(X)$ is the cumulative probability of interest, $\Gamma(.)$ is the gamma function, and r must be non-negative.

For a simple scaling process, it can be shown that the relation between the r^{th}-order PWMs of rainfalls for two different rainfall durations t and (λt) can be expressed as:

$$\beta_r(\lambda t) = \lambda^{\eta_r}\beta_r(t) = \lambda^{\eta}\beta_r(t) \tag{3-18}$$

where $\eta_r = \eta_0$ is the scaling exponent and can be estimated based on the means, $E\{X\}$, (that is, the PWM of order $r = 0$) of different rainfall durations.

This infers that the scaling exponents η_r are constant for all PWM orders r within the same rainfall scaling regime. In other words, the plot of the scaling exponents η_r (y-axis) with the PWM order r (x-axis) should display a horizontal line rather than a linear sloping line as for the case of the NCMs (Nguyen et al., 2002b).

Furthermore, let $\tau_3(t)$ and $\tau_3(\lambda t)$ denote the L-skewness of the data samples for two different time scales t and λt respectively (Hosking, 1990). L-skewness is the dimensionless version of the third order L-moment. It is obtained by dividing the third-order L-moment by the second-order L-moment. Hence, for a simple scaling process it can be shown that:

$$\tau_3(\lambda t) = \frac{6\beta_2(\lambda t) - 6\beta_1(\lambda t) + \beta_0(\lambda t)}{2\beta_1(\lambda t) - \beta_0(\lambda t)} = \frac{\lambda^\eta}{\lambda^\eta}.\frac{[6\beta_2(t) - 6\beta_1(t) + \beta_0(t)]}{[2\beta_1(t) - \beta_0(t)]} = \tau_3(t) \tag{3-19}$$

Equation (3-19) indicates that the L-skewness is constant over different time scales. Consequently, for the simple scaling process, the shape parameter of the GEV distribution, κ, which is a function of the L-skewness, is also constant over the time scale, that is,

$$\kappa(\lambda t) = \kappa(t) \tag{3-20}$$

From Eqn. (3-17) and after some mathematical manipulations, the zero- and first-order PWMs can be written as follows:

$$\beta_0 = \xi + \frac{\alpha}{\kappa}\{1 - \Gamma(1+\kappa)\} \tag{3-21}$$

$$\beta_1 = \frac{1}{2}\left[\beta_0 + \frac{\alpha}{\kappa}(1 - 2^{-k})\Gamma(1+k)\right] \tag{3-22}$$

On the basis of Eqns. (3-18), (3-20)-(3-22) the location and scale parameters of the GEV distribution for different time scales can be related as follows:

$$\alpha(\lambda t) = \lambda^{\eta} \alpha(t) \tag{3-23}$$

$$\xi(\lambda t) = \lambda^{\eta} \xi(t) \tag{3-24}$$

and the quantiles for different time scales can also be expressed as:

$$X_T(\lambda t) = \lambda^{\eta} X_T(t) \tag{3-25}$$

In summary, based on these equations, for a simple scaling regime, it is possible to derive the distributions and statistical properties of short-duration extreme rainfalls from those of longer durations at a given study site as described in the following section.

3.3.3.2 Quantile estimates

Similar to the NCM-based scaling method, there are two different manners to estimate the sub-daily extreme rainfall quantiles from the daily ones: the direct and indirect methods. The direct method scales the rainfall quantiles for duration (λt) from those for duration t directly using Eqn. (3-25). Note that the daily extreme rainfall quantiles computed based on the two different PWM and NCM methods are not the same. Consequently, the scaled sub-daily extreme rainfall quantiles obtained by these two approaches are therefore different. Similarly, even though the parameter scaling relationships are identical for both NCM and PWM methods, the computed scaling parameters by these two estimation methods could be different. For the indirect method, the first three PWMs of sub-daily AMSs are first estimated using the scaling relationships of PWMs over different rainfall durations (see Figure 3-5a, for example). These three estimated PWMs are then utilized to solve for the three GEV parameters in order to compute the rainfall quantiles using Eqn. (3-17). Both methods are investigated and compared in Section 3.4.1.

3.3.3.3 Special case

For the special case when the shape parameter $\kappa = 0$, the scaling relationships between the scaling parameters (or location) of the sub-daily and daily AMSs as shown in Eqn. (3-23) (or (3-24) continue to hold true. The quantile scaling relationship provided in Eqn. (3-25) also holds true. These properties are referred to as the scaling properties of the GUM distribution model using the PWMs (a special case of the GEV/PWM model proposed in this study) as described in the work by Yu et al. (2004).

3.3.4 Model Comparison Criteria

In the present study, six common goodness-of-fit (GOF) criteria were selected for assessing the feasibility and accuracy of the proposed scaling model for estimating short-duration extreme design rainfalls at a local site in the context of climate change. These criteria include the root mean square error (RMSE), the root mean square relative error (RMSEr), the mean absolute deviation (MAD), the mean absolute relative deviation (MADr), the adjusted coefficient of determination (R^2_{adj}), and the correlation coefficient (CC).

$$RMSE = \left\{\sum \frac{(x_i - y_i)^2}{(n-m)}\right\}^{\frac{1}{2}} \tag{3-26}$$

$$RMSEr = \left[\frac{1}{(n-m)} \sum \left\{\frac{(x_i - y_i)}{x_i}\right\}^2\right]^{\frac{1}{2}} \tag{3-27}$$

$$MAD = \frac{1}{(\mathrm{n-m})} \sum |x_i - y_i| \tag{3-28}$$

$$MADr = \frac{1}{(\mathrm{n-m})} \sum \left\{\frac{|x_i - y_i|}{x_i}\right\} \tag{3-29}$$

$$R_{adj}^2 = 1 - \frac{(n-1)}{(n-m-1)} \times (1 - R^2) \tag{3-30}$$

$$CC = \frac{\sum\{(x_i - \bar{x})(y_i - \bar{y})\}}{\{\sum(x_i - \bar{x})^2 \sum(y_i - \bar{y})^2\}^{\frac{1}{2}}} = R \tag{3-31}$$

where $x_i, i = 1, 2, \ldots, n$ are the observed values and $y_i, i = 1, 2, \ldots, n$ are the estimated values for the same probability level p_i; n is the sample length; $\bar{x}$ and $\bar{y}$ denote the average value of the observed and estimated quantiles, respectively; m is the number of model parameters and by default $m = 0$ when comparing between the observed and estimated values. However, for the case of comparing the performance of the four scaling models (i.e. GEV/PWM, GEV/NCM, GUM/PWM, and GUM/NCM models) in estimating the distributions of sub-daily extreme rainfall series from those of the daily extreme rainfall series, the number of model parameters, m must be taken into account to make a fair comparison. Depending on the approach, $m = 3$ was used for the GEV/PWM and GEV/NCM models, and $m = 2$ for the GUM/PWM and GUM/NCM models.

The Cunnane's plotting position formula was used to estimate the non-exceedance probabilities, p_i, because of its ability to yield approximately unbiased quantiles for a wide range of distributions (Nguyen et al., 2017; Nguyen and Nguyen, 2019a):

$$p_{i:n} = \frac{i - 0.4}{n + 0.2} \tag{3-32}$$

After computing the six GOF statistical tests, a ranking scheme is utilized to rank all the selected distributions. Ranking scores are assigned to each model according to the value computed for each criterion. A distribution with the lowest RMSE, RMSEr, MAD, MADr, MAE, or highest R^2_{adj} is given the rank of 1 for the corresponding assessment category. In case of ties, equal ranks are given to those corresponding models. Furthermore, for each numerical criterion, the overall rank associated with each distribution is computed by summing the individual ranks.

3.4 Results and Discussion

3.4.1 Scaling analysis

The main objective of the scaling analysis is to be able to identify the scaling behaviour of the extreme rainfall processes for different time scales at the location of interest. Extreme rainfall events of short durations (e.g., from several minutes to a few hours) may be governed by a totally different physical mechanism as compared to those events of longer durations (e.g., several hours to a couple of days). The scaling behaviour of these different physical phenomena could be discovered through investigating the relationships between the statistical moments of extreme rainfall amounts and the rainfall durations.

Notice that the statistical moments of extreme rainfalls computed based on the NCMs and the PWMs are quite different. The conventional (or ordinary) moments involve the increase in the powers of the quantile function $x(u)$ and thus give a higher weight to the outliers in the dataset. When the order of the statistical moment increases, the values of the moments increase by an amount proportional to the mean raised to the power of the order. For instance, for the Montreal P.E.T Intl. Airport Station presented in Figure 3-5a, the first-order NCMs (i.e., the means) of the rainfall amounts of different rainfall durations range from 10^1 mm to 10^2 mm, while the second-order NCMs range from 10^2 mm to 10^4 mm, and the third-order NCM range from 10^4 mm to 10^6 mm. If the order continues to be raised to a much higher value, for example, to the fifth order, the NCM values become very large due to the very large weights applied to the very high outliers.

Hence, it can be seen that the differences between the NCMs of rainfall amounts for the smallest and the largest rainfall durations become much larger for higher orders of the NCMs. In contrast to the ordinary NCMs, the PWMs involve the powers of u and may be regarded as integrals of $x(u)$ weighted by the polynomials u^r. Since the values of u are between 0 and 1, hence, when the order of moment increases, the values of the PWMs of rainfall amounts decrease gradually. For instance, for the Montreal P.E.T Intl. Airport Station presented in Figure 3-5a, the zero-order PWMs (i.e., the means or the first-order NCMs) of rainfall amounts for different rainfall durations varied in a range from 10^1 mm to 10^2 mm. However, the first- and second-order PWMs are almost in the same range of rainfall values as for the first-order PWMs, while the ranges of values for the equivalent second- and third-order NCMs are very much larger as indicated previously. Even when the power of the PWMs is raised to the fifth-order, the values of the corresponding PWMs are still within a range of low values from 10^0 mm to10^1 mm. Therefore, it can be seen that the computed PWMs of extreme rainfalls are more robust against the high outliers than the computed NCMs.

Some previous studies have indicated that extreme rainfall processes for durations ranging from several minutes to several days could exhibit one or two distinct scaling regime(s) (see, e.g., Nguyen et al., 1998; Yu et al., 2004; Bairwa et al., 2016). In other words, if the log-log plot of rainfall statistical moments versus rainfall durations displays a straight line and does not indicate any breaking point, one can conclude that there exists only one scaling regime for these extreme rainfall processes over the selected time scales. On the other hand, if the plot shows a breaking point, for instance at 30-minute duration as shown in Figure 3-5 for Montreal PE Trudeau Airport station, then one could identify two different scaling regimes of extreme rainfalls for two distinct ranges of rainfall durations; that is, the first scaling regime is defined for the range from 5-minute duration to 30-minute duration, and the second scaling regime for the range from 30-minute duration to 1-day duration.

To avoid the subjectivity in the identification of the breaking point location on the log-log plot, a numerical criterion was employed. This criterion relies on the residuals and the ranking of the residuals computed by fitting a linear regression model to the log-log plot of rainfall statistical moments (i.e., NCMs or PWMs) versus rainfall durations. For each plot, straight lines were fitted by a linear regression method such that the group-wide and the total residuals of the first three statistical moments are minimized. Hence, the number of fitted lines needed is equal to the number of scaling regimes visually identified. Notice also that to estimate the parameters of a three-parameter distribution such as GEV, only the first three statistical moments are required. In addition, this method is limited to the identification of the breaking point at a given observed rainfall duration within the range from D_1 = 5 minutes to D_9 = 1440 minutes and should not be used to detect the breaking point location for an unobserved duration (e.g., 45 minutes) since there is no physical basis associated with it.

For purposes of illustration, Figure 3-5b shows the result of detection of breaking durations using both the NCMs and PWMs for the Montreal P.E.T Intl. Airport Station. In this case, results are similar for both statistical moments. The breaking point is identified at 30 minutes and there are two different scaling regimes: the first scaling regime is from 1440 minutes to 30 minutes and the second scaling regime from 30 minutes to 5 minutes. It is also noted that the computed NCM-based scaling exponents for the orders smaller than three can be well-approximated by a straight line representing a given simple scaling regime, while the scaling exponents given by the NCMs of orders higher than three display a small deviation from the simple scaling line. For the computed PWM-based scaling exponents, notice that this deviation for the higher order PWM is much smaller. This result indicates that estimation of the scaling exponents using the PWMs are more robust than using the NCMs.

The results of scaling analysis of all 74 study stations are spatially represented in Figure 3-6. In general, it can be seen that the estimation results using both NCMs and PWMs are highly comparable for a larger number (more than 96%) of stations, especially for those with long rainfall records. Furthermore, by observing the two plots, the PWM-based breaking point graph indicates a more consistent results and a better agreement among the neighboring stations. The PWM-based empirical scaling exponents are computed for both scaling regimes of each station.

In particular, Figure 3-6b indicates that, for the Atlantic region, two stations on the East coast of Newfoundland and Labrador show a 15-minute breaking point, while the remaining station exhibits the same 360-minute breaking point as many stations in Nova Scotia and New Brunswick of the Maritime region. There are two stations located in the North of New Brunswick with a 10-minute breaking point; and two stations located in the West of Nova Scotia with a 60-minute breaking point stations.

For Quebec and Ontario of Eastern Canada, among the 29 stations, a total of 62% of these stations exhibit a 30-minute breaking point. These stations are mainly located in the Southern Quebec, Southern Ontario, and Northwestern Ontario. For North-Eastern Ontario, the breaking points are located at 15-minute duration or 30-minute duration. There are five stations with a 60-minute breaking point in Ontario; interestingly, four of them located next to the Great Lakes region. In particular, the Kingston Pumping (#44) and Trenton Airport (#56) Stations are situated in the Northwest of Lake Ontario; the North Bay (#43) Station is situated in the Northeast of Lake Nipissing; the Thunder Bay (#39) Station is situated in the Northwest of Lake Superior. There is only one station with a 120-minute breaking point – the Kenora RCS (#36) Station located on the Lake of the Woods. This station has also recorded the largest 120-minute and 360-minute extreme rainfall events as described in Section 3.2.

For the Prairies region, most stations located in Southern Manitoba and Saskatchewan show a 30-minute breaking point, while the stations located in the North of these two provinces exhibit a 15-minute breaking point. Only station Saskatoon RCS (#27) shows the 60-minute breaking point. For Alberta province, all stations exhibit the breaking point at 15-minute rainfall duration, except one station shows a 10-minute breaking point. Note that there is one station showing the breaking point at 1-hour duration, the Red Deer Regional Airport (#17) Station. However, the difference in scaling exponents between the two scaling regimes is less than 1% (see Figure 3-7). Thus, this station can be considered to have only a single scaling regime (i.e., from 1-day to 5-minute).

The westernmost province of Canada – British Columbia, located between the Pacific Ocean and the Rocky Mountains, displays the most complex scaling behaviour. This is due to the complicated and diverse geography of the province varying from coastal islands to mountainous interiors. The 12 investigated stations indicate that the breaking point ranges from a very short duration of 10 minutes to a much longer duration of 6 hours. There are two stations (Station #5 – Comox Airport and Station #6 – Tofino Airport located respectively on the West and East Coasts of the Vancouver Island bordering with the Pacific) show a 120-minute breaking duration. Similar to the province of Alberta, the differences in scaling exponents between the two scaling regimes are approximately 5% (see Figure 3-7). Thus, these stations could be considered to have only a single scaling regime (i.e., from 1-day to 5-minute). Station #14 – Blue River Airport – shows the breaking point at 360-minute duration with approximately 9% difference in scaling exponents between the two scaling regimes.

For the Territories, the two stations located in Yukon and Northwest Territories exhibit the same breaking point at 15-minute duration which are also similar to the stations located in Northeastern British Columbia and Northern Prairies provinces.

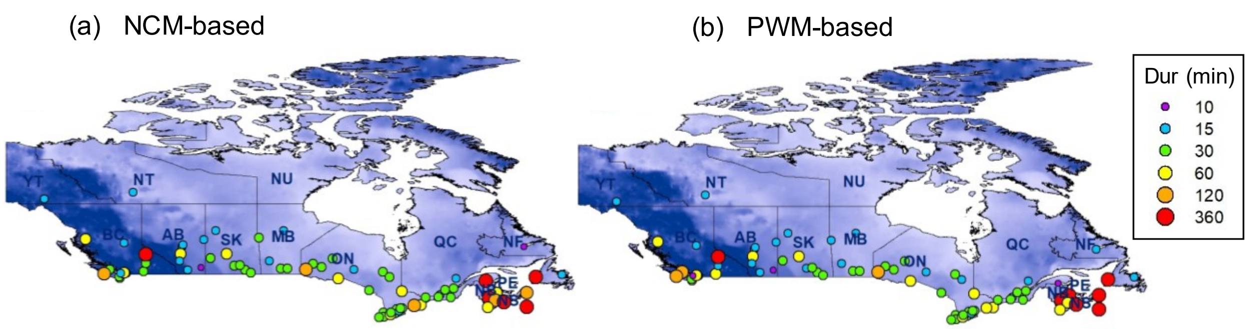

Figure 3-6. Locations of breaking points of 74 stations based on (a) NCMs (b) PWMs. Circle markers with different colors and sizes show the breaking durations

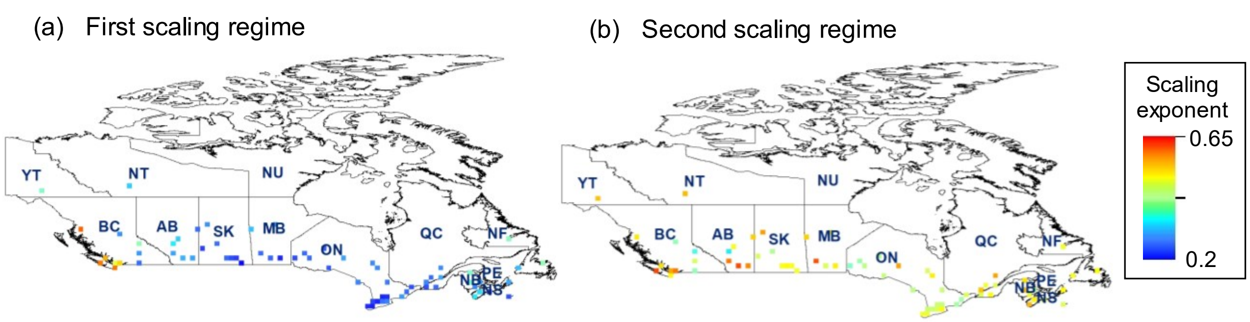

Figure 3-7. The PWM-based empirical scaling exponents for (a) the first scaling regime and (b) the second scaling regime. The first and second scaling regimes are defined from 1 day to the breaking point and from the breaking point to 5 minutes, respectively.

To investigate the robustness of the empirical scaling exponent estimates, the first five NCM-based and PWM-based empirical scaling exponents are plotted with the theoretical simple scaling exponents on Figure 3-8 for both scaling regimes. The first scaling regime is defined from the 24-hour duration to the breaking duration, whereas the second scaling regime is defined from the breaking duration to the 5-minute duration. Results show that the four- and fifth-order empirical scaling exponents divert significantly from the simple scaling exponents, especially for the NCM-based estimation. The coefficient of determination R^2 between the empirical and simple scaling exponents are calculated and provided in Table 3-3. These results point out that the PWM-based estimation yields a much better result than the NCM-based estimation for all the moment estimators and for both scaling regimes. For example, R^2 values for PWM-based estimations are 0.98 for the first scaling regime and 0.87 for the second scaling regime, while the corresponding values for the NCM-based estimation are 0.96 and 0.81, respectively.

Table 3-3. Values of R^2 between the empirical and theoretical simple scaling exponents for the first five moments. Bold values indicate a higher R^2 value between the PWM and NCM methods for each scaling regime. Note that the first moments are equal to the means.

Moments	**1st scaling regime**		**2nd scaling regime**	
	PWM	NCM	PWM	NCM
1	**1**	1	**1**	1
2	**0.994**	0.990	0.947	**0.953**
3	**0.982**	0.955	**0.874**	0.812
4	**0.972**	0.897	**0.812**	0.653
5	**0.962**	0.834	**0.757**	0.531

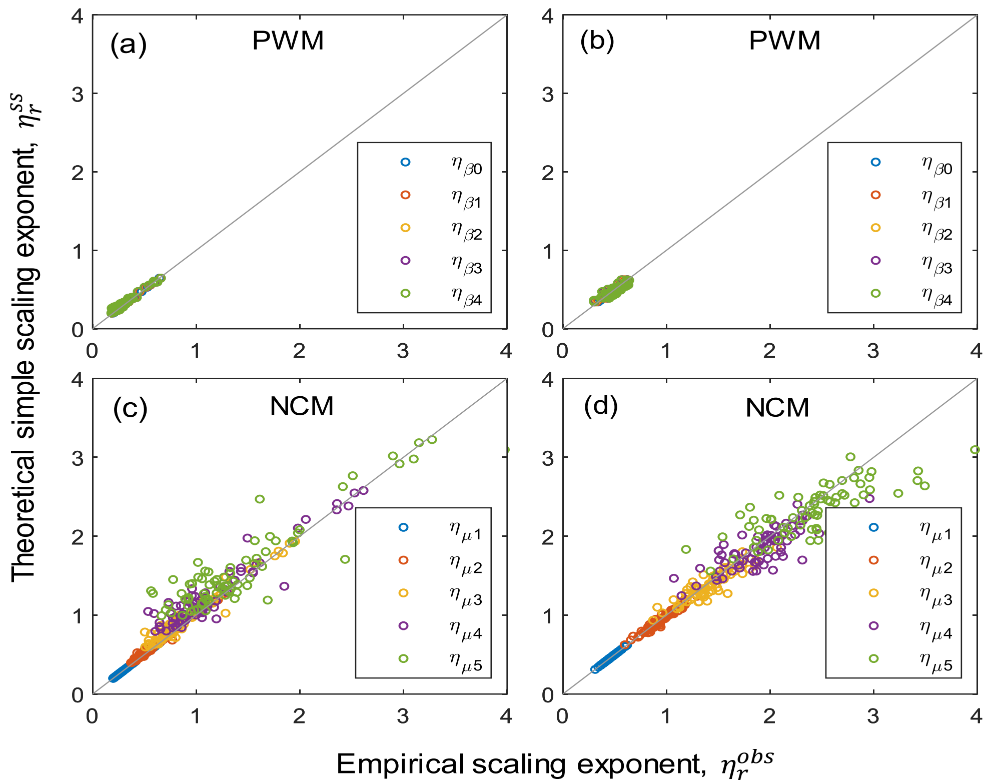

Figure 3-8. Empirical versus simple scaling exponent plot for (a) PWM-based first and (b) second scaling regimes; (c) NCM-based first and (d) second scaling regimes. The first and second scaling regimes are defined from the 24-hour to the breaking duration, and from the break to the 5-min duration, respectively.

3.4.2 Direct and indirect quantile scaling

In this section, the direct and indirect scaling methods for computing the sub-daily extreme rainfall quantiles from those of daily data based on the scaling GEV/PWM distribution model as described in Section 3.3.3 are investigated and compared. In particular, they are employed to estimate the distributions and quantiles of the sub-daily extreme rainfalls from those daily extreme rainfalls. The estimated values are compared to the at-site frequency analysis of the observed values using both graphical and numerical comparisons.

For purposes of illustration, results of four representative stations located in different provinces across Canada are presented as shown in Figure 3-9. These stations, which contain one of the longest extreme rainfall records and/or contain the largest rainfall amounts in one or several durations, are: Montreal P.E.T. Intl. Airport Station (1943-2014), Dauphin CS Station (1954-2016), Regina Airport Station (1941-1995), and Vancouver Airport Station (1953-2017). For each station, the probability plots as shown in Figure 3-9 were used to compare the estimated extreme rainfall quantiles given by the scaling-invariant (either direct or indirect) method and those given by the at-site frequency analysis for 1-hour and 5-minute AMS. It can be seen that the estimated probability distributions for 1-hour and 5-minute AMS by the indirect method provided a better fit to the observed points (or closer to the theoretical fitted distribution) than those given by the direct method. Thus, the indirect method yields better quantile estimates for these four stations as compared to the direct method. More specifically, the direct method tends to over-estimate the left tail portion of the distributions, and more importantly, it tends to under-estimate the right tail portion, which is a critical area where the extreme rainfall values are often used for the design of various hydraulic structures.

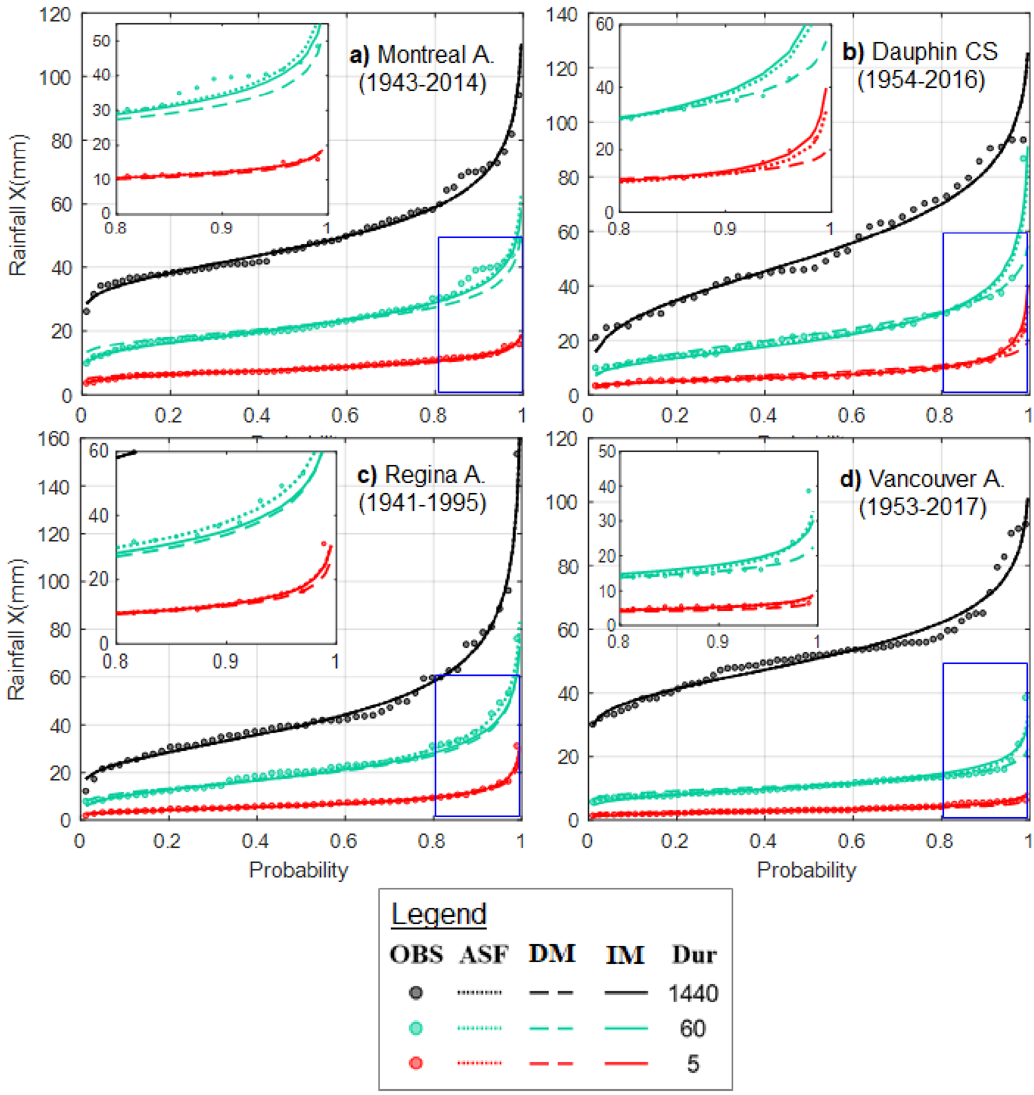

Figure 3-9. Probability plots of 1-hour and 5-minute AMS scaled from 1-day AMS using the direct method (DM, dash lines) and indirect method (IM, continuous line). Empirical distribution of observed data (OBS, circle markers) and theoretical fitted distribution using at-site frequency analysis (ASF, dotted lines) are also plotted for comparisons. Small graph on each plot shows the zoomed-in blue window.

Figure 3-9 only shows the comparison of the distributions of 1-hour and 5-minute AMS for the four representative stations. For a full comparison of all rainfall durations and all stations, the graphical comparison using quantile-quantile (Q-Q) plots and numerical comparison using different statistical criteria are employed as shown in Figure 3-10 and Figure 3-11, respectively. The observed extreme design rainfalls are plotted with the downscaled ones for six return periods (T = 2, 5, 10, 25, 50, and 100 years) and for eight rainfall durations (D = 5, 10, 15, 30, 60, 120, 360, and 720 minutes). The observed values are estimated based on the at-site frequency analysis approach using the GEV distribution. The downscaled values are estimated from the daily extreme rainfalls using both the direct and indirect methods.

The Q-Q plots in Figure 3-10 show a high correlation between the estimated and observed values for both methods. However, the indirect method performs better with a narrower spread of points along the perfect agreement line (i.e. the 45-degree line). The boxplots in Figure 3-11 indicate that the indirect method outperforms the direct method for all criteria. This difference in accuracy of the estimates between these two methods is due to the form of parameterization that each method applied. The direct method used only the zero-order moments of extreme rainfall data series to estimate the rainfall quantiles, while the indirect method involved all three moments of order 0, 1, and 2 in the estimation. Consequently, the indirect procedure used much more information from the data than the direct method and, therefore, produced higher accuracy.

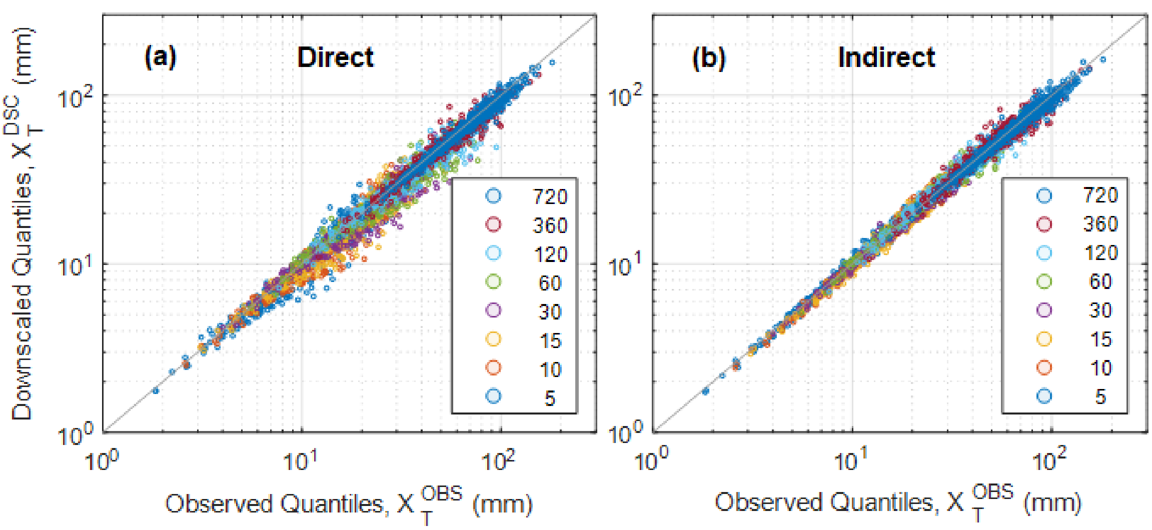

Figure 3-10. Quantile-quantile (Q-Q) plot of the observed (X_T^{obs}, mm) and the downscaled (X_T^{dsc}, mm) extreme design rainfalls for six return periods (T=2, 5, 10, 25, 50, and 100 years) and for eight rainfall durations (D=5, 10, 15, 30, 60, 120, 360, and 720 minutes). The observed values are estimated using the at-site frequency analysis approach. The downscaled values are estimated from the daily extreme rainfalls using (a) direct and (b) indirect methods.

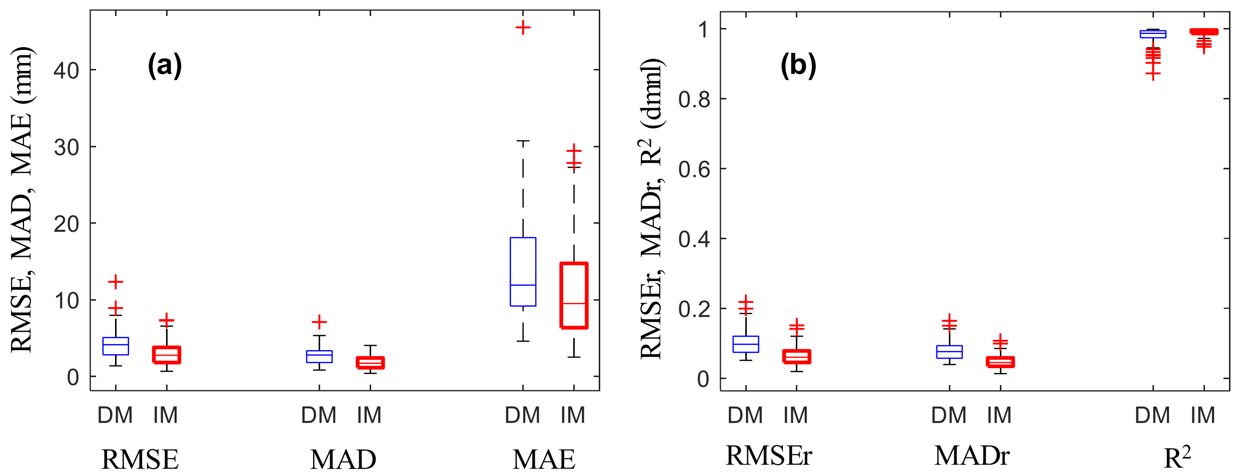

Figure 3-11. Boxplots of numerical comparisons of the estimated extreme design rainfall quantiles produced using the direct method (DM, blue box) and indirect method (IM, red box) for 74 stations using different statistical criteria: (a) RMSE, MAD, MAD (mm) and (b) RMSEr, MADr, R^2 (dmnl).

3.4.3 Comparison of scale-invariance models

This section presents the comparison of the performance between the GEV/PWM model proposed in this study, the existing scale-invariance GEV/NCM model, and their special cases – the scaling GUM/PWM and GUM/NCM models. Furthermore, as indicated in the previous section, the indirect scaling methods was used in this comparison since it can produce more accurate results than the direct procedure for these scale-invariance models.

For purpose of illustration, Figure 3-12 presents the graphical comparisons of the cumulative distribution functions (CDFs) of the sub-daily AMS (for rainfall duration ranging from D = 720 to 5 minutes) derived from the distribution of daily AMS data (D = 1440 minutes) using the four scale-invariance models for Montreal P.E.T. Intl. Airport Station. For each model, a visual assessment can be performed by visually comparing the estimated CDFs of the sub-daily extreme rainfalls to the empirical CDFs of the observed data and to the fitted theoretical CDFs. Note that, the scaling model allows to derive the distributions of the sub-daily AMS from the fitted distribution of the daily data by considering the relationship between the PWMs or NCMs of extreme rainfall amounts over different rainfall durations. Whereas the ASFA method does not take into account this relationship and the theoretical distribution is fitted independently to each daily and sub-daily AMS. Results in Figure 3-12 indicate that the extreme rainfall quantiles estimated using these scaling models highly agree with the observed values. From the visual standpoint, all the scale-invariance models seem to perform well at these two stations. However, the significance of the differences between these models is difficult to assess based on the graphical display. A more objective evaluation using numerical comparison criteria is thus necessary.

Different goodness-of-fit test criteria presented in Section 3.3.4 were thus utilized to evaluate the performance of the four models. In detail, the six statistical GOF tests were calculated based on the estimated and empirical extreme rainfall quantiles of sub-daily data (i.e., the empirical CDFs are the same for all four models). The use of different theoretical distributions yields different results of extreme rainfall quantiles even using the same parameter estimation method (for example, GEV/PWM model versus GUM/PWM model; or GEV/NCM model versus GUM/NCM model, see Figure 3-12). Furthermore, assuming that the distributions of sub-hourly and sub-daily AMS follow the GEV distribution, different parameter estimation methods yield different results of extreme rainfall quantiles (for instance, GEV/PWM model versus GEV/NCM model, see Figure 3-12). While the empirical CDF/quantiles are independent with theoretical distributions and parameter estimation methods.

Using these numerical criteria, the results for Montreal P.E.T. Intl. Airport Station indicated that the GUM/PWM produced the best results for the RMSE (1.63 mm) and the MAE (9.5 mm) criteria, while the GEV/PWM yielded the best results for the RMSEr (5.4 %) and MADr (4.3 %) which is the same as the GUM/NCM. For the R^2, the GUM/PWM and GUM/NCM models produced slightly better results with R^2_{adj}=0.99. Ranking of these values are also presented in Figure 3-13. Similar calculations were carried out for all 74 stations and the results were also presented in Figure 3-13 for 5 to 720-minute observed and estimated AMS data. The observed data are shown as boxplots on the left for all stations with provincial names. Numerical values of the six indices are synthesized and displayed as boxplots on top of Figure 3-13. Note that the GEV/PWM, GEV/NCM, GUM/PWM, and GUM/NCM scale-invariance models are denoted as M1, M2, M3, and M4, respectively.

In general, results for the downscaled sub-daily AMS show that all four scale-invariance performed well. For instance, as can be seen from the boxplots, to the whisker extents, the worst model produces RMSEr and MADr less than 18% and 12% respectively, RMSE and MAD less than 4.5 mm and 2.5mm, and R^2_{adj} at least 0.95. On average, as compared to the medians, the worst model produces RMSEr and MADr less than 9% and 6% respectively, RMSE and MAD less than 2.5 mm and 1.5mm, and R^2_{adj} at least 0.98. Based on these boxplots, especially, boxplots of the dimensionless indices (i.e., RMSEr, MADr, and R^2_{adj}), it can be seen that the GEV/PWM model performs best for these criteria with the smallest box widths, lowest (or highest) medians and shortest upper (or lower) whisker extents for the cases of RMSEr and MADr (or R^2_{adj}).

The ranking of the four candidate scaling models for each of the selected 74 stations based on the six indices are also presented in Figure 3-13. Ranking from number 1 to 4 indicates the gradual decrease from the best to the worst distributions. On the basis of these goodness-of-fit numerical comparison results, it was found that no unique scaling model ranked consistently best for all criteria and all locations. However, the proposed GEV/PWM seems to perform well for the majority of stations and for all six indices. To investigate this, the overall rank (or total score) of each numerical index was obtained by summing the individual point rank at each station for each model. Ranking of the total score (i.e., from 1 to 4) was also computed. Results are shown at the bottom of Figure 3-13. In addition, the number of first score was also calculated for each model of each criterion. Results are displayed in the form of the bar graphs right below the ranking of the total score in Figure 3-13. Note that the equal scores were used for tie cases. Hence, the sum of the first score for each numerical index based on the four models can be higher than the total number (74) of stations considered.

In general, based on the three criteria (i.e., RMSEr, MAD, and MADr), the GUM/NCM is the least accurate with the total scores (or first scores) for these indices are 249 (7), 257 (6), and 251 (9), respectively. However, it produces comparable results to the GUM/PWM model for the RMSE criterion and performs better than the GUM/PWM model for the MAE index. The R^2_{adj} criterion should not be used to compare these two models as the relationship between their quantiles can be described by a linear function. In fact, using the same reduced Gumbel variates, the quantile functions of the two models are linear. This means that the plots of quantiles estimated using the two models with the same Gumbel reduce variates are straight lines on a same graph. In contrast to the GUM/NCM, the GEV/PWM is the best model among the four considered models with the lowest total scores (or highest first scores) for all six indices (RMSE, RMSEr, MAD, MADr, MAE, and R^2_{adj}), which are 122 (49), 110 (51), 102 (55), 99 (56), 150 (38), and 110 (56), respectively. If only the MAE criterion is considered, the GEV/NCM model produces comparable results with the GEV/PWM model with a close total score (i.e. 155 vs 150), an approximate box width and a similar whisker extent.

The quantile-quantile (Q-Q) plot was also used to visually compare the scaling-based and empirical-based 5-to-720-minute extreme rainfall quantiles. Results are shown in Figure 3-14.

Results again confirm that the GEV/PWM model is the best model with the smallest spread of points along the perfect result line (i.e. the 45-degree line).

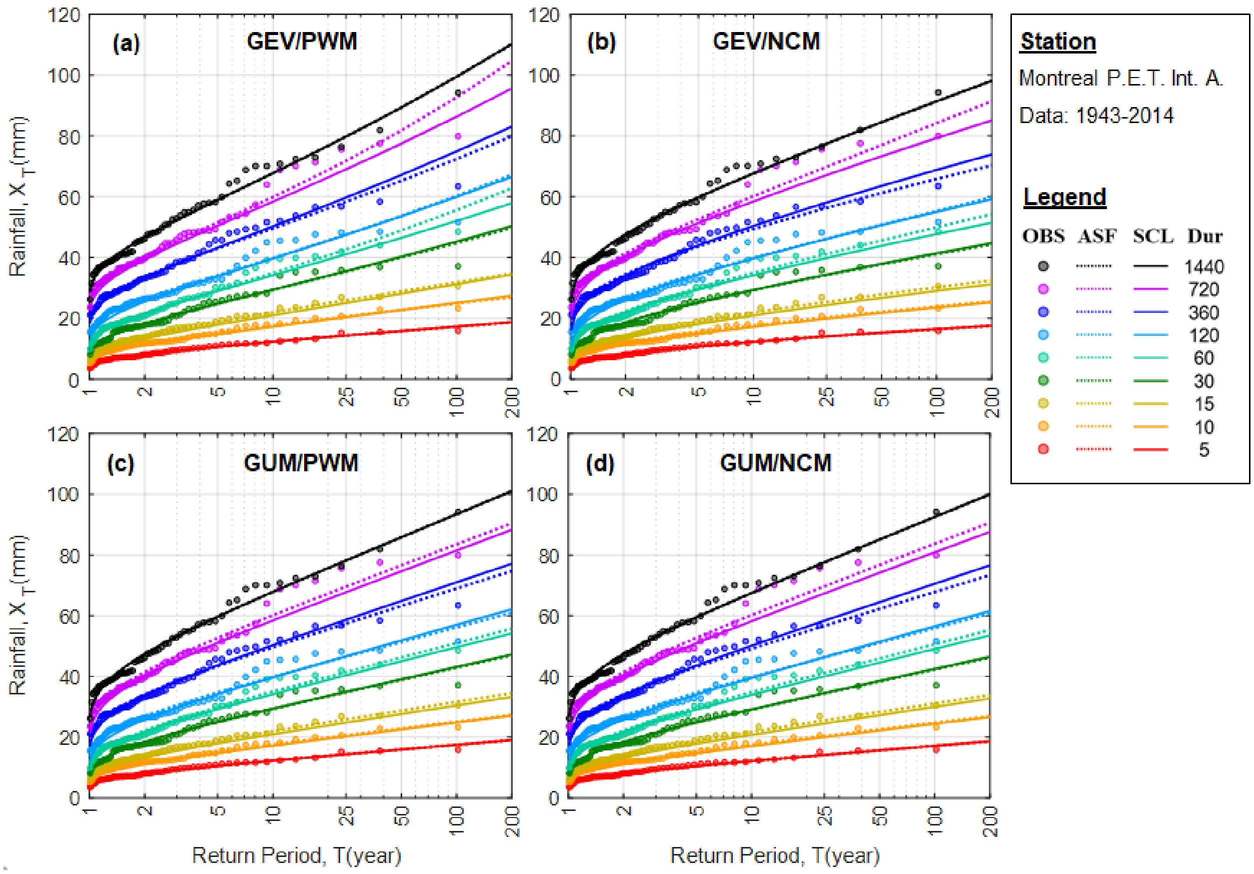

Figure 3-12. Probability plots of the estimated sub-daily and sub-hourly AMS (D = 720 to 5 minutes) derived from the daily AMS (D = 1440 minutes) for Montreal P.E.T. Intl. Airport Station using the scaling approach (SCL, continuous lines) and at-site frequency analysis (ASF, dotted lines) of the observed data (OBS, circle markers).

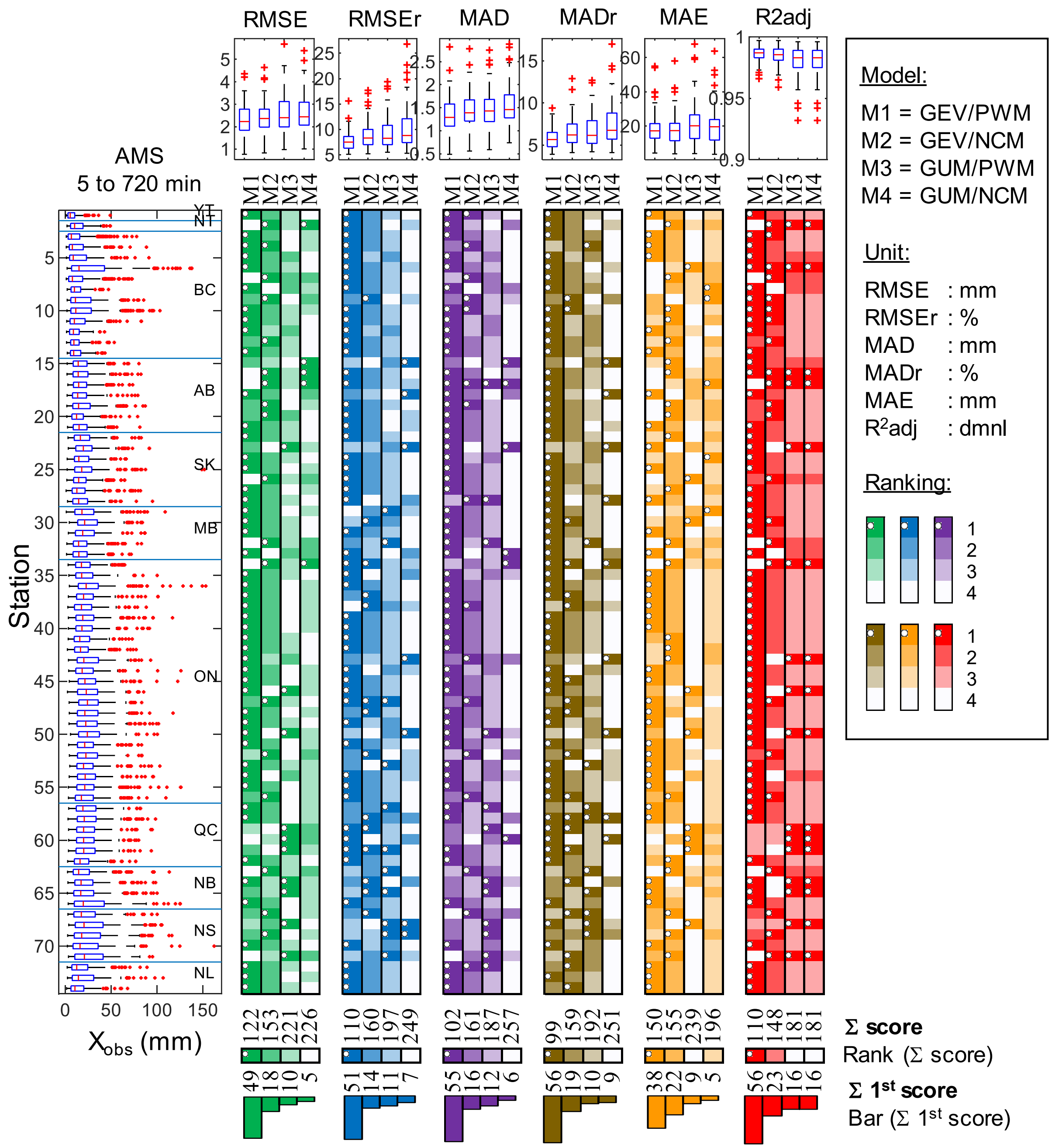

Figure 3-13. Statistical test results of observed and estimated 5- to 720-minute extreme rainfall quantiles produced using the four scaling models. Observed AMS data from 5 to 720 minutes are shown on the left for all stations with provincial names. Numerical values of each criterion for 74 stations are summarized in the form of boxplots on the top. For each station, the four scaling models are ranked from the best (rank = 1, darkest color with a diamond) to the worst model (rank = 4, white). The total score for a model is computed by summing the individual ranks. Equal ranks are used for ties. Similarly, the total first score is computed by counting only the number of stations that the model performs best.

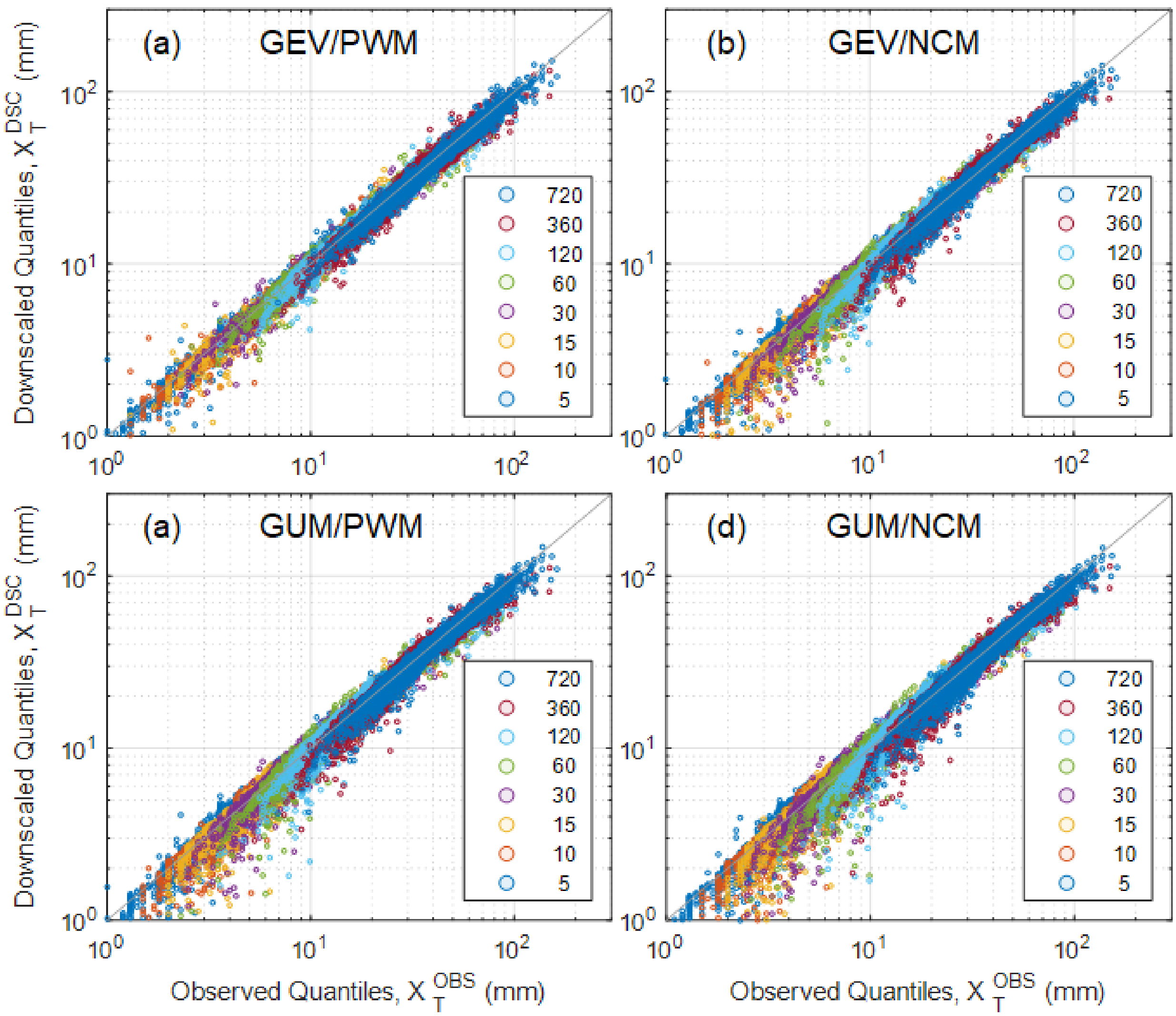

Figure 3-14. Quantile-quantile (Q-Q) plots of the scaling-based (downscaled) and empirical-based (observed) extreme rainfall quantiles of 720-minute to 5-minute rainfall duration for (a) GEV/PWM, (b) GEV/NCM, (c) GUM/PWM, and (d) GUM/NCM models.

3.5 Summary and Conclusions

Short-duration extreme rainfall data (e.g., a few minutes to hours) are often required for the simulation and assessment of runoff and inundation for the fast response areas, such as the urban and small rural watersheds. However, this data is often limited or unavailable at the given study location while those of daily scale are widely available. The present study proposed a special mathematical framework based on the scale-invariance Generalized Extreme Value (GEV) distribution model to establish the linkages between the non-central moments (NCMs) or the probability weighted moments (PWMs) of extreme rainfalls over different time scales (e.g., from several minutes to one day). On the basis of this framework, the distributions and quantiles of short-duration extreme rainfalls can be derived from those of longer-duration data.

The NCM-based mathematical framework and the scaling properties of the GEV distribution were critically reviewed and presented in this Chapter. This includes the scaling GEV/NCM model proposed by Nguyen et al. (1998) and its special case, the scaling GUM/NCM model as described in Menabde et al. (1999). The traditional NCMs have been commonly used to estimate model parameters by raising the power of each element in the sample to the same order. It is thus considered to be sensitive to outliers, especially for moments of high orders such as skewness. In contrast, the PWM system puts the weight on the probability and therefore produces a more robust estimate. The PWM-based mathematical framework and scaling properties of the GEV distribution (referred to as the GEV/PWM model) was first introduced in this study. The GUM/PWM model as suggested in a previous study by Yu et al. (2004) is hence a special case of the proposed GEV/PWM model.

The long-record short-duration extreme rainfall data from a network of 74 raingages located across Canada were used to investigate the feasibility and accuracy of the proposed scaling GEV/PWM model. The observed data from each station contains annual maximum rainfall series (AMS) of nine different rainfall durations ranging from 5 to 1440 minutes with at least 40 years of record. In total, 666 AMS dataset were considered in the present study.

Firstly, the scaling behaviours of the AMS for all 74 stations were analyzed based on both NCMs and PWMs. Results of this scaling analysis have indicated that the estimates of the empirical scaling exponents based on the PWMs are more accurate and more robust than those given by the NCMs for different extreme rainfall scaling regimes and for higher order rainfall statistical moments. For instance, the R^2 between the empirical and theoretical scaling exponents of the second-order PWM for two distinct scaling regimes are 0.982 and 0.874, respectively, while those values given by the third-order NCM are only 0.955 and 0.812, respectively. Note that the zero-order PWMs are equivalent to the first-order NCMs and they are both equal to the AMS means.

Secondly, following the scaling analysis, the direct and indirect scaling methods for estimating the quantiles of sub-daily AMS from those of daily AMS based on the proposed scaling GEV/PWM model were investigated and compared. The direct method estimates the quantiles of sub-daily AMS directly from those of daily AMS without the need of estimating the GEV model parameters. On the other hand, the indirect method computes the PWMs of sub-daily AMS from those of the daily AMS and then used these estimated PWMs to estimate the GEV model parameters for computing the quantiles of the sub-daily extreme rainfalls. Results based on different graphical displays (probability plots and quantile-quantile plots) as well as six numerical indices (RMSE, RMSEr, MAD, MADr, MAE, R^2_{adj}) have indicated that the indirect method outperformed the direct method for all these criteria. This method was then employed to compare the performance of the proposed GEV/PWM model with other exisisting scale-invariance models.

Graphical and numerical comparisons of the performances of the GEV/PWM model and three existing scaling models (GUM/PWM, GEV/NCM, and GUM/NCM) were conducted using data from a network of 74 stations across Canada. Results of these comparisons have indicated that no distribution performed best for all stations and for all criteria. However, it was found that the proposed GEV/PWM model was superior to all three existing models for the majority of stations and criteria. For example, the model can produce the lowest errors for a large number of stations (69% and 76% of stations) based on the RMSEr and MADr criteria, respectively.

In summary, the present study has deveoped an improved method for estimating more accurately the extreme rainfalls at a given location of interest by taking into account the relationships between the statistical moments of extreme rainfall amounts for different rainfall durations as compared to the traditional estimation approach in which the statitical properties of extreme rainfalls for different durations were considered independently. Hence, the proposed method could also be used in the regional rainfall estimation context to estimate extreme rainfalls at locations with limited or missing data (partially-gauged sites with missing sub-daily data for instance) or at locations with no available data (ungaged sites) by transfering the scaling properties of AMS from the neighboring stations located within a same homogeneous region. Furthermore, the proposed method can also be used to provide projected short-duration extreme rainfalls from the projected daily extreme rainfalls for updating the IDF relations in the context of a changing climate as described in the following chapters.

Chapter 4. Linking Climate Change to Urban Storm Drainage System Design: An Innovative Approach to Modeling of Extreme Rainfall Processes Over Different Spatio-Temporal Scales

4.1 Introduction

The design of urban storm drainage systems requires a "design storm" that represents the time distribution of rainfalls within an extreme storm event. More specifically, in engineering practice, the design storm of a specified exceedance probability and duration is commonly estimated from the extreme rainfall intensity-duration-frequency (IDF) relations (Hershfield, 1961; Chow, 1964; WMO, 2009). However, in recent years, climate change has been recognized as having a profound impact on the hydrologic cycle at different temporal and spatial scales. The temporal scales could vary from a very short time interval of a few minutes (for urban water cycle) to a yearly time scale (for annual water balance computation). The spatial resolutions could be from a few square kilometers (for urban and rural watersheds) to several thousand square kilometers (for large river basins). In particular, the intensity and frequency of extreme precipitation events in most regions will be likely increased in the future (Alexander et al., 2006; Lenderink and Van Meijgaard, 2008; Kharin et al., 2013; Shephard et al., 2014; Zhang et al., 2017). Hence, there exists an urgent need to assess the possible impacts of climate variability and climate change on the IDF relations in general and on the design storm in particular for improving the design of urban drainage systems in the context of a changing climate (Willems et al., 2012; CSA, 2012; Madsen et al., 2014; Simonovic et al., 2016).

To achieve this, the projected annual maximum rainfall series for different rainfall durations from short time scales (e.g., a few minutes) to long time intervals (e.g., one day or longer) under different possible climate change scenarios are required. Consequently, global climate models (GCMs) have been extensively used currently to provide projected precipitations for future periods (e.g., next hundred years) based on different Representative Concentration Pathways (RCP) scenarios. These models have been recognized to be able to represent reasonably well the main features of the global distribution of basic climate parameters (Lambert and Boer, 2001), but could not reproduce well details of regional climate conditions at temporal and spatial scales of relevance to hydrological impact studies (Nguyen and Nguyen, 2007). This is because outputs from GCMs are usually at resolutions that are too coarse (generally greater than 200 km and mostly available at a daily time scale) and are not suitable for many climate change impact studies in urban areas. A new rainfall modeling approach is thus needed to establish an accurate linkage between climate projections from GCMs and extreme rainfall (ER) processes at a site of interest.

To refine the GCM coarse grid resolution climate projection data to much finer spatial resolutions (regional or local scales) for reliable assessment of climate change impacts, different downscaling methods have been proposed (Wilby et al., 2002; Fowler et al., 2007; Maraun et al., 2010; Gooré Bi et al., 2017). These methods can be classified into two broad categories: dynamical downscaling (DD) and statistical downscaling (SD). The DD techniques involve the extraction of regional scale information from large-scale GCM data based on the modeling of regional climate dynamical processes (Laprise, 2008; Xue et al., 2014; Xu et al., 2019). These models use physical principles to reproduce local climates, thus, are comprehensive physical models, but are computationally intensive. Whereas the SD techniques rely on the empirical relationships between observed (or analyzed) large-scale atmospheric variables and observed (or analyzed) surface environment parameters (Wilby et al., 2002; Nguyen and Nguyen, 2007, 2008; Bürger et al., 2012, 2013; Werner and Cannon, 2016). The SD methods are thus flexible to adapt to specific study purposes and inexpensive computing resource requirement (Nguyen and Nguyen, 2007). Both downscaling methods therefore have their strengths and limitations (Wilby et al., 2002; Teutschbein et al., 2011), and both are currently used for downscaling the GCM outputs to the regional scales (approximately 10 to 50 km resolutions) for climate-related studies. There are many different downscaled climate projection data sources available at the national or global level provided by different organizations. For example, in North America, just to list a few, the NA-CORDEX dataset available at roughly 25 or 50 km resolution covering most of North America (NA-CORDEX, 2018), NEX-GDDP dataset available at about 25 km resolution covering the entire globe (NEX-GDDP, 2018), the NEX-DCP30 dataset available at approximately 1km resolution for the conterminous United States (NEX-DCP30, 2018), PCIC statistically downscaled climate scenarios available at roughly 10 km for Canada (PCIC, 2018). However, downscaled data from these methods are still considered bias when comparing to observed data at a local site in a same grid cell and need to be bias-corrected. A bias-correction method is therefore required to correct the data before it can be used for impact assessments and adaptation studies (Willems et al., 2012).

In addition to the spatial downscaling, the temporal downscaling is also required to derive the distributions of sub-daily extreme rainfalls from that of the daily values since the climate projections are normally available at the daily scale. Several approaches have been developed in the literature, such as the chaotic method, the scale-invariance approach, the point-process model, the neural networks techniques (Sivakumar et al., 2001; Nguyen et al., 2002b; Coulibaly et al., 2005; Marani and Zanetti, 2007; Nguyen et al., 2007; Lee and Jeong, 2014; Herath et al., 2016).

Among these methods, the scale-invariance (or scaling) concept has increasingly become a new methodology in the analysis and modeling of various extreme hydrological processes across a wide range of temporal scales (Gupta and Waymire, 1990; Sposito, 1998; Hubert, 2001; Veneziano and Furcolo, 2002; Veneziano and Lepore, 2012; Lovejoy and Schertzer, 2012). Scale invariance implies that the distributions and statistical properties of ERs over different time scales are related to each other by an operator involving only the scale ratio and the scaling exponent (Gupta and Waymire, 1990). In particular, the scaling method has been used in the construction of the IDF relations for the current and future climates (Burlando and Rosso, 1996; Nguyen et al., 2002b; Yu et al., 2004; Bougadis and Adamowski, 2006; Nguyen et al., 2007; Blanchet et al., 2016; Ghanmi et al., 2016). More specifically, several scaling models have been proposed in the literature, such as the scaling Gumbel (GUM) model based on the non-central moments and the probability weighted moments (Menabde et al., 1999; Yu et al. 2004). The scaling Generalized Extreme Values (GEV) model based on the non-central moments (Nguyen et al., 1998). More recently, a novel scaling probability weighted moments-based GEV model has been shown to outperform other existing scaling models (Nguyen and Nguyen, 2018a).

In view of the above issues, the present paper proposes an innovative SD approach that can be used for establishing the linkage between climate change information to extreme rainfall estimation for urban storm drainage systems design; a difficult and challenging task in current engineering practices. This SD approach was based on a new procedure for modeling the ER processes over different spatial and temporal scales. The feasibility and accuracy of the proposed approach were assessed for a case study in Ontario (Canada) using the IDF data from a network of seven raingauges. These data are provided in Sections 4.2. Details of the proposed methodology are described in Section 4.3. Results are presented and discussed further in Section 4.4. Finally, a summary of the research findings is provided in Section 4.5.

4.2 Study Sites and Data

The observed IDF data from a network of seven raingauges located in Ontario (Canada) were used for this study. The station information and locations are presented in Table 4-1 and Figure 4-1. Observed IDF data at each site contain annual maximum rainfall series (AMS) of nine different durations (ranging from 5 minutes to 1440 minutes). Note that the observed IDF data have been provided by Environment Canada to produce the at-site IDF relations for the various practical engineering application purposes (Environment Canada, 2019). The selection of the stations relied on the quality of the data, the adequate length of available historical ER records, and the representative spatial distribution of the raingauges. To ensure the quality of data, only data from recording raingauges provided by the Atmospheric Environmental Service of Environment Canada were used. Furthermore, the raingauges were selected from different geography locations to represent diverse climatic conditions of Ontario.

Regarding the climate change information, the climate simulation outputs from 21 global climate models (GCMs) conducted under the Coupled Model Inter-comparison Project Phase 5 (CMIP5) were used. These models are provided by nine different countries from different continents, including Canada (one model), USA (five models), Australia (two models), France (three models), Germany (two models), Norway (one model), China (two models), Russia (one model), and Japan (four models). Details of the 21 GCMs are provided in Table 4-2. These models are operated at different spatial resolutions with the finest resolution approximately 1^o x 1^o (Japan and USA) to the coarsest resolution 3^o x 3^o (Japan, Canada, and France). The grid resolutions of these models are plotted on Figure 4-2. The resolution of a common GCM grid of 2.5° x 2° (approximately 250 km x 200 km) is also plotted on Figure 4-1 and Figure 4-2 for the comparison.

Table 4-1. Information on the seven raingauges used in this study. Note: Lat = latitude (°), Lon = Longitude (°), Elv = Elevation (meter), and RCL = record length (from year to year)

No	Station ID	Station name	Lat (°)	Lon (°)	Elv (m)	RCL
1	6057592	Sault Ste Marie A	46.48	-84.51	192	1961-2007
2	6104175	Kingston Pumping Stn	44.24	-76.48	76	1961-2007
3	6137362	St Thomas WPCP	42.77	-81.21	209	1961-2004
4	6139525	Windsor A	42.28	-82.96	189	1961-2007
5	6144478	London CS	43.03	-81.15	278	1961-2016
6	6153301	Hamilton RBG CS	43.29	-79.91	102	1961-2016
7	6158731	Toronto Intl A.	43.68	-79.63	173	1961-2017

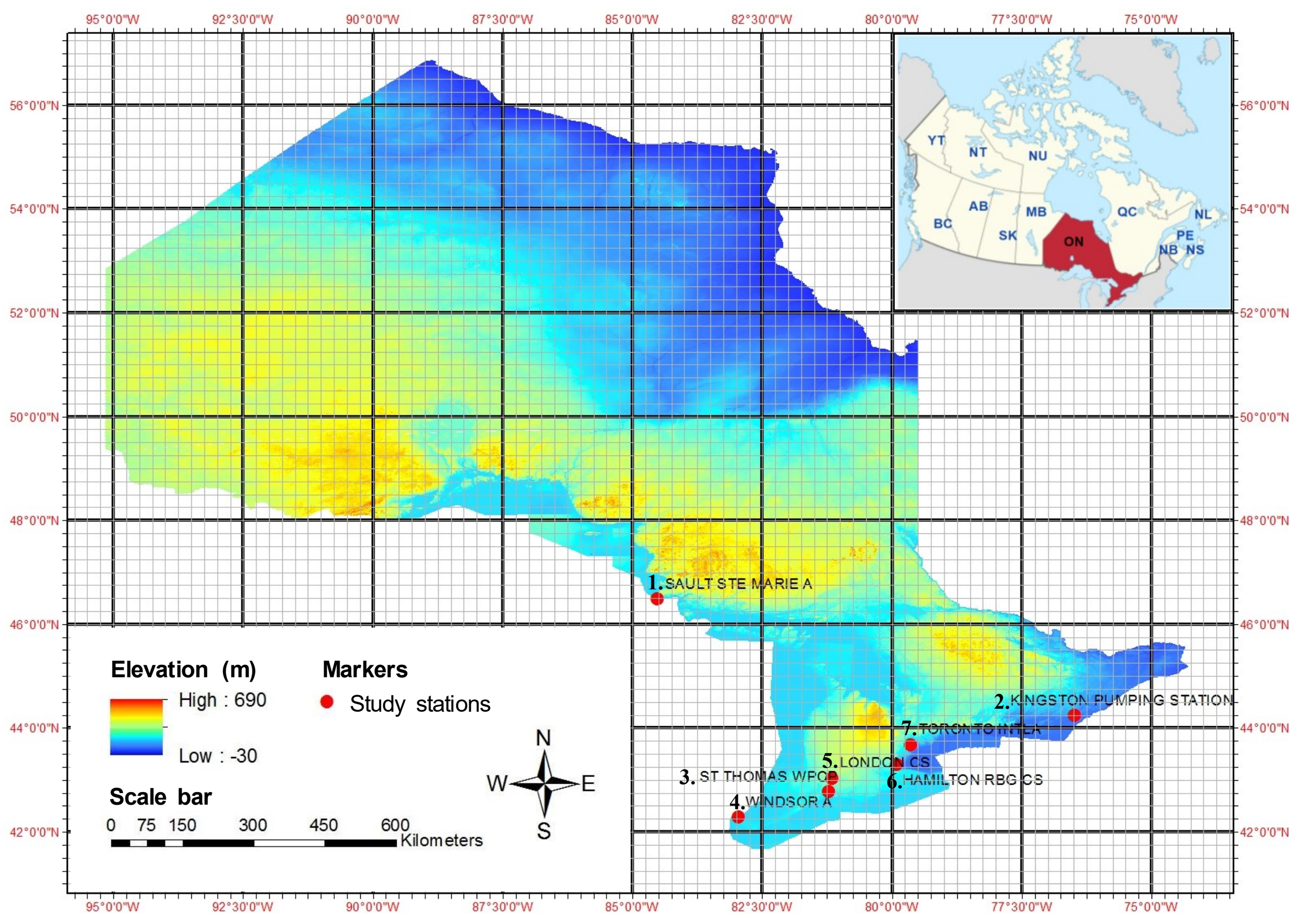

Figure 4-1. Locations of the seven study raingauges (red circle markers). The bold black lines show a common GCM grid of 2.5°x2°, while the gray lines show the NASA grid of 0.25°x0.25°. The provincial digital elevation model was obtained from LIO (2016).

Table 4-2. List of the 21 GCMs used in the research, adapted from IPCC (2019), ENES (2019), and CCIA (2019)

No	Model Name	Model Country	Model Agency/Institution	Grid Resolution	
				Lat (°)	Lon (°)
1	CanESM2	Canada	Canadian Centre for Climate Modelling and Analysis	2.79	2.81
2	CCSM4	USA	National Center for Atmospheric Research	0.94	1.25
3	CESM1-BGC		National Science Foundation, Department of Energy, National Center for Atmospheric Research	0.94	1.25
4	GFDL-CM3		NOAA's Geophysical Fluid Dynamics Laboratory	2.00	2.50
5	GFDL-ESM2G			2.02	2.50
6	GFDL-ESM2M			2.02	2.50
7	ACCESS1-0	Australia	Commonwealth Scientific and Industrial Research Organization (CSIRO) and Bureau of Meteorology (BOM), Australia	1.25	1.88
8	CSIRO-MK3-6-0		Commonwealth Scientific and Industrial Research Organization (CSIRO) in collaboration with Queensland Climate Change Centre of Excellence	1.87	1.88
9	CNRM-CM5	France	National Centre of Meteorological Research, France	1.40	1.41
10	IPSL-CM5A-LR		Institute Pierre-Simon Laplace	1.89	3.75
11	IPSL-CM5A-MR			1.27	2.50
12	MPI-ESM-LR	Germany	Max Planck Institute for Meteorology (MPI-M)	1.87	1.88
13	MPI-ESM-MR			1.87	1.88
14	NorESM1-M	Norway	Norwegian Climate Centre	1.89	2.50
15	BCC-CSM1-1	China	Beijing Climate Center, China Meteorological Administration	2.79	2.81
16	BNU-ESM		College of Global Change and Earth System Science, Beijing Normal University	2.79	2.81
17	INMCM4	Russia	Institute for Numerical Mathematics, Russia	1.50	2.00
18	MIROC5	Japan	Atmosphere and Ocean Research Institute (The University of Tokyo), National Institute for Environmental Studies,and Japan Agency for Marine-Earth Science and Technology	1.40	1.41
19	MIROC-ESM			2.79	2.81
20	MIROC-ESM-CHEM			2.79	2.81
21	MRI-CGCM3		Meteorological Research Institute	1.12	1.13

Note that the climate simulation outputs used in this study are from these models but have been statistically downscaled by NASA to the same regional scale of 0.25° x 0.25° (approximately 25 km x 25 km) for the Representative Concentration Pathways 4.5 scenario (i.e. RCP 4.5) based on the bias-correction spatial disaggregation approach (Thrasher et al., 2012). NASA grid is also plotted on Figure 4-1 and Figure 4-2. Each of the precipitation projections contains data for the periods from 1950 through 2005 ("Retrospective Run") and from 2006 to 2100 ("Prospective Run"). Note that only the data from 1961 to 1990 (reference period or baseline) were used for the calibration processes while those from 1991 to 2005 were used for the validation purposes. The prospective precipitation projections were used to construct future IDF relations for three different periods, including 2011-2040 (2020s), 2041-2070 (2050s), and 2071-2100 (2080s).

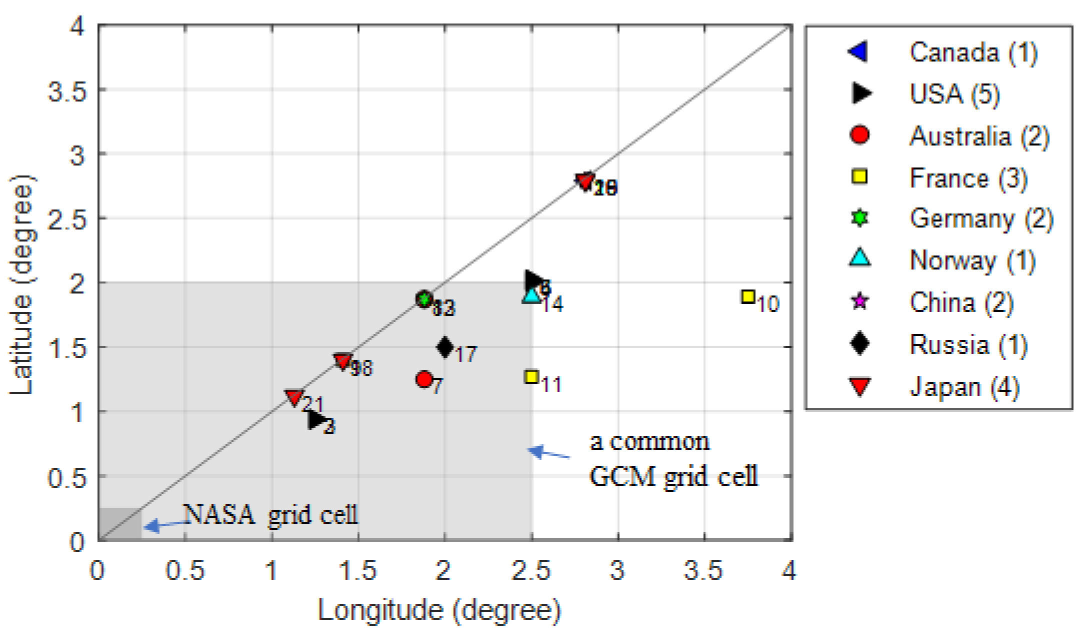

Figure 4-2. Grid resolutions of the 21 GCMs (numbered from 1 to 21 in the plot) from nine different countries (different markers and colors). The resolution of a common GCM grid cell (2.5°x2°) is shown in the big light gray box for the purpose of illustration. The resolution of the NASA grid cell (0.25°x0.25°) is shown in the small dark gray box. The number in bracket in the legend box show the number of GCMs corresponding to those countries.

4.3 Methodology

4.3.1 A statistical approach to modeling extreme rainfall processes over different spatial and temporal scales

The proposed statistical modeling approach consists of two main steps. The first step is to establish the linkage between projected daily extreme rainfalls (ERs) available at a regional scale and daily extreme amounts at a local site of interest; and the second step is to determine the distribution of sub-daily ERs from the estimated daily ERs at the given location. A detailed description of these two steps is given in Figure 4-3 and in the following sections.

4.3.1.1 Linking projected regional climate simulations to local daily extreme rainfalls

As mentioned previously, to construct the extreme rainfall IDF relations at a local site, the first step is to derive the distribution of daily ERs at that location using the daily ER series available at the regional scale (see Figure 4-3). Hence, a spatial statistical downscaling technique is needed to describe the linkage between regional climate variables to weather variables at a local site. In the present study, two approaches were employed for linking the NASA extreme rainfalls available at the regional 25-km scale, $\hat{X}$, to a given local site, X_i. The first method was based on the use of a scaling factor (δ_i) to correct the mean of the regional data and the mean of the at-site data as shown by Eqn. (1). The second method relies on a bias correction function $[e(F)]$ to correct the differences between the empirical cumulative distribution functions (ECDF) of regional and at-site daily ERs as indicated by Eqn. (2). This bias correction function can be represented by a regression model (i.e., a second-degree polynomial function) as shown by Eqn. (3) (Nguyen and Nguyen, 2008; Willems et al., 2012).

$$X_i(F) = \delta_i \cdot \hat{X}(F) \; ; \tag{4-1}$$

$$X_i(F) = \hat{X}(F) + e(F) \; ; \tag{4-2}$$

$$e(F) = c_o + c_1 \cdot \hat{X}(F) + c_2 \cdot [\hat{X}(F)]^2 + \varepsilon \tag{4-3}$$

where $X_i(F)$ is the adjusted daily ER at the local site of interest i; $\hat{X}(F)$ is the daily regional ER at the grid containing that site; F is the cumulative probability of interest; $\delta_i = \mu_i / \hat{\mu}$ is the scaling factor at site i; μ_i and $\hat{\mu}$ are respectively the mean of the daily ERs at the local site i and the mean of the regional values at the grid containing that particular site; $e(F)$ is the bias correction function associated with $\hat{X}(F)$; $c_o, c_1, and\ c_2$ are the coefficients of this function derived using the least square technique and ε is the error term.

4.3.1.2 Linking estimated local daily to sub-daily extreme rainfalls

After estimating the daily ER series at the site of interest, the second step is to derive the statistical properties of sub-daily ER series from the estimated daily series at the same location (see Figure 4-3). In the present study, this sub-daily ER derivation was performed using the scale-invariance probability weighted moment-based Generalized Extreme Values (GEV/PWM) model. The GEV distribution has been widely used for representing the probability distribution of ERs and for constructing the rainfall IDF relations as recommended in a number of guidelines for hydrological practices by the World Meteorological Organization (WMO, 2009a) as well as by many other countries such as Australia, Austria, Germany, Italy, and Spain (Salinas et al., 2014b; Ball et al., 2016; Nguyen et al., 2017). In addition, the GEV/PWM model has been recently shown to perform superior than other existing scale-invariance models (Nguyen and Nguyen, 2018a). More specifically, the quantile, X_T, corresponding to a given return period $T = 1/(1 - F)$, of the

GEV model can be estimated using Eqn. (4-4), and the PWM method can be used for estimating the GEV parameters as shown in Eqn. (4-5) for the *r*th-order PWM β_r (Hosking et al., 1985).

$$X_T = \xi + \frac{\alpha}{\kappa}\{1 - [-\ln(F)]^{\kappa}\} \tag{4-4}$$

$$\beta_r = M_{1,r,0} = E[X\,\{F(X)\}^r] = (r+1)^{-1}\left(\xi + \frac{\alpha}{\kappa}\{1 - (r+1)^{-\kappa}\,\Gamma(1+\kappa)\}\right) \tag{4-5}$$

in which $\xi, \alpha,$ and κ are the location, scale, and shape parameters respectively; and F is the cumulative probability of interest. $\Gamma(.)$ is the gamma function and r must be non-negative;

For a simple scaling process, it can be shown that the relation between the r^{th}-order PWMs of rainfalls for two different rainfall durations t and λt can be expressed by Eqn. (4-6) (Nguyen and Nguyen, 2018a).

$$\beta_r(\lambda t) = \lambda^{\eta_r}\beta_r(t) = \lambda^{\eta}\beta_r(t) \tag{4-6}$$

where $\eta_r = \eta$ is the scaling exponent and can be estimated based on the mean $E\{X\}$ (that is, the PWM of order $r = 0$.

This infers that the scaling exponents η_r are constant across all PWM orders r for the same rainfall scaling regime. In other words, the plot of the scaling exponents η_r (y-axis) with the PWM orders r (x-axis) should display a horizontal line rather than a linear sloping line as for the case of the ordinary statistical moments (Nguyen et al., 2002b). Furthermore, for the simple scaling process, it can be shown that the parameters and quantiles of the GEV/PWM model of time scale λt and t are related as follows:

$$\kappa(\lambda t) = \kappa(t)\ \ ;\ \ \alpha(\lambda t) = \lambda^{\eta}\alpha(t)\,;\ \ \ \xi(\lambda t) = \lambda^{\eta}\xi(t); \tag{4-7}$$

$$X_T(\lambda t) = \lambda^{\eta}X_T(t); \tag{4-8}$$

In summary, based on these equations, it is possible to derive the distributions and statistical properties (quantiles and parameters) of short-duration ERs from those of longer durations at a given study site. The indirect method is employed as it yields better result than the direct method (see Chapter 3). The first three PWMs of the sub-daily and sub-hourly AMS are computed from those of the daily AMS at the local site of interest obtained from the spatial downscaling step. These PWMs are then used for estimating the three parameters and the distributions as well as quantiles of the GEV/PWM model.

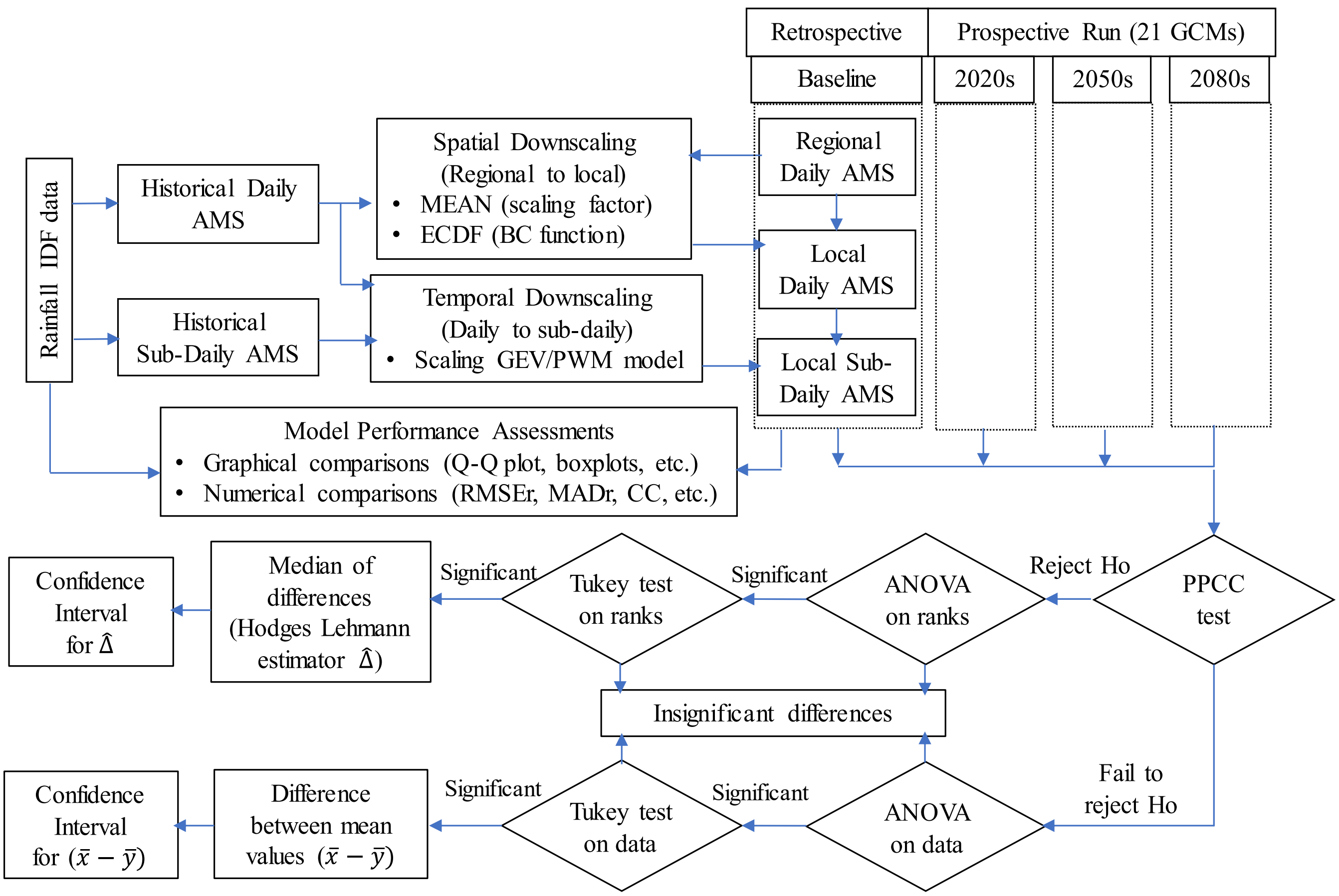

Figure 4-3. Flowchart of the proposed method for assessing climate change impacts on local short-duration extreme storm

4.3.2 Model comparison criteria

4.3.2.1 Goodness-of-fit tests

In the present study, six common goodness-of-fit (GOF) criteria were selected for assessing the feasibility and accuracy of the proposed spatio-temporal statistical downscaling (STSD) procedure for estimating short-duration (sub-daily) extreme design rainfalls (or IDF relations) at a local site in the context of climate change. These criteria include the root mean square error (RMSE), the root mean square relative error (RMSEr), the mean absolute deviation (MAD), the mean absolute relative deviation (MADr), the adjusted coefficient of determination (R_{adj}^2), and the correlation coefficient (CC) as follows:

$$RMSE = \left\{\sum \frac{(x_i - y_i)^2}{(n-m)}\right\}^{\frac{1}{2}} \tag{4-9}$$

$$RMSEr = \left[\frac{1}{(n-m)}\sum\left\{\frac{(x_i - y_i)}{x_i}\right\}^2\right]^{\frac{1}{2}} \tag{4-10}$$

$$MAD = \frac{1}{(\mathrm{n-m})}\sum|x_i - y_i| \tag{4-11}$$

$$MADr = \frac{1}{(\mathrm{n-m})}\sum\left\{\frac{|x_i - y_i|}{x_i}\right\} \tag{4-12}$$

$$R_{adj}^2 = 1 - \frac{(n-1)}{(n-m-1)} \times (1 - R^2) \tag{4-13}$$

$$CC = \frac{\sum\{(x_i - \bar{x})(y_i - \bar{y})\}}{\{\sum(x_i - \bar{x})^2 \sum(y_i - \bar{y})^2\}^{\frac{1}{2}}} = R \tag{4-14}$$

where $x_i, i = 1,2, \dots, n$ are the observed values and $y_i, i = 1,2, \dots, n$ are the estimated values for the same probability level p_i; n is the sample length; $\bar{x}$ and $\bar{y}$ denote the average value of the observed and estimated quantiles, respectively; m is the number of model parameters and by default $m = 0$ when comparing between the observed and estimated values. However, for the case of comparison of two different approaches used in the bias correction step (Section 4.3.1.1), the number of model parameters m must be taken into account to provide a fair comparison. Depending on the approach, $m = 1$ for the simple scaling factor (i.e. the MEAN approach), and $m = 2$ for the second-degree polynomial function (i.e. the ECDF approach). Note that for a simple linear regression between two variables, the coefficient of determination R^2, also known as fraction of the variance explained by regression, equals to the square of the correlation coefficient (Helsel and Hirsch, 2002; Berthouex and Brown, 2002).

4.3.2.2 Multiple comparison tests

To test whether there is a significant change in the estimated extreme design rainfalls between different time periods (reference period and projected periods or between different projected periods), a two-stage test for comparing several independent groups are required (Helsel and Hirsch, 2002; Berthouex and Brown, 2002). In the first stage, the main purpose of the test is to determine if all k groups have the same central value or whether at least one of the groups differs from the others. Following this stage, another test is carried out to identify what pairs are significantly different in the second stage. To achieve this, different parametric or non-parametric approaches can be used. The choice of a parametric or non-parametric method depends upon the normality assumption of the data distribution. To check this assumption, the probability plot correlation coefficient (PPCC) test is employed in this research (Helsel and Hirsch, 2002).

When data within each of the groups are normally distributed and possess identical variances, the popular parametric test known as an analysis of variance (ANOVA) can be used to determine whether each group's mean is identical (Helsel and Hirsch, 2002; Berthouex and Brown, 2002). This is an extension of t-test between two groups and often known as a t-test between three or more groups. When there are only two groups, the ANOVA becomes identical to a t-test. That is, the F statistic becomes equal the square of the two-sample t-test statistic $F = t^2$, and will have the same p-value. Hence, ANOVA is restricted by the same types of assumptions as is a t-test.

When every group of data cannot be assumed to be normally distributed or have identical variance, a nonparametric test equivalent to ANOVA known as Kruskal-Wallis test should be used to determine whether each group's median is identical (Helsel and Hirsch, 2002). This test is much similar to a rank-sum test extended to more than two groups. The exact version of Kruskal-Wallis test is only useful for small sample sizes (normally less than or equal to 10). When the sample sizes become larger, this is rarely required as the tables of the exact p-values for all sample sizes would be huge and cumbersome due to many possible combinations of numbers of groups and sample sizes per group. With sample sizes of greater than or equal to 20, the large-sample approximation (a chi-square approximation) or the rank transformation test (i.e. by ranking the data and performing ANOVA on the ranks, also known as F approximations) are computed. The F and chi-square approximations will result in very similar p-values (Helsel and Hirsch, 2002).

The ANOVA F-test on the original data or on the ranks of the data are thus used in this research to detect whether there is a statistically significant difference among the groups. Details of how to perform an ANOVA test is provided in the appendix.

Following the ANOVA step, the Tukey's HSD (also called Tukey's range) post-hoc test is utilized to identify what pairs are significantly different. Note that if one only wishes to compare the difference in extreme rainfalls between the baseline (reference period) and the projected period, then the Dunnett's method can be applied to figure out what treatments are significantly different from the control. In this case, instead of k treatments to compare, there are now only $(k-1)$ treatments. Note that since they are post-hoc tests, hence, if ANOVA is conducted on the ranks of data, then Tukey's or Dunnett's approach must be performed on the ranks as well. In this paper, since we are interested in all possible differences in extreme rainfalls between the reference period and the projected periods as well as between different projected periods, the Tukey's test is selected. Details of how to conduct a Tukey's test is provided in the appendix.

The magnitude of difference as well as the associated confidence interval for a selected pair can also be computed using the Hodges-Lehmann estimator for the non-parametric approach or simply the difference between the two mean values for the parametric approach (see the appendix).

4.4 Results and Discussion

4.4.1 Estimation of bias-corrected daily extreme rainfalls at a local site

The performance of the two methods for downscaling of daily extreme rainfalls from regional to local scale were first investigated and compared using different graphical displays and numerical criteria. Historical data from the seven raingauges and the "Retrospective Run" data from NASA in the same time period from 1961-2005 were used for the result assessments. The split-half sample was employed to compare the two methods. The first half of data were used for estimating the scaling factors $(\delta)$and the bias correction functions $[e(F)]$ as described in Section 4.3.1.1, while the remaining data were employed for validation of these estimations. Note that similar to the previous study by Nguyen et al. (2007), the use of a second-order polynomial function in the ECDF method has been found acceptable for correcting the bias between the daily extreme regional and at-site rainfall values for all seven study sites.

For purposes of illustration, Figure 4-4 shows the graphical comparison of the probability plots before and after bias corrections for the Windsor Airport Station using the two considered bias-correction methods and the data of all 21 climate models. The medians of the ensemble of 21 models and observed data are also plotted for comparison. Numerical comparisons based on different goodness-of-fit (GOF) tests between observed data and estimated values (medians of 21 models) were also carried out to evaluate the accuracy of the proposed bias-correction methods. Results are shown in Figure 4-5 for the Windsor Airport station. Similar plots were produced for all other study sites and provided in the supplemental document.

Based on the graphical and numerical comparisons of all seven stations, it can be concluded that the ECDF method produces a more accurate result for the calibration period (i.e. from 1961 to 1983) than the MEAN method. This is expected since the ECDF approach uses a more complex functions with more parameters (i.e. a second-degree polynomial function) to correct the whole empirical distribution, it should be able to capture the moments of higher orders of the observed data in the calibration step much better than the MEAN method which uses only a simple scaling ratio between the regional and local values. The question then arises whether the ECDF is stable and continues to perform well for the validation period. This question is critical as the calibrated parameters will be then applied to different projected periods to correct the projected daily extreme rainfalls.

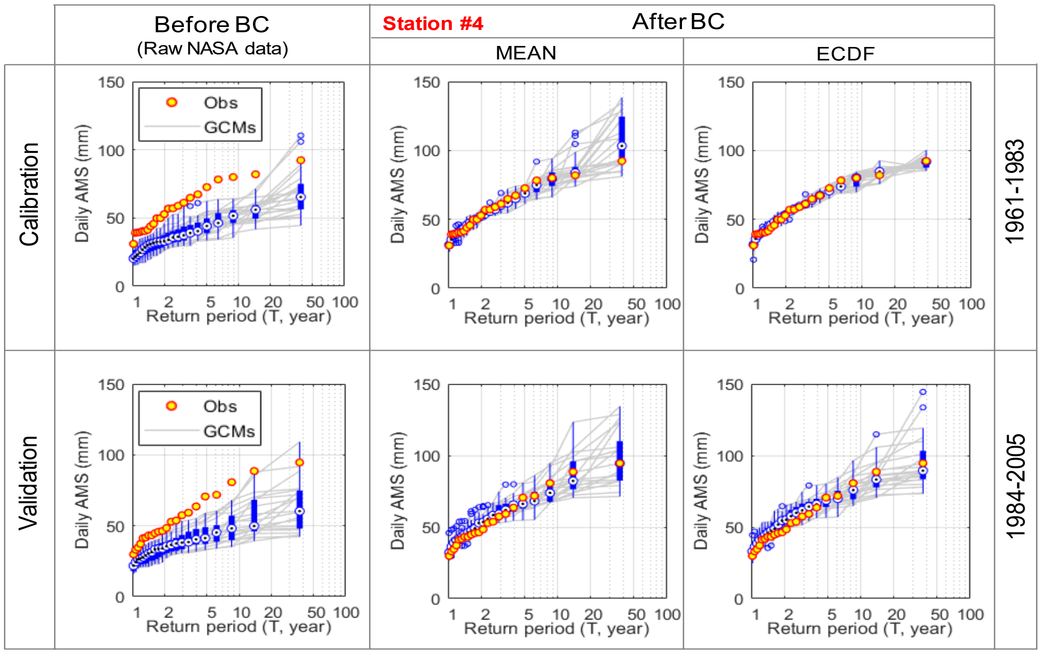

Figure 4-4. Comparison between the distributions of the observed local daily annual maximum series (AMS, yellow markers) and the NASA regional daily AMS (gray lines and boxplots of the 21 models) before and after bias correction (BC) for calibration (1961-1990) and validation (1991-2005) periods using a scaling factor to correct the mean (MEAN) and using a BC function to correct the empirical cumulative distribution function (ECDF) at Windsor Airport station.

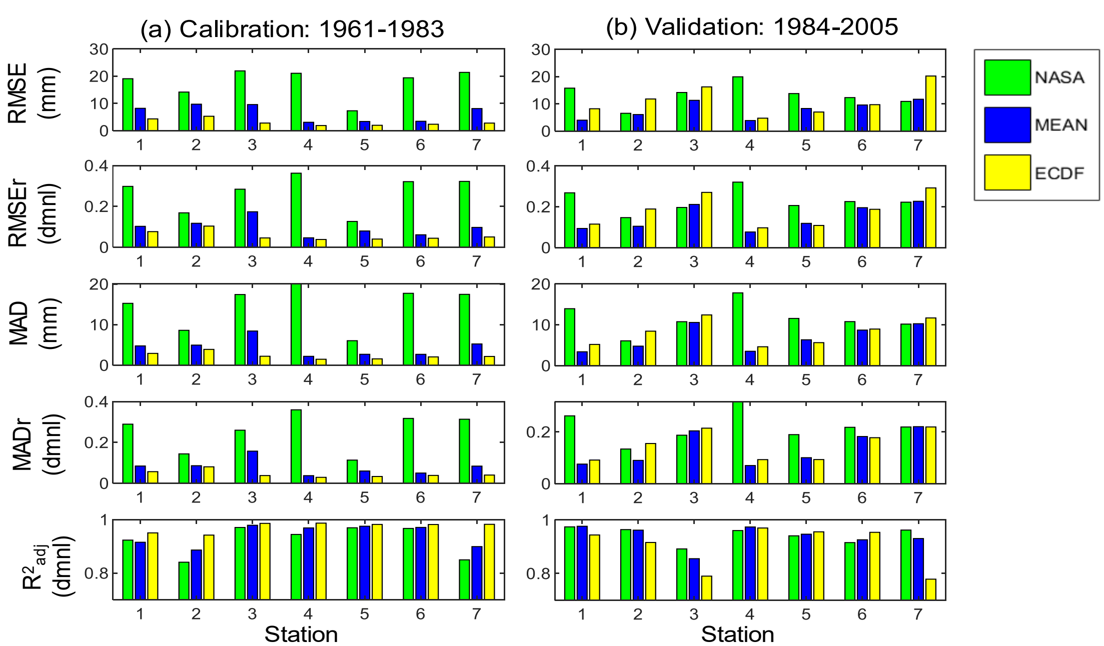

Figure 4-5. Comparison of goodness-of-fit results of the two bias-correction methods (i.e. MEAN and ECDF) for the spatial downscaling at all stations. The green column shows the results before bias correction (i.e. NASA gridded data). Units: mm = millimetre, dmnl = dimensionless.

Graphical and numerical comparisons of the performance of the two bias-correction approaches over the validation period are also presented in Figure 4-4 and Figure 4-5 for the Windsor Airport Station. It can be seen that the two methods provide comparable results for this station based on the comparison of the median and the observation of the boxplot sizes and whiskers. However, this is not the case for other study sites. More specifically, for these sites, it was found that the ECDF method not only produces less accurate results (for the median of the ensemble of 21 models) but more importantly, this method is highly unstable (see the size of the boxes and whiskers of the ensemble of 21 models). The reason is that when using a more complex function to correct the bias, this correction could provide a better fit to the calibrated data range (i.e., interpolation). Hence, if the data range for the validation period is almost in the same range of data used for model calibration (i.e. involving only interpolation), the ECDF method could work well as it was shown in Figure 4-4 for the Windsor Airport station. However, when applying the computed bias-correction function to the validation data that are beyond the selected calibrated data range (i.e. involving extrapolation), the bias-corrected values obtained might be not in good agreement with the observed values and this difference depends on the degree of extrapolation required. The bias in that case is thus not reduced but could be inflated instead. The severity of the inflation is proportional to the degree of extrapolation. For example, Station #5 – London CS Station, is much less severe compared to Station #7 – Toronto International Airport Station. The more complex the bias-correction function is (i.e., the better fit to the calibrated data is achieved), the less flexible the model can capture the validated data representing different conditions that have not been observed in the calibration period. Even with the use of a second-degree polynomial in the ECDF approach, the extrapolation could yield very different and unrealistic results, especially under different climate change scenarios under which the future extreme rainfalls are expected very likely to increase.

Hence, the bias correction of the whole empirical distribution function by the ECDF method to obtain a perfect agreement with the observations during calibration as suggested in some previous studies (Willems et al., 2012) is unnecessary since it may result in less accurate and unstable results for validation purposes. Therefore, in the present study, the MEAN method was selected to estimate the bias-corrected daily ER series at all seven study sites based on the available regional 25-km NASA extreme rainfalls for both the Retrospective Run (from 1961 to 2005) and the Prospective Run (from 2006 to 2100). Note that to be consistent, data from the reference period (1961-1990) was used to calibrate the model before applying to three future projected periods. The split-half sample discussed above is only applied to the comparison of the two bias correction methods.

4.4.2 Estimation of sub-daily extreme rainfalls at a local site

4.4.2.1 Validation of the scaling GEV/PWM approach

To estimate the distribution of sub-daily ER series at a given site for future climate, the scale-invariance GEV/PWM model presented in Section 4.3.1.2 was used. The feasibility and accuracy of the scaling model in reproduction of the historical record data was first assessed using the observed daily and sub-daily annual maximum series (AMS) at all study sites. Data from 1961-1990 at each site were selected for calibration while the remaining data (see Table 4-1) were utilized for validation.

Figure 4-6 shows the comparison of the distributions of the eight sub-daily AMS (from D = 5 to 720 minutes) that were estimated based on the scaling model and the traditional at-site frequency analysis (ASFA) approach for two different stations: Sault Ste Marie Airport and Windsor Airport stations. According to the at-site frequency analysis method, the theoretical GEV distribution was independently fitted to each daily and sub-daily AMS without considering the relationships between the statistical properties of these AMS over different rainfall durations. The scaling model considers these temporal relationships and computes the distributions of the sub-daily AMS from the fitted distribution of the daily data. Results from Figure 4-6 indicates that the extreme rainfall quantiles estimated using the proposed scaling model agree very well with those values given by the independently fitted distributions based on the ASFA approach (with very low RMSEr and MADr values, less than 5%; and high CC values, about 0.99) for both stations even the two stations display quite different tail behaviors.

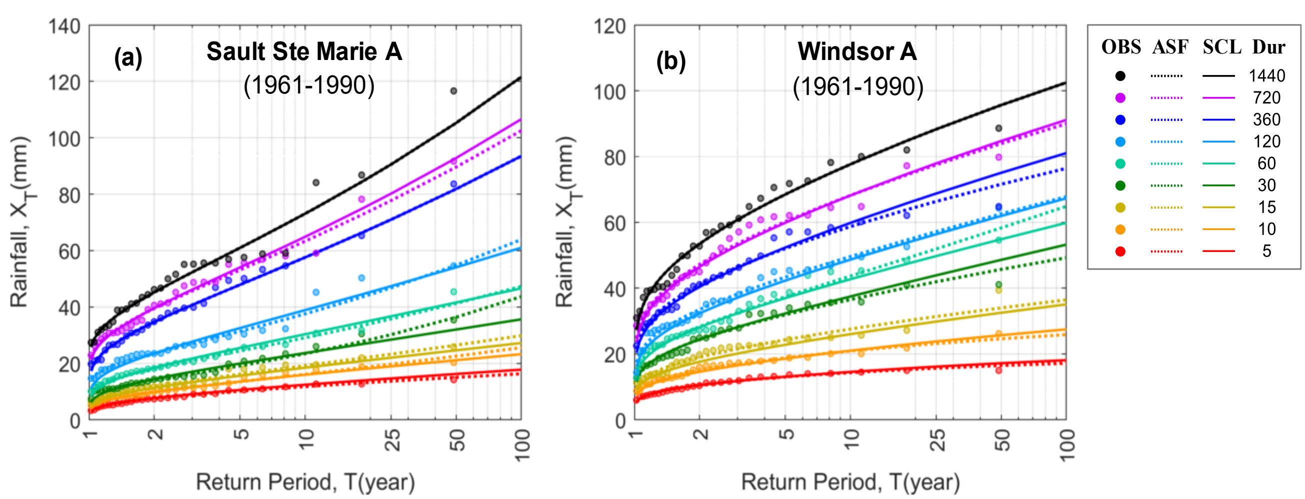

Figure 4-6. Depth-duration-frequency curves derived based on the at-site frequency analysis approach (ASF, dash lines) and the scaling GEV/PWM model (SCL, continuous lines) at (a) Sault Ste Marie Airport and (b) Windsor Airport stations. Markers shows the observed (OBS) data of rainfall durations ranging from D = 1440 to 5minutes

Graphical and numerical evaluations of the proposed scaling model in the estimation of the sub-daily extreme design rainfalls (for six return periods from T = 2 to 100 years and for eight rainfall durations from D = 5 to 720 to minutes) for the calibration period at all seven study sites are shown in Figure 4-7(a) and Table 4-3. Results again point out that the proposed scaling model performs very well in reproduction of the historical data with values of RMSEr and MADr ranging from 3 to 10%, and CC all higher than 0.98.

Validation of the proposed scaling model for the remaining data using graphical comparison and numerical criteria are presented in Figure 4-7(b) and Table 4-3. Note that the data for this period are much shorter with the average sample length is about 20 years. The extreme design rainfalls were thus computed for only five short return periods from T = 2 to 50 years. Results show a wider range of computed values for all numerical criteria; that is, from 7 to 23% for the RMSEr and MADr values, and from 0.97 to 0.99 for the CC values (i.e. lower accuracy compared to the calibration period as expected).

In summary, based on the superior performance of the proposed scaling GEV/PWM model in its capability to describe accurately the distribution of historical extreme rainfall data at all sites, this scaling model can be used to derive the distributions of projected sub-daily extreme rainfalls.

Table 4-3. GOF results of the extreme rainfall quantiles estimated based on the at-site frequency analysis and the scaling approach using historical record at each study site. Extreme rainfall quantiles are computed for return periods up to T = 100 years for the calibration period and up to T = 50 years for the validation period.

Stn	Calibration period (T = 2, 5, 10, 25, 50, 100 years)				Validation period (T = 2, 5, 10, 25, 50 years)			
	Data	RMSEr	MADr	CC	Data	RMSEr	MADr	CC
1	1961-1990	0.05	0.03	0.998	1991-2007	0.14	0.11	0.981
2		0.06	0.04	0.996	1991-2007	0.15	0.12	0.983
3		0.07	0.05	0.994	1991-2004	0.16	0.13	0.986
4		0.04	0.03	0.998	1991-2007	0.13	0.10	0.990
5		0.10	0.08	0.983	1991-2016	0.23	0.14	0.974
6		0.08	0.07	0.992	1991-2016	0.09	0.07	0.991
7		0.06	0.05	0.996	1991-2017	0.15	0.12	0.984

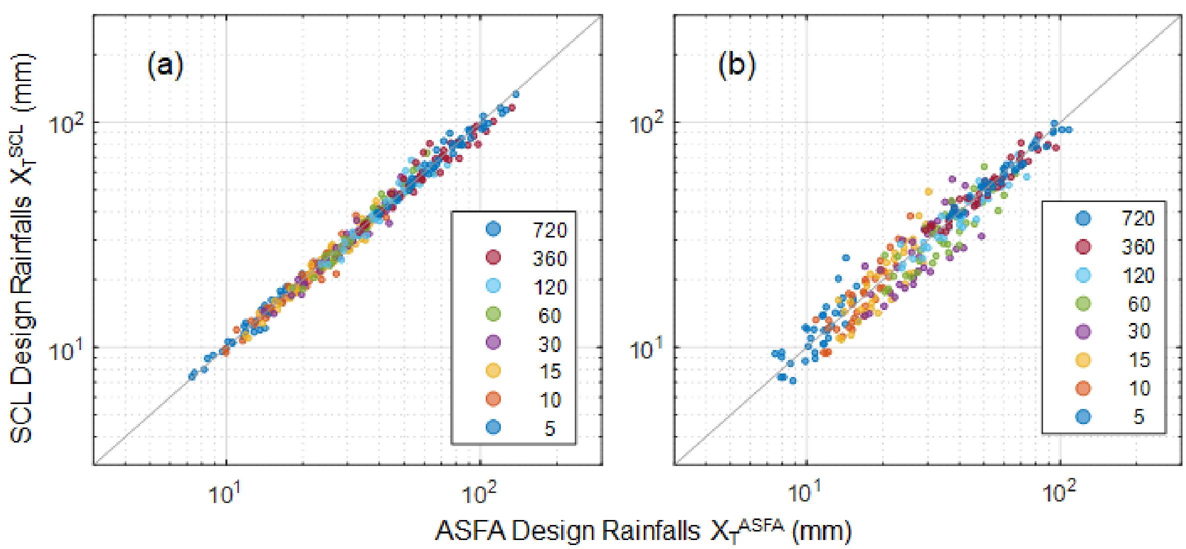

Figure 4-7. Q-Q plots of the extreme design rainfalls of all seven study stations estimated using the at-site frequency analysis approach (ASFA design rainfalls X_T^{ASFA}, mm) and the scaling GEV/PWM model (SCL design rainfalls X_T^{SCL}, mm) for different sub-daily rainfall durations (different marker colors, D = 720 minutes to 5 minutes) for (a) the calibration period with return periods up to T = 100 years and (b) the validation period with return periods up to T = 50 years. Note that the return period values T = 2, 5, 10, 25, 50, and 100 years.

4.4.2.2 Estimation of projected sub-daily extreme rainfalls at a local site

The proposed scaling model was applied to the bias-corrected daily extreme rainfalls given by all 21 models for the "Retrospective Run" data to derive the sub-daily extreme rainfalls. For purposes of illustration, Figure 4-8 shows the probability plots of the observed and computed extreme rainfalls X_T (mm) for different rainfall durations at Windsor Airport Station for the reference period (1961-1990). The uncertainties associated with the estimation of these values are displayed in the form of standard boxplots based on the ensemble of 21 GCM's. In general, it can be seen that the observed values fall in the range of the estimated values of 21 models. Numerical comparisons based on the medians of the 21 models and the observed data indicate a high agreement between them with RMSEr, MADr, and CC approximately 7%, 5%, and 0.99, respectively. Similar computations were carried out for each study site and for the validation period (1991-2005). Results are provided in Table 4-4.

For all seven study sites, the Q-Q plots of the estimated extreme design rainfalls derived based on the scale-invariance GEV/PWM and the at-site frequency analysis using the GEV distribution are presented in Figure 4-9. Note that the median values of the results from 21 GCMs are used for the computation. There are six plots for six return periods from T = 2 to 100 years. Each of these plots contains the design rainfalls values for all nine rainfall durations from D = 5 to 1440 minutes. Numerical comparisons were also conducted to evaluate the overall results for all sites as shown in Table 4-5.

The low values of RMSEr and MADr as well as the high values of CC indicate that the proposed spatio-temporal statistical downscaling procedure are feasible and accurate in estimating extreme design rainfalls for a given location. The procedure was then applied for estimating the projected sub-daily ER series for three future periods using the daily "Prospective Run" (2011-2100) data at each site.

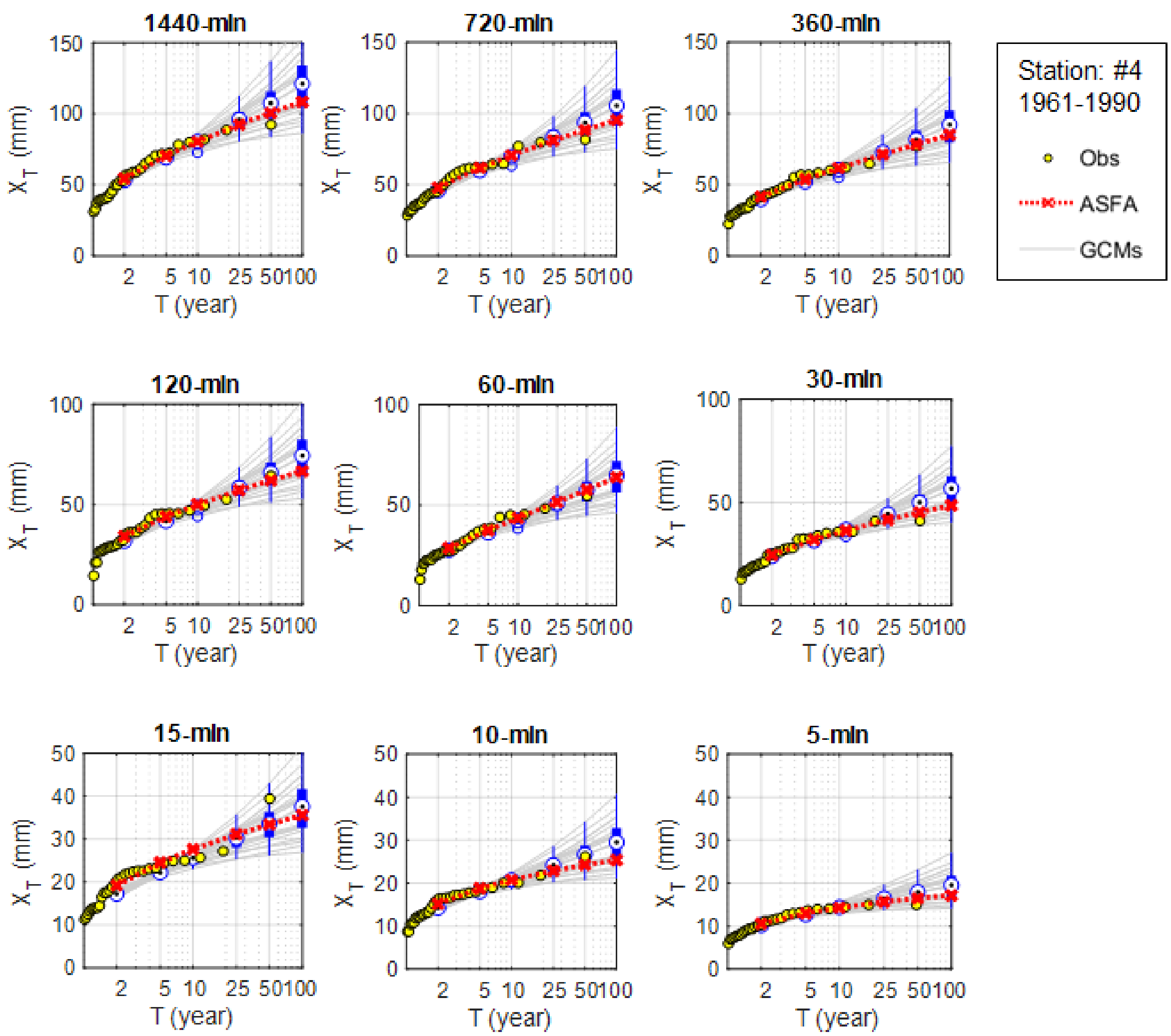

Figure 4-8. Cumulative distribution function (CDF) plots of the computed extreme design rainfalls X_T (mm) for all nine different durations (nine subplots from D = 1440 to 5 minutes) at station #4 - Windsor Airport Station. For each subplot, the yellow markers show the empirical CDF of the observed extreme rainfall data from 1961-1990, the red discontinuous lines show the theoretical CDF based on at-site frequency analysis using the GEV distribution, and the gray lines show the estimated CDF derived using the proposed procedures for all 21 models. In addition, the red cross markers show the extreme design rainfalls X_T (for return periods T = 2, 5, 10, 25, 50, 100 years) using the at-site frequency analysis, while the boxplots show the uncertainty in estimation of those values using the ensemble of 21 models.

Table 4-4. GOF results of the estimated and observed IDF data at each study site

Stn	Calibration period 1961-1990			Validation period 1991-2005		
	RMSEr	MADr	CC	RMSEr	MADr	CC
1	0.136	0.109	0.989	0.207	0.165	0.932
2	0.120	0.102	0.987	0.123	0.106	0.985
3	0.137	0.121	0.991	0.241	0.198	0.987
4	0.065	0.051	0.995	0.159	0.138	0.984
5	0.086	0.064	0.980	0.198	0.165	0.956
6	0.169	0.128	0.973	0.169	0.135	0.948
7	0.176	0.147	0.967	0.241	0.189	0.968

Table 4-5. GOF results of the estimated and observed IDF data for different return periods

	Calibration period 1961-1990					Validation period 1991-2005			
T (year)	2	5	10	25	50	2	5	10	25
RMSEr	0.050	0.058	0.086	0.135	0.172	0.215	0.171	0.143	0.155
MADr	0.044	0.046	0.072	0.119	0.152	0.165	0.140	0.119	0.126
CC	0.995	0.996	0.993	0.979	0.961	0.979	0.980	0.974	0.954

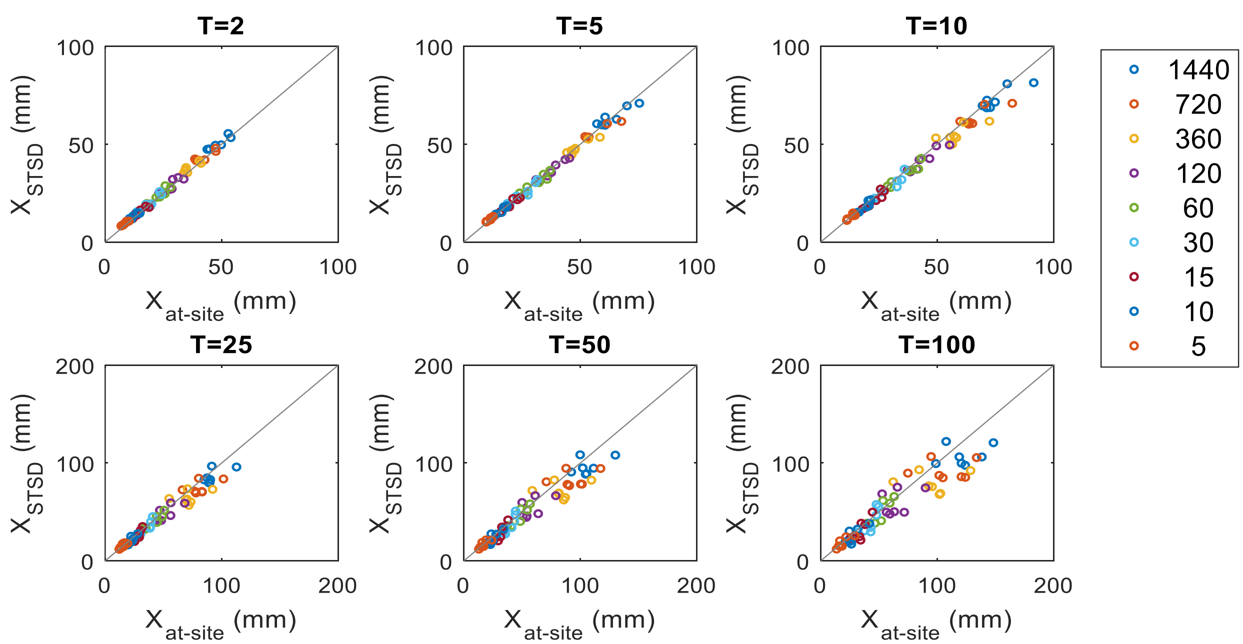

Figure 4-9. Q-Q plots of extreme rainfalls computed using the proposed spatial-temporal statistical downscaling procedure (X_{STSD}, mm) and the at-site frequency analysis ($X_{at\text{-}site}$, mm) for different rainfall durations (from D = 1440 to 5 minutes) and for different return periods (T = 2 to 100 years) of the 1961-1990 calibration period.

4.4.3 Climate change impacts on local extreme storms

Figure 4-10 shows the projected ERs at Windsor Airport Station for three different return periods (T = 10, 50, and 100 years) and three different rainfall durations (D = 5, 60, and 1440 minutes) for three future periods 2020s (2011-2040), 2050s (2041-2070), and 2080s (2071-2100) under the RCP 4.5 scenario as compared to the ERs for the reference "baseline" period (1961-1990). Similar plots were produced for other stations. It can be seen that, for Windsor Airport Station, there are small differences in the median values between the baseline and projected periods as well as between the projected periods. However, for other stations, the differences are much larger.

To evaluate whether the differences are statistically significant or not, the multiple comparison tests described in Section 4.3.2.2 were used. For each multiple comparison test, there are four different groups (i.e. four treatments), including the reference period and three projected periods. Each group contains the design rainfalls from 21 models. To decide whether the ANOVA test and Tukey's HSD test should be performed on the data or on the ranks, PPCC tests were first conducted with the significant level $\alpha = 0.05$ (i.e. the critical value $r* = 0.95$).

Results of PPCC tests are presented in Figure 4-11.(a) for Windsor Airport Station as an example. For this station, 4% of the data did not pass the test (i.e. the null hypothesis H_0 was rejected). Similar things occurred to station number #1 – Sault Ste. Marie Airport (17%), number #2 – Kingston pumping (8%), number #6 – Hamilton RBG CS (14%), and especially number #7 – Toronto International Airport (26%). Only station #3 – St. Thomas WPCP and station #5 – London CS passed the test at $\alpha = 5\%$ (i.e. failed to reject H_0). Plots similar to Figure 4-11 are produced for all other stations and provided in the appendix. Note that if $\alpha = 1\%$ ($r* = 0.93$) is used instead, then all stations could be considered passing the test. Observation of the distribution of each data group (i.e. boxplots in Figure 4-11) indicates that data is not normally distributed and there are also outliers. Therefore, the ANOVA and Tukey's tests were performed on the ranks. The tests on the original data were also conducted as a reference.

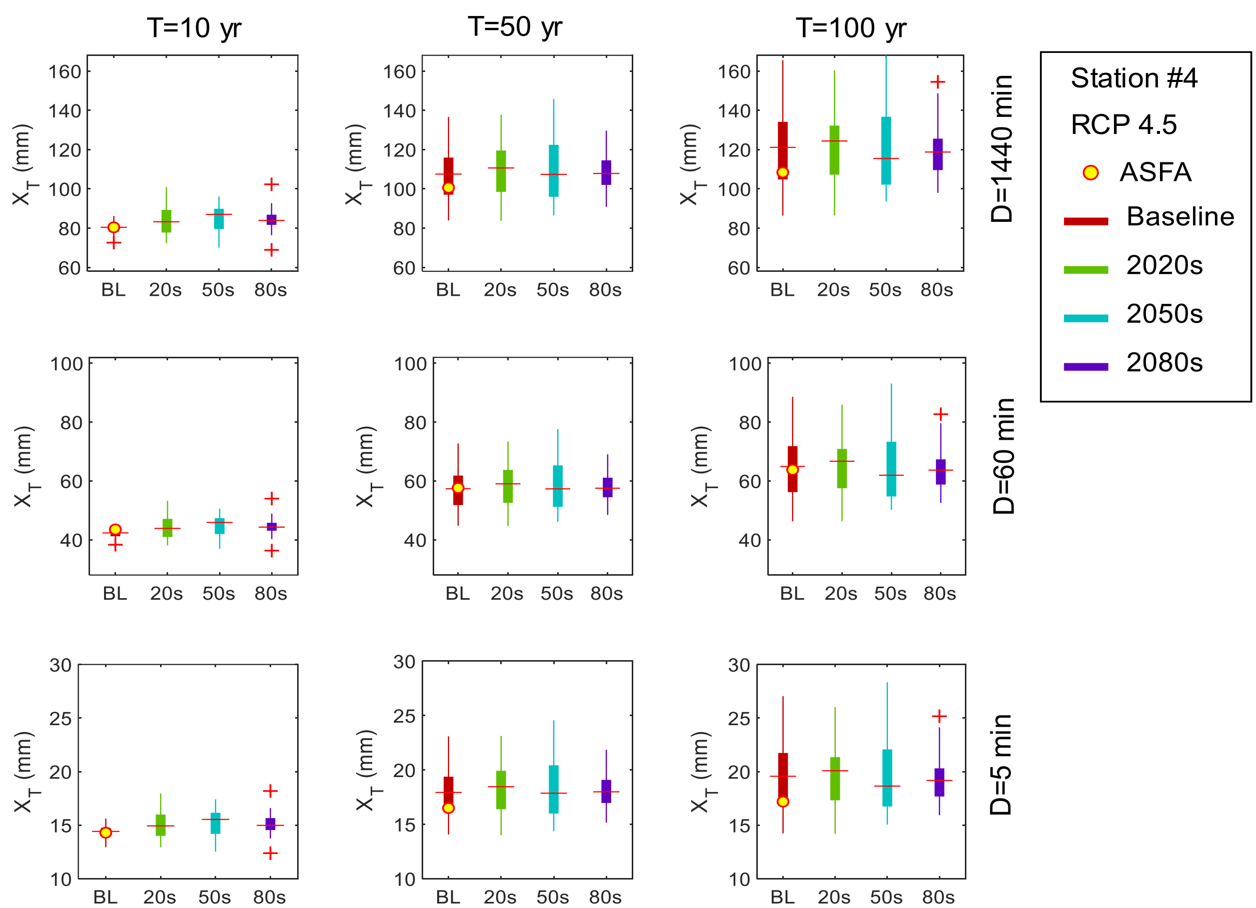

Figure 4-10. Projected extreme design rainfalls at station #4 – Winsor Airport Station, for three return periods (T = 10, 50, and 100 years) and for three durations (D = 1440, 60, and 5 minutes) using data for the current period of 1961-1990 (Baseline), and for future periods 2011- 2040 (2020s), 2041-2070 (2050s), and 2071-2100 (2080s) under the RCP 4.5 scenario. The yellow circles show the at-site frequency analysis (ASFA) values.

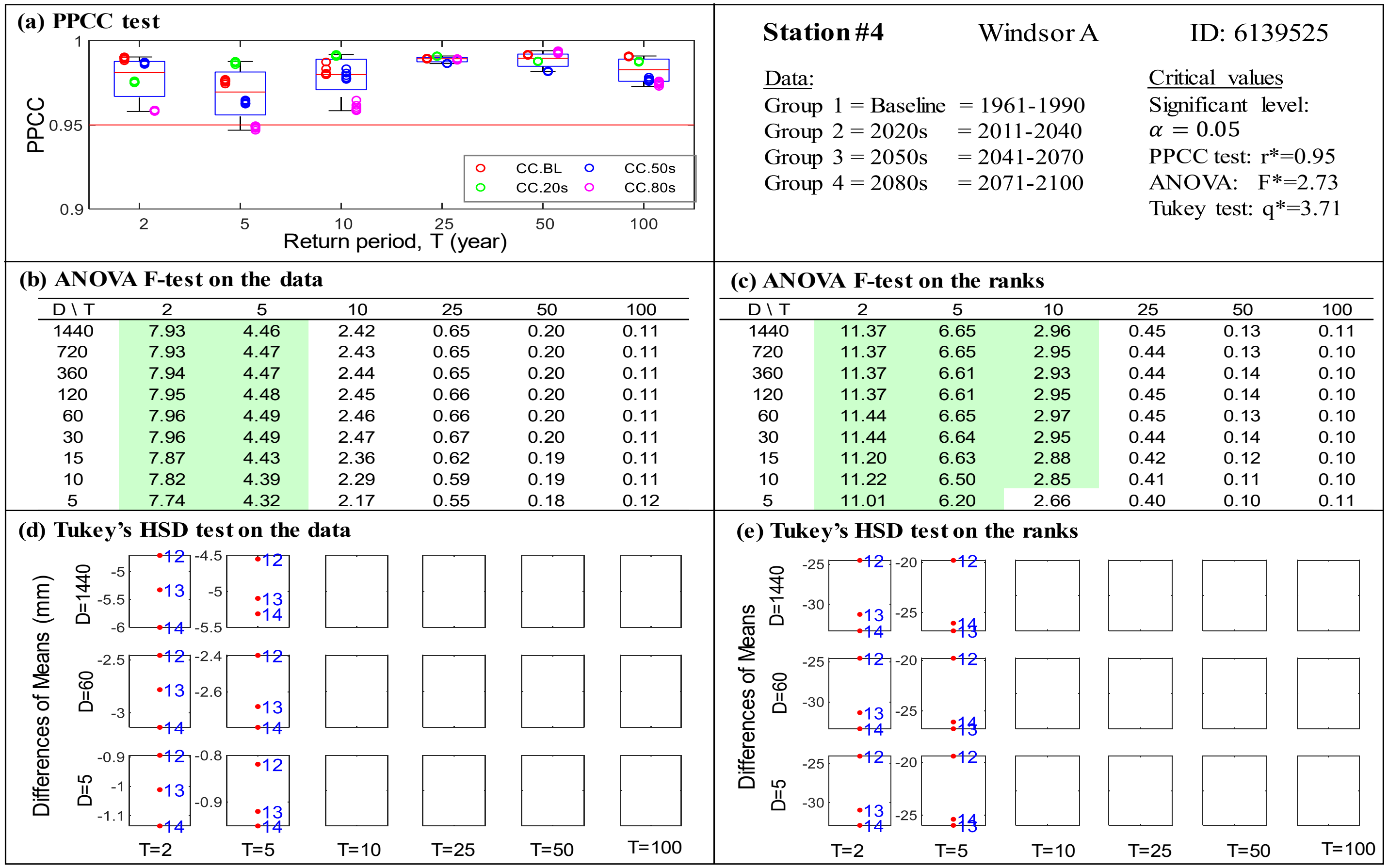

(b) ANOVA F-test on the data

D \ T	2	5	10	25	50	100
1440	7.93	4.46	2.42	0.65	0.20	0.11
720	7.93	4.47	2.43	0.65	0.20	0.11
360	7.94	4.47	2.44	0.65	0.20	0.11
120	7.95	4.48	2.45	0.66	0.20	0.11
60	7.96	4.49	2.46	0.66	0.20	0.11
30	7.96	4.49	2.47	0.67	0.20	0.11
15	7.87	4.43	2.36	0.62	0.19	0.11
10	7.82	4.39	2.29	0.59	0.19	0.11
5	7.74	4.32	2.17	0.55	0.18	0.12

(c) ANOVA F-test on the ranks

D \ T	2	5	10	25	50	100
1440	11.37	6.65	2.96	0.45	0.13	0.11
720	11.37	6.65	2.95	0.44	0.13	0.10
360	11.37	6.61	2.93	0.44	0.14	0.10
120	11.37	6.61	2.95	0.45	0.14	0.10
60	11.44	6.65	2.97	0.45	0.13	0.10
30	11.44	6.64	2.95	0.44	0.14	0.10
15	11.20	6.63	2.88	0.42	0.12	0.10
10	11.22	6.50	2.85	0.41	0.11	0.10
5	11.01	6.20	2.66	0.40	0.10	0.11

Figure 4-11. Multiple comparison tests for station #4 – Windsor Airport station; (a) Results of PPCC tests for four groups: group 1 (baseline), group 2(2020s), group 3(2050s), and group 4 (2080s). For each group, there are nine rainfall durations (D = 1440 to 5 minutes) and six return period values (T = 2 to 100 years). Boxplots summarize the PPCC results of all four groups for each return period; (b) and (c) ANOVA F-test results for a selected rainfall duration and return period on data and ranks respectively, statistically significant results are highlighted with green; (d) and (e) Tukey's test results for a selected rainfall duration and return period on data and ranks respectively, significant difference pairs are displayed on the graph (e.g., 12 means the difference between group 1 and 2 is statistically significant).

Results of the ANOVA and Tukey's tests are also presented in Figure 4-11. The critical values to make decisions for these tests are $F^*_{(1-\alpha),(k-1),(N-k)} = F^*_{0.95,3,80} = 2.73$ and $q^*_{(1-\alpha),(k),(N-k)} = q^*_{0.95,4,80} = 3.7$. Note that the Tukey's test was only carried out if there was a statistically significant difference in the F-test (which is highlighted in Figure 4-11). For several cases, when F is not much bigger than F^* (i.e. approximate 10% difference), the F-test still shows a significant different, but the post-hoc Tukey's test does not point out which pair is different among the four groups as for the case of T = 10 year in Figure 4-11.(e). Otherwise, the Tukey's test will indicate all possible different pairs. For example, for T = 5 years and D = 5 minutes in Figure 4-11(e), the difference between group 1 (baseline) and group 2 (2020s) is statistically significant. The same thing happens with group 1 and group 3 (2050s); and group 1 and group 4 (2080s). However, there is no statistically significant difference between group 2, 3, and 4. As a reference, the ANOVA and Tukey tests on the original data were computed for comparison. Results showed a high agreement with those performed on the ranks. However, the tests on the data (i.e. parametric approach) provided lower power (e.g. lower F-statistic values) than the tests on the ranks in making decision of rejection of the null hypothesis due to being applied to non-normal data. The skewness and outliers in the data inflate the sample standard deviation used in those tests. This makes their power to detect differences between groups become weaker than that for the equivalent nonparametric test (Helsel and Hirsch, 2002).

To calculate the magnitude of the difference (i.e. absolute or relative change) of a selected pair, the non-parametric Hodges-Lehmann estimator was used. This estimator computes the median of the difference as well as the confidence interval associated with $\alpha = 5\%$. Results are shown in Figure 4-12 for all seven sites. If the difference of a pair is significant (obtained from

Tukey's test), then it will be displayed as a continuous line. On the other hand, it is plotted with a dash line to indicate an insignificant difference.

Results show that there is an increase in extreme design rainfalls for all stations (based on the median values), but these changes are not always statistically significant. For each station, for a same return period, the differences in the relative change between different durations are small (less than 3%), except station #7 which is about 6%. Among all seven stations, only station #1 shows a significant increase in extreme design rainfalls between the reference and projected periods for different rainfall durations and different return periods. This station is located apart (approximately 600 km or more) from the remaining stations. The relative change increases with the increase in return periods from T = 2 to 25 years and is approximately 13% to 18% on average. However, it is almost the same for higher return period which is about 18% on average. Opposite to station #1, the relative change decreases with the increase in return periods for station #4 (by 10% to 2% on average) and station #2 (by 14% to 8% on average). These changes are however only significant for T = 2 to 5 years for station #4, and for T = 2 to 25 years for station #2. For station #4, the difference could be also negative for T = 50 to 100 years (meaning that a decrease of extreme design rainfalls for future periods). However, the decrease is small (less than 2%) and is also not statistically significant. Station #3 and #5 (about 25 km from each other) show pretty similar results with the changes are almost the same across all return periods (i.e. approximately 13% for station #3 and 10% for station #5). These changes are only statistically significant for return periods up to T = 25 years. Station #6 and #7 (roughly 60 km from each other) also display same behaviour with the changes are almost similar for T = 2 to 10 years (i.e. approximately 10% for station #6 and 12% for station #7) and then decrease with the increase of return periods. These changes are significant for return periods up to T = 10 years.

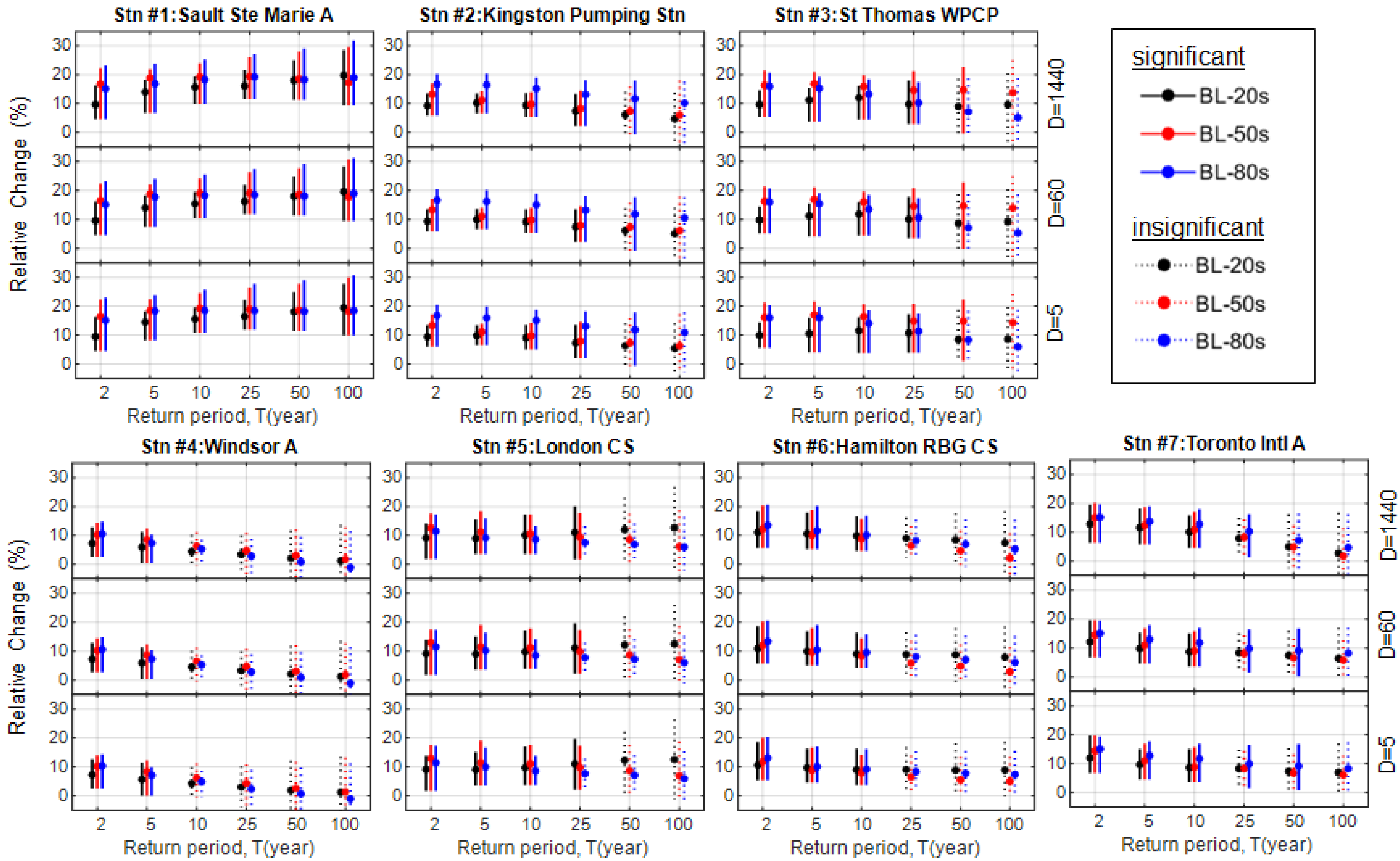

Figure 4-12. Comparison of relative changes (%) in the future extreme design rainfalls between different rainfall durations (D = 1440, 60, and 5 minutes) for three periods (Baseline-2020s, baseline-2050s, and baseline-2080s). A positive change means an increase of extreme rainfall between the baseline and the projected period. If a change is statistically significant, the median and confidence interval are displayed with a dot and continuous line. Otherwise, they are plotted with a dot and dash line.

The confidence intervals were also computed for these changes or differences. As presented in Figure 4-12, many of them are asymmetric. This reflected the truth that data used for the comparison was non-normal and also confirmed that the use of a nonparametric approach was suitable. The widths of the confidence intervals vary between different projected periods, between different design rainfall values, and between different stations. In general, the significant differences were found to be between 5% to 22%.

4.5 Conclusion

An innovative statistical downscaling (SD) procedure was proposed for estimating short-duration (sub-daily) extreme design rainfalls at a given local site in the context of climate change. The proposed approach involves two steps: (i) the spatial downscaling step using the scaling factors or the bias correction functions to transfer the daily downscaled global climate model (GCM) extreme rainfall projections at a regional scale to a given local site and (ii) the temporal downscaling step using the scale-invariance GEV/PWM model to derive the distributions of sub-daily extreme rainfalls (ERs) from that of daily values at the same study location. Results from a case study using the climate simulation outputs from 21 GCMs conducted under the CMIP5 project and the observed daily ERs from a network of seven raingauges located in Ontario (Canada) have indicated the feasibility, reliability, and accuracy of the proposed SD method.

To assess the possible differences (i.e., relative changes) between the reference and projected periods as well as between different projected periods, several statistical tests were conducted in sequence. These tests included the probability plot correlation coefficient (PPCC) test to check for the normality of data, the analysis of variance (ANOVA) F-test to detect whether there was a significant difference among the groups, and Tukey's honestly significant difference

(Tukey's HSD) test to indicate what pairs were significant difference. The magnitudes of the differences as well as the associated uncertainties (i.e. confidence intervals) were also computed for each significant difference pair.

Using the climate projection outputs from 21 GCMs under the RCP 4.5 scenario, for the majority of stations, results showed significant changes between the baseline and three future periods for different extreme design rainfall values of different return periods up to T = 25 years, and up to T = 50 years for a few stations. It was found that an important increase (varying from 8% to 18% for the median values) in the estimated extreme design rainfall amounts depending upon the station locations and the value of design return periods. For T = 100 years, only Sault Ste Marie Airport Station showed a significant increase in the estimated rainfall amounts. There were also increases from 3% to 8% in design rainfalls for T = 50 years and T = 100 years for some stations, but they were found to be not statistically significant.

It is important to notice that estimation of rainfall quantiles based on the at-site frequency analysis approach for high return periods (i.e. T = 100 years) involve high uncertainty, especially for short data samples. Thus, the method is often recommended for estimation of rainfall quantiles of return periods that are less than the length of the data sample (i.e. interpolation), and for return periods that are as twice as the sample length (i.e. extrapolation) (WMO, 2009a). Hence, for sample length of 30 years, the estimation of design rainfalls should be limited to T = 50-year return period. To reduce uncertainty and increase the robustness of the at-site estimation, several probabilistic models could be used together, such as the generalized normal (GNO) and Pearson type III (PE3) distributions as suggested by Nguyen et al. (2017) and Nguyen and Nguyen (2019a) for the Ontario region. New scale-invariance models based on these probability distribution models could be developed to tackle the temporal downscaling step. Another option is to increase the sample size used for the frequency analysis (e.g. using sample of 45 or 50-year record length). Of course, with the advancement of computer, the upgrade of database, and the improvement of physical-based modelling, the data sources have been improved significantly for each coming CMIP generation with a larger number of embedded GCMs and a longer “Retrospective” and “Prospective” simulation periods. For many regions, such a long record of data is often unavailable, regional frequency analysis is an alternative option to reduce uncertainty of the estimation by “trading space for time”. However, the use of this approach is subject to the difficulty and uncertainty of determining the homogeneous regions.

In summary, further studies could be carried out for other regions with different climatic conditions to assess the feasibility and accuracy of the proposed approach. In addition, the proposed approach could be used to estimate extreme rainfalls and to construct IDF relations for a gauged site or for an ungauged location for the current climate as well as for future climate under different climate change scenarios.

Chapter 5. Mathematical Frameworks and Scaling Properties of Several Probability Distribution Models Commonly Used in Hydrologic Frequency Analysis

5.1 Introduction

The estimation of extreme design rainfalls in the context of potential climate change impacts has become essential in current engineering practices due to recent recognition of climate variability (Williems et al., 2012; Kharin et al., 2013; Simonovic et al., 2016; Zhang et al., 2017). This estimation requires hence a suitable rainfall (spatial) downscaling approach to establishing an accurate linkage between daily climate projections from global or regional climate models (GCMs or RCMs) and daily extreme rainfall (ER) processes at a local site (Willems et al., 2012; Fowler et al., 2007; Maraun et al., 2010; Gooré Bi et al., 2017). Furthermore, this linkage so far has been commonly established at the daily timestep since current climate models have some major limitations in their detailed physical modeling ability and their limited computational capability. Consequently, it requires an improved (temporal) rainfall modeling approach to describe the linkages between the ER processes over a wide range of time scales (e.g., from one day to several minutes) (Nguyen et al., 2007; Herath et al., 2016; Li et al., 2017; Lee and Park., 2017).

The spatial resolution problems of GCM and RCM outputs has been examined in detail in several previous studies. In particular, several different downscaling methods have been proposed to spatially disaggregate GCM or RCM projected outputs to much finer regional scales or local/point scales (single-site or multi-site cases) for reliable assessments of climate change impacts (Wilby et al., 2002; Fowler et al., 2007; Maraun et al., 2010; Gooré Bi et al., 2017; Wilby and Dawson, 2013; Khalili and Nguyen, 2016; Werner et al., 2016). However, very few studies have tackled the temporal downscaling problem of GCM or RCM outputs. More specifically, some procedures have been proposed to derive the key statistics of the sub-daily ER series from those of the daily series (Herath et al., 2016; Lee and Park, 2017). Among these methods, the statistical models based on the scale-invariance (or scaling) concept has recently increasingly become an essential tool for modeling ER processes over a wide range of temporal scales (Hubert, 2001; Veneziano and Furcolo, 2002; Veneziano and Lepore, 2012; Lovejoy and Scherzer, 2012).

Scale invariance implies that the statistical properties of ER over different time scales are related to each other by an operator involving only the scale ratio and the scaling exponent (Gupta and Waymire, 1990). Applications of the scale-invariance (scaling) concept has begun since the last decades. However, only a few scale-invariance models have been reported in the literature, including the scaling generalized extreme value (GEV) distribution and its special case, the scaling Gumbel (GUM) distribution (Nguyen et al., 1998; Nguyen et al., 2002b; Menabde et al., 1999; Yu et al., 2004). These scaling models have been extensively applied to the estimation of short-duration ERs at gauged and ungauged sites, as well as to the construction of IDF curves in the current climate and in a changing climate (Nguyen et al., 2007; Nguyen et al., 2002b; Yu et al., 2004; Bougadis and Adamowski, 2006; Blanchet et al., 2016; Bairwa et al., 2016; Ghanmi et al., 2016; Vu et al., 2016). Recently, Nguyen and Nguyen (2018a) has introduced a new scaling GEV model based on the probability weighted moment system (i.e. the scaling GEV/PWM model). Using long record IDF data from a network of 21 raingauged stations located in the Ontario province of Canada, they showed that the GEV/PWM model out perform the other existing scaling models, including the GEV/NCM model (Nguyen et al., 1998), and their special cases, the GUM/PWM model (Yu et al., 2004) and the GUM/NCM model (Menabde et al., 1999).

Scaling approach has been applied to the discharge data series too. Gupta and Dawdy (1995) showed that, depending on the flood generating mechanism, annual flood flows could follow either simple scaling or multi-scaling laws. Snowmelt generating floods tend to exhibit simple scaling laws, whereas rainfall generating floods tend to follow multi-scaling laws. Smith (1992) stated that the index flood – a well-known method to transfer data from the at-site values to the regional values and vice versa, involved the assumption that the regional flood series possessed a simple scaling behavior. Pandey (1998) studied many annual maximum flood series in Québec and Ontario, Canada, and observes that the first nine NCM orders exhibited a simple scaling with the basin areas, while those of PWMs showed a multi-scaling relationship. Vogel and Sankarasubramanian (2000) also found that stream discharges in some regions of the United States displayed the simple scaling property. Eaton et al. (2002) demonstrated that flood flows in British Columbia, Canada, follow a simple scaling law. The scaling properties of Canadian annual stream flows were investigated in the studies of Yue and Gan (2004, 2009), while those of regional floods in New South Wales, Australia, were studied by Ishak et al. (2011). All of these studies have showed that conventional moments of flood data series are scaling with basin areas. Gado and Nguyen (2015) applying this property to propose a new method for homogeneous region delineations based on the case study of Quebec. Their results showed that the scaling approach was more efficient than the two existing techniques known as region of influence and canonical correlation analysis. Gupta (2017) presents a scaling theory of floods for developing a physical basis of statistical flood frequency relations.

In practice, in addition to the GEV and GUM distributions, there are other probability models that have been used for describing the distribution of the extreme hydrologic variables in general and the annual extreme rainfalls in particular (Stedinger et al., 1993; Hosking and Wallis, 1997; Rao and Hamed, 2002; WMO, 2009; Nguyen et al., 2017). Some countries recommend the use of a specific distribution in their national guidelines for flood or rainfall frequency analyses. For example, the GEV distribution is a recommended choice in many countries in Europe, including Austria, Germany, Italy, and Spain (Salinas et al., 2014a, 2014b). Log-Pearson Type 3 distribution has been used in the US in Bulletin 17B for flood frequency analysis (Griffis and Stedinger, 2007) while GEV distribution for rainfall frequency analysis (NOAA's Atlas 14, 2014). The GEV and LP3 distribution are also recommended in Australia (Ball et al., 2016). Some other distributions have also been used popularly, including the Gumbel (GUM) distribution in Finland and Spain, the generalized Pareto (GPA) distribution in Belgium, the generalized logistic (GLO) distribution in the UK. In addition, the generalized normal (GNO), which has the same distribution as the Log-Normal 3-parameter (LN3) with slight parameter modifications, could also be a suitable choice depending on the size of the study area and the climate conditions (Salinas et al., 2014b; Faulkner et al., 2016). The Pearson 3 (PE3) is also a good model as it can fit the full daily precipitation remarkably well at both the point and catchment scales (Ye et al., 2018). PE3 was also identified as the best fitting distribution with GEV is the next candidate based on IDF data from 51 station across Canada. The quantiles computed based on both distributions are virtually indistinguishable (Burn and Taleghani, 2013). Nguyen et al. (2017) shows that, among the 11 study models that could be used for describing the distribution of short-duration AMS in Ontario (Canada), the GEV, GNO, and PE3 are the top models and they could be used interchangeably for constructing the IDF curves.

In view of the above-mentioned issues, the main objective of the present study is therefore to derive the mathematical frameworks and scaling properties of several popular probability distribution models that are frequently used in the frequency analyses of hydrologic extreme variables. These scaling models then can be used as the tools for modelling the extreme rainfall processes over a wide range of time scales (e.g., from several minutes to one day) so that the quantiles and distributions of short-duration extreme rainfalls can be estimated from those of longer durations. These probability models include different types of extreme family distribution, including the GLO, GNO, and PE3 distributions. The general mathematical framework as well as the scaling properties of these distributions are formulated and derived based on two different estimation methods (i.e. the non-central moment (NCM) and probability weighted moment (PWM) systems) as presented in Section 5.2. This results in six different scaling models: GLO/NCM, GLO/PWM, GNO/NCM, GNO/PWM, PE3/NCM, and PE3/PWM models. The feasibility and accuracy of the proposed models are assessed and compared with the existing scaling GEV/NCM and GEV/PWM models using IDF data from a network of 74 raingauges across Canada as described in Sections 5.3. Results are presented in Section 5.4 along with some discussion. A summary of research findings is provided in Section 5.5.

5.2 Mathematical frameworks and scaling properties of several probability distribution models commonly-used in hydrologic frequency analysis

This section presents the derivations of mathematical frameworks and scaling properties of the GLO, GNO, and PE3 distributions based on both the NCM and PWM systems. Similar to the GEV distribution, these probability models also belong to the extreme value family and have been used frequently in the frequency of extreme hydrologic variables.

5.2.1 General mathematical frameworks and scaling properties

5.2.1.1 Non-central moment system

For a distribution of a random variable X with a probability density function $f(x)$ and a cumulative distribution function $F(x)$, the r^{th}-order non-central moment (NCM) is given by:

$$\mu_r = \mathrm{E}(\mathrm{X}^\mathrm{r}) = \int_{-\infty}^{+\infty} x^r f(x)dx = \int_{-\infty}^{\infty} x^r dF(x) \tag{5-1}$$

Applying the transformation $u = F(x)$ and provided that the integral in the Eqn. (5-1) exists, the r^{th}-order NCM, μ_r, can be expressed as in Eqn. (5-2) (Hosking and Wallis, 1997):

$$\mu_r = \mathrm{E}(\mathrm{X}^\mathrm{r}) = \int_{0}^{1} \{x(u)\}^r du \tag{5-2}$$

where $0 < u < 1$ and $x(u)$ is a unique value satisfying $F(x(u)) = u$.

The cumulative distribution function, $F(x)$, and quantile function, $x(F)$, of each distribution (GLO, GNO, and PE3) are given in the following sub-sections for each distribution respectively.

The general NCM of r^{th}-order, μ_r, and the first three NCMs of the study probability distribution models (GLO, GNO, and PE3) are derived and/or re-formulated for each distribution and are given in the following sub-sections for each distribution respectively. These non-central moment (NCM) estimators (and method of moment, MOM) can be used for estimating the parameters of these distributions in consideration of the scaling property of these NCMs over different rainfall durations.

For a simple scaling process, it can be shown that (Nguyen et al., 2002b):

$$\mu_r(\lambda t) = \lambda^{\eta_r}\mu_r(t) = \lambda^{r\eta}\mu_r(t) \tag{5-3}$$

where $\eta_r = r\eta_1$ with η_1 is the scaling exponent which can be estimated based on the 1st-order NCM (i.e. the mean).

In addition, for a simple scaling process, it can be shown that the skewness is constant over different time scales. Indeed, let $g(t)$ and $g(\lambda t)$ denote the skewness of the data samples for two different time scales t and (λt) respectively, we have:

$$g(\lambda t) = \frac{[\mu_3(\lambda t) - 3\mu_2(\lambda t)\mu_1(\lambda t) + 2\mu_1^3(\lambda t)]}{[\mu_2(\lambda t) - \mu_1^2(\lambda t)]^{\frac{3}{2}}} = \frac{\lambda^{3\eta}}{\lambda^{3\eta}}\frac{[\mu_3(t) - 3\mu_2(t)\mu_1(t) + 2\mu_1^3(t)]}{[\mu_2(t) - \mu_1^2(t)]^{\frac{3}{2}}} = g(t) \tag{5-4}$$

The skewness of each study distribution (GLO, GNO, and PE3 distributions) is a function of the shape parameter only. These equations are given in the following sub-sections for each distribution respectively. Since the skewness is constant over different time scales, the shape parameter, κ (of the GLO and GNO distributions) and γ (of the PE3 distribution) of each distribution model is also constant over time scales as a result.

Using the equations of the first two NCMs of each distribution and the relations between NCMs of different time scales, the relationships between the scale parameters, α (of the GLO and GNO distributions) and location parameters, μ (of the PE3 distribution) of two different time scales can be established. Substitute these parameters into the quantile function of each distribution to obtain the scaling relationship between quantiles of two different time scale (see Figure 5-1). In summary, for a simple scaling process, it can be shown that the statistical properties (parameters and quantiles) of these scaling models of two different time scales t and λt are related as follows:

$$\kappa(\lambda t) = \kappa(t);\ \alpha(\lambda t) = \lambda^{\eta}\alpha(t);\ \xi(\lambda t) = \lambda^{\eta}\xi(t);\quad \text{for GLO and GNO distributions} \tag{5-5}$$

$$\gamma(\lambda t) = \gamma(t);\ \sigma(\lambda t) = \lambda^{\eta}\sigma(t);\ \mu(\lambda t) = \lambda^{\eta}\mu(t)\ ;\quad \text{for PE3 distribution}$$

$$X_T(\lambda t) = \lambda^{\eta}X_T(t); \tag{5-6}$$

5.2.1.2 *Probability weighted moment system*

Probability weighted moments of a random variable X with a function F(X) are defined by (Greenwood et al., 1979):

$$\mathrm{M_{p,r,s}} = E[X^p\{F(X)\}^r\{1 - F(X)\}^s] \tag{5-7}$$

A special case that is particularly useful and commonly used in practice is $\beta_r = M_{1,r,0}$. For a distribution of a random variable X that has a quantile function, $x(u)$, the PWM of r^{th}-order can be expressed as in Eqn.(5-8) (Hosking and Wallis, 1997):

$$\beta_r = \mathrm{E}(\mathrm{X}\{F(X)\}^r) = \int_0^1 x(u)u^r du \tag{5-8}$$

The general PWM of r^{th}-order, β_r, and the first three PWMs of the GLO, GNO, and PE3 probability distribution models are derived and/or re-formulated for each distribution and are given in the following sub-sections for each distribution respectively. The probability weighted moments

(PWMs) and its linear combination forms (L-moments) can be used for estimating the parameters of these distributions in consideration of the scaling property of these PWMs over different rainfall durations.

For a simple scaling process, it can be shown that the relation between the r^{th}-order PWMs of rainfalls for two different rainfall durations t and λt can be expressed as:

$$\beta_r(\lambda t) = \lambda^{\eta_r}\beta_r(t) = \lambda^{\eta}\beta_r(t) \qquad (5\text{-}9)$$

In addition, for a simple scaling process, it can be shown that the L-skewness is constant over different time scales. Indeed, let $\tau_3(t)$ and $\tau_3(\lambda t)$ denote the L-skewness of the data samples for two different time scales t and λt respectively, we have:

$$\tau_3(\lambda t) = \frac{6\beta_2(\lambda t) - 6\beta_1(\lambda t) + \beta_0(\lambda t)}{2\beta_1(\lambda t) - \beta_0(\lambda t)} = \frac{\lambda^{\eta}}{\lambda^{\eta}} . \frac{[6\beta_2(t) - 6\beta_1(t) + \beta_0(t)]}{[2\beta_1(t) - \beta_0(t)]} = \tau_3(t) \qquad (5\text{-}10)$$

The L-skewness of each study distribution (GLO, GNO, and PE3 distributions) is a function of the shape parameter only. These equations are given in the following sub-sections for each distribution respectively.

Since the L-skewness is constant over different time scales, the shape parameter, κ (of the GLO and GNO distributions) and γ (of the PE3 distribution) of each distribution model is also constant over time scales as a result. Furthermore, using the equations of the first two PWMs of each distribution and the relations between PWMs of different time scales, the relationships between the scale parameters, α (of the GLO and GNO distributions) and location parameters, μ (of the PE3 distribution) of two different time scales can be established. Similarly, the quantile scaling relationship can also be obtained by substituting these scaling parameters into the quantile functions (see Figure 5-1). The equations received are identical with Eqn. (5-5) and (5-6) provided for the NCM system above.

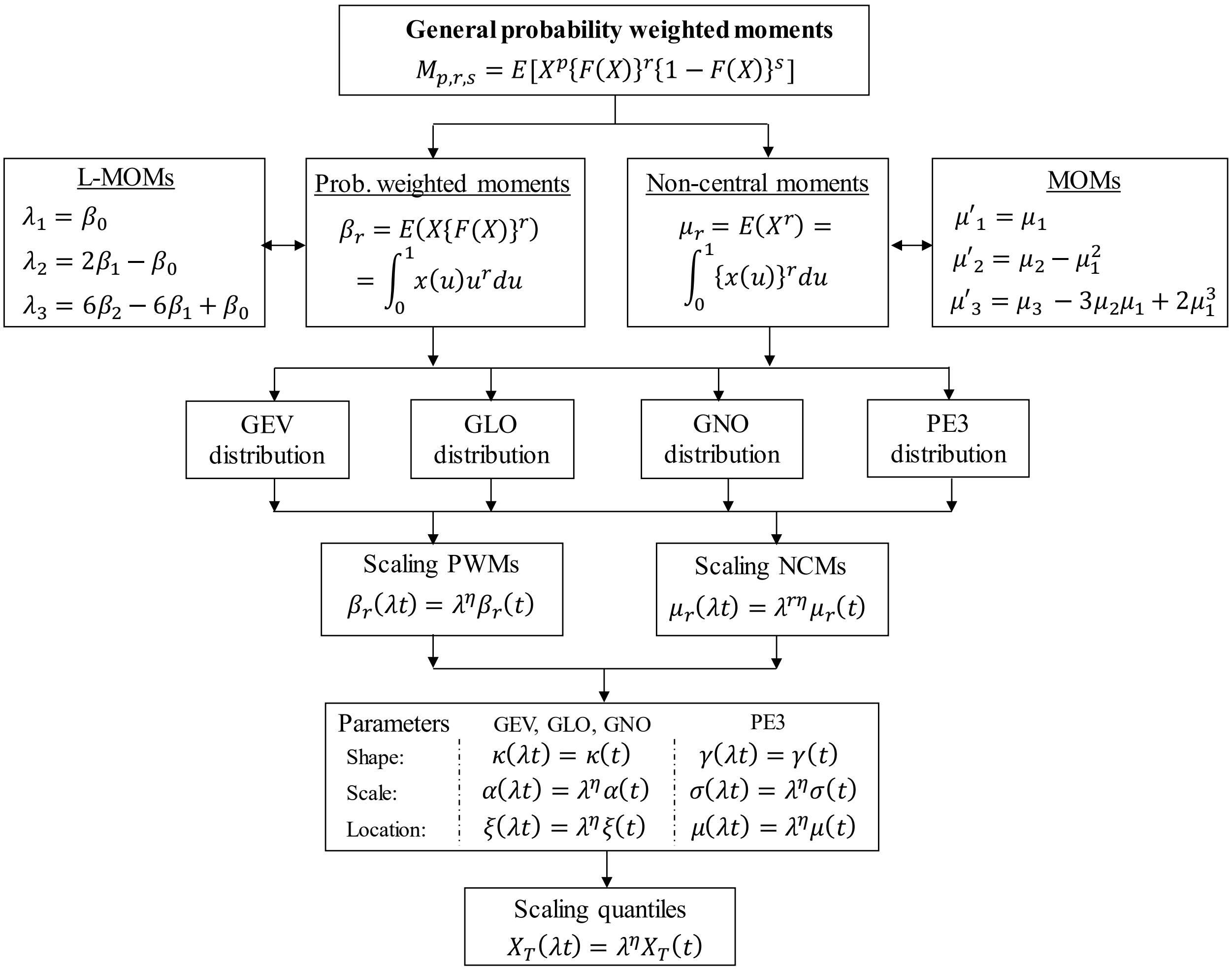

Figure 5-1. Mathematical frameworks and scaling properties of several popular distributions (GEV, GLO, GNO, PE3) based on the probability weighted moment and non-central moment systems

5.2.2 Novel Scaling Generalized Logistic (GLO) model

5.2.2.1 The Generalized Logistic (GLO) distribution

The cumulative distribution function (CDF) of the GLO distribution, $F(x)$, and its quantile function, $x(F)$, are defined by (Hosking and Wallis, 1997):

$$F(x) = \frac{1}{1+\exp(-y)} \quad \text{where} \quad y = \begin{cases} -k^{-1}log\left\{1 - \frac{k(x-\xi)}{\alpha}\right\}, & k \neq 0 \\ \frac{(x-\xi)}{\alpha} & , \ k = 0 \end{cases} \tag{5-11}$$

$$x(F) = \begin{cases} \xi + \alpha \frac{\left\{\frac{1-F}{F}\right\}^k}{k} & , \ \kappa \neq 0 \\ \xi - \alpha log\left\{\frac{(1-F)}{F}\right\} & , \ \kappa = 0 \end{cases} \tag{5-12}$$

in which $\xi, \alpha,$ and κ are the location, scale, and shape parameters, respectively. For the special case, $k = 0$ is the logistic distribution.

5.2.2.2 A novel NCM-based scaling GLO model

The generalized r^{th}-order NCM, μ_r, of the GLO distribution has been derived in Nguyen and Nguyen (2018b) and is presented in Eqn. (5-13):

$$\mu_r = \left(\xi + \frac{\alpha}{\kappa}\right)^r + (-1)^r \left(\frac{\alpha}{\kappa}\right)^r \Gamma(1 + r\kappa)\Gamma(1 - r\kappa) + r\sum_{i=1}^{r-1}(-1)^i \left(\frac{\alpha}{\kappa}\right)^i \left(\xi + \frac{\alpha}{\kappa}\right)^{r-\mathrm{i}} \Gamma(1 + i\kappa)\Gamma(1 - i\kappa) \tag{5-13}$$

in which $\Gamma(.)$ is the gamma function.

Based on Eqn. (5-13), the first three order NCMs are:

$$\mu_1 = \left(\xi + \frac{\alpha}{\kappa}\right) - \left(\frac{\alpha}{\kappa}\right)\Gamma(1 + \kappa)\Gamma(1 - \kappa) \tag{5-14}$$

$$\begin{aligned} \mu_2 &= \left(\xi + \frac{\alpha}{\kappa}\right)^2 - 2\left(\frac{\alpha}{\kappa}\right)\left(\xi + \frac{\alpha}{\kappa}\right)\Gamma(1 + \kappa)\Gamma(1 - \kappa) + \left(\frac{\alpha}{\kappa}\right)^2 \Gamma(1 + 2\kappa)\Gamma(1 - 2\kappa) \\ &= \mu_1^2 + \left[\frac{\alpha}{\kappa}\right]^2 [\Gamma(1 + 2k)(1 - 2k) - \Gamma^2(1 + k)\Gamma^2(1 - k)] \end{aligned} \tag{5-15}$$

$$\mu_3 = \left(\xi + \frac{\alpha}{\kappa}\right)^3 - 3\left(\frac{\alpha}{\kappa}\right)\left(\xi + \frac{\alpha}{\kappa}\right)^2 \Gamma(1 + \kappa)\Gamma(1 - \kappa) \tag{5-16}$$

$$+ 3\left(\frac{\alpha}{\kappa}\right)^2\left(\xi + \frac{\alpha}{\kappa}\right)\Gamma(1+2\kappa)\Gamma(1-2\kappa) - \left(\frac{\alpha}{\kappa}\right)^3\Gamma(1+3\kappa)\Gamma(1-3\kappa)$$

The skewness of the GLO distribution is only a function of the shape parameter, κ, and is given by (Rao and Hamed, 2000):

$$g(.) = \frac{\kappa}{|\kappa|}[-\Gamma(1+3\kappa)\Gamma(1-3\kappa) + 3\Gamma(1+\kappa)\Gamma(1-\kappa)\Gamma(1+2\kappa)\Gamma(1-2\kappa) - 2\Gamma^3(1+\kappa)\Gamma^3(1-\kappa)]/[\Gamma(1+2\kappa)\Gamma(1-2\kappa) - \Gamma^2(1+\kappa)\Gamma^2(1-\kappa)]^{\frac{3}{2}} \quad (5\text{-}17)$$

5.2.2.3 <u>A novel PWM-based scaling GLO model</u>

The generalized r^{th}-order PWMs, β_r, of the GLO distribution has been derived in Nguyen and Nguyen (2018b) and is presented in Eqn. (5-18):

$$\beta_r = (r+1)^{-1}\left(\xi + \frac{\alpha}{\kappa}\left[1 - \frac{\Gamma(1+\kappa)\,\Gamma(r+1-\kappa)}{\Gamma(r+1)}\right]\right) \quad (5\text{-}18)$$

Based on Eqn. (5-18), the first three order PWMs are:

$$\beta_o = \left(\xi + \frac{\alpha}{\kappa}[1 - \Gamma(1+\kappa)\Gamma(1-\kappa)]\right) \quad (5\text{-}19)$$

$$\beta_1 = \frac{1}{2}\left(\xi + \frac{\alpha}{\kappa}[1 - \Gamma(1+\kappa)\Gamma(2-\kappa)]\right) \quad (5\text{-}20)$$

$$\beta_2 = \frac{1}{3}\left(\xi + \frac{\alpha}{\kappa}\left[1 - \frac{1}{2}\Gamma(1+\kappa)\Gamma(3-\kappa)\right]\right) \quad (5\text{-}21)$$

The L-skewness of the GLO distribution is a function of the shape parameter, κ, only and is given by (Hosking and Wallis, 1997):

$$\tau_3(.) = -\kappa \quad (5\text{-}22)$$

5.2.3 *Novel Scaling Generalized Normal (GNO) model*

5.2.3.1 The Generalized Normal (GNO) distribution

The three-parameter lognormal (LN3) distribution is usually defined by (Hosking and Wallis, 1997):

$$F(x) = \Phi[\{\log\frac{(x-\zeta)-\mu\}}{\sigma}], \quad \zeta \leq x < \infty \tag{5-23}$$

in which $\mu, \sigma, and\ \zeta$ are model parameters.

This version only includes the lognormal distributions with positive skewness and a lower bound. A re-parameterized version known as GNO that includes both the positive skewness ($\kappa < 0$), negative skewness ($\kappa > 0$), and the Normal distribution as a special case ($\kappa = 0$) has been presented in Hosking and Wallis (1997). With this form, the GNO distribution exhibits many similar structures to the GEV and GPA distributions. The CDF of the GNO distribution model are defined by Eqn. (5-24). The quantile function, $x(F)$, has no explicit analytical form and must be solved by inversing the CDF function.

$$F(x) = \Phi(\mathrm{y}) \quad \text{where} \quad y = \begin{cases} -\frac{1}{k}\log\left[1 - \frac{k(x-\xi)}{\alpha}\right]; k \neq 0 \\ (x-\xi)/\alpha\,; \quad k = 0 \end{cases} \tag{5-24}$$

$$\Phi(x) = \int_{-\infty}^{x} \phi(t)dt \ \text{ and } \phi(t) = (2\pi)^{-\frac{1}{2}} \exp\left(-\frac{1}{2}t^2\right) \tag{5-25}$$

in which $\xi, \alpha,$ and κ are the location, scale, and shape parameters, respectively. For the special case, $k = 0$ is the normal distribution. These parameters relate to those of the LN3 version as follows:

$$\kappa = -\sigma \ ; \quad \alpha = \sigma \exp(\mu) \quad ; \quad \xi = \zeta + \exp(\mu) \tag{5-26}$$

5.2.3.2 A novel NCM-based scaling GNO model

The generalized r^{th}-order NCM, μ_r, of the LN3 distribution has been described in Singh (1998) and is presented in Eqn. (5-27):

$$\mu_r = \sum_{i=1}^{r-1} \binom{r}{i} \exp\left[(r-i)\mu + \frac{(r-i)^2\sigma^2}{2}\right]\zeta^i \tag{5-27}$$

Based on Eqn. (5-27), the first three order NCMs are:

$$\mu_1 = exp\left(\mu + \frac{\sigma^2}{2}\right) + \zeta \tag{5-28}$$

$$\mu_2 = \exp(2\mu + 2\sigma^2) + 2\zeta \exp\left(\mu + \frac{\sigma^2}{2}\right) + \zeta^2 \tag{5-29}$$

$$\mu_3 = \exp\left(3\mu + \frac{9}{2}\sigma^2\right) + 3\zeta \exp(2\mu + 2\sigma^2) + 3\zeta^2 \exp\left(\mu + \frac{\sigma^2}{2}\right) + \zeta^3 \tag{5-30}$$

The generalized r^{th}-order NCM, μ_r, of the GNO distribution can be re-formulated as follows:

$$\mu_r = \sum_{i=1}^{r-1} \binom{r}{i} \left(-\frac{\alpha}{k}\right)^{(r-i)} exp\left[\frac{(r-i)^2k^2}{2}\right]\left(\xi + \frac{\alpha}{k}\right)^i \tag{5-31}$$

Based on Eqn. (5-27), the first three order NCMs are:

$$\mu_1 = \left(-\frac{\alpha}{k}\right)\exp\left(\frac{k^2}{2}\right) + \left(\xi + \frac{\alpha}{k}\right) \tag{5-32}$$

$$\mu_2 = \left(\frac{\alpha}{k}\right)^2 \exp(2k^2) - \frac{2\alpha}{k}\exp\left(\frac{k^2}{2}\right)\left(\xi + \frac{\alpha}{k}\right) + \left(\xi + \frac{\alpha}{k}\right)^2 \tag{5-33}$$

$$\mu_3 = \left(-\frac{\alpha}{k}\right)^3 \exp\left(\frac{9k^2}{2}\right) + 3\left(\frac{\alpha}{k}\right)^2 \exp(2k^2)\left(\xi + \frac{\alpha}{k}\right) - 3\frac{\alpha}{k}\exp\left(\frac{k^2}{2}\right)\left(\xi + \frac{\alpha}{k}\right)^2 + \left(\xi + \frac{\alpha}{k}\right)^3 \tag{5-34}$$

The skewness of the LN3 distribution is given by (Singh, 1998):

$$g(.) = [\exp(\sigma^2) + 2][\exp(\sigma^2) - 1]^{1/2} \tag{5-35}$$

It can be re-formulated for the GNO as follows:

$$g(.) = [\exp(\kappa^2) + 2][\exp(\kappa^2) - 1]^{1/2} \tag{5-36}$$

Therefore, it is possible to estimate the three parameters of the scaling GNO/NCM probability distribution model using the first three NCMs.

5.2.3.3 A novel PWM-based scaling GNO model

The PWM expressions for the GNO distribution are difficult to obtain. The first two order PWMs of the GNO distribution are given by Hosking and Wallis (1997) as follows:

$$\beta_0 = \xi + \frac{\alpha}{k}\left[1 - exp\left(\frac{k^2}{2}\right)\right] \tag{5-37}$$

$$\beta_1 = \frac{1}{2}\beta_0 + \frac{\alpha}{2k}\exp\left(\frac{k^2}{2}\right)\left[1 - 2\phi\left(-\frac{k}{\sqrt{2}}\right)\right] \tag{5-38}$$

For β_2 and L-skewness, there are no simple expression. Hosking and Wallis (1997) notes that L-skewness of the GNO distribution is a function of the shape parameter, κ, alone and can be approximated as:

$$\tau_3(.) = \mathrm{f}(\kappa) \approx -k\frac{A_0 + A_1k^2 + A_2k^4 + A_3k^6}{1 + B_1k^2 + B_2k^4 + B_3k^6} \tag{5-39}$$

where A_i ($i = 0\ to\ 3$) and B_j ($j = 1\ to\ 3$) are the coefficients. Their values are provided in Table A.1 of Hosking and Wallis (1997) and can be found in Appendix D.

5.2.4 *Novel Scaling Pearson Type 3 (PE3) model*

5.2.4.1 *The Pearson type 3 (PE3) distribution*

The CDF of the PE3 distribution model are defined by Eqn.(5-40) (Hosking and Wallis, 1997). The quantile function, $x(F)$, has no explicit analytical form and must be solved by inversing the CDF function.

$$F(x) = \frac{G\left(\alpha, \frac{x-\xi}{\beta}\right)}{\Gamma(\alpha)} \quad ; \qquad \text{for } \gamma > 0 \; and \; \xi \leq x < \infty; \tag{5-40}$$

$$F(x) = \frac{G\left(\alpha, \frac{x-\xi}{\beta}\right)}{\Gamma(\alpha)} \quad ; \qquad \text{for } \gamma < 0 \; and - \infty < x \leq \xi;$$

$$F(x) = \Phi\left(\frac{x-\mu}{\sigma}\right) \quad ; \qquad \text{for } \gamma = 0 \; and - \infty < x < \infty;$$

$$G(\alpha, x) = \int_0^x t^{\alpha-1} e^{-t} dt \tag{5-41}$$

$$\alpha = \frac{4}{\gamma^2}, \qquad \beta = \frac{\sigma|\gamma|}{2}, \qquad \xi = \mu - \frac{2\sigma}{\gamma} \tag{5-42}$$

in which $\mu, \sigma,$ and γ are the location, scale, and shape parameters, respectively. $G(.)$ is the incomplete gamma function. For the special case, $\gamma = 0$ is the normal distribution.

5.2.4.2 *A novel NCM-based scaling PE3 model*

The generalized r^{th}-order NCM, μ_r, of the PE3 distribution in term of the standard parameters has been described in Singh (1998) and is presented as follows:

$$\mu_r = \sum_{i=0}^{r} \binom{r}{i} \frac{\beta^{r-i}}{\Gamma(\alpha)} \Gamma(r - i + \alpha) \xi^i \tag{5-43}$$

Based on Eqn. (5-43), the first three order NCMs are:

$$\mu_1 = \xi + \alpha\beta \tag{5-44}$$

$$\mu_2 = (\xi + \alpha\beta)^2 + \alpha\beta^2 \tag{5-45}$$

$$\mu_3 = (\xi + \alpha\beta)^3 + 3\alpha\beta^2(\xi + \alpha\beta) + 2\alpha\beta^3 \tag{5-46}$$

The generalized r^{th}-order NCM, μ_r, of the re-parameterized PE3 distribution in term of $\mu, \sigma,$ and γ can be formulated as follows:

$$\mu_r = \sum_{i=0}^{r} \binom{r}{i} \frac{(\sigma|\gamma|/2)^{r-i}}{\Gamma(4/\gamma^2)} \Gamma(r - i + 4/\gamma^2)(\mu - 2\sigma/\gamma)^i \tag{5-47}$$

The first three order NCMs of the re-parameterized version are:

$$\mu_1 = \mu \tag{5-48}$$

$$\mu_2 = \mu^2 + \sigma^2 \tag{5-49}$$

$$\mu_3 = \mu^3 + 3\sigma^2\mu + \sigma^3|\gamma| \tag{5-50}$$

The skewness of the PE3 distribution is given by (Singh, 1998):

$$g(.) = 2/\alpha^{0.5} \tag{5-51}$$

It can be re-formulated for the re-parameterized PE3 as a function of the shape parameter, κ, only as follows:

$$g(.) = \gamma \tag{5-52}$$

5.2.4.3 <u>A novel PWM-based scaling PE3 model</u>

The PWM expressions for the PE3 distribution are difficult to obtain. The first two order PWMs of the PE3 distribution in terms of the standard parameter are given by Hosking and Wallis (1997) as follows:

$$\beta_0 = \xi + \alpha\beta \tag{5-53}$$

$$\beta_1 = \frac{1}{2}\left(\beta_0 + \pi^{-\frac{1}{2}}\beta\Gamma\left(\alpha + \frac{1}{2}\right)/\Gamma\left(\alpha\right)\right) \tag{5-54}$$

In terms of the re-parameterization, it can be formulated as follows:

$$\beta_0 = \mu \tag{5-55}$$

$$\beta_1 = \frac{1}{2}\left(\beta_0 + \frac{1}{2}\pi^{-\frac{1}{2}}\sigma|\gamma|\Gamma\left(\frac{4}{\gamma^2} + \frac{1}{2}\right)/\Gamma\left(\frac{4}{\gamma^2}\right)\right) \tag{5-56}$$

For β_2 and L-skewness, there are no simple expression. Hosking and Wallis (1997) notes that the L-skewness of the PE3 distribution is a function of the standard parameter, α, or of the re-parameterized shape parameter, γ, alone and can be approximated as:

$$\tau_3 = \mathrm{f}(\alpha) = 6I_{1/3}(\alpha, 2\alpha) - 3\ ; \text{ or } \quad \tau_3 = \mathrm{f}(\gamma) = 6I_{1/3}\left(\frac{4}{\gamma^2}, \frac{8}{\gamma^2}\right) - 3 \tag{5-57}$$

$$I_x(p,q) = \frac{\Gamma(p+q)}{\Gamma(p)\Gamma(q)}\int_0^x t^{p-1}(1-t)^{q-1}\,\mathrm{d}t \tag{5-58}$$

$$\tau_3 \approx \alpha^{-0.5}\frac{A_0 + A_1\alpha^{-1} + A_2\alpha^{-2} + A_3\alpha^{-3}}{1 + B_1\alpha^{-1} + B_2\alpha^{-2}}\ ; \text{if } \alpha \geq 1 \tag{5-59}$$

$$\tau_3 \approx \frac{1 + E_1\alpha + E_2\alpha^2 + E_3\alpha^3}{1 + F_1\alpha + F_2\alpha^2 + F_3\alpha^3}\ ; \text{if } \alpha < 1$$

where $I_x(p,q)$ is the incomplete beta function ratio; A_i (i = 0 to 3), B_j (j = 1 to 2), E_k (k = 1 to 3), and F_k are coefficients and their values can be found in Table A.2 of Hosking and Wallis (1997) and can be found in Appendix D.

5.3 Numerical application

5.3.1 Study sites and Data

To assess the feasibility and accuracy of the proposed scaling models, the long record IDF data from a network of 74 stations located across Canada were selected for this study (see Figure 5-2). These stations were chosen based on the quality of the data, the adequate length of available historical records, and the representative spatial distribution of the raingauges. To ensure the quality of data, only data from recording raingauges provided by the Atmospheric Environmental Service of Environment Canada were used. Each station contains at least 40 years of record of nine rainfall durations (from D = 5 to 1440 minutes). The data must pass the three selected statistical tests of the independence and stationarity of the input data series at the 5% significant level. These tests include the Mann-Whitney test for homogeneity and stationarity (jumps), the Mann–Kendall test for trend detection, and the Wald-Wolfowitz test for independence and stationarity (Rao and Hamed, 2000; WMO, 2009a).

Several sample statistics are calculated, including the maximum, mean, standard deviation, and skewness values as shown in Figure 5-3. The range of each statistic (minimum to maximum) for each rainfall duration is also summarized based on values from all 74 stations. Color scales are used to display and compare these values for each statistic and each duration. For each statistic and each duration, color is scaled from white to dark green/blue/purple/brown (i.e. from the minimum to maximum value, provided in the table below each column). In addition, for the ease of comparison, yellow and red markers are added to the plot to indicate stations with rainfall depths greater than or equal to 95 and 99 percentiles respectively.

The AMS maximum values have been analyzed in depth in Chapter 3. Results show that the largest short-duration storms (ranging from 5 minutes to 1 hour) were mostly observed in the Prairies of Canada. Particularly, at the Lethbridge CDA Station (Alberta), the Regina International Airport Station (Saskatchewan), and Dauphin CS Station (Manitoba). Whereas, for longer durations (D = 2 to 6 hours), they were mostly recorded in the Western Ontario at the Kenora RCS Station. For the longest durations (D = 12 to 24 hours), they were measured in the British Columbia coast (Tofino Airport Station) and the Eastern coast (Saint John Airport and Sydney CS Stations).

For the AMS mean values, the picture is quite different from the AMS max values for rainfall durations of 5 minutes to 2 hours. The largest means were mostly recorded in the Western Ontario (i.e. Kenora RCS Station) and Southern Ontario (Chatham WPCP and Winsor Airport Stations) with the rainfall depths approximately 10 mm (5 minutes), 15 mm (10 minutes), 18 mm (15 minutes), 24 mm (30 minutes), 29 mm (1 hour), and 36 mm (2 hours). For longer rainfall durations (i.e. 6 hours and more), the largest means were mostly recorded in the Western (Tofino Airport Station) and Eastern (Saint John Airport Station) Canada coasts. The rainfall depths are approximately 64 mm (6 hours), 94 mm (12 hours), and 133 mm (1 day).

For the rainfall variation (i.e. standard deviation), on average, it is approximately 40% of the mean value for all rainfall durations. However, it can be as small as 19% and can be as large as 76%. The largest standard deviation observed based on the 74 stations for different durations are: 5 mm (5 minutes), 7 mm (10 minutes), 9 mm (15 minutes), 13 mm (30 minutes), 14 mm (1 hour), 20 mm (2 hours), 25 mm (6 hours), 29 mm (12 hours), 31 mm (1 day). Regarding the AMS skewness, the computed values indicate that many AMS are highly skew. On average, the skewness ranges from 1.1 to 1.6 for different rainfall durations. However, they can be extremely skew with values range from 2.9 to 4.6.

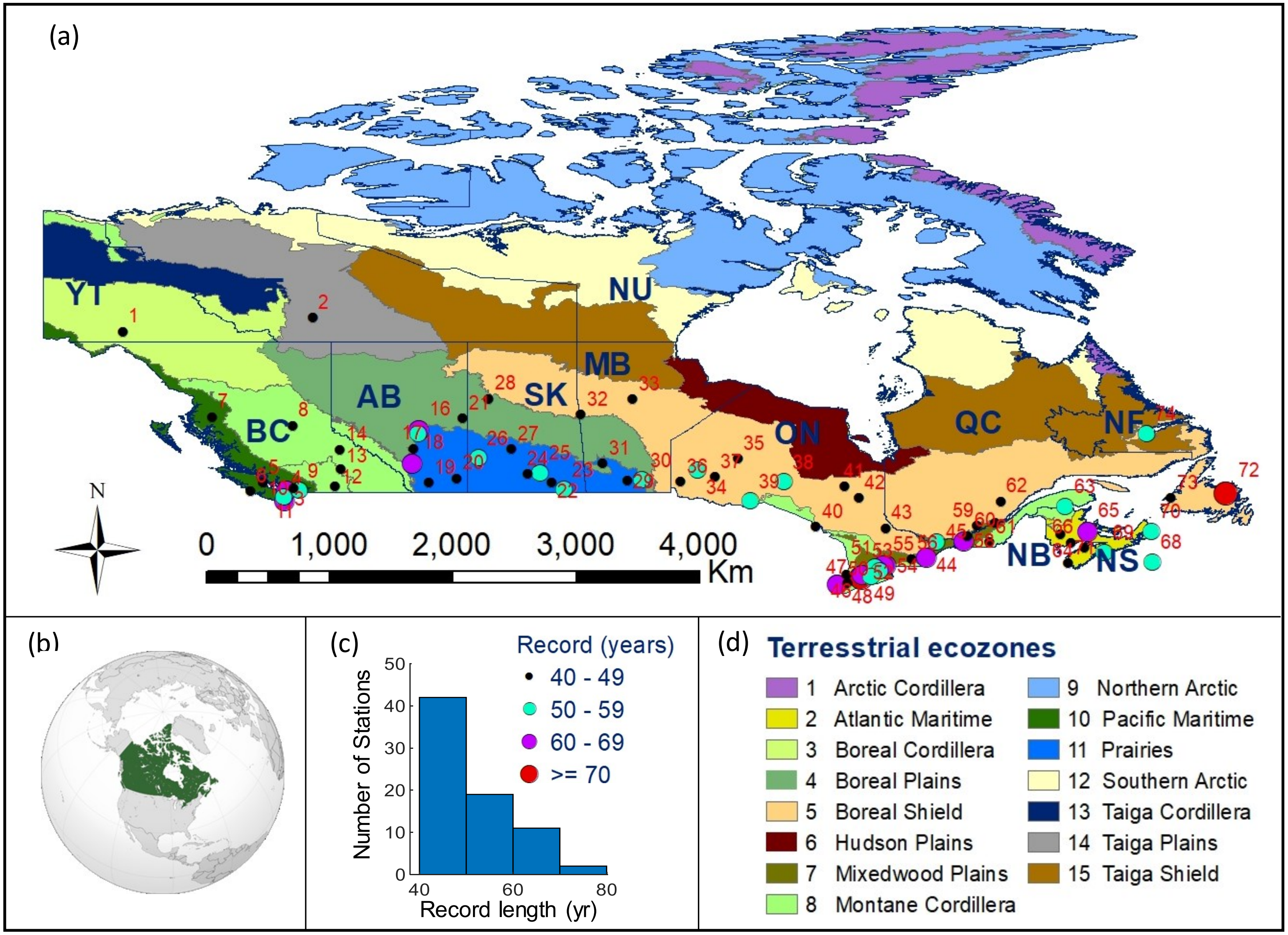

Figure 5-2. (a) Locations and record lengths (circle markers with different sizes and colors) of the 74 study raingauges; (b) map of Canada in the world; (c) Histogram of record lengths; (d) Names of 15 different terrestrial ecoregions in Canada. Adapted from Government of Canada (2019)

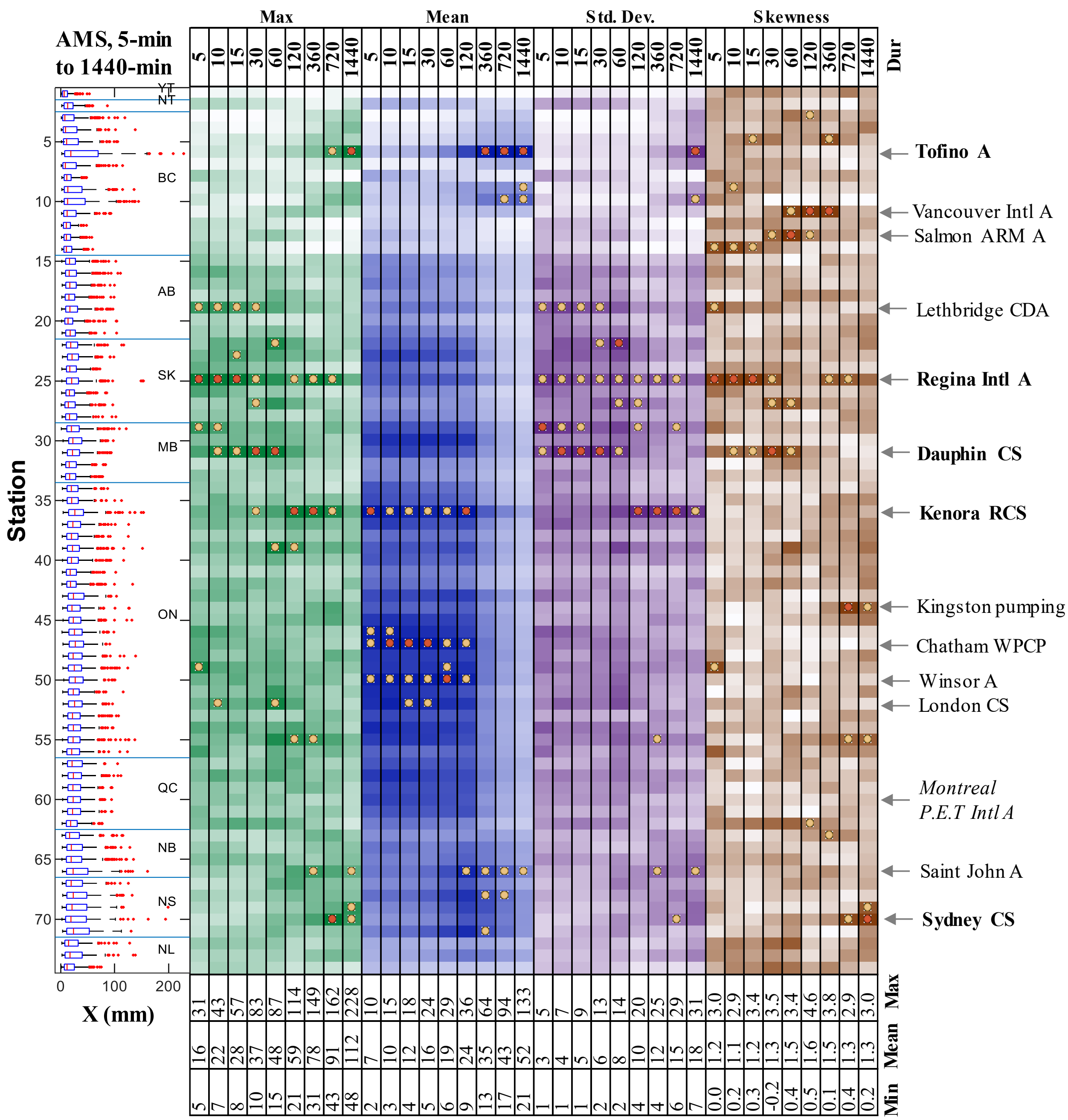

Figure 5-3. Several basic statistics (maximum, mean, standard deviation, and skewness) of 5-minute to 1440-minute AMS (boxplots on the left) of 74 stations. For each statistic and each duration, color is scaled from white to dark green/blue/purple/brown (i.e. from the minimum to maximum value, provided in the table below each column). Yellow and red markers are also added to each column to indicate stations with values greater than or equal to 95 and 99 percentiles respectively.

5.3.2 Model Assessment Criteria

In this study, five indices are used for comparing the performance of the eight study models. These criteria include the root mean square error (RMSE), the root mean square relative error (RMSEr), the mean absolute deviation (MAD), the mean absolute relative deviation (MADr), and the correlation coefficient (CC). RMSE and MAD have the same unit with the rainfall depth (mm), while RMSEr, MADr, and CC are dimensionless (dmnl). They are calculated as follows:

$$RMSE = \left\{\sum \frac{(x_i - y_i)^2}{n}\right\}^{\frac{1}{2}} \tag{5-60}$$

$$RMSEr = \left[\frac{1}{n}\sum\left\{\frac{(x_i - y_i)}{x_i}\right\}^2\right]^{\frac{1}{2}} \tag{5-61}$$

$$MAD = \frac{1}{n}\sum|x_i - y_i| \tag{5-62}$$

$$MADr = \frac{1}{n}\sum\left\{\frac{|x_i - y_i|}{x_i}\right\} \tag{5-63}$$

$$CC = \frac{\sum\{(x_i - \bar{x})(y_i - \bar{y})\}}{\{\sum(x_i - \bar{x})^2 \sum(y_i - \bar{y})^2\}^{\frac{1}{2}}} \tag{5-64}$$

where $x_i, i = 1, 2, \dots, n$ are the observed values and $y_i, i = 1, 2, \dots, n$ are the estimated values for the same probability level p_i; n is the sample length; $\bar{x}$ and $\bar{y}$ denote the average value of the observed and estimated quantiles, respectively. The non-exceedance probabilities, p_i, is estimated using the Cunnane's plotting position formula (Nguyen et al., 2017; Nguyen and Nguyen, 2019a).

5.4 Results and Discussion

This section compares the performance of the six novel scaling models proposed in Section 5.2 (i.e. GLO/PWM, GLO/NCM, GNO/PWM, GNO/NCM, PE3/PWM, and PE3/NCM models) with two existing scale-invariance models (i.e. GEV/PWM and GEV/NCM models). The comparisons were performed based on a number of different graphical displays and numerical indices. For all eight scaling models, the model parameters are estimated based on the indirect method (i.e. based on the scale-invariance property of the first three statistical moments (PWMs or NCMs) over different rainfall durations) as described in Chapter 3. The distributions and the quantiles of the sub-daily and sub-hourly extreme rainfalls can be then easily obtained by substituting these parameters into the corresponding quantile function of each model.

Figure 5-4 presents the probability plots of the sub-daily and sub-hourly AMS (D = 5 to 720 minutes) derived from the distribution of daily AMS data using the eight scale-invariance models for the Montreal P.E.T. Intl. Airport Station. For each model (i.e. each sub-plot), a visual assessment can be carried out by visually comparing the estimated cumulative distribution functions (CDFs) of the sub-daily and sub-hourly extreme rainfalls to the empirical CDFs of the observed data or to the theoretical CDFs fitted to the observed data. From the visual point, all models seem to fit well to the observed data though they exhibit quite different tail behaviors on the right-hand side (i.e. for T = 50 years and up). Even using the same distribution but with different moment systems (e.g. GEV/PWM versus GEV/NCM model), the estimated rainfall quantiles can be quite different. For this station, it can be seen that the estimations based on the PWM system produce higher quantile values, especially for those corresponding to high return periods, compared to the estimation using the NCM system. In particular, the GLO distribution yields the highest difference while PE3 distribution produces the least difference for quantiles computed using the two different moment systems. Comparing the four distributions, based on the PWM system and the observation of the right tail behaviours, the GLO distribution yields the largest quantile while the PE3 distribution yields the smallest quantile; the GEV and GNO distributions produce almost the same values. However, the differences are much smaller when computing the quantile using the NCM system.

To discriminate these models, the five indices presented in Section 5.3 were used. For the results to be comparable among different models, the empirical extreme rainfall quantiles of sub-daily and sub-hourly data were used as the reference values to compare with the estimated values. The empirical values are independent with the theoretical distributions and parameter estimation methods and therefore the same for all eight models. Using these numerical indices, results of Montreal P.E.T. Intl. Airport Station indicate that, among the eight considered models, the PE3/PWM model provided the best fit to the observed data of this station. In detail, it yields the best results for the three indices, including RMSE (1.54 mm), MAD (1.01 mm), and CC (0.996), and the tied results for the two remaining criteria, including RMSEr (5.4%, tied with the GEV/PWM model), and MADr (4.2%, tied with the GEV/PWM and GNO/PWM models). Similar calculations were conducted for all 74 stations. Results are presented in Figure 5-5.

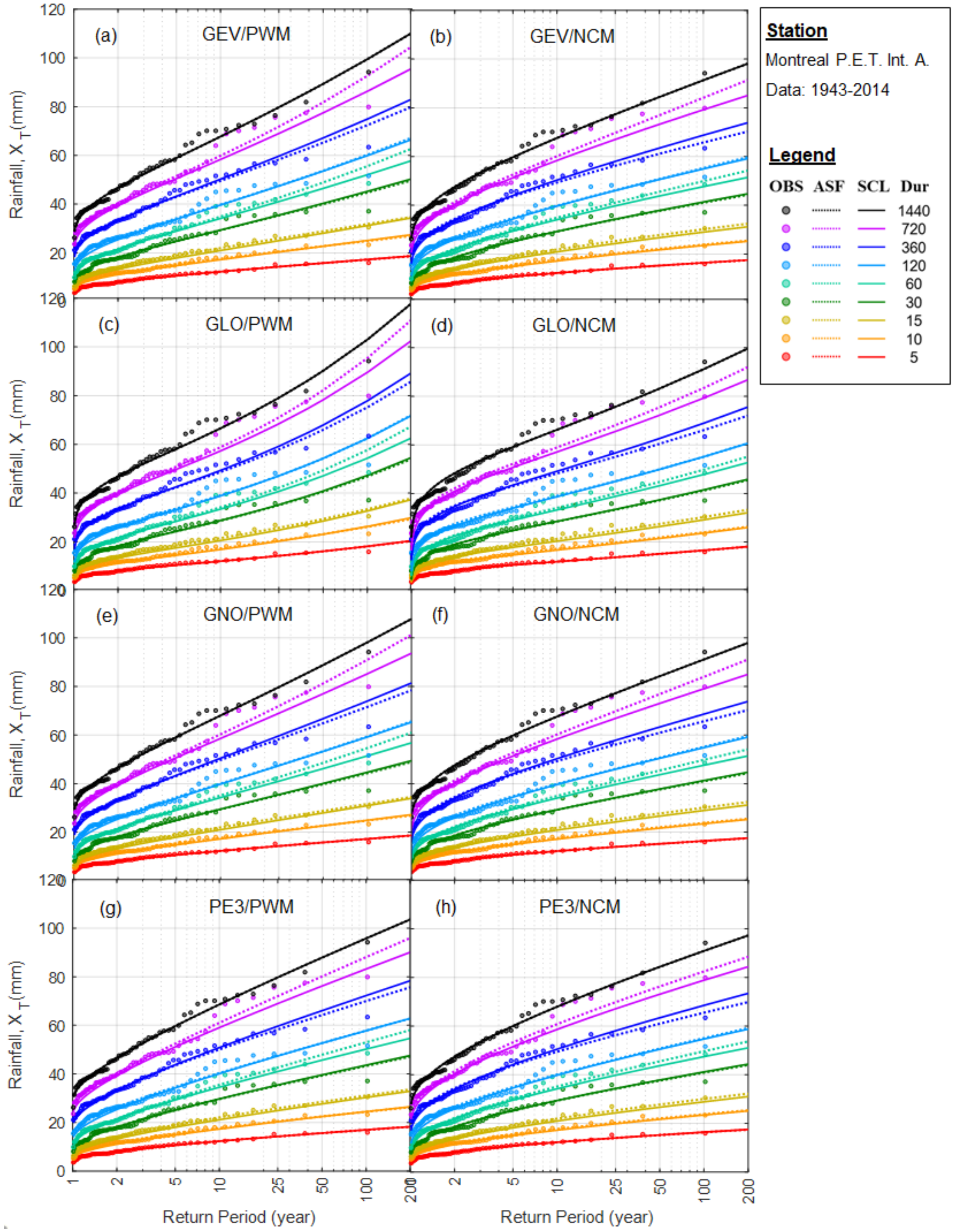

Figure 5-4. Probability plots of the estimated sub-daily and sub-hourly AMS (D = 720 to 5 minutes) derived from the daily AMS (D = 1440 minutes) for Montreal P.E.T. Intl. Airport Station using the scaling approach (SCL, continuous lines) and at-site frequency analysis (ASF, dotted lines) of the observed data (OBS, circle markers).

Figure 5-5 shows the boxplots of the results of the five numerical comparison indices for 5- to 720-minute observed and estimated AMS data for all 74 stations. In general, on the basis of these goodness-of-fit numerical comparison results, it is found that no unique scaling model ranked consistently best for all criteria and all locations. Results based on these models are quite comparable, except the GLO/NCM model consistently produces the worst results for all indices. For the remaining seven scaling models, as can be seen from the boxplots, to the whisker extents, these models produce RMSEr and MADr less than 15% and 10% respectively, RMSE and MAD less than 4 mm and 2 mm, and CC at least 0.98. On average, to the medians, these models produce RMSEr and MADr less than 8% and 6% respectively, RMSE and MAD less than 2.2 mm and 1.2 mm, and CC at least 0.99. Based on the boxplots of the dimensionless indices (i.e. RMSEr and MADr), it can be seen that for each distribution, the PWM estimators yield better results than the NCM estimators. That is, results of PWM-based models display smaller box widths, lower medians and shorter upper whisker extents for the cases of RMSEr and MADr than those of NCM-based models. However, results are almost similar for the four PWM-based scaling models. A ranking scheme is utilized to rank all the models.

Ranking scores (from 1 to 8) are assigned to each model according to the value computed for each index. The model with the lowest RMSE, RMSEr, MAD, MADr, or highest CC is given the rank of 1 for the corresponding assessment category. Thus, ranking from 1 to 8 indicates the gradual decrease from the best to the worst candidates. In case of ties, equal ranks are given to those corresponding models. Furthermore, for each numerical criterion, the overall rank (or total score) of each numerical index was obtained by summing the individual point rank at each station for each model. The total score of each model ranges from 74 (the best) to 592 (the worst) based on 74 stations. In addition, the number of first score was also calculated for each model of each criterion by counting only the number of stations with first score. The total first score of each model ranges from 74 (the best) to 0 (the worst). Note that equal scores were used for tie cases. Hence, for each index, if we sum the total first score across all eight models, the sum can be higher than 74. Results are shown in Figure 5-6. The total scores are displayed in the form of bar graph to the left, while those of the first score are plotted to the right for each criterion. Ranks of the total scores and total first scores are also plotted next to them to help the comparison easier.

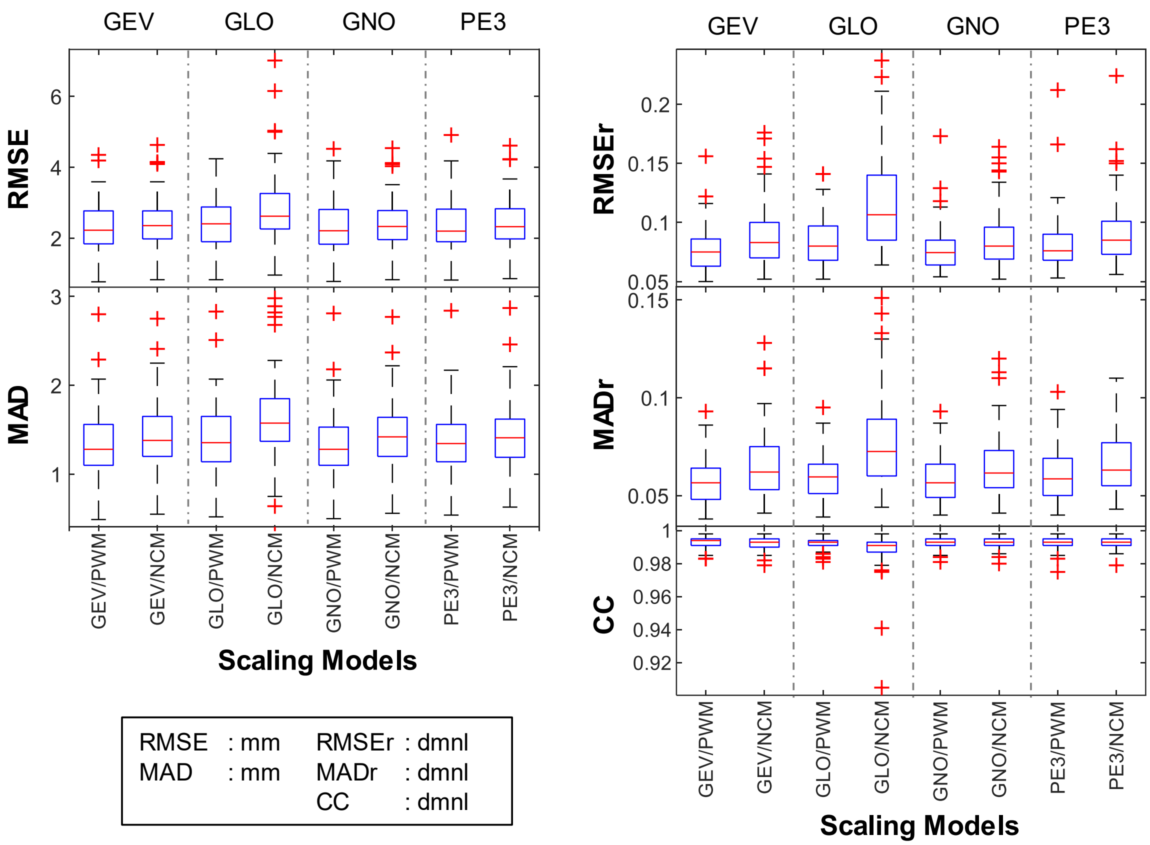

Figure 5-5. Numerical comparisons of the performance of eight scaling models in deriving the distributions and quantiles of sub-daily and sub-hourly (i.e. 5- to 720-minute) AMS from those of daily AMS. The comparisons are based on the real values computed using five criteria: RMSE (mm), RMSEr (dmnl), MAD (mm), MADr (dmnl), and CC (dmnl).

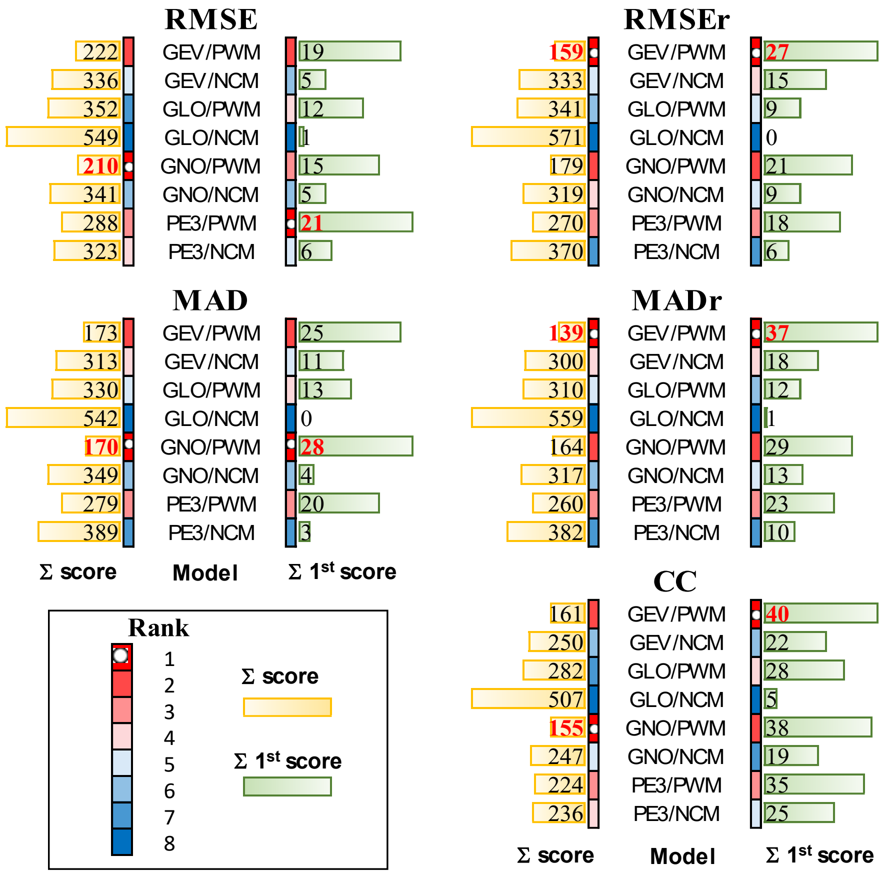

Figure 5-6. Numerical comparisons of the performance of eight scaling models in deriving the distributions and quantiles of sub-daily and sub-hourly (i.e. 5- to 720-minute) AMS from those of daily AMS. The comparisons are based on the rankings of the real values computed using five different criteria: RMSE (mm), RMSEr (dmnl), MAD (mm), MADr (dmnl), and CC (dmnl). For each index, the scores shown on the left are the total score of each model computed by summing the individual rank at each station. While the scores shown on the right are the total first score calculated by counting the number of stations with the first score.

Figure 5-6 shows that, in general, the GNO/PWM and GEV/PWM models are the best models among the eight considered candidates though they do not always perform best at all study stations. In fact, each model performs best for about 1/3 the number of stations (based on RMSE, RMSEr, and MAD criteria), and 1/2 the number of stations (based on MADr and CC criteria). This could be due to the strong spatial variation of rainfall characteristics across the study region. Depending on the criteria, for example, the GNO/PWM model yield the best estimates based on the RMSE and MAD indices. Whereas, the GEV/PWM model yield the best estimates based on the RMSEr and MADr. The two models produce almost the same results for the CC category. Therefore, these two scaling models can be used interchangeably in deriving the distributions of short-duration extreme rainfalls from those of longer duration to improve the accuracy and robustness of the results. In addition, it is necessary to note that the difference in quantile estimates between the top models are small. These values are investigated and plotted in Figure 5-7 and Figure 5-8.

Figure 5-7 and Figure 5-8 show the comparison of the 1-hour and 5-minute design rainfall quantiles for the 100- and 10-year return periods, respectively. These values are estimated using the at-site frequency analysis and the scale-invariance approaches based on both GEV/PWM and GNO/PWM models. From the figures, it is easy to see that the uncertainty of the design rainfall quantiles estimations using two different methods (e.g., ASFA method versus scaling method based on the GEV/PWM or the GNO/PWM model) are much larger than using two different models (e.g., ASFA or downscaled values based on the GEV/PWM model versus the GNO/PWM model). In detail, the difference between the ASFA quantiles and the downscaled quantiles are tiny for the two models. For the low return period (T=10 year), the quantiles estimated using the GNO/PWM model are mostly higher (between 0 and 4%) than those computed using the GEV/PWM model for both rainfall durations. However, for the high return period (T=100 year), the GEV/PWM model yield mostly higher quantile values (between 0 and 3%) for both rainfall durations. Whereas, comparing between the ASFA and the downscaled methods using either the GEV/PWM or the GNO/PWM model show a much larger difference. For the low return period (T=10 year) and for the 1-hour duration, about 40% the downscaled quantiles are overestimated (between 0 and 15%), while the remaining values are underestimated (between 0 and 10%); while for the 5-minute duration, more than 50% values are overestimated (between 0 and 9%), and the remaining values are underestimated (between 0 and 8%). For the high return period (T=100 year) and for the 1-hour duration, about 50% of the downscaled quantiles are either over- or under-estimated (between 0 and 22%); while for the 5-minute duration, about 60% values are overestimated (between 0 and 22%), and the remaining values are underestimated (between 0 and 14%).

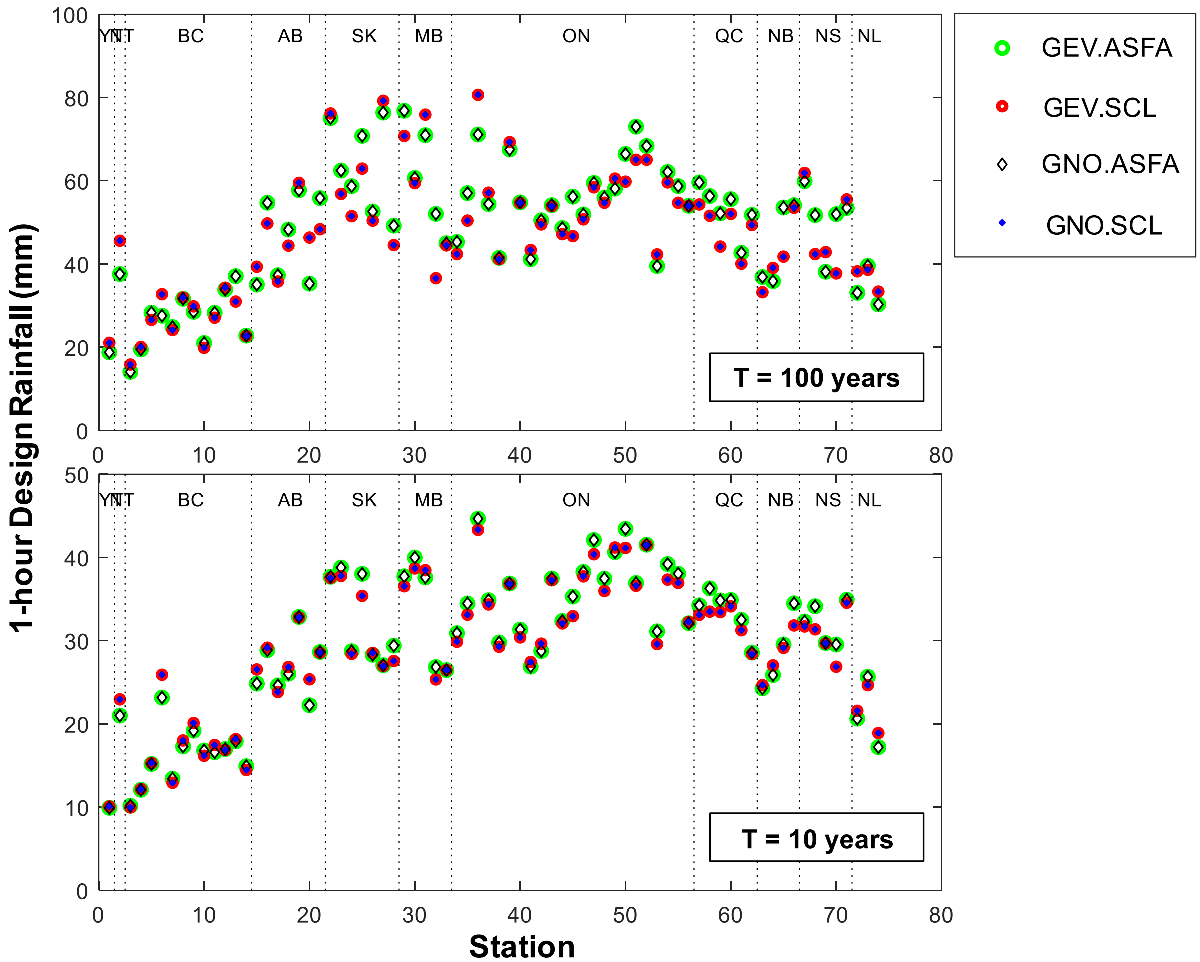

Figure 5-7. Comparison of the 1-hour design rainfalls (mm) estimated using two different distributions (i.e. GEV and GNO) in combination with two different estimation methods (i.e. the at-site frequency analysis, ASFA, and the scaling methods, SCL) for two different return periods (T = 100 and 10 years).

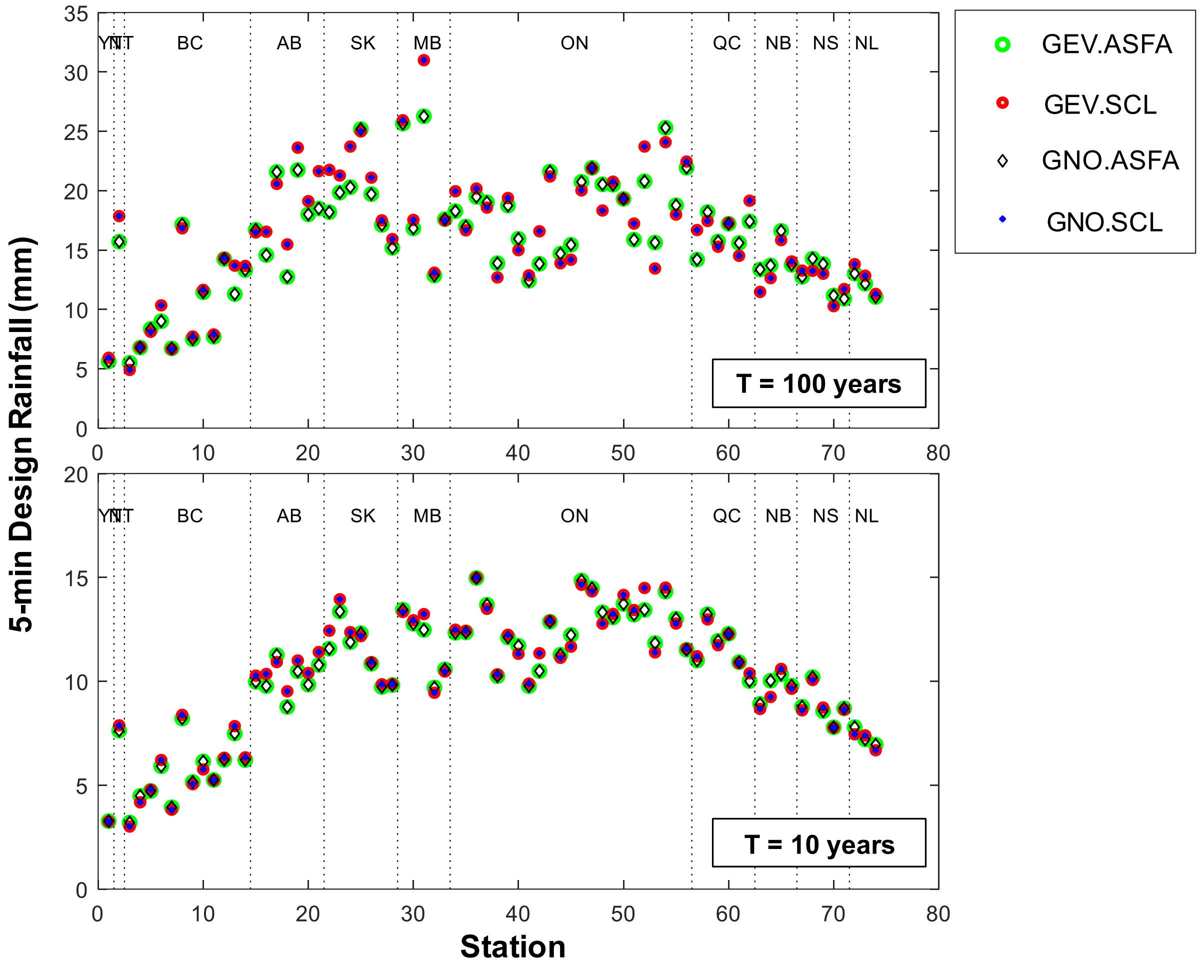

Figure 5-8. Similar to Figure 5-7 but for 5-minute design rainfalls (mm)

5.5 Conclusion

Global and regional climate models along with different (spatial) statistical downscaling approaches have been extensively used to link projected climate change simulations to the daily extreme rainfalls at a given location of interest. Projected data of high temporal resolutions (i.e. sub-daily or sub-hourly) at these local sites are often limited or unavailable due to current limitations on detailed physical modelling and computational capability of these climate models. A few statistical models based on the scale-invariance concepts have been introduced as a tool to overcome this problem. These models can be used for modeling extreme rainfall processes over a wide range of time scales. In particular, in the context of climate change these scaling models can be used to describe the linkages between the distributions of sub-daily extreme rainfalls (ERs) and the distribution of daily ERs that is commonly provided by global or regional climate simulations.

From the literature review, it has been found that the scaling GEV distribution (i.e. GEV/PWM and GEV/NCM models) and its special cases, the scaling GUM distribution (i.e. GUM/PWM and GUM/NCM models) have been used in a number of publications. Nevertheless, there is still no general agreement as to which statistical model should be used for describing the distribution of annual rainfall extremes over a wide range of temporal scales (e.g., from one day to several minutes). The GEV distribution has been widely used as a reasonable candidate. However, some countries recommend the use of a specific distribution model other than the GEV distribution. The present study therefore introduces several novel scale-invariance models that are developed based on some popular probability distributions. These distributions have been recommended in several national guidelines and frequently used in the frequency analysis of extreme hydrologic variables. They are the generalized logistic (GLO), generalized normal (GNO), and Pearson Type 3 (PE3) distributions. Their mathematical frameworks and scaling properties are first derived and formulated in this research based on both the non-central moment (NCM) and probability weighted moment (PWM) system. This results in six different novel scaling models, including the GLO/NCM, GLO/PWM, GLO/NCM, GLO/PWM, PE3/NCM, and PE3/PWM models that can be utilized for representing the distributions of AMS over different time scales.

The feasibility and accuracy of the six proposed scaling models in estimating the quantiles and distributions of short-duration ERs were assessed and compared with the observed data. In addition, they are compared with other two existing scaling models, including the GEV/NCM and

GEV/PWM models (Nguyen and Nguyen, 2018). Long record ER data (containing at least 40 years) of nine different rainfall durations (from 5 minutes to one day) from a network of 74 raingauges located across Canada were used for the assessments and comparisons. The estimated short-duration extreme rainfall quantiles highly agree with the observed data with RMSEr and MADr less than 15% and 10% respectively, and CC at least 0.98 for all models, except the GLO/NCM model which produced higher errors and lower correlation coefficients. Results also showed that the PWM-based scaling models produced better estimations than the NCM-based ones. Among the eight candidates considered, the GNO/PWM and GEV/PWM models are the top two models. Their results are virtually indistinguishable on graphical displays. Numerical comparisons of 5-minute and 1-hour design rainfall quantiles estimated from those of 1-day duration showed that for the low return period (T=10 year), the quantiles estimated using the GNO/PWM model are mostly higher (between 0 and 4%) than those computed using the GEV/PWM model for both rainfall durations. However, for the high return period (T=100 year), the GEV/PWM model yielded mostly higher quantile values (between 0 and 3%) for both rainfall durations. Hence, in practice, the two scaling models can be used interchangeably or used together to enhance the accuracy and reliability of the estimation of extreme design rainfalls in the current climate and in the context of climate change.

The scaling GLO/PWM model though performed poorer than the GEV/PWM and GNO/PWM models in terms of goodness-of-fit (GOF) test, it tends to yield more conservative results (i.e. higher quantile estimates) for quantiles of return periods beyond the available record lengths than the other models (i.e. GEV/PWM and GNO/PWM models). This model thus could be used for assessing the climate change impacts on the IDF relations to increase the confidence, especially in the UK where the GLO distribution has been recommended for modeling of extreme hydrologic variables. An example could be found in Nguyen and Nguyen (2018b)

The scaling PE3/PWM model was the third best model after the scaling GEV/PWM and GNO/PWM models. It produced better GOF test values compared to the GEV/NCM model that has been used as the temporal downscaling model in some water-related climate change impact assessments studies (Nguyen et al., 2007; Nguyen and Nguyen, 2008; Herath et al., 2016; Hassanzadeh et al., 2019). It is also better than the scaling GLO/PWM model in terms of GOF test. However, the model tends to yield lower quantile estimates (of return periods beyond the available record lengths) than the other models (i.e. GEV/PWM and GNO/PWM models). Thus, if the AMS is believed to follow the PE3 distribution, then the scaling PE3/PWM model is a good choice to modelling extreme rainfall processes across a wide range of time scale for both the historical and projected data. Otherwise, it should be used with cautious since the quantiles of high return periods could be underestimated.

This work could be extended in the future to consider the mathematical framework and scaling properties of the log-Pearson Type 3 distribution that has not been covered in this research yet. This model has been recommended as an appropriate distribution for modelling annual maximum peak flow in some national guidelines and the flood process has been shown to possess some scaling properties in some publications. In addition, regional flood/rainfall frequency analysis based on the scaling approach could be an alternative solution to the current index flood/rainfall approach.

Chapter 6. Decision-Support Tool for Constructing Robust Rainfall IDF Relations in Consideration of Model Uncertainty and Climate Change Information for The Design and Management of Urban Water Systems

6.1 Introduction

Rainfall frequency analyses are commonly used for the design of various urban hydraulic structures, such as dams, culverts, and storm sewers. Results of these analyses are often summarized by "intensity-duration-frequency" (IDF) relations for a given site or they are presented in the form of "rainfall frequency atlas", which provides rainfall accumulation depths for various durations and return periods over the region of interest (see, e.g., WMO, 2009a; NOAA's Atlas 14, 2014; Environment Canada, 2014). It should be noted that the word "duration" refers to the length of a time-window used to statistically characterize the precipitation intensities rather than the storm duration. In current engineering practices, the IDF relations are derived based on statistical frequency analyses of annual maximum rainfall series (AMS) data where available rainfall records of adequate lengths could be used to estimate the parameters of a selected probability distribution (WMO, 2009a; CSA, 2012).

In general, selection of a suitable distribution to representing AMS is the most difficult and time-consuming task since there are many recommended probability models available in the literature as well as in the national design guidelines from different countries (Stedinger et al., 1993; Hosking and Wallis, 1997; Rao and Hamed, 2000; WMO, 2009a; CSA, 2012; Salinas et al., 2014; Ball et al, 2016). Recently, a systematic approach has been proposed by Nguyen et al. (2017) to identify the most appropriate probability distributions among several candidate models for providing the most accurate and most robust extreme rainfall estimates. This systematic approach has been shown to be more efficient and more robust than the traditional model selection method since it was based on two main steps: (i) a detailed evaluation of both descriptive and predictive abilities of a probability model as well as its uncertainty (rather than only the descriptive ability as in most previous studies); and (ii) a systematic comparison of the accuracy and robustness of all candidate models based an extensive set of graphical and numerical performance criteria.

Descriptive ability relates to the goodness-of-fit of the theoretical probability model to the empirical frequency distribution given by the observed extreme rainfall data while the predictive ability is concerned with the accuracy and robustness of the extreme rainfall quantile estimates given by the selected model using the rainfall data in the validation period (that are different from those data used in the calibration of the selected model). This predictive ability assessment, however, is a highly time-consuming task since it requires the generation of a large number of random rainfall samples (for instance, by bootstrap method) for different rainfall durations (from several minutes to hours or days) for establishing the IDF relations for a given site, or for constructing the regional rainfall frequency maps using the data from many different locations over a given region.

Consequently, based on the advanced computing capability of existing computer systems it is necessary to develop a decision-support tool that could facilitate the application of the proposed systematic model selection approach in an efficient manner in order to be able to identify automatically and objectively the best probability models for a large number of datasets. There are several tools published and available to solve partly the issues, for example, the Rainbow (Raes et al., 2006), RainIDF (Chang et al., 2013), HEC-SSP (Bartles et al., 2016). These tools rely only on the descriptive ability with a limited number of goodness-of-fit tests to identify the best distribution. In addition, they allow to perform frequency analyses without the IDF construction using only a limited number of probability models. The other tools allow construction of IDF curves but for only a specific distribution or a specific regression model.

In addition, climate change has been recognized as having a profound impact on the hydrologic cycle at various spatial and temporal scales in recent years. The intensity and frequency of extreme rainfall events in most regions will be likely increased in the future (Shephard et al., 2014, Zhang et al., 2017). Hence, there exists an urgent need to assess the possible impacts of climate variability and climate change on the IDF relations for improving the design of urban drainage systems in the context of a changing climate (Willems et al., 2012, CSA, 2012, Madsen et al., 2014, Simonovic et al., 2016). To assess the potential impacts of climate change and climate variability, the global and regional climate models have been extensively used in many studies. However, due to current limitations on the detailed physical modelling and computational capability, these models could only provide output scenarios at the macro and meso scales and on a daily time step which are ineffective to inform decision-making at the micro (or local) scales (Nguyen and Nguyen, 2008; 2018a). Thus, resolving the spatial and temporal scale issues are crucial for reliable assessment of climate change impacts, so that local decision makers can possibly evaluate what the likely climate change impacts are, such as maximum rainfalls, at the urban or local scales. Recently, a spatiotemporal statistical downscaling approach has been proposed by Nguyen and Nguyen (2019b) to modelling extreme rainfall processes over a wide range of space scales (e.g., from regional to local) and time scales (e.g., from several minutes to one day). This procedure allows establishing the linkage between daily extreme rainfalls at regional scales and daily and sub-daily extreme rainfalls at a local (point) scale.

In view of the above issues, the main objective of the present study is to propose a decision-support tool (hereafter referred to as SMExRain – Statistical Modelling of Extreme Rainfalls). The tool has been first developed to consolidate the weather extreme data and to help visualize the descriptive and predictive scenarios of different probability distribution models commonly-used in modeling extreme hydrologic processes. This aids the decision-makers in identifying the most suitable probability models for performing rainfall frequency analyses in general and for constructing IDF relations in particular. This user-friendly and freely available tool was developed based on the recent publication by Nguyen et al. (2017) and Nguyen and Nguyen (2019a). Furthermore, the tool is also capable of establishing the linkage between climate projections of climate change available at large-scale to local scales (i.e. to see smaller regional impacts of climate change) with or without empirical data.

Details on SMExRain structure and its methodology are described in Section 6.2. Two case studies are presented as the illustrative applications of the decision-support tool in estimating the extreme design rainfall values for the current climate and assessing the impacts of climate changes on these design values. The first case study, presented in Section 6.3, shows the application of SMExRain in identification of the best distribution for Ontario region and for construction of IDF relations using a 252 AMS from a network of 84 stations. The second case study, presented in Section 6.4, shows the application of SMExRain in assessing climate change impacts on local extreme rainfall processes. The climate simulation outputs from 21 global climate models (GCMs) and the observed extreme rainfall data over Ontario region, Canada, were used for the case study.

Results of these numerical applications have indicated the feasibility and high efficiency of the proposed SMExRain software. The conclusions and discussion are then provided in Section 6.5.

6.2 The Decision-Support Tool: SMExRain

6.2.1 General description

SMExRain has been coded in Matlab environment and equipped with a user-friendly ribbon interface (see Figure 6-1). It can independently run without any requirement of a Matlab version. However, it requires the installation of the free-of-charge Matlab Compiler Runtime (MCR) v9.1 corresponding to the Matlab R2016b version (Mathworks, 2016). Note that using an incompatible MCR may cause the program to be malfunction. The different steps involved in the structure of the SMExRain tool is depicted in Figure 6-2.

Inputs for SMExRain are annual maxima of different specified rainfall durations. Notice however that if rainfall data are collected at fixed observation times, for example clock hours, they may not provide the correct maximum amounts for the specified durations. Hence, it is important to apply some adjustment procedure to convert the measured (fixed-observation time) constrained annual maxima to (moveable observation time) unconstrained values if the dataset has not already been adjusted by the providers (CSA, 2012; NOAA’s Atlas 14, 2014). For the climate change impact assessment studies, SMExRain also requires the projected extreme rainfall series available at the regional scales.

Figure 6-1. The graphical user interface (GUI) of the SMExRain software

In the data screening and preliminary analysis step, SMExRain provides users with several computed common statistical properties. In addition, it also provides users with many useful graphs for statistical analyses, including the histogram plot for empirical probability density function analysis, the time series plot for trend analysis, and the boxplot for outlier detection. Note that outlier values (i.e. significantly different from the other observations in the sample) are not excluded from the frequency analyses of the extreme rainfall series if they pass the quality check (CSA, 2012). Furthermore, three statistical tests were included for testing the independence and stationarity of the input data series: the Mann-Whitney test for homogeneity and stationarity (jumps), the Mann–Kendall test for trend detection, and the Wald-Wolfowitz test for independence and stationarity (Rao and Hamed, 2000; WMO, 2009a).

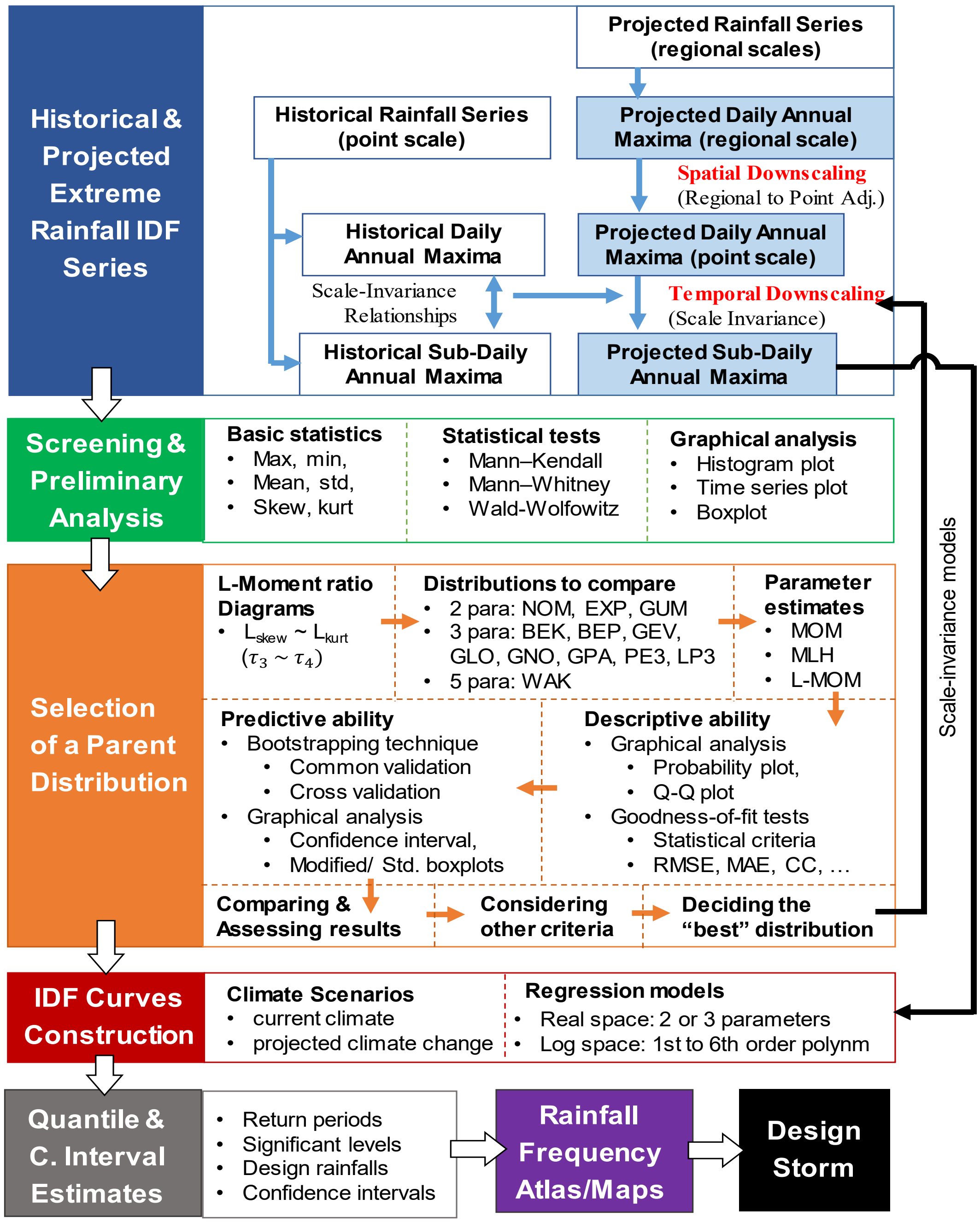

Figure 6-2. SMExRain structure and functions

For selecting a best-fit probability distribution, various numerical and graphical criteria could be employed. This descriptive ability assessment includes most common tools such as the popular L-moment ratio diagram, different statistical goodness-of-fit (GOF) tests, and various graphical displays. In addition, SMExRain provides necessary tools for evaluating the predictive ability of a model. For convenience, SMExRain allows users to perform the assessment and comparison of up to twelve probability distributions simultaneously rather than to evaluate a single distribution at a time.

6.2.2 Estimation of extreme design rainfalls for the design of urban water systems

The extreme design rainfall values necessary for the design and management of urban water systems at a given small urban watershed could be computed based on the rainfall frequency analyses of historical extreme rainfall values available at that location or at the nearby locations. The frequency analysis could be carried out by first selecting an appropriate distribution and parameter estimation method among many candidates available and then fitting the selected distribution to the observed dataset to estimate the design rainfall quantiles corresponding to the desired return periods

6.2.2.1 Probability distributions and parameter estimation procedures

SMExRain includes several common probability distributions that have been selected based on their popularity in hydrologic frequency analyses: Beta-K (BEK), Beta-P (BEP), Generalized Extreme Value (GEV), Generalized Normal (GNO), Generalized Logistic (GLO), Generalized Pareto (GPA), Gumbel (GUM), Log-Pearson Type III (LP3), Pearson Type III (PE3), and Wakeby (WAK) distributions. Other special cases of these distributions, such as exponential

(EXP) and normal (NOM) were also included in the software. Regarding the estimation of the distribution parameters, the method of L-moments is used for all distributions (Hossking and Wallis, 1997) except for the BEK and BEP models that are estimated by the method of maximum likelihood (Mielke and Johnson, 1974). GEV parameters are estimated by both the L-moments (denotes as GEV) and non-central moments (denotes as GEV*) methods (Nguyen et al., 2017).

Furthermore, it is noted that the parameter (or quantile) estimates of some distributions, such as BEK, BEP, GEV*, GNO, PE3, LP3, are in implicit forms and they require iterative solving methods. Numerical methods are thus utilized to obtain approximate solutions. SMExRain relies on the accuracy of the f-solve function supported by MATLAB with the three well-known and powerful algorithms, including the trust-region dogleg, the trust-region-reflective, and the Levenberg-Marquardt to achieve feasible solutions (Mathworks, 2016). For the case of BEK, BEP, and GEV*, different initial parameter values other than the default values might be used if the solutions do not converge (which can be easily check using the probability or Q-Q plots described in the following sub-section). In addition, to enhance the accuracy and to speed up the quantile estimates processes of the GNO/NOM and PE3/LP3 distributions, SMExRain was equipped with the normal inverse and incomplete gamma inverse functions (Mathworks, 2016).

6.2.2.2 Goodness-of-fit (GOF) tests for assessing the descriptive ability of a distribution

To visually assess the GOF of a fitted distribution to an observed rainfall dataset, the SMExRain provides probability plots and quantile-quantile (Q-Q) plots. Many commonly-used empirical plotting position (EPP) formulas available in the literature are included in this software as shown in Table 6-1. In addition, it also provides a general user-customized EPP formula. The review and selection of an appropriate EPP formula can be found in several publications, for example, Cunnane (1978), Nguyen et al. (1989), Inna and Nguyen (1989), and Helsel and Hirsch (2002).

Table 6-1. Empirical plotting position formulas equipped in SMExRain

Method	Formula
Hazen (1914)	$\frac{m-0.5}{N+0}$
Weibull (1939)	$\frac{m-0}{N+1}$
Beard (1943)	$\frac{m-0.3}{N+0.38}$
Benard and Bos-Levenbach (1953)	$\frac{m-0.3}{N+0.2}$
Chegodajev (1955)	$\frac{m-0.3}{N+0.4}$
Blom (1958)	$\frac{m-\frac{3}{8}}{N+\frac{1}{4}}$
Tukey (1962)	$\frac{m-\frac{1}{3}}{N+\frac{1}{3}}$
Gringorten (1963)	$\frac{m-0.44}{N+0.12}$
Cunnane (1978)	$\frac{m-0.4}{N+0.2}$
Adamowski (1981)	$\frac{m-0.25}{N+0.5}$
Nguyen et al. (1989)	$\frac{m-0.42}{N+(0.3\gamma+0.05)}$
In-na and Nguyen (1989)	$\frac{m-(0.13\gamma+0.27)}{N+(-0.08\gamma+0.38)}$

Note: General formula: $\frac{m-A}{N+B}$, where m = rank of the data point; N = sample size (or number of data points); and γ = sample skewness coefficient. A and B are constants and receive different values for different formulas or can be specified by users.

In addition to the visual assessment, SMExRain includes also four popular numerical indices to provide a more accurate evaluation of the best fit of a distribution; namely, the root mean square error (RMSE), the relative root mean square error (RRMSE), the maximum absolute error (MAE), and the correlation coefficient (CC) (see Chapter 2). Furthermore, to facilitate the identification of the probability models with the best descriptive ability, a convenient ranking scheme has been developed to judge the overall GOF of each distribution. Rankings are assigned to each distribution according to the computed values of these numerical indices. For instance, a distribution with the lowest RMSE, RRMSE, MAE and highest CC would be given the rank of 1. In the case of a tie, average ranks are assigned to those tied distributions.

6.2.2.3 *Bootstrap method for assessing the predictive ability of a distribution*

The bootstrap method repeatedly draws, with replacement, n observations from the available data set of size N (N>n) (Efron and Tibshirani, 1994). First, a portion of "n" data points from the original sample of size N (n < N) is selected. In SMExRain, two options are provided: common validation and cross validation. In the former option, users can select the first or second half of a given sample to do bootstrapping. In the latter option, a portion of the sample of size n can be extracted with the starting point selected randomly. Then the bootstrap samples (hundreds to thousands) are generated based on these "n" selected values. The default value is 1000 samples for reliable results and efficient computation costs. Each candidate distribution is then fitted to the generated bootstrap samples and is extrapolated to estimate the right-tail quantiles corresponding to the k largest (k=4 by default) observed rainfall amounts in the full data set (N values). The variability in the estimation of these extrapolated quantiles is presented in the form of modified boxplots by default. However, users can also easily switch to the standard boxplots (Helsel and

Hirsch, 2002). Large box widths or long whiskers imply high uncertainty in the estimation of these k largest rainfall values. If the observed values fall outside the box, then the distribution fitted to the bootstrap samples has overestimated or underestimated the true values and this distribution is therefore not recommended since it does not provide accurate rainfall estimates. Note that SMExRain allows user to compare the predictive ability of up to twelve models simultaneously using the same generated samples to ensure a fair comparison.

6.2.3 Updating extreme design rainfalls considering climate change information for the design and management of urban water systems

The are two main steps to assess the potential climate change impacts on the local short-duration extreme rainfalls. The first step is to establish the linkage between projected daily extreme rainfalls available at a regional scale and daily extreme amounts at a local site of interest. The second step is to determine the distribution of sub-daily extreme rainfalls from the estimated daily extreme rainfalls at the given location. A detailed description of these two steps is presented in Figure 6-3 and in the following sections.

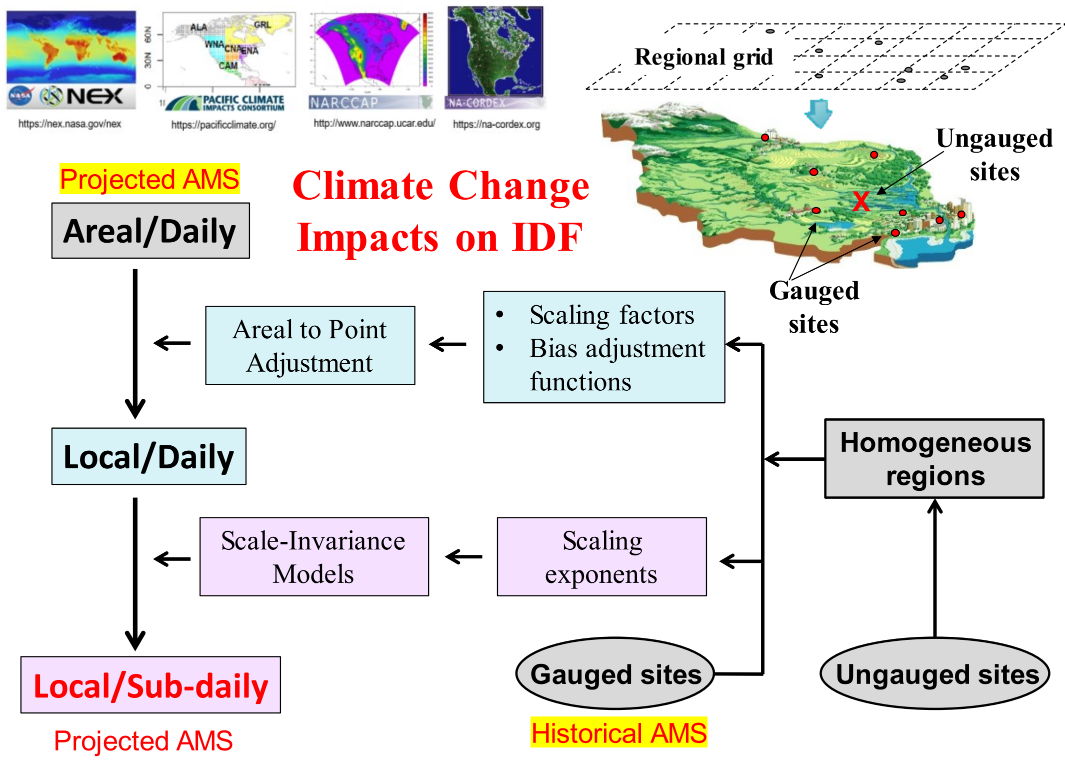

Figure 6-3. The two steps in SMExRain to link the regional daily climate change projections to the local sub-daily extreme rainfalls at a given location of interest

6.2.3.1 Linking the projected regional climate simulations to local daily extreme rainfalls

In SMExRain, the spatial linkage between the extreme rainfalls available at a regional scale $\hat{X}$ and at a given local site X_i could be established using different statistical models based on two different manners. The first approach is based on the use of a scaling factor η_i to correct the mean of the regional data and the mean of the at-site data as shown by Eqn. (6-1). The second method relies on a bias correction function $e(F)$ to correct the differences between the empirical cumulative distribution functions (ECDF) of regional and at-site daily extreme rainfalls as indicated by Eqn. (6-2). This bias correction function can be represented by a regression model (i.e., a second-degree polynomial function) as shown by Eqn. (6-3) (Nguyen and Nguyen, 2008;

Willems et al., 2012). For gauged sites, both approaches could be used and estimated based on the empirical data at the study sites (Nguyen and Nguyen, 2019b). For ungauged sites, where observed data is unavailable, the scaling factors at a given location could be computed based on the interpolated mean at that site transferred from those of the neighboring stations located within a same homogeneous region (Nguyen et al., 2018).

$$X_i(F) = \delta_i \cdot \hat{X}(F) \tag{6-1}$$

$$X_i(F) = \hat{X}(F) + e(F) \tag{6-2}$$

$$e(F) = c_o + c_1 \cdot \hat{X}(F) + c_2 \cdot [\hat{X}(F)]^2 + \varepsilon \tag{6-3}$$

where $X_i(F)$ is the adjusted daily extreme rainfall at the local site of interest i; $\hat{X}(F)$ is the daily regional ER at the grid containing that site; F is the cumulative probability of interest; $\delta_i = \mu_i/\hat{\mu}$ is the scaling factor at site i; μ_i and $\hat{\mu}$ are respectively the mean of the daily extreme rainfalls at the local site i and the mean of the regional values at the grid containing that particular site; $e(F)$ is the bias correction function associated with $\hat{X}(F)$; $c_o, c_1, and\ c_2$ are the coefficients of this function which can be estimated based on the least square technique and ε is the error term.

6.2.3.2 Linking the estimated local daily to sub-daily extreme rainfalls

In SMExRain, the temporal linkages between local daily and sub-daily extreme rainfalls are performed based on the scale-invariance models. Scale invariance implies that the statistical properties of extreme rainfalls over different time scales are related to each other by an operator involving only the scale ratio and the scaling exponent. In particular, the distributions of sub-daily extreme rainfalls are derived using the scale-invariance probability weighted moment-based Generalized Extreme Values (GEV/PWM) model. The GEV/PWM model has been recently shown to perform superior than other existing scale-invariance models (Nguyen and Nguyen, 2018a). More specifically, the quantile, X_T, corresponding to a given return period $T = 1/(1 - F)$, of the GEV model can be estimated once the parameters are known as in Eqn. (6-4). These parameters could be estimated based on the method of PWMs and L-moments (Hosking and Wallis, 1997). For a simple scaling process, it can be shown that the r^{th}-order PWMs, β_r, of rainfall data, parameters and quantiles of the GEV distribution model for two different rainfall durations t and λt can be related as in Eqn. (6-6) and Eqn. (6-7). For gauged sites, the scaling exponents could be computed based on the empirical data at the study sites (Nguyen and Nguyen, 2019b). For ungauged sites, where observed data is unavailable, the scaling exponents at a given location could be interpolated from those of the neighboring stations located within a same homogeneous region (Nguyen et al., 2018).

$$X_T = \xi + \frac{\alpha}{\kappa}\{1 - [-\ln(F)]^{\kappa}\} \tag{6-4}$$

$$\beta_r = M_{1,r,0} = E[X\{F(X)\}^r] = (r+1)^{-1}\left(\xi + \frac{\alpha}{\kappa}\{1 - (r+1)^{-\kappa}\,\Gamma(1+\kappa)\}\right) \tag{6-5}$$

$$\beta_r(\lambda t) = \lambda^{\eta_r}\beta_r(t) = \lambda^{\eta}\beta_r(t) \tag{6-6}$$

$$\alpha(\lambda t) = \lambda^{\eta}\alpha(t);\ \xi(\lambda t) = \lambda^{\eta}\xi(t); \kappa(\lambda t) = \kappa(t);\ \ X_T(\lambda t) = \lambda^{\eta}X_T(t); \tag{6-7}$$

in which $\xi, \alpha,$ and κ are the location, scale, and shape parameters respectively; and F is the cumulative probability of interest. $\Gamma(.)$ is the gamma function and r must be non-negative; $\eta_r = \eta$ is the scaling exponent and can be estimated based on the mean $E\{X\}$ (that is, the PWM of order $r = 0$).

6.2.4 Graphical and tabular forms of IDF relations for engineering practice

In SMExRain, IDF relations are provided in both tabular and graphical forms for the computed rainfall intensities (or depths) for different durations (usually from five minutes to one day) and for different return periods of interests (commonly from two to a hundred years).

Depending upon the empirical mathematical model selected for representing the IDF relations, the coefficients (parameters) of this model are computed using the least-square technique. In general, the mathematical form of the empirical model is chosen such that it can facilitate the interpolation of rainfall intensities for a given observed duration or interpolated (unobserved) duration. SMExRain supports many popular regression equations in both real-space (with two or three coefficients) and log-space (with polynomial up to order 6) as shown in Table 6-2 based on some available practical guidelines (WMO, 2009a; Ball et al., 2016). It is noted that even using the same mathematical expression, for example, the well-known model $I = \frac{a}{t^b}$, the computed values of the empirical coefficients "a" and "b" could be completely different depending on whether the estimation was performed in the real space or in the log-space (see Figure 6-4). A further detail related to the use of different regression-based methods in hydrologic frequency analysis can be found in Pandey and Nguyen (1999).

Table 6-2. Regression formulas supported in SMExRain

Optimization	**Formula**
Real-space least squares	$I = \frac{a}{t^b}$; $I = \frac{a}{t^b + c}$; $I = \frac{a\,T}{t^b + c}$; $I = \frac{a}{(t+c)^b}$; $I = \frac{a + b.\log(T)}{(1+t)^c}$
Log-space least squares	$\log(I) = \sum_{k=1}^{p+1} C_k\,(\log t)^{p+1-k}$ $= C_1(\log t)^p + C_2(\log t)^{p-1} + \cdots + C_p(\log t) + C_{p+1}$

Note: I = average rainfall intensity, that is, depth per unit time (generally expressed in mm/hr); t = precipitation duration (min or hr); T = return period (years), p = polynomial order (supported lowest and highest orders are $p = 1$ and $p = 6$, respectively); and a, b, c, and C_k ($k = 1,2, \ldots, p$) = coefficients varying with the locations and return periods.

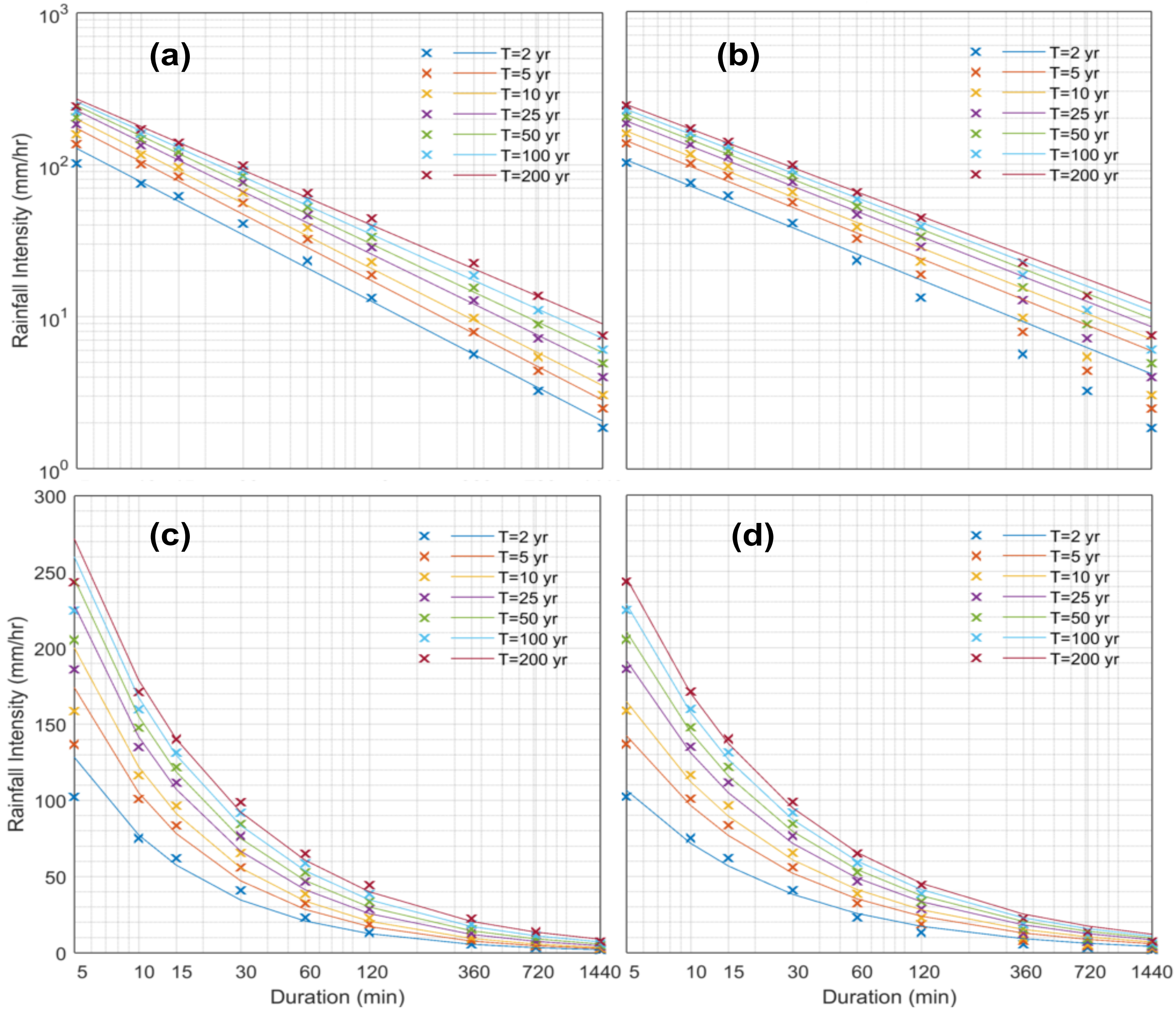

Figure 6-4. Fitting the regression model $RI = \frac{a}{t^b}$ in the log-space (a & c) and real space (b & d). The results are displayed in the log(x)-log(y) (a & b) and semi-log(x) (c & d).

6.3 Numerical Application: Estimation of historical extreme design rainfalls

This section presents the application of SMExRain in supporting users in making decision on the best distribution model(s) among several considered candidates for a large number of study sites. It also shows the uncertainty of design rainfall estimates using different selected distribution models.

6.3.1 Database

The feasibility of the proposed decision-support tool SMExRain has been tested using IDF data available from a wide-range rain-gauge network located in different provinces of Canada, including Quebec (Nguyen and Nguyen, 2015), British Columbia (Lim, 2016), and extensively in Ontario (Nguyen et al., 2017). In this paper, for illustrative purposes, only results from the application of the SMExRain for Ontario were presented based on a total of 252 rainfall datasets for three rainfall durations (5 minutes, 1 hour, and 24 hours) from a network of 84 stations (see Figure 6-5).

Preliminary analysis using L-moment ratio diagrams for all stations and all three durations with record lengths of at least 40 years, 30 years, and 20 years were performed. Figure 6-6 shows the L-moment ratio diagram of annual maximum series of all study stations and three rainfall durations as an illustration. The wide spread of data points from one group of the same rainfall duration or from three groups of different durations on the diagram show that no distribution can be selected at the best distribution for all the datasets. On average, the GEV and GNO models could be considered the most suitable models.

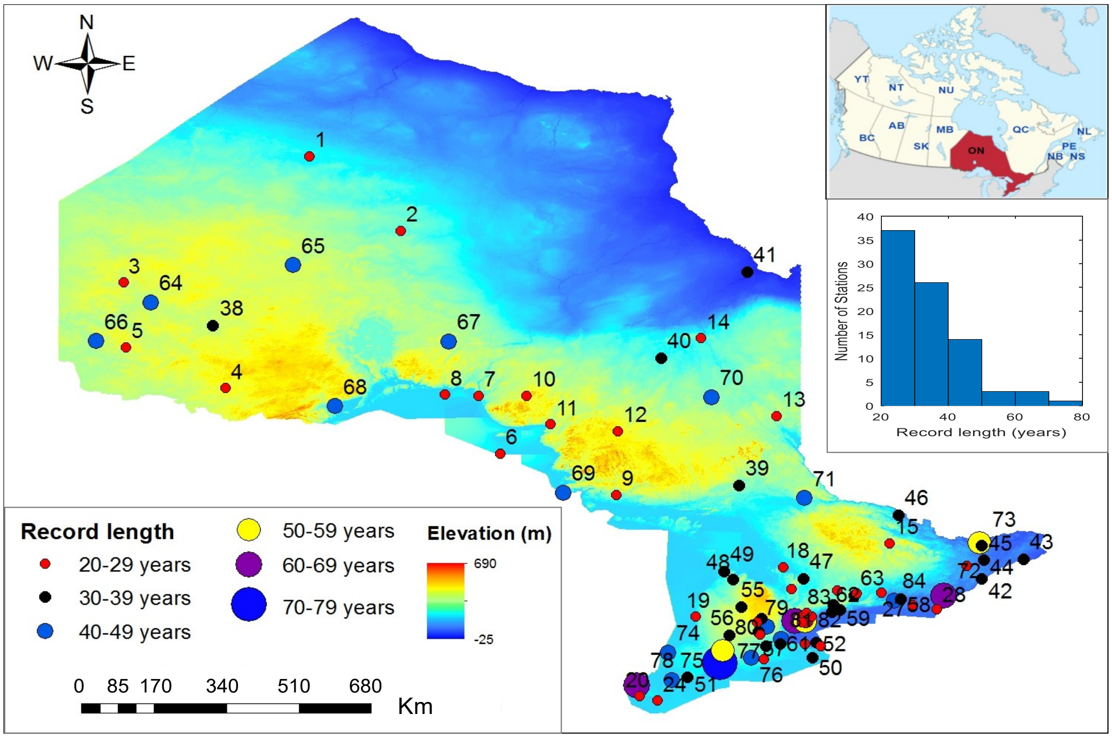

Figure 6-5. Locations of the 84 study raingauges in Ontario. Station names are provided in the appendix.

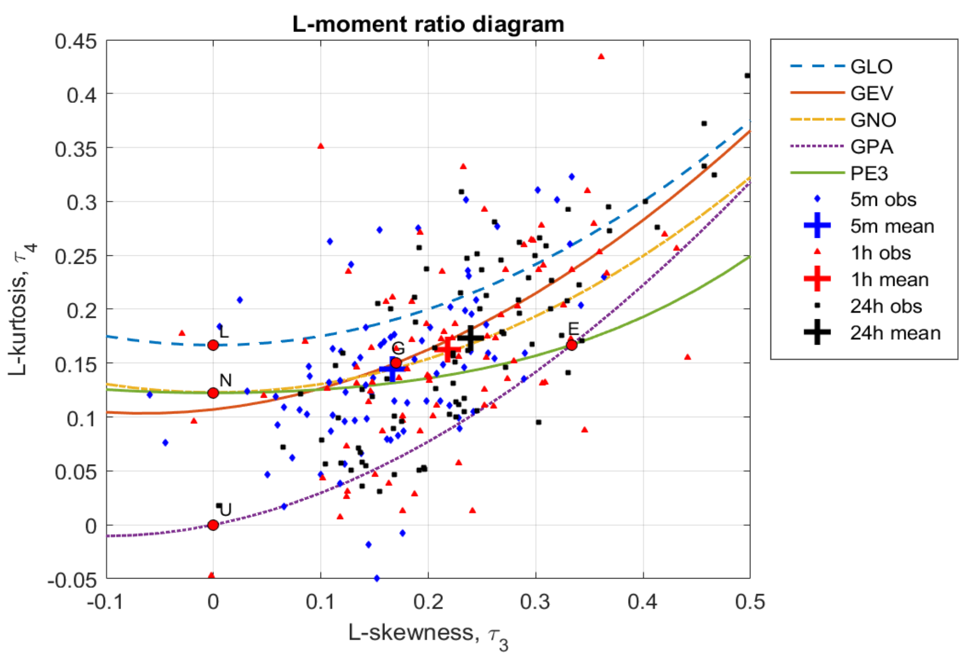

Figure 6-6. L-moment ratio diagram of 252 AMS from 84 rain-gauges containing at least 20-year records. The blue diamond and '+', red triangle and '+', and black rectangle and '+' markers denote 5-min, 1-hour, and 24-hour dataset L-skewness and L-kurtosis and their corresponding group average values respectively

6.3.2 Decision-support process

6.3.2.1 Descriptive ability assessment results

The Q-Q plots of all 252 AMS shows that all distributions closely described the left-tail and central parts. The right-tail parts, however, are less well described and there are no obvious trends. These values can be accurately estimated, over-estimated, or under-estimated by any of the 11 candidates.

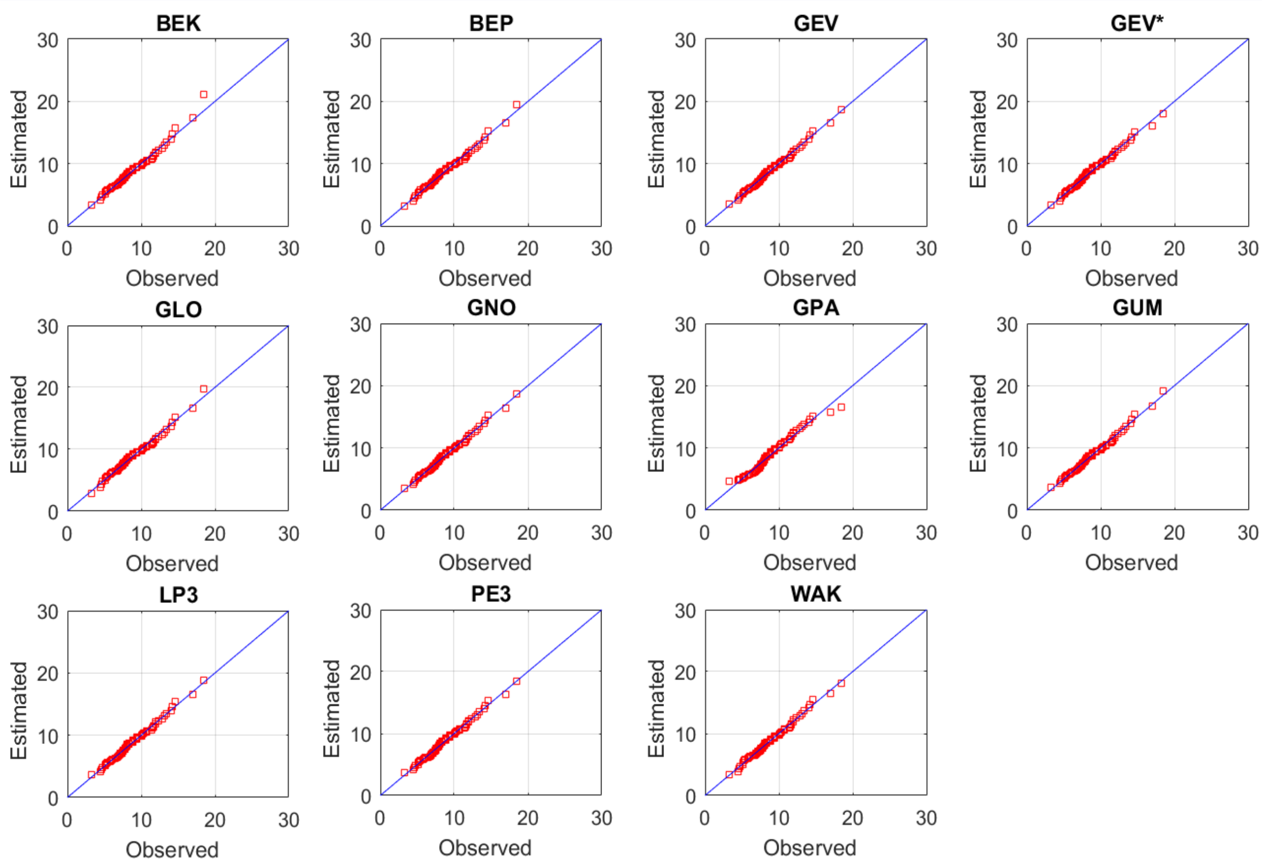

Figure 6-7. Q-Q plots for distributions fitted to 5-min AMS at Toronto Int. Airport station

For purposes of illustration, Figure 6-7 shows the results for 1-hour AMS from the longest rainfall record available at Toronto Int. Airport station. From the visual standpoint, all distributions seem to perform well in this case, except the BEK and GPA distributions. However, the significance of the differences between the remaining models is difficult to judge merely based on the graphical display, as the differences are minor. A more objective evaluation using numerical comparison criteria is thus required.

The goodness-of-fit tests based on the four statistical criteria (RMSE, RRMSE, MAE, and CC) were computed for the 11 candidates for numerical comparisons of the 5-min AMS. These criteria were calculated for stations containing at least 40-year, 30-year, and 20-year records, respectively. Results are presented in Figure 6-8.

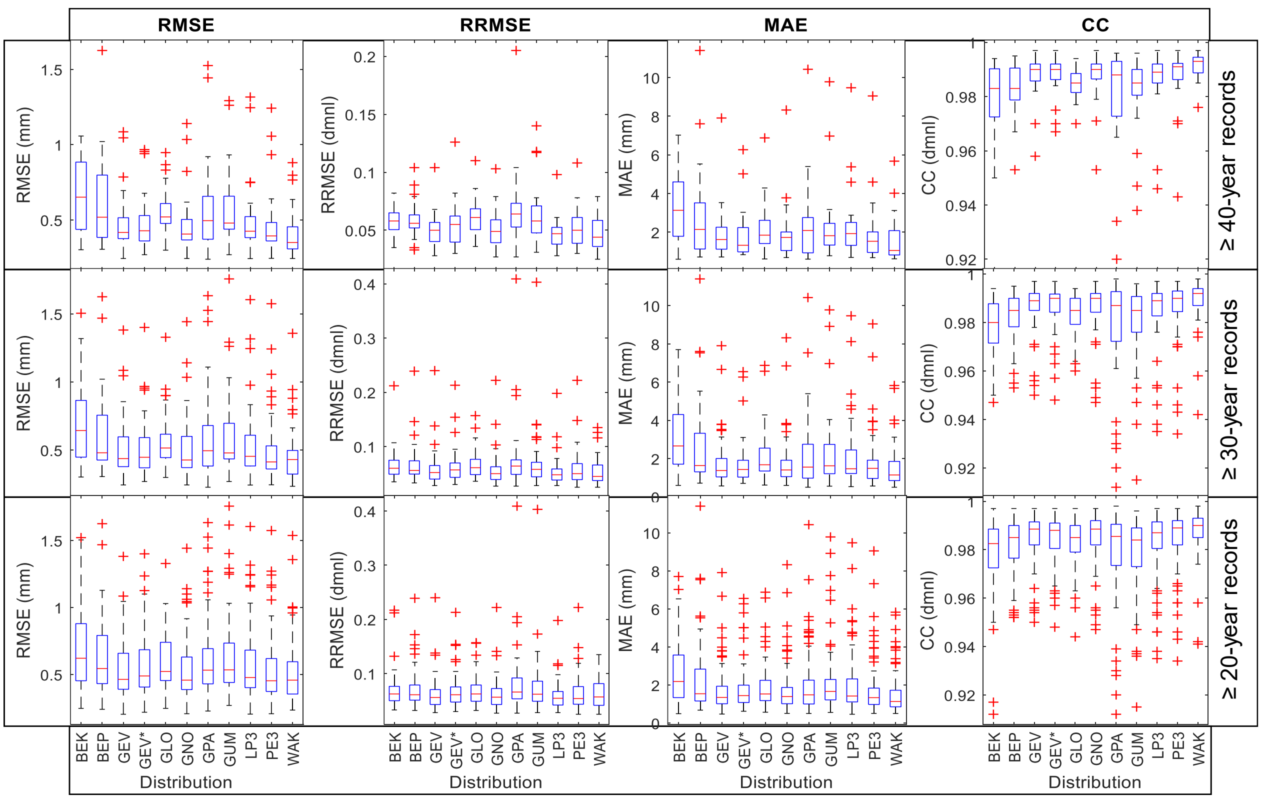

Figure 6-8. Comparing boxplots of RMSE, RRMSE, MAE, and CC results of 11 selected candidates using 5-min AMS of stations containing at least 40-year, 30-year, and 20-year records

Results show that for the 5-min rainfall duration, the WAK model is the best following by the PE3, GNO, GEV, and GEV* for the three indices RMSE, MAE, and CC with slight differences in the values between them. On average, for data containing at least 20-year records, these values are approximately 0.5 mm for RMSE, 1.5 mm for MAE, and 0.985 for CC. The third quarter values (i.e. 75th percentiles) and the whiskers extend to about 0.35 to 1.1 mm for RMSE, 1 to 3 mm for MAE, and at least 0.97 to 0.96 for CC. However, for the relative error (RRMSE), the LP3 model is the best following by the WAK, GNO, and GEV models. On average, these values are about 5% while the third quarter values and the whiskers extend to about 7.5 to 10% for RRMSE. Similar plots were produced for 1-hour and 1-day rainfall durations and provided in the appendix.

Ranking of the 11 candidate distributions for each of the 84 selected stations based on the four indices are presented in Figure 6-9. Ranking from number 1 to 11 indicates the gradual decrease in accuracy from the best to the worst distributions. On the basis of these GOF numerical comparison results, it was found that no unique distribution ranked consistently best for all locations and for all three selected rainfall durations. The overall rank for each distribution was obtained for each numerical index by summing the individual rank at each location for different record lengths (at least 40 years, 30 years, and 20 years). The overall rank for only the 5-min AMS is presented at the end of Figure 6-9 and for all three durations is presented in Figure 6-10.

It can be seen that the WAK model outperforms the others in describing the distribution of daily and sub-daily AMS. The GEV, GNO, and PE3 models also performed well overall and their scores are close to each other. This can be expected since these models have been recommended for use in frequency analyses of the hydrologic extreme variables by many previous studies. It is also noticed that the PE3 model performed slightly better than the GEV and GNO models for 5-min duration data. However, for data set of longer durations – 1-hour and 24-hour, the GEV and GNO models are slightly better. The GLO, LP3, and GEV* distributions provided an average performance as they stand among the middle positions. Notice in particular that if only RRMSE criterion is considered, the LP3 distribution can be considered as the best candidate for data of all durations. However, in practice the use of more than one performance criteria is commonly recommended.

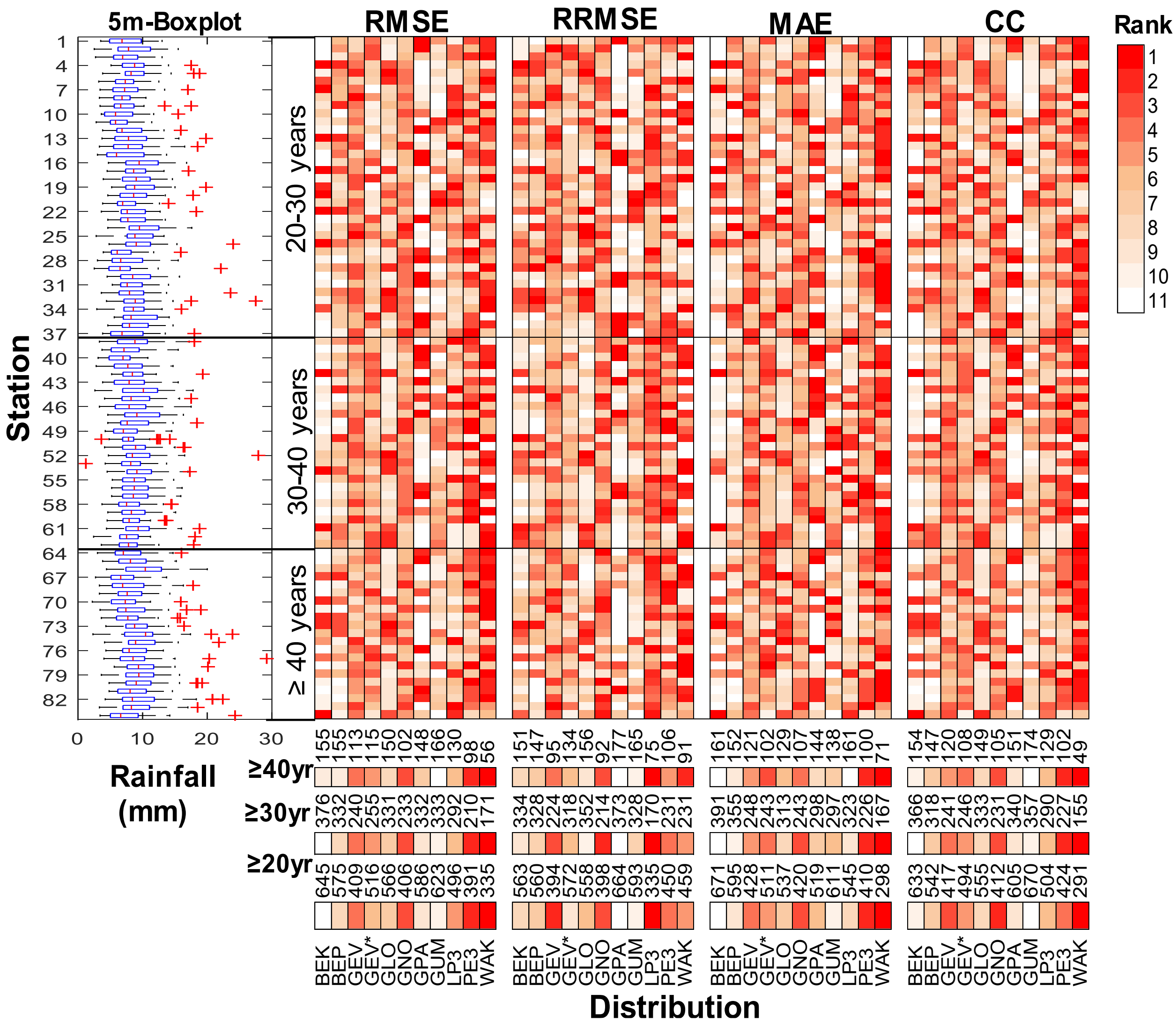

Figure 6-9. Ranking of 11 models for 5-min AMS for each station individually and the overall rank for 84 stations based on the four criteria. Rank = 1 (or close to 1) indicates the best model(s) and rank = 11 (or close to 11) indicates the worst model(s). Boxplots of the 5-min data are shown on the left.

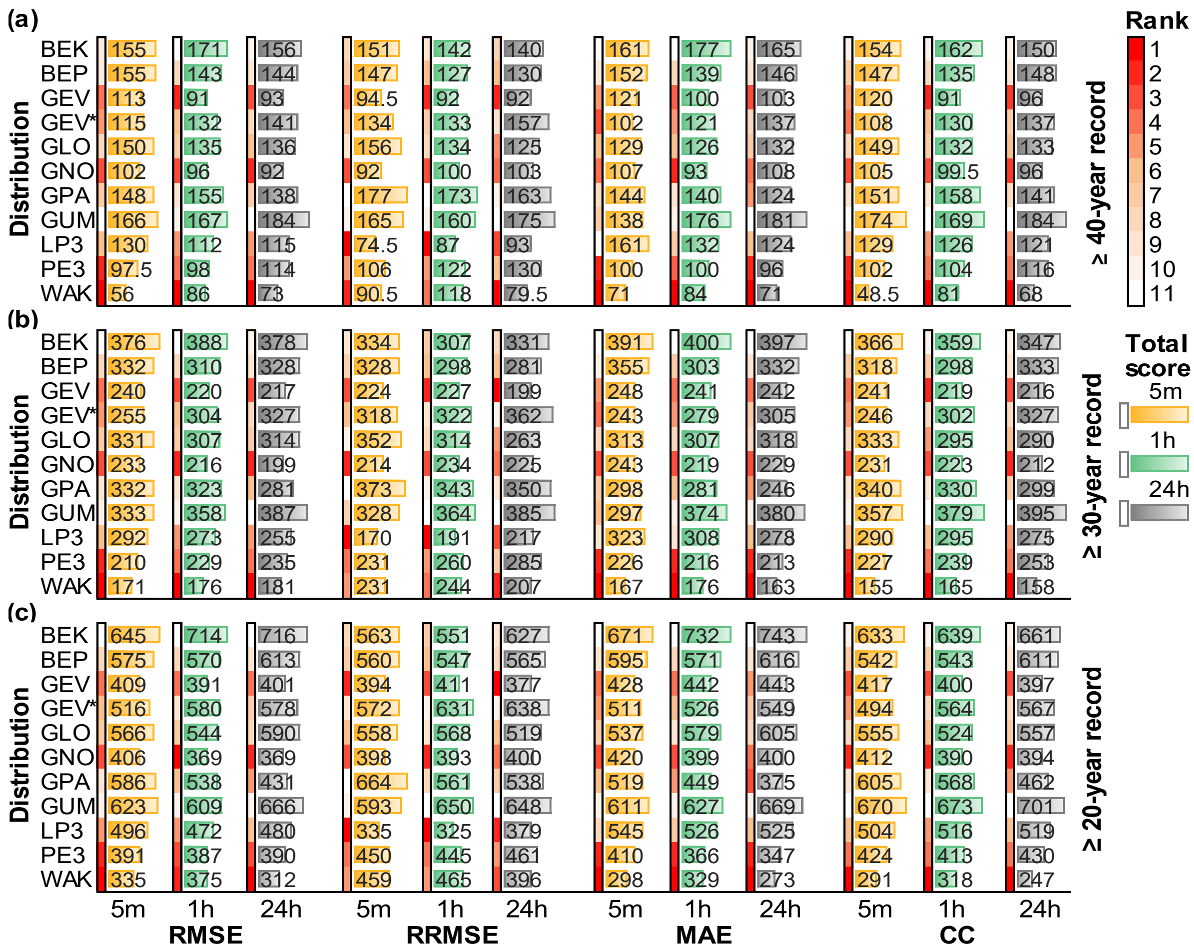

Figure 6-10. Overall rank for all stations containing at least (a) 40-year, (b) 30-year, and (c) 20-year records based on the four statistical tests for all three durations of 5-min, 1-hour, and 24-hour AMS (The lowest scores or the shortest bar indicates the best models)

6.3.2.2 Predictive ability assessment results

In this study, one thousand bootstrap samples were generated with replacement. The size of a generated bootstrap sample is equal to half (i.e. 50%) of the full sample with a rainfall record length of at least 40 years or approximate two third (i.e. 65%) of the full sample size if the record length is between 30-40 years. This process is required to ensure that the generated bootstrap samples contain at least a sufficient length of 20 years for more reliable statistical results. Each candidate distribution was then fitted to the generated samples and was used to extrapolate the right-tail quantiles corresponding to the four largest values in the full data set. For instance, Figure 6-11 shows the results for 5-min AMS at Toronto Int. Airport station.

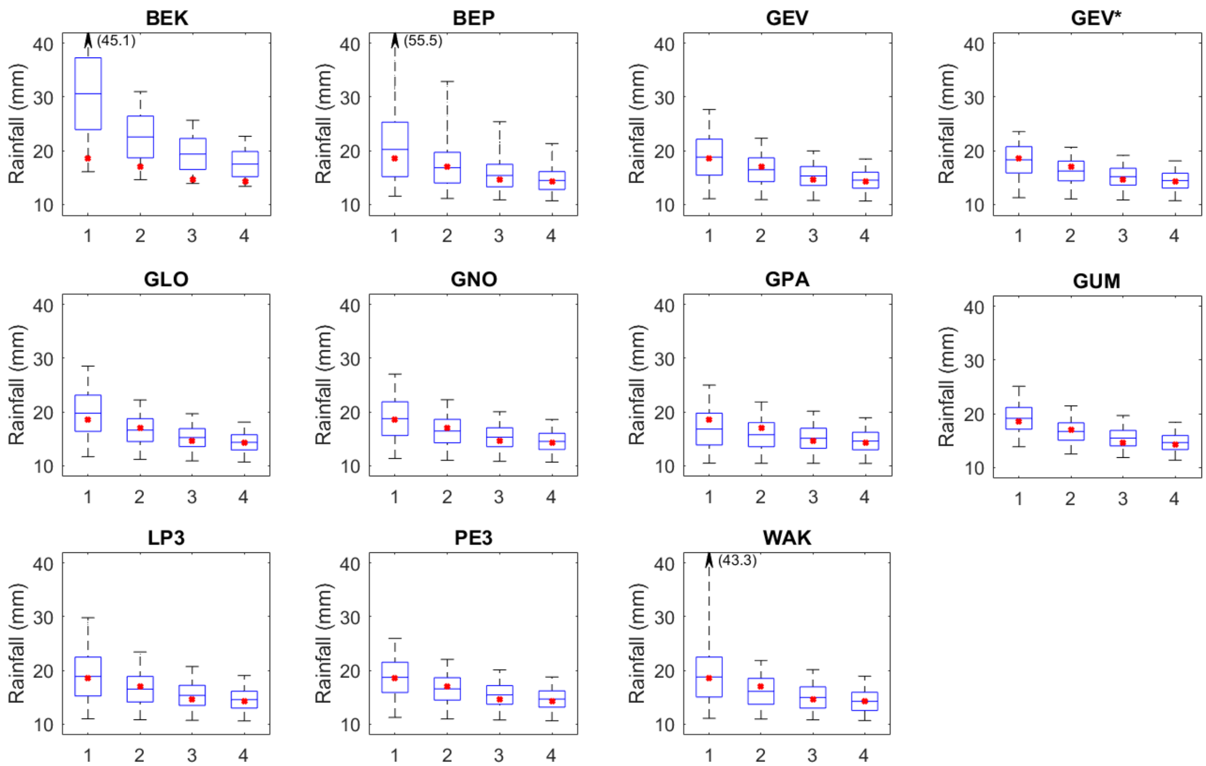

Figure 6-11. Boxplots of extrapolated right-tail bootstrap data for 5-min AMS at Toronto Int. Airport station

The modified boxplots of 141 AMS show that in general the Beta-K, Beta-P gave consistently the worst performance with large sampling variation and bias for all three durations. Unlike the BEK and BEP models, the boxplots for the WAK model do not show large box widths, however, they reveal long upper whiskers. In addition, results reveal that, the LP3 model produced larger box widths than other remaining distributions, yet it was not as poorly performed as the BEK, BEP or WAK models. Although the Gumbel model exhibited the lowest sample variation in most cases, it tended to over- or under-estimate the observed values most frequently. The GEV, GEV*, GLO, GNO, GPA, and PE3 models produced satisfactory results at most stations where the box enclosed the observed right-tail values with a reasonable whisker spread and good correlation with the observed values. In particular, the GEV, GNO, and PE3 models produced almost identical results. Occurrences of over- or under-estimation of largest rainfall amounts did occur for all distributions at several locations.

6.3.3 Decision-making process

In general, it can be observed that no one particular distribution performed the best at every station for each selected performance criterion. This could be due to the strong spatial variation of rainfall characteristics within this Ontario region. While it is difficult to provide a clear physical interpretation of the regional variability of the computed model parameters, however based on the proposed tool, one is still able to identify in an objective way the GEV, GNO, and PE3 as the best candidates for a large number of cases considered. Hence, these three models could be recommended as appropríte models for use in the frequency analysis of AMS for a given site in Ontario as shown in Figure 6-12, for instance for Toronto Int. Airport station.

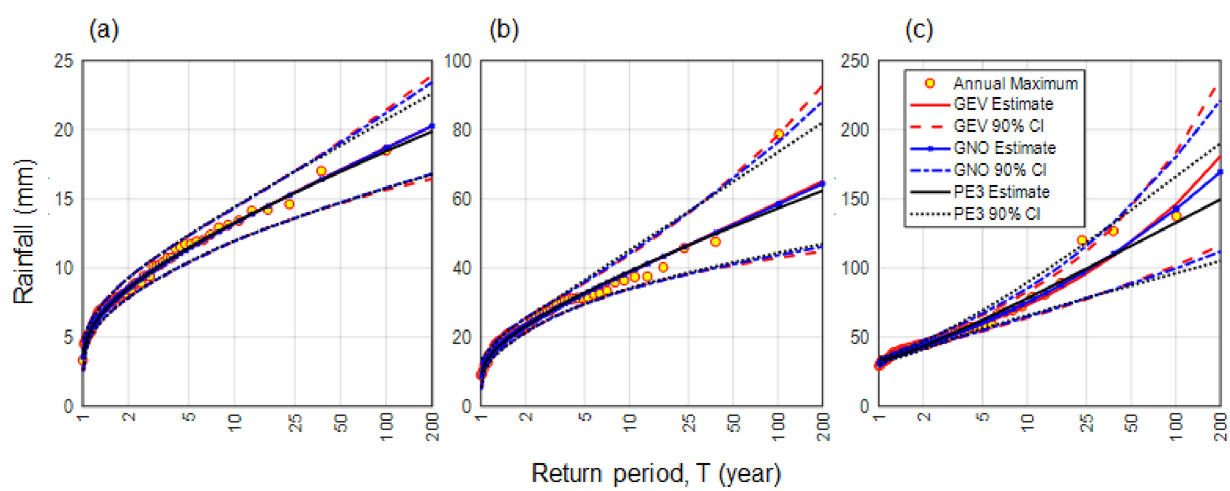

Figure 6-12. Frequency curves (solid lines) and 90% confidence limits (90% CI, dashed lines) of (a) 5-minute, (b) 1-hour, and (c) 24-hour AMS (blue circle markers) at Toronto Int. Airport station using the top three distributions – GEV, GNO, and PE3

The difference in extreme design rainfall estimates produced by these three distributions can be also further investigated for those stations containing at least 30-year records as shown in Figure 6-13. Results reveal that the estimated values for return periods within the twice sample lengths are almost identical for the three distributions. However, the GEV model tends to provide slightly higher values for high return periods, while the PE3 model tends to give slightly higher values for low return periods. The three models, therefore, could be used interchangeably in computing IDF relations and extreme design rainfalls for Ontario region as shown in Figure 6-14 for example. Nonetheless, if only one model is preferred, other criteria should be thus considered in the choice of an appropriate distribution. For instance, the GEV model is based on a more solid theoretical basis than the other two distributions because it was derived from the statistical theory of extreme random variables (Coles, 2001). In addition, it tends to produce more conservative results for high return periods compared to the other models. Therefore, the GEV model could be considered as the most suitable distribution if only a unique probability model is required for describing the distribution of AMS in Ontario region.

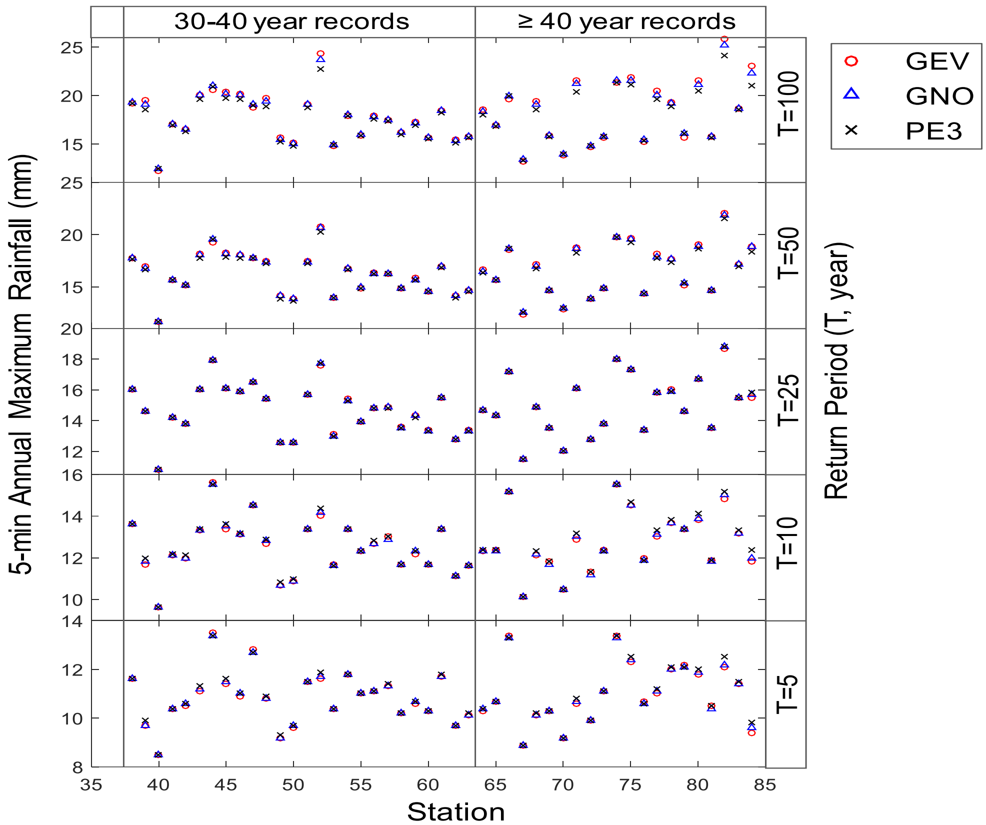

Figure 6-13. Comparing 5-min extreme design rainfalls estimates using the top three distributions (GEV, GNO, and PE3) for different return periods (T, years) for 47 stations containing at least 30-year records

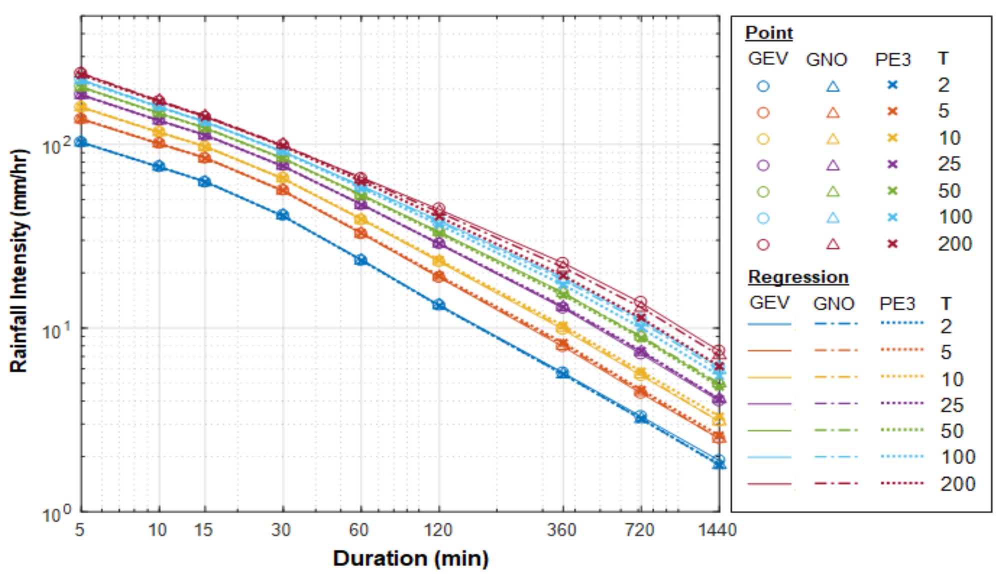

Figure 6-14. IDF curves for Toronto Int. A. station (T=2 to 200 years) produced using the top three distributions and represented as marker symbols (circles for GEV, triangles for GNO, and crosses for PE3). Regressions were performed using the sixth order polynomial functions and represented as lines (continuous for GEV, discontinuous for GNO, and dot for PE3).

6.4 Numerical Application: Updating IDF Relations Considering Climate Change Impacts

This section presents the evaluation of the feasibility and accuracy of SMExRain in reproducing the distributions and quantiles of the historical extreme rainfall data at a given location of interest. For the gauged sites, the results have been presented in detail in Chapter 4. Therefore, this section only focuses on the application of SMExRain to compute the design rainfall quantiles at a give ungauged location for the baseline period (e.g. 1961-1990) using the GCM-based data. The assessment of climate change impacts on local extreme rainfalls can be done by replacing the data of reference period with those of different projected periods (e.g. 2041-2070) as described in detail in Chapter 4.

6.4.1 Study sites and data

To assess the feasibility and accuracy of the tool in reproducing the distributions and quantiles of the historical data at an ungauged site, the NASA climate simulation outputs from 21 global climate models conducted under the CMIP5 and the observed IDF data in the period of 1961-2005 from a network of 15 raingauges located in the Ontario province, Canada, were selected for this study.

The climate simulation outputs from 21 global climate models (GCMs) conducted under the Coupled Model Inter-comparison Project Phase 5 (CMIP5) and the observed IDF data in the period of 1961-2005 from a network of 15 raingauges located in the Ontario province, Canada, were selected for this study (see Figure 6-15). The climate simulation outputs have been statistically downscaled by NASA (i.e., NASA Earth Exchange) from the global scales (a few degrees or 10^2 km) to the regional scale (approximately 25 km x 25 km) for two different Representative Concentration Pathways scenarios (i.e. RCP 4.5 and 8.5) based on the bias-correction spatial disaggregation approach (Thrasher et al., 2012).

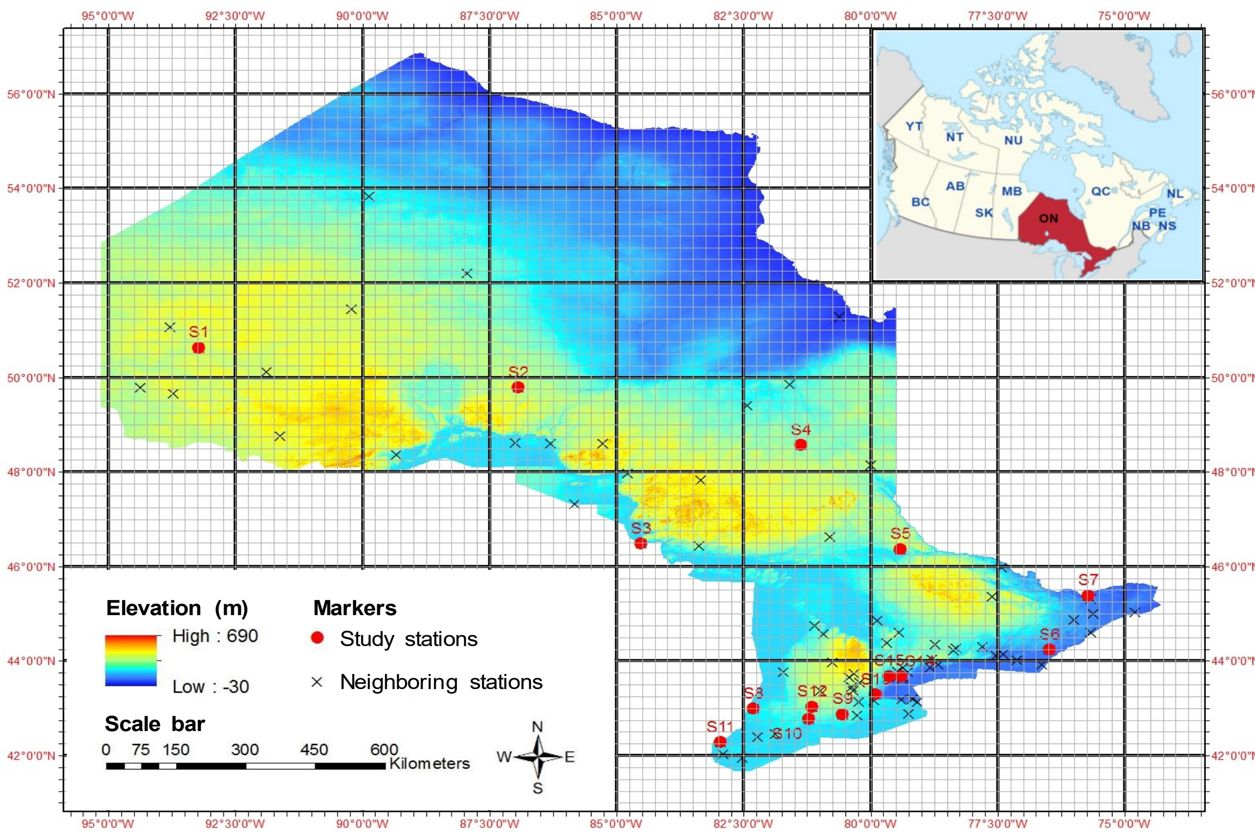

Figure 6-15. Locations of the 15 study raingages (red circle markers) and 69 neighboring stations (black cross markers) used for the study. The bold black lines show a common GCM grid of 2.5°x2°, while the gray lines show the NASA grid of 0.25°x0.25°. The provincial digital elevation model was obtained from

Observed IDF data at each site consists of annual maximum rainfall series for nine different durations (ranging from 5 minutes to 1440 minutes). Note that the observed IDF data have been provided by the Environment Canada to produce the at-site IDF relations for the various practical engineering application purposes (Environment Canada, 2014). The jackknife technique was used to represent the ungauged site condition at the study sites. In addition to these sites, IDF data from other 69 neighbouring stations were also used for the interpolation of the means and scaling exponents at the ungauged sites. Data of 1961-1990 were used for the calibration of the scaling factors and scaling exponents while those of 1991-2005 were used for the validation of these calibrated scaling factors and scaling exponents. Selection of these stations relied on the quality of the data, the adequate length of available historical ER records, and the representative spatial distribution of raingauges.

6.4.2 Results

6.4.2.1 <u>Derivation of local daily extreme rainfalls at an ungauged site</u>

To transfer the NASA extreme rainfalls at the 25-km regional scale, $\hat{X}$, to a given ungauged site, scaling factors were used. Figure 6-16 shows the comparisons of different GOF test results between the daily estimated (i.e., regional and the bias-corrected values) and the daily observed extreme rainfalls for both the calibration (1961-1990) and the validation periods (1991-2005). It is important to note that there was a systematic bias between the extreme rainfalls at the regional scale and at a local site. Indeed, the correlation coefficients between the regional and observed values are high (higher than 0.9) but the errors are also large (about 30%) for both the calibration and validation periods. The use of a transfer function (i.e. a scaling factor or areal-reduction factor) is thus necessary. Furthermore, it can be clearly seen that the bias-corrected (areal-reduction adjustment) extreme rainfalls derived for an ungauged site using the estimated scaling factor produced lower values of RMSEr and MADr as well as higher values of CC as compared to the raw data (i.e. 25x25 km regional values) obtained directly from NASA. In addition, the low values of RMSEr and MADr (about 10% and 15% or less for the calibration and validation respectively) and high values of CC (about 0.95 or higher) have indicated the feasibility and accuracy of the proposed spatial downscaling (or areal-reduction adjustment using scaling factors) approach in the estimation of extreme design rainfalls for an ungauged location.

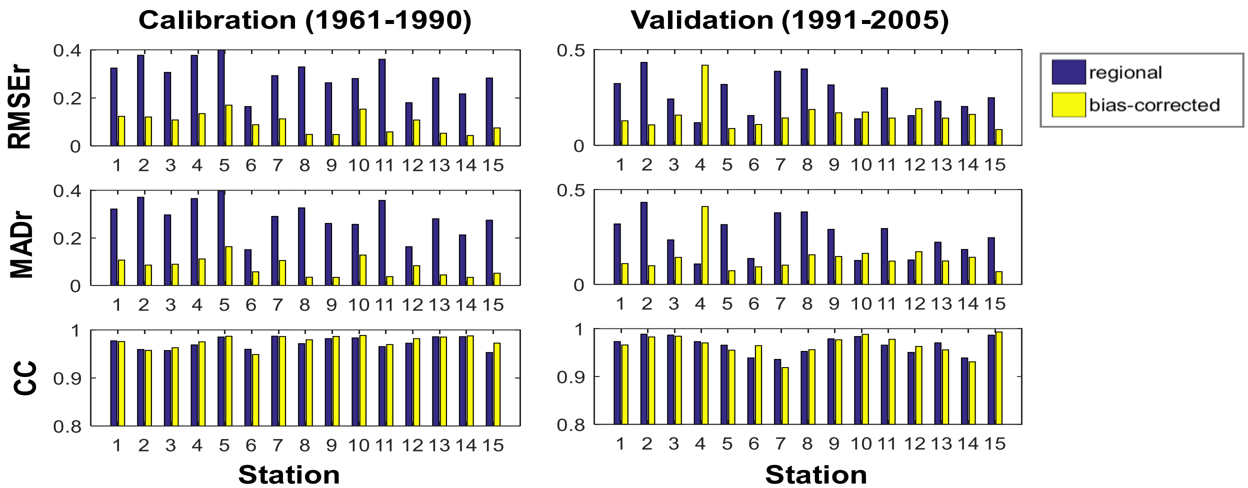

Figure 6-16. Comparisons of GOF results between observed and estimated (i.e., regional and bias-corrected) extreme rainfalls at the 15 study sites for the calibration (1961-1990) and validation (1991-2005) periods

6.4.2.2 Derivation of local sub-daily extreme rainfalls at an ungauged site

To obtain the sub-daily extreme rainfall series from the daily extreme rainfall series at a given site, the proposed scale-invariance GEV/PWM method was applied. Different graphical visualization and goodness-of-fit (GOF) tests were used to evaluate the feasibility and accuracy of this method. For purpose of illustration, Figure 6-17 a presents the probability plots of the computed extreme design rainfalls X_T (mm) for two different durations at station #13 – the Hamilton RBG CS station for both the calibration (1961-1990) and validation (1991-2005) periods respectively. Uncertainty associated with the estimation of the extreme design rainfalls is displayed in the form of standard boxplots. It can be seen that the distributions of the estimated sub-daily extreme rainfalls derived based on the distribution of local daily extreme rainfall (adjusted from regional values) using SMExRain agreed well with the observed data.

Figure 6-18 shows the Q-Q plots of the estimated extreme design rainfalls derived from the NASA regional data using SMExRain and the at-site frequency analysis using the GEV distribution for different rainfall durations and return periods for all 15 selected stations. Note that the median values of the results from 21 GCMs were used for the computation. A numerical comparison was conducted to evaluate the results using the three selected dimensionless GOF indices (i.e. RMSEr, MADr, and CC) for all sites as shown in Table 6-3. The low values of RMSEr and MADr as well as the high values of CC have indicated the feasibility and accuracy of the proposed temporal GEV/PWM statistical downscaling in the estimation of the extreme design rainfalls for a given ungauged location. Note that, for accuracy, only the estimated quantiles within the twice sample lengths (i.e. up to 50-year and 25-year return periods for the calibration and validation respectively) were used for comparisons.

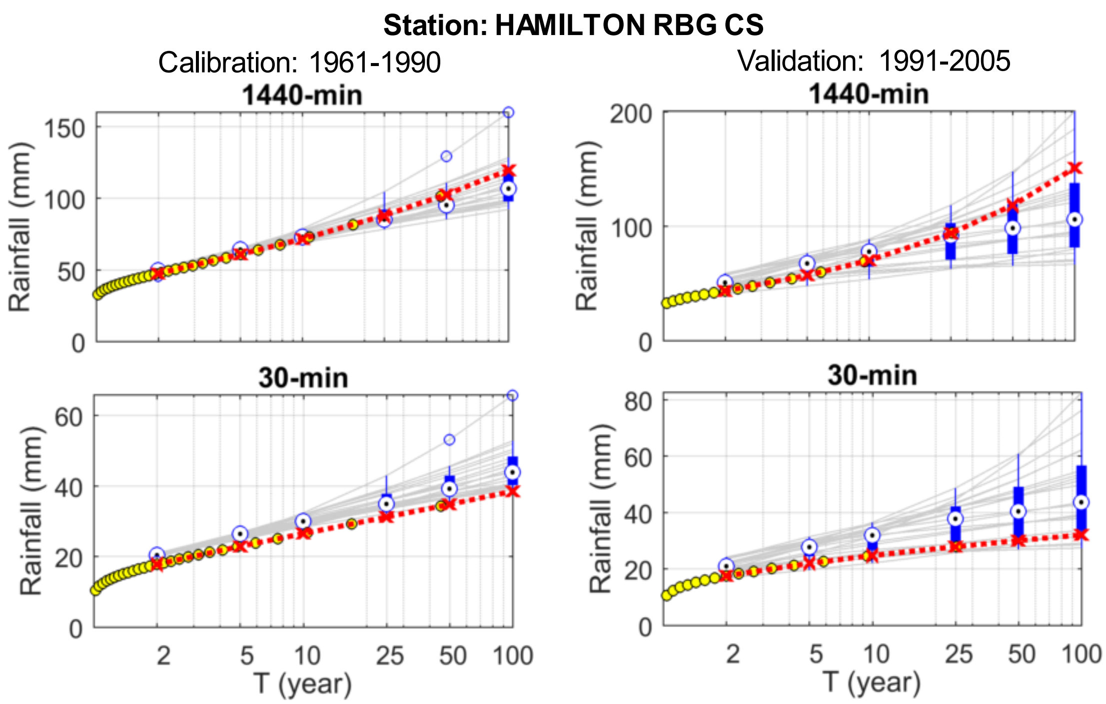

Figure 6-17. CDF plots of the computed extreme design rainfalls X_T (mm) for two different durations (D=30 and 1440 minutes) at the Hamilton RBG CS station for both the calibration (1961-1990) and validation (1991-2005) periods,

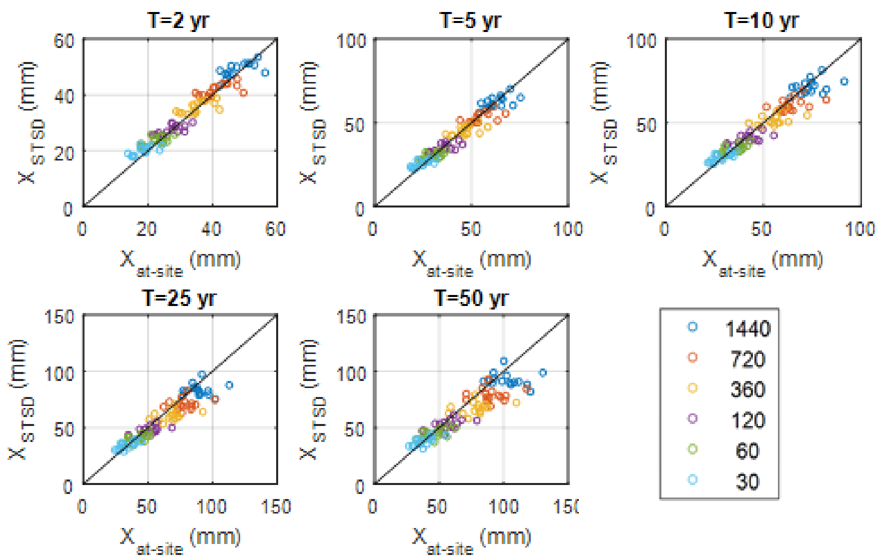

Figure 6-18. Q-Q plots of the estimated extreme rainfalls using SMExRain (X_{STSD}, mm) and the at-site frequency analysis ($X_{at\text{-}site}$, mm) for different rainfall durations (D=30 to 1440 minutes) and for different return periods (T=2 to 50 years).

Table 6-3. Goodness-of-fit test results for both calibration and validation periods

	Calibration period 1961-1990					**Validation period 1991-2005**			
T (year)	**2**	**5**	**10**	**25**	**50**	**2**	**5**	**10**	**25**
RMSEr (%)	10.3	10.3	11.4	13.9	16.3	15.9	15.2	16.5	20.2
MADr (%)	8.0	8.1	9.3	11.8	13.8	13.4	12.5	12.8	15.9
CC (dmnl)	0.965	0.958	0.950	0.931	0.910	0.929	0.903	0.885	0.866

6.5 Conclusion and Discussion

A decision-support tool (SMExRain) has been developed for evaluating systematically the performance of various commonly-used probability distributions in hydrologic frequency analyses in order to identify the most suitable model for representing the distribution of extreme rainfalls for a study region of interest. Based on an extensive set of several different graphical and numerical assessment criteria, and being equipped with a user-friendly ribbon interface, this tool can be used to assess in an efficient and objective manner the descriptive and predictive abilities of each distribution for a large amount of extreme rainfall datasets of different durations for a given location as well as for a large number of sites. It can also be used for constructing robust IDF relations based on historical data considering model uncertainty. In addition, the tool can be used to update the IDF relations by taking into account the possible impacts of different climate change scenarios on the short-duration extreme rainfall process a given local gauged or ungauged site.

The proposed SMExRain tool has been successfully tested using extreme rainfall data for various regions in Canada. In this paper, for illustrative purposes, only results from the application of this tool for Ontario region were presented to demonstrate its efficiency and usefulness in the selection of the best models for representing accurately the distribution of AMS in this region. More specifically, it was found that, among the eleven selected candidates, the GEV, GNO and PE3 models provided the most accurate and the most robust extreme rainfall estimates for this study area. The estimated rainfall values for different return periods are quite comparable for these three distributions. However, the GEV model tends to provide slightly higher values for high return periods, while the PE3 model tends to give slightly higher values for low return periods. These three models, therefore, could be recommended for use in the construction of the IDF relations and for estimating extreme design rainfalls. Nonetheless, for practical engineering design purposes, the GEV model could be preferable to the GNO and PE3 models because it has a more solid theoretical basis and it produces more conservative results (i.e., higher design rainfall estimates for high return periods).

It has been demonstrated in this study that SMExRain is a powerful decision-support tool that could be conveniently used in engineering practice to identify in an efficient and objective manner the best probability models for constructing IDF relations for a given location or for many sites over a given region. Furthermore, these IDF relations can provide accurate and robust design rainfall estimates since they are based on a detailed evaluation of the descriptive and predictive abilities and the uncertainty of various candidate models; and they were also relied on a systematic comparison procedure to assess the accuracy and robustness of each selected model using an extensive set of graphical and numerical performance criteria.

SMExRain can be used to perform rainfall frequency analyses and to construct IDF curves for a single site or for a number of sites. However, it is necessary to know the credible limits of extrapolation of frequency analyses based on site record lengths. In general, it is held that "a quantile of return period T can be reliably estimated from a data record of length n only if T≤n" (Hosking and Wallis 1997, page 2). For extrapolating distributions, no general guidance is available, but "a common rule of thumb is to restrict extrapolation of at-site quantile estimates to return periods (years) of up to twice as long as the record length" (WMO, 2009a, page 5-16). As an example, in the paper, the estimated design rainfalls for return periods within the twice sample lengths are almost identical for the top three distributions in Ontario region.

Rather than single point (at-site) IDF curves, regional rainfall frequency analyses and other data sources are being used for enhancing knowledge of rainfall IDF characteristics. Regional approaches are expected to provide more robust estimates for rainfall quantiles of high return periods as compared to those given by the at-site procedures (Hosking and Wallis, 1997; Nguyen et al., 2002b; Madsen et al., 2009; Burn, 2014; Goudenhoofdt et al., 2017; Forestieri et al., 2018). Regionalization techniques are hence the basis for developing regional rainfall IDF atlases at the national level for some countries such as U.S. (NOAA's Atlas 14, 2014), Australia (Ball et al., 2016), and U.K. (FEH, 1999). However, for Canada, the at-site (or single point) IDF is still one of the most commonly used tools for the design of various urban water infrastructure such as urban storm drainage systems, detention ponds, and so on (CSA, 2012). Many of these assets are typically designed with the return periods of 10 or 25 years. Environment Canada continues to provide the at-site IDF of more than 550 sites across Canada (CSA, 2012; Environment Canada, 2014). Hence, the anticipated common usage of SMExRain is to estimate the rainfall depth-duration values for return periods lying within twice sample record lengths of an observed series. Given that the record lengths tend to be short, normally less than 30 years on average, these values are estimated for return periods such as 2, 5, 10, 20, 25, 50-year. For those return periods, regionalization techniques are relatively less important than they are for high return periods of 100 years or more. Notice also that one of the main difficulties in the application of regionalization techniques is related to the definition of “homogeneous” regions. Various methods have been proposed for determining regional homogeneity, but there is still no generally accepted procedure in practice (WMO, 2009a).

The decision-support tool SMExRain can be also used for assessing the climate change impacts on extreme rainfalls for design and management of urban water systems. More specifically, it has been demonstrated that the proposed tool was able to describe accurately the linkage between the climate change information at large spatial and temporal scales given by global (or regional) climate models and the short-duration extreme rainfalls at a local site where observed historical rainfall record are available (a gauged site) or unavailable (an ungauged site). To evaluate the feasibility and accuracy of the proposed SMExRain, the climate simulation outputs from 21 global climate models and the observed extreme rainfall data over Ontario region, Canada were used. These climate simulations have been downscaled by NASA to a regional 25-km scale for different climate change scenarios. Results of these numerical applications have indicated the feasibility and accuracy of the SMExRain in the assessment of the climate change impacts on the extreme rainfalls at a given gauged or ungauged site.

Finally, the inferences made in this paper are based upon case studies using the observed extreme rainfall IDF data from Ontario (Canada) and the daily downscaled climate projections available at the 25-km regional scale from NASA. Similar studies should be carried out to assess the feasibility and accuracy of the proposed SMExRain tool based on available data in other regions with different climatic conditions.

Chapter 7. Conclusions and Recommendations

7.1 Conclusions

The primary purpose of this research is to develop novel methods and tools for improving the estimations of extreme design rainfalls in the current climate and in consideration of a changing climate at gauged and ungauged locations for the design and management of various water-related infrastructures. The following main conclusions can be drawn from the present study:

(1) A general procedure was developed for assessing systematically the performance of descriptive and predictive abilities of many different probability distributions. Based on this, the most appropriate candidate was then identified for representing the distribution of annual maximum rainfall series (AMS). A case study using 63 long-record short-duration AMS data from a network of 21 raingauges located in Ontario have indicated the feasibility of the proposed model evaluation method. It was found that, among the 11 models considered, the GEV, GNO, and PE3 are the top three distributions that provided the greatest goodness-of-fit and robust quantile extrapolations for different rainfall durations and for a number of locations in the study region. These distributions can be thus alternately used for the frequency analysis of daily and sub-daily annual extreme rainfalls in this area. For practical application purposes, the GEV is preferable to the GNO and PE3 due to its more solid theoretical basis and the inherent scale-invariance property of its non-central

moments over different time scales, which is useful for the modelling of sub-daily extreme rainfall processes in the context of climate change.

(2) A holistic mathematical framework and scaling properties was developed for the scaling Generalized Extreme Value (GEV) distribution model based on the probability weighted moment (PWM) system. It can be used to estimate short-duration extreme design rainfalls of sub-daily or sub-hourly scales from those of longer time scale. The new scale-invariant model has a simpler mathematical derivation which helps to reduce the computational costs significantly when dealing with a large amount of data. Furthermore, it is more robust and accurate compared to the existing models. Results based on 666 long-record AMS dataset from a network of 74 raingauges located across Canada showed that the estimates of PWM-based empirical scaling exponents are more accurate and robust for different scaling regimes and for higher order moments. Additionally, results of various graphical and numerical comparisons pointed out that the novel scaling GEV/PWM model is superior to the three existing models for the majority of stations and criteria.

(3) An innovative spatiotemporal statistical downscaling (STSD) procedure was proposed for assessing climate change impacts on the short-duration extreme rainfalls processes at a given local site in the context of climate change. Climate simulation outputs from 21 global climate models conducted under the CMIP5 project and the observed daily extreme rainfalls from a network of seven raingauges located in Ontario was used for the case study. Results have indicated the feasibility, reliability, and accuracy of the proposed approach. In addition, a new procedure using a series of statistical tests in sequence has been proposed to test for the magnitudes of the differences as well as to compute the associated uncertainties of extreme rainfalls for the current and projected periods as well as between

different projected periods. Results showed significant changes (varying from 8% to 18%) between the baseline and three future periods for different extreme design rainfall values of different return periods up to T = 25 years, and up to T = 50 years for a few stations. For T = 100 years, only one station showed a significant increase in the estimated rainfall amounts. There were also increases from 3% to 8% in design rainfalls for T = 50 years and T = 100 years for some stations, but they were found to be not statistically significant.

(4) Many procedures have been developed to tackle the spatial downscaling, however, only a few methods have been proposed to deal with the temporal downscaling. In this research, in addition to the scaling GEV/PWM model, several novel scale-invariance models have been developed to enhance the accuracy and reliability of the temporal linkage between the low and high temporal resolution extreme rainfalls. In other words, these scaling models could be used to derive the distributions and quantiles of the projected sub-daily and sub-hourly extreme rainfalls from those of projected daily data. Several probability distributions commonly-used in the frequency analysis of extreme hydrologic variables were selected, including the Generalized Logistic (GLO), Generalized Normal (GNO), and Pearson Type III (PE3) distribution models. The mathematical frameworks and scaling properties were derived for these distributions based on both the non-central moment (NCM) and PWM systems. This results in six novel scaling models. The IDF data from a network of 74 raingauges located across Canada were used for investigating the feasibility and accuracy of these new scaling models. The results were also compared with the two existing scaling models (i.e. GEV/PWM and GEV/NCM models). Results showed that the PWM-based scaling models produced better estimations than the NCM-based ones. Additionally, among the eight models, the scaling GNO/PWM and GEV/PWM model are

the best models with virtually identical results. Hence, in practice, they can be used interchangeably or used together to enhance the accuracy and reliability of the estimation of extreme design rainfalls in the current climate and in the context of climate change.

(5) A decision-support tool, referred to as SMExRain, has been developed. The tool can be used by professionals and engineers in practice to obtain an accurate and robust estimation of a suitable design rainfall for sustainable design of water infrastructure. The tool is highly convenient and efficient for performing statistical modeling and analysis of extreme rainfall processes for a large number of sites and for estimating accurately extreme rainfalls for design purposes. In addition, it assists users, stakeholders, and decision-makers in understanding and recognizing the uncertainties and assumptions in projecting how they could change in the future under different climate scenarios. The tool includes the standard technique and the most recent developments in the area of extreme rainfall modeling and frequency analyses to identify the most suitable probability distributions for extreme rainfalls in terms of their descriptive and predictive abilities. Furthermore, the tool allows users to quantify climate change impacts and their uncertainties on extreme rainfall IDF relations using projected climate simulations from many different global or regional climate models. The tool has been tested using extreme rainfall data for different regions in Canada.

7.2 Recommendations for Future Research

Based on the findings of this research, the following recommendations are suggested for future studies:

(1) The conventional method of construction of extreme rainfall intensity-duration-frequency (IDF) relations could be improved based on the new scale-invariance techniques and models derived in this research. In particular, the conventional independently-fitting technique doesnot take into account the temporal relationships among extreme rainfall amounts of different rainfall durations. In the end, a regression model has to be added either in the real-space or log-space in order to interpolate and estimate the design values of unobserved/missing rainfall durations such as 45 minutes or 3 hours. Based on the results from this research, extreme rainfall amounts of different rainfall durations showed an inherent scale-invariance property of its non-central moments or probability-weighted-moments over different time scales. Therefore, this property can be utilized along with a scaling model to improve the estimation of the design rainfall quantiles and to construct more robust at-site (or point scale) rainfall IDF relations.

(2) Annual maximum rainfall series (AMS) have been widely used in construction of IDF relations due to its simple structure. Beside this, the peak-over-threshold (POT) approach has increasingly received attention as it offers more information that may be lost when using the AMS approach. However, application of the scaling approach to estimate the short-duration POT data from that of long-duration is extremely limited due to the complex nature of determining the threshold for different durations (Salvadori and De Michele, 2001; Rajulapati and Mujumdar, 2017). With the development of the new scaling models for different moment systems in this research, this could open a new door to conduct further research on the application of the scaling approach to the POT data.

(3) Regional frequency analysis based on the newly derived scaling models could be a promising technique to improve the estimation of the extreme design rainfalls as partially-

gauged locations (missing sub-daily data but daily data available) or ungauged location (no data available) by transfering the scaling properties from the neigboring stations located within a same homogeneous region. In addition, since the area has been shown to possess the scaling property in some researches, it is possible to incorporate the areal reduction factor into the IDF relations to form a new rainfall intensity-duration-area-frequency (IDAF) relations (Gado and Nguyen, 2015; Melese et al., 2019). The IDAF relations has a significant advantage over the point scale IDF relations in the simulation of runoff models over different spatial resolutions. This is also particularly useful when combining the observed data of different spatial resolutions from different measuring sources, such as raingauges, radar, and satellite rainfalls (Thorndahl et al., 2017; Mekis et al., 2018; Pathak and Teegavarapu, 2018; Ochoa-Rodriguez, 2019).

(4) For the assessment of climate change impacts on local short-duration extreme rainfall processes, further studies could be carried out for other regions with different climatic conditions to assess the feasibility and accuracy of the proposed spatiotemporal downscaling procedure. In addition, several newly derived scaling models such as scaling GNO/PWM and PE3/PWM models could be used along with the scaling GEV/PWM in the temporal downscaling step in order to improve the robustness of the estimation and construction of IDF relations for a gauged or an ungauged location for the current climate as well as for future climate under different climate change scenarios.

(5) The decision-support tool SMExRain can be upgraded to include a number of design storm shapes suggested in a number of design guidelines from different countries. This helps to facilitate the uncertainty assessment in the simulation of urban runoff and inundation under different climate change scenarios. Additionally, the tool can be expanded to allow the

assessment of climate change impacts on some other extreme hydrologic variables. For example, the minimum and maximum temperatures have a profound impact on the transportation network and public health problems.

Chapter 8. Statement of Originality

To the best of the author's knowledge, the followings are the original contributions from the present study to the hydrological science and engineering:

(1) A systematic procedure has been developed for assessing systematically the performance of different commonly used probability distributions in rainfall frequency analyses based on their descriptive as well as predictive abilities. This assessment procedure relies on an extensive set of graphical and numerical performance criteria to identify the most suitable models that could provide the most accurate and most robust extreme rainfall estimates. The proposed systematic assessment approach has been shown to be more efficient and more robust than the traditional model selection method based on only limited goodness-of-fit criteria.

(2) A novel scale-invariance probability-weighted-moment-based Generalized Extreme Value (GEV/PWM) probability distribution model has been developed for modeling rainfall extremes across a wide range of time scales (e.g., several minutes to one day). The mathematical framework and scaling properties of the proposed model are derived. The relations to its special case and between the ordinary moment and probability weighted moment systems are described. The scaling behaviours were also analyzed for the two moment systems. Results showed that the estimates of PWM-based empirical scaling exponents are more accurate and robust for different scaling regimes and for higher order moments. In addition, results based on an extensive graphical and numerical comparisons

have indicated the superior performance of the proposed model as compared to the other existing popular models.

(3) An innovative spatiotemporal statistical downscaling (STSD) approach has been developed for establishing the linkage between daily extreme rainfalls at regional scales and daily and sub-daily extreme rainfalls at a local (point) scale. The proposed STSD contains two steps: (i) the spatial downscaling step using the scaling factors or the bias correction functions to transfer the daily downscaled global climate model (GCM) extreme rainfall projections at a regional scale to a given local site, and (ii) the temporal downscaling step using the new scale-invariance GEV/PWM model to derive the distributions of sub-daily extreme rainfalls from that of daily values at the same study location. In addition, a new procedure has been introduced for robust assessment of the climate change impacts on the extreme rainfalls for urban drainage system design using a series of statistical tests in sequence to evaluate the significant changes of rainfalls among different time periods.

(4) Several novel scale-invariant models have been proposed for modeling rainfall extremes across a wide range of time scales in the context of climate change. Their mathematical frameworks and scaling properties are first derived in this research. These models are developed based on several popular probability distributions that are often used in the frequency analysis of extreme hydrologic variable and have been recommended in several national guidelines, including the Generalized Logistic (GLO), Generalized Normal (GNO), and Pearson Type III (PE3) distribution models. This helps to improve the accuracy and reliability of the temporal linkage between extreme rainfall of low and high

temporal resolutions. In addition, it helps to facilitate the application of the scaling methods in some countries where the use of these distributions are compulsory.

(5) A decision-support tool, referred to as SMExRain, has been developed for constructing robust extreme rainfall intensity-duration-frequency (IDF) relations in consideration of model uncertainty and climate change information for the design and management of urban water systems. The tool that can be used by professionals and engineers in practice to obtain an accurate and robust estimation of a suitable design rainfall for sustainable design of water infrastructure. The tool is highly convenient and efficient for performing statistical modeling and analysis of extreme rainfall processes for a large number of sites and for estimating accurately extreme rainfalls for design purposes. In addition, it assists users, stakeholders, and decision-makers in understanding how extreme rainfalls and IDF values are changing in the current climate and recognizing the uncertainties and assumptions in projecting how they could change in the future. The tool includes the standard technique and the most recent developments in the area of extreme rainfall modeling and frequency analyses to identify the most suitable probability distributions for extreme rainfalls in terms of their descriptive and predictive abilities. Furthermore, the tool allows users to quantify climate change impacts and their uncertainties on extreme rainfall IDF relations using projected climate simulations from many different global or regional climate models. The tool has been tested using extreme rainfall data for different regions in Canada.

The list of the peer-reviewed journals and refereed conference papers and their relations to different chapters in the thesis are as follows:

Chapter 2: a paper has been published in the Journal of Hydrology with the following citation:

Nguyen, T.-H., El Outayek, S., Lim, S.H., Nguyen, V.-T.-V., 2017. A systematic approach to selecting the best probability models for annual maximum rainfalls – A case study using data in Ontario (Canada). J. Hydrol., 553: 49-58.

Chapter 3: a peer-review conference paper has been published in the proceeding of the ASCE EWRI 2018 conference and a manuscript has been prepared to submit to the Journal of Hydrology with the following citations:

Nguyen, T.-H., and Nguyen, V.-T.-V., 2018a. A novel scale-invariance generalized extreme value model based on probability weighted moments (GEV/PWM) for estimating extreme design rainfalls in the context of climate change. Proceedings of the World Environmental and Water Resources Congress 2018, Minneapolis, Minnesota, June 3-7, 2018. DOI:doi:10.1061/9780784481417.025

Nguyen, T.-H., Nguyen, V.-T.-V, and Nguyen, L., 2019. A Novel Scale-Invariance Probability-Weighted-Moment-Based Generalized Extreme Value Distribution for Modeling Rainfall Extremes Across A Wide Range of Time Scale. J. Hydrol. (draft for submission).

Chapter 4: a paper has been accepted for publication in the Journal of Hydro-Environment Research with the following citation:

Nguyen, T.-H., Nguyen, V.-T.-V., 2019b. Linking climate change to urban storm drainage system design: An innovative approach to modeling of extreme rainfall processes over different *spatial and temporal scales. Journal of Hydro-environment Research. JHER-10 Anniversary: (Manuscript number: JHER_2018_146_R0, accepted for publication).*

Chapter 5: a peer-review conference paper (best student paper) has been published in the proceeding of the HIC 2018 conference and a manuscript has been prepared to submit to the Journal of Water Resources Research with the following citations:

Nguyen, T.-H., Nguyen, V.-T.-V., 2018b. Scale-Invariance Generalized Logistic (GLO) Model for Estimating Extreme Design Rainfalls in the Context of Climate Change. In: La Loggia, G., Freni, G., Puleo, V., De Marchis, M. (Eds.), HIC 2018. Proceeding of the 13th International Conference on Hydroinformatics. EPic series in Engineering, Palermo, Italy, pp. 1531-1538.

Nguyen, T.-H., Nguyen, V.-T.-V., 2019d. Mathematical Frameworks and Scaling Properties of Several Probability Distribution Models Commonly Used in Hydrologic Frequency Analysis. Water Resour. Res. (draft for submission).

Chapter 6: three peer-review conference papers have been published in the conference proceedings of the CSCE 2017, 2019 annual conferences and the HIC 2018 conference, and a journal paper has been published in the Journal of Hydrologic Engineering with the following citations:

Nguyen, T.-H., Nguyen, V.-T.-V., 2017. Statistical Modeling of Extreme Rainfall Processes (SMExRain): A Decision Support Tool for Constructing Intensity-Duration-Frequency Relations for Urban Water Infrastructure Design. Proceeding of the CSCE 2017 Annual Conference: Leadership in Sustainable Infrastructure, May 31 - June 03, 2017, Vancouver, Canada, pp. HYD745-1 – HYD745-10.

Nguyen, T.-H., Nguyen, V.-T.-V., Nguyen, H.-L., 2018. A spatio-temporal statistical downscaling approach to deriving extreme rainfall IDF relations at ungauged sites in the context of climate change. In: La Loggia, G., Freni, G., Puleo, V., De Marchis, M. (Eds.). The 13th International hydroinformatics conference HIC 2018. EPiC Series in Engineering, Palermo, Italy, pp. 1539-1546

Nguyen, T.-H., Nguyen, V.-T.-V., 2019c. A Decision-Support Tool for Assessing Climate Change Impacts on Design and Management of Urban Water Systems. Proceeding of the CSCE 2019 annual conference: Growing with youth, June 12 - 15, 2019, Laval, Quebec, Canada, pp. HYD023-1 - HYD023-10.

Nguyen, T.-H., Nguyen, V.-T.-V., 2019a. Decision-Support Tool for Constructing Robust Rainfall IDF Relations in Consideration of Model Uncertainty. J. Hydrol. Eng., 24(7): 06019004.

References

Adamowski, K., Alila, Y., Pilon, P.J., 1996. Regional rainfall distribution for Canada. Atmos. Res., 42(1): 75-88. DOI: http://dx.doi.org/10.1016/0169-8095(95)00054-2

Ahmad, M.I., Sinclair, C.D., Werritty, A., 1988. Log-logistic flood frequency analysis. J. Hydrol., 98(3-4): 205-224. DOI:10.1016/0022-1694(88)90015-7

Alexander, L.V. et al., 2006. Global observed changes in daily climate extremes of temperature and precipitation. Journal of Geophysical Research: Atmospheres, 111(D5): n/a-n/a. DOI:10.1029/2005JD006290

Alila, Y., 1999. A hierarchical approach for the regionalization of precipitation annual maxima in Canada. Journal of Geophysical Research: Atmospheres, 104(D24): 31645-31655. DOI:10.1029/1999JD900764

Arnbjerg-Nielsen, K. et al., 2013. Impacts of climate change on rainfall extremes and urban drainage systems: a review. Water Sci Technol, 68(1): 16-28. DOI:10.2166/wst.2013.251

Arora, K., Singh, V.P., 1989. A comparative evaluation of the estimators of the Log Pearson Type (LP) 3 distribution. J. Hydrol., 105: 19-37. DOI:10.1016/0022-1694(89)90094-2

Bairwa, A.K., Khosa, R., Maheswaran, R., 2016. Developing intensity duration frequency curves based on scaling theory using linear probability weighted moments: A case study from India. J. Hydrol., 542: 850-859. DOI: 10.1016/j.jhydrol.2016.09.056

Ball, J. et al., 2016. Australian Rainfall and Runoff: A Guide to Flood Estimation, Commonwealth of Australia.

Bartles, M., Brunner, G., Fleming, M., Faber, B., Slaughter, J., 2016. HEC-SSP: Statistical software package. Version 2.1. User's Manual, US Army Corps of Engineers, Davis, CA, US.

Bernardara, P., Lang, M., Sauquet, E., Schertzer, D., Tchiriguyskaia, 2007. Multifractal Analysis in Hydrology: Application to Time Series. Versailles, France.

Blanchet, J., Ceresetti, D., Molinié, G., Creutin, J.D., 2016. A regional GEV scale-invariant framework for Intensity–Duration–Frequency analysis. J. Hydrol., 540: 82-95. DOI: 10.1016/j.jhydrol.2016.06.007

Bobée, B., Ashkar, F., 1991. The gamma family and derived distributions applied in hydrology. Water resources publications, Colorado, USA, 203 pp.

Bougadis, J., Adamowski, K., 2006. Scaling model of a rainfall intensity-duration-frequency relationship. Hydrol. Processes, 20(17): 3747-3757. DOI:10.1002/hyp.6386

Bürger, G., Murdock, T.Q., Werner, A.T., Sobie, S.R., Cannon, A.J., 2012. Downscaling Extremes—An Intercomparison of Multiple Statistical Methods for Present Climate. Journal of Climate, 25(12): 4366-4388. DOI:10.1175/jcli-d-11-00408.1

Bürger, G., Sobie, S.R., Cannon, A.J., Werner, A.T., Murdock, T.Q., 2013. Downscaling Extremes: An Intercomparison of Multiple Methods for Future Climate. Journal of Climate, 26(10): 3429-3449. DOI:10.1175/jcli-d-12-00249.1

Burlando, P., Rosso, R., 1996. Scaling and muitiscaling models of depth-duration-frequency curves for storm precipitation. J. Hydrol., 187(1): 45-64. DOI: http://dx.doi.org/10.1016/S0022-1694(96)03086-7

Burn, D.H., 2014. A framework for regional estimation of intensity–duration–frequency (IDF) curves. Hydrol. Processes, 28(14): 4209-4218. DOI:10.1002/hyp.10231

Burn, D.H., Taleghani, A., 2013. Estimates of changes in design rainfall values for Canada. Hydrol. Processes, 27(11): 1590-1599. DOI:10.1002/hyp.9238

CCIA (Climate Change in Australia), 2019. Projections for Australia's NRM regions. Retrieved from https://www.climatechangeinaustralia.gov.au/en/climate-projections. Accessed on July 07, 2019.

Chang, K.B., Lai, S.H., Faridah, O., 2013. RainIDF: Automated derivation of rainfall intensity-duration-frequency relationship from annual maxima and partial duration series. J. Hydroinformatics, 15(4): 1224-1233. DOI:10.2166/hydro.2013.192

Chow, K.C.A., Watt, W.E., 1992. Use of Akaike information criterion for selection of flood frequency distribution. Canadian Journal of Civil Engineering, 19(4): 616-626. DOI:10.1139/l92-071

Chow, V.T., 1964. Handbook of Applied Hydrology. McGraw-Hill, New York, USA.

Coleman, T.F., Li, Y., 1994. On the Convergence of Reflective Newton Methods for Large-Scale Nonlinear Minimization Subject to Bounds. Mathematical Programming, 67(2).

Coleman, T.F., Li, Y.Y., 1996. An interior trust region approach for nonlinear minimization subject to bounds. Siam J Optimiz, 6(2): 418-445. DOI: 10.1137/0806023

Coles, S., 2001. An Introduction to Statistical Modelling of Extreme Values. Springer, London, UK, 219 pp.

Coulibaly, P., Dibike, Y.B., Anctil, F., 2005. Downscaling Precipitation and Temperature with Temporal Neural Networks. Journal of Hydrometeorology, 6(4): 483-496. DOI:10.1175/jhm409.1

CSA, 2012. Technical guide: Development, interpretation and use of rainfall intensity-duration-frequency (IDF) information: Guideline for Canadian water resources practitioners. Canadian Standard Association, 214 pp.

Cunnane, C., 1978. Unbiased plotting positions - A review. J. Hydrol., 37(3): 205-222.

Cunnane, C., 1989. Statistical distributions for flood frequency analysis, WMO-report no. 781 (Operational Hydrology Report no. 33). World Meteorological Organization, Geneva, Switzerland.

Dalrymple, T., 1960. Flood-frequency analyses, U.S. Geol. Surv. Water Supply Pap., no. 1543A.

Eaton, B., Church, M., Ham, D., 2002. Scaling and regionalization of flood flows in British Columbia, Canada. Hydrol. Processes, 16(16): 3245-3263. DOI:10.1002/hyp.1100

Efron, B., Tibshirani, R.J., 1994. An introduction to the bootstrap. Chapman & Hall/CRC Monographs on Statistics & Applied Probability. CRC Press, New York, USA, 456 pp.

El Adlouni, S., Bobée, B., Ouarda, T.B.M.J., 2008. On the tails of extreme event distributions in hydrology. J. Hydrol., 355(1-4): 16-33. DOI: 10.1016/j.jhydrol.2008.02.011

ENES (European Network for Earth System Modelling), 2019. CMIP5 Models and Grid Resolution. Retrieved from https://portal.enes.org/data/enes-model-data/cmip5/. Accessed on July 07, 2019.

Environment Canada, 2014. Rainfall Intensity-Duration-Frequency (IDF) Tables and Graphs. Version 2.3. Released date: December 2014. Retrieved from https://climate.weather.gc.ca/ prods_servs/ engineering_e.html. Accessed on May 1st, 2015.

Environment Canada, 2019. Rainfall Intensity-Duration-Frequency (IDF) Tables and Graphs. Version 3.0. Released date: February 2019. Retrieved from https://climate.weather.gc.ca/ prods_servs/ engineering_e.html. Accessed on March 1st, 2019.

Faulkner, D., Warren, S., Burn, D., 2016. Design floods for all of Canada. Canadian Water Resources Journal / Revue canadienne des ressources hydriques, 41(3): 398-411. DOI:10.1080/07011784.2016.1141665

Forestieri, A. et al., 2018. Regional frequency analysis of extreme rainfall in Sicily (Italy). 38(S1): e698-e716. DOI: 10.1002/joc.5400

Fowler, H.J., Blenkinsop, S., Tebaldi, C., 2007. Linking climate change modelling to impacts studies: recent advances in downscaling techniques for hydrological modelling. Int. J. Climatol., 27(12): 1547-1578. DOI:10.1002/joc.1556

Gado, T.A., Nguyen, V.-T.-V., 2015. Comparison of Homogenous Region Delineation Approaches for Regional Flood Frequency Analysis at Ungauged Sites. J. Hydrol. Eng.: 04015068. DOI:10.1061/(asce)he.1943-5584.0001312

Ghanmi, H., Bargaoui, Z., Mallet, C., 2016. Estimation of intensity-duration-frequency relationships according to the property of scale invariance and regionalization analysis in a Mediterranean coastal area. J. Hydrol., 541: 38-49. DOI: 10.1016/j.jhydrol.2016.07.002

Gooré Bi, E., Gachon, P., Vrac, M., Monette, F., 2017. Which downscaled rainfall data for climate change impact studies in urban areas? Review of current approaches and trends. Theor. Appl. Climatol., 127(3): 685-699. DOI:10.1007/s00704-015-1656-y

Government of Canada, 2018. Topographic Data of Canada - CanVec. Retrieved from: ftp://ftp.maps.canada.ca/pub/nrcan_rncan/vector/canvec. Accessed on Jan 01, 2018.

Government of Canada (2019). Terrestrial Ecoregions of Canada. Retrieved from: https://open.canada.ca/data/en/dataset/ade80d26-61f5-439e-8966-73b352811fe6. Accessed on October 1st 2019.

Goudenhoofdt, E., Delobbe, L., Willems, P., 2017. Regional frequency analysis of extreme rainfall in Belgium based on radar estimates. Hydrol. Earth Syst. Sci., 21(10): 5385-5399. DOI:10.5194/hess-21-5385-2017

Greenwood, J.A., Landwehr, J.M., Matalas, N.C., Wallis, J.R., 1979. Probability weighted moments: Definition and relation to parameters of several distributions expressable in inverse form. Water Resour. Res., 15(5): 1049-1054. DOI:10.1029/WR015i005p01049

Griffis, V.W., Stedinger, J.R., 2007. Evolution of Flood Frequency Analysis with Bulletin 17. J. Hydrol. Eng., 12(3): 283-297. DOI:10.1061/(asce)1084-0699(2007)12:3(283)

Gumbel, E.J., 1958. Statistics of extremes. Columbia University Press, New York. DOI: citeulike-article-id:3346664

Gupta, V., 2017. Scaling Theory of Floods for Developing a Physical Basis of Statistical Flood Frequency Relations. Oxford University Press. DOI:10.1093/acrefore/9780199389407.013.301

Gupta, V.K., Dawdy, D.R., 1995. Physical interpretations of regional variations in the scaling exponents of flood quantiles. Hydrol. Processes, 9(3-4): 347-361. DOI: 10.1002/hyp.3360090309

Gupta, V.K., Waymire, E., 1990. Multiscaling properties of spatial rainfall and river flow distributions. Journal of Geophysical Research: Atmospheres, 95(D3): 1999-2009. DOI: 10.1029/JD095iD03p01999

Gupta, V.K., Waymire, E.C., 1993. A Statistical Analysis of Mesoscale Rainfall as a Random Cascade. Journal of Applied Meteorology, 32(2): 251-267. DOI:10.1175/1520-0450(1993)032<0251:asaomr>2.0.co;2

Hansen, C.R., 2015. Comparison of regional and at-site frequency analysis methods for the estimation of southern Alberta extreme rainfall. Canadian Water Resources Journal / Revue canadienne des ressources hydriques, 40(4): 325-342. DOI:10.1080/07011784.2015.1060871

Hassanzadeh, E., Nazemi, A., Adamowski, J., Nguyen, T.-H., Van-Nguyen, V.-T., 2019. Quantile-based downscaling of rainfall extremes: Notes on methodological functionality, associated uncertainty and application in practice. Adv. Water Resour. DOI: https://doi.org/10.1016/j.advwatres.2019.07.001

Helsel, D.R., Hirsch, R.M., 2002. Statistical Methods in Water Resources Techniques of Water Resources Investigations, Book 4, chapter A3. U.S. Geological Survey, US, 522 pp.

Herath, S.M., Sarukkalige, P.R., Nguyen, V.T.V., 2016. A spatial temporal downscaling approach to development of IDF relations for Perth airport region in the context of climate change. Hydrol. Sci. J., 61(11): 2061-2070. DOI:10.1080/02626667.2015.1083103

Hershfield, D.M., 1961. Rainfall Frequency Atlas of the United States, Technical Paper No. 40., Weather Bureau, US Department of Commerce, Washington, DC.

Hosking, J.R.M., 1990. L-Moments: Analysis and Estimation of Distributions Using Linear Combinations of Order Statistics. Journal of the Royal Statistical Society. Series B (Methodological), 52(1): 105-124.

Hosking, J.R.M., Wallis, J.R., 1997. Regional Frequency Analysis: An Approach Based on L-Moments. Cambridge University Press, Cambridge, UK, 224 pp.

Hosking, J.R.M., Wallis, J.R., Wood, E.F., 1985. Estimation of the Generalized Extreme-Value Distribution by the Method of Probability-Weighted Moments. Technometrics, 27(3): 251-261. DOI:10.2307/1269706

Houghton, J.C., 1978. Birth of a parent: The Wakeby Distribution for modeling flood flows. Water Resour. Res., 14(6): 1105-1109.

Hubert, P., 2001. Multifractals as a tool to overcome scale problems in hydrology. Hydrol. Sci. J., 46(6): 897-905. DOI:10.1080/02626660109492884

Hyndman, R.J., Koehler, A.B., 2006. Another look at measures of forecast accuracy. International Journal of Forecasting, 22(4): 679-688.

IBC, 2018. (Insurance Bureau of Canada): Facts of the Property and Casualty Insurance Industry in Canada, Toronto: Insurance Bureau of Canada.

IPCC (Intergovernmental Panel on Climate Change), 2019. DDC AR5 reference snapshot. Retrieved from https://www.ipcc-data.org/sim/gcm_monthly/AR5. Accessed on July 07, 2019.

Ishak, E., Haddad, K., Zaman, M., Rahman, A., 2011. Scaling property of regional floods in New South Wales Australia. Natural Hazards, 58(3): 1155-1167. DOI:10.1007/s11069-011-9719-6

Jenkinson, A.F., 1955. The frequency distribution of the annual maximum (or minimum) values of meteorological elements. Quarterly Journal of the Royal Meteorological Society, 81(348): 158-171. DOI:10.1002/qj.49708134804

Katz, R.W., Parlange, M.B., Naveau, P., 2002. Statistics of extremes in hydrology. Adv. Water Resour., 25(8-12): 1287-1304. Doi 10.1016/S0309-1708(02)00056-8

Khalili, M., Van Nguyen, V.T., 2016. An efficient statistical approach to multi-site downscaling of daily precipitation series in the context of climate change. Climate Dynamics, 49(7-8): 2261-2278. DOI:10.1007/s00382-016-3443-6

Kharin, V.V., Zwiers, F.W., Zhang, X., Hegerl, G.C., 2007. Changes in Temperature and Precipitation Extremes in the IPCC Ensemble of Global Coupled Model Simulations. Journal of Climate, 20(8): 1419-1444. DOI:10.1175/jcli4066.1

Kharin, V.V., Zwiers, F.W., Zhang, X., Wehner, M., 2013. Changes in temperature and precipitation extremes in the CMIP5 ensemble. CLIM. CHANGE, 119(2): 345-357. DOI:10.1007/s10584-013-0705-8

Kite, G.W., 1977. Frequency and Risk Analyses in Hydrology. Water Resources Publications, Fort Colling, Colorado, USA.

Kumar, P., Guttarp, P., Foufoula-Georgiou, E., 1994. A probability-weighted moment test to assess simple scaling. Stochastic Hydrol Hydraul, 8(3): 173-183. DOI: 10.1007/bf01587233

Lambert, S.J., Boer, G.J., 2001. CMIP1 evaluation and intercomparison of coupled climate models. Climate Dynamics, 17(2): 83-106. DOI:10.1007/pl00013736

Lang, M., Ouarda, T.B.M.J., Bobee, B., 1999. Towards operational guidelines for over-threshold modeling. J. Hydrol., 225(3-4): 103-117. DOI:Doi 10.1016/S0022-1694(99)00167-5

Laprise, R., 2008. Regional climate modelling. J. Comput. Phys., 227(7): 3641-3666. DOI: 10.1016/j.jcp.2006.10.024

Lee, T., Jeong, C., 2014. Nonparametric statistical temporal downscaling of daily precipitation to hourly precipitation and implications for climate change scenarios. J. Hydrol., 510: 182-196. DOI: https://doi.org/10.1016/j.jhydrol.2013.12.027

Lee, T., Park, T., 2017. Nonparametric temporal downscaling with event-based population generating algorithm for RCM daily precipitation to hourly: Model development and performance evaluation. J. Hydrol., 547: 498-516. DOI: https://doi.org/10.1016/j.jhydrol.2017.01.049

Lemmen, D.S., Warren, F.J., James, T.S., Mercer Clarke, C.S.L., 2016. Canada's Marine Coasts in a Changing Climate, Government of Canada, Ottawa, ON.

Lenderink, G., van Meijgaard, E., 2008. Increase in hourly precipitation extremes beyond expectations from temperature changes. Nature geoscience, 1: 511-514.

Levenberg, K., 1944. A Method for the Solution of Certain Problems in Least-Squares. Quarterly Applied Mathematics, 2: 164-168.

Li, J., Johnson, F., Evans, J., Sharma, A., 2017. A comparison of methods to estimate future sub-daily design rainfall. Adv. Water Resour., 110(Supplement C): 215-227. DOI: https://doi.org/10.1016/j.advwatres.2017.10.020

Lim, S.H., 2016. "Statistical modeling of extreme rainfall processes in British Columbia, Master thesis." Department of Civil Engineering and Applied Mechanics, 168 pages

LIO, 2016. Land Information Ontario. Retrieved from https://www.ontario.ca/page/land-information-ontario. Accessed on Dec 01, 2016

Lovejoy, S., 1982. Area-perimeter relation for rain and cloud areas. Science (New York, N.Y.), 216(4542): 185-7. DOI:10.1126/science.216.4542.185

Lovejoy, S., Schertzer, D., 2012. The Weather and Climate: Emergent Laws and Multifractal Cascades. Cambridge University Press, Cambridge. DOI:10.1017/CBO9781139093811

Madsen, H., Arnbjerg-Nielsen, K., Mikkelsen, P.S., 2009. Update of regional intensity–duration–frequency curves in Denmark: Tendency towards increased storm intensities. Atmos. Res., 92(3): 343-349. DOI: https://doi.org/10.1016/j.atmosres.2009.01.013

Madsen, H., Lawrence, D., Lang, M., Martinkova, M., Kjeldsen, T.R., 2014. Review of trend analysis and climate change projections of extreme precipitation and floods in Europe. J. Hydrol., 519: 3634-3650. DOI: 10.1016/j.jhydrol.2014.11.003

Marani, M., Zanetti, S., 2007. Downscaling rainfall temporal variability. Water Resour. Res., 43(9): n/a-n/a. DOI:10.1029/2006WR005505

Maraun, D. et al., 2010. Precipitation downscaling under climate change: Recent developments to bridge the gap between dynamical models and the end user. Rev. Geophys., 48(3): n/a-n/a. DOI:10.1029/2009RG000314

Marquardt, D.W., 1963. An Algorithm for Least-Squares Estimation of Nonlinear Parameters. J Soc Ind Appl Math, 11(2): 431-441.

Martin, J.C., Perez, C.J., 2009. Bayesian analysis of a generlized lognormal distribtuion. Computational Statistics and Data Anlaysis 53: 1377-1387.

Mathworks. (2016). “Matlab R2016b Documentation”. Retrieved from https://www.mathworks.com/help/index.html. Accessed on January 01, 2016

Mekis, E. et al., 2018. An Overview of Surface-Based Precipitation Observations at Environment and Climate Change Canada. Atmosphere-Ocean, 56(2): 71-95. DOI:10.1080/07055900.2018.1433627

Mélèse, V., Blanchet, J., Creutin, J.-D., 2019a. A Regional Scale-Invariant Extreme Value Model of Rainfall Intensity-Duration-Area-Frequency Relationships. Water Resour. Res., 55(7): 5539-5558. DOI:10.1029/2018wr024368

Mélèse, V., Blanchet, J., Creutin, J.D., 2019b. A Regional Scale-Invariant Extreme Value Model of Rainfall Intensity-Duration-Area-Frequency Relationships. Water Resour. Res., 55(7): 5539-5558. DOI:10.1029/2018wr024368

Mélèse, V., Blanchet, J., Molinié, G., 2018. Uncertainty estimation of Intensity–Duration–Frequency relationships: A regional analysis. J. Hydrol., 558: 579-591. DOI: https://doi.org/10.1016/j.jhydrol.2017.07.054

Menabde, M., Seed, A., Pegram, G., 1999. A simple scaling model for extreme rainfall. Water Resour. Res., 35(1): 335-339. DOI:10.1029/1998wr900012

Mielke, P.W., Johnson, E.S., 1974. Some generalized beta distributions of the second kind having desirable application features in hydrology and meteorology. Water Resour. Res., 10 (2): 223-226.

Moré, J.J., 1977. The Levenberg-Marquardt Algorithm: Implementation and Theory. Numerical Analysis: 105-116.

Moré, J.J., Garbow, B.S., Hillstrom, K.E., 1980. User Guide for MINPACK 1. Argonne National Laboratory, Rept. ANL-80-74.

Murshed, M.S., Kim, S., Park, J.-S., 2011. Beta-κ distribution and its application to hydrologic events. Stochastic Environmental Research and Risk Assessment, 25(7): 897-911. DOI:10.1007/s00477-011-0494-4

NA-CORDEX (The North American CORDEX Program), 2018. Regional climate change scenario data and guidance for North America, for use in impacts, decision-making, and climate science. Retrieved from https://na-cordex.org/. Accessed on February 02, 2018.

NEX-DCP30 (NASA Earth Exchange (NEX) Downscaled Climate Projections), 2018. Retrieved from https://cds.nccs.nasa.gov/nex/. Accessed on February 02, 2018.

NEX-GDDP (NASA Earth Exchange Global Daily Downscaled Projections), 2018. Retrieved from https://cds.nccs.nasa.gov/nex-gddp/. Accessed on February 02, 2018.

Nguyen, T.-H., El Outayek, S., Lim, S.H., Nguyen, V.-T.-V., 2017. A systematic approach to selecting the best probability models for annual maximum rainfalls - a case study using data in Ontario (Canada). J. Hydrol. DOI: https://doi.org/10.1016/j.jhydrol.2017.07.052

Nguyen, T.-H. and Nguyen, V.-T.-V., 2015. Statistical Modeling of Extreme Rainfall Processes: A Decision-Support Tool for Rainfall Frequency Analyses. FloodNet Annual Workshop 2015. Sep 17-18, 2015. Toronto, ON, Canada.

Nguyen, T.-H., Nguyen, V.-T.-V., 2017. Statistical Modeling of Extreme Rainfall Processes (SMExRain): A Decision Support Tool for Constructing Intensity-Duration-Frequency Relations for Urban Water Infrastructure Design, CSCE 2017 Annual Conference: Leadership in Sustainable Infrastructure, May 31 - June 03, 2017, Vancouver, Canada.

Nguyen, T.-H., Nguyen, V.-T.-V., 2018a. A Novel Scale-Invariance Generalized Extreme Value Model Based on Probability Weighted Moments for Estimating Extreme Design Rainfalls in the Context of Climate Change, World Environmental and Water Resources Congress 2018. DOI: 10.1061/9780784481417.025

Nguyen, T.-H., Nguyen, V.-T.-V., 2018b. Scale-Invariance Generalized Logistic (GLO) Model for Estimating Extreme Design Rainfalls in the Context of Climate Change. In: La Loggia, G., Freni, G., Puleo, V., De Marchis, M. (Eds.), HIC 2018. 13th International Conference on Hydroinformatics. EPic series in Engineering, Palermo, Italy, pp. 1531-1538.

Nguyen, T.-H., Nguyen, V.-T.-V., 2019a. A Decision-Support Tool for Assessing Climate Change Impacts on Design and Management of Urban Water Systems, CSCE 2019 annual conference: Growing with youth, June 12 - 15, 2019, Laval, Quebec, Canada, pp. HYD023-1 - HYD023-10.

Nguyen, T.-H., Nguyen, V.-T.-V., 2019b. Decision-Support Tool for Constructing Robust Rainfall IDF Relations in Consideration of Model Uncertainty. J. Hydrol. Eng., 24(7): 06019004. DOI: 10.1061/(ASCE)HE.1943-5584.0001802

Nguyen, T.-H., Nguyen, V.-T.-V., 2020. Linking climate change to urban storm drainage system design: An innovative approach to modeling of extreme rainfall processes over different spatial and temporal scales. Journal of Hydro-environment Research. DOI: https://doi.org/10.1016/j.jher.2020.01.006.

Nguyen, T.-H., Nguyen, V.-T.-V., Nguyen, H.-L., 2018. A spatio-temporal statistical downscaling approach to deriving extreme rainfall IDF relations at ungauged sites in the context of climate change. In: La Loggia, G., Freni, G., Puleo, V., De Marchis, M. (Eds.), 13th

International hydroinformatics conference HIC 2018. EPiC Series in Engineering, Palermo, Italy, pp. 1539-1546.

Nguyen, T.D., 2003. Regional Estimation of Extreme Rainfall Events, McGill University, Montréal, Québec, Canada, 240 pp.

Nguyen, T.D., Nguyen, V.T.V., Desramaut, N., 2008. Estimation of urban design storms in consideration of GCM-based climate change scenarios, Water and Urban Development Paradigms. CRC Press, pp. 347-356. DOI: 10.1201/9780203884102.pt3

Nguyen, V.-T.-V., Tao, D., Bourque, A., 2002a. On selection of probability distributions for representing annual extreme rainfall series, Ninth International Conference on Urban Drainage (9ICUD). ASCE Library, Portland, Oregon, United States.

Nguyen, V.T., Nguyen, T.D., Ashkar, F., 2002b. Regional frequency analysis of extreme rainfalls. Water science and technology: a journal of the International Association on Water Pollution Research, 45(2): 75-81.

Nguyen, V.T.V., Inna, N., Bobee, B., 1989. New Plotting-Position Formula for Pearson Type-III Distribution. J Hydraul Eng-Asce, 115(6): 709-730.

Nguyen, V.T.V., Nguyen, T.D., 2007. Chapter 16: Statistical downscaling of precipitation process for climate-related impact studies. Water Resources Publications.

Nguyen, V.T.V., Nguyen, T.D., 2008a. A spatial-temporal statistical downscaling approach to estimation of extreme precipitations for climate-related impact studies at a local site, World Environmental and Water Resources Congress 2008: Ahupua'a, Honolulu, HI. DOI:10.1061/40976(316)401

Nguyen, V.T.V., Nguyen, T.D., 2008b. A Spatial-Temporal Statistical Downscaling Approach to Estimation of Extreme Precipitations for Climate-Related Impact Studies at a Local Site, World Environmental and Water Resources Congress 2008. DOI: 10.1061/40976(316)401

Nguyen, V.T.V., Nguyen, T.D., Cung, A., 2007. A statistical approach to downscaling of sub-daily extreme rainfall processes for climate-related impact studies in urban areas. In: Fang, H.H.P., Lee, J.H.W. (Eds.), Water Science and Technology: Water Supply, pp. 183-192. DOI:10.2166/ws.2007.053

Nguyen, V.T.V., Nguyen, T.D., Gachon, P., 2006. On the linkage of large-scale climate variability with local characteristics of daily precipitation and temperature extremes: an evaluation of statistical downscaling methods Advances in Geosciences, 4(16): 1-9.

Nguyen, V.T.V., Nguyen, T.D., Wang, H., 1998. Regional estimation of short duration rainfall extremes. Water Science and Technology, 37(11): 15-19. DOI :http://dx.doi.org/10.1016/S0273-1223(98)00311-4

Nguyen, V.T.V., Pandey, G.R., 1994. Estimation of Short-Duration Rainfall Distribution Using Data Measured at Longer Time Scales. Water Science and Technology, 29(1-2): 39-45.

Nguyen, V.T.V., Wang, H., 1996. Regional Estimation of Short-Duration Rainfall Distribution Using Available Daily Rainfall Data. Journal of Water Management Modeling. DOI:10.14796/JWMM.Rl91-ll

NOAA Atlas 14, Volume 6., 2014. Precipitation-Frequency Atlas of the United States, California, Version 2.3, S. Perica, S. Dietz, S. Heim, L. Hiner, K. Maitaria, D. Martin, S. Pavlovic, I. Roy, C. Trypaluk, D. Unruh, F. Yan, M. Yekta, T. Zhao, G. Bonnin, D. Brewer, L. Chen, T. Parzybok, J. Yarchoan, National Weather Service, Silver Spring, MD

Ochoa-Rodriguez, S., Wang, L.-P., Willems, P., Onof, C., 2019. A Review of Radar-Rain Gauge Data Merging Methods and Their Potential for Urban Hydrological Applications. Water Resour. Res., 55(8): 6356-6391. DOI:10.1029/2018wr023332

Ojha, C.S.P., Berndtsson, R., Bhunya, P., 2008. Engineering hydrology. Oxford University Press, Oxford; New York.

Öztekin, T., 2005. Comparison of Parameter Estimation Methods for the Three Parameter Generalized Pareto Distribtuion. Turkish Journal of Agriculture and Foresty, 29: 419-428.

Öztekin, T., 2007. Wakeby distribution for representing annual extreme and partial duration rainfall series. Meteorological Applications, 14(4): 381-387. DOI:10.1002/met.37

Pandey, G.R., 1998. Assessment of Scaling Behavior of Regional Floods. J. Hydrol. Eng., 3(3): 169-173. DOI: doi:10.1061/(ASCE)1084-0699(1998)3:3(169)

Pandey, G.R., Nguyen, V.T.V., 1999. A comparative study of regression-based methods in regional flood frequency analysis. J. Hydrol., 225(1): 92-101. DOI: http://dx.doi.org/10.1016/S0022-1694(99)00135-3

Pathak, C.S., Teegavarapu, R.S.V., 2018. Radar Rainfall Data Estimation and Use. Radar Rainfall Data Estimation and Use. DOI:10.1061/9780784415115

PCIC (Pacific climate impacts consortium), 2018. Statistically downscaled climate scenarios. Retrieved from https://www.pacificclimate.org/data. Accessed on February 02, 2018.

Pearson, K., 1893. Contributions to the Mathematical Theory of Evolution. [Abstract]. Proceedings of the Royal Society of London, 54: 329-333.

Powell, M.J.D., 1970. A Fortran Subroutine for Solving Systems of Nonlinear Algebraic Equations. Numerical Methods for Nonlinear Algebraic Equations. Ch. 7.

Raes, D., Willems, P., GBaguidi, F., 2006. RAINBOW – a software package for analyzing data and testing the homogeneity of historical data sets, 4th International Workshop on 'Sustainable management of marginal drylands, Islamabad, Pakistan, 27-31 January 2006.

Rao, A.R., Hamed, K.H., 2000. Flood frequency analysis. CRC Press, Boca Raton, London, 350 pp.

Robson, A., Reed, D., 1999. Flood Estimation Handbook, Volume 3, Statistical procedures for flood frequency estimation. Institute of Hydrology, Wallingford, Oxfordshire, United Kingdom.

Rosso, R., Burlando, P., 1990. Scale invariance in temporal and spatial rainfall, KV General Assembly European Geophysical Society. Annales Geophysicae, 23-27 April, Copenhagen, pp. 145.

Salinas, J.L., Castellarin, A., Kohnová, S., Kjeldsen, T.R., 2014a. Regional parent flood frequency distributions in Europe - Part 2: Climate and scale controls. Hydrology and Earth System Sciences, 18(11): 4391-4401. DOI:10.5194/hess-18-4391-2014

Salinas, J.L., Castellarin, A., Viglione, A., Kohnová, S., Kjeldsen, T.R., 2014b. Regional parent flood frequency distributions in Europe - Part 1: Is the GEV model suitable as a pan-European parent? Hydrology and Earth System Sciences, 18(11): 4381-4389. DOI:10.5194/hess-18-4381-2014

Sandink, D., Simonovic, S.P., Schardong, A., Srivastav, R., 2016. A decision support system for updating and incorporating climate change impacts into rainfall intensity-duration-frequency curves: Review of the stakeholder involvement process. Environmental Modelling & Software, 84: 193-209. DOI: http://dx.doi.org/10.1016/j.envsoft.2016.06.012

Schaefer, M., 1990. Regional analyses of precipitation annual maxima in Washington State. Water Resour. Res., 26(1): 119–131.

Schertzer, D., Lovejoy, S., 1987. Physical modeling and analysis of rain and clouds by anisotropic scaling multiplicative processes. Journal of Geophysical Research: Atmospheres, 92(D8): 9693-9714. DOI:10.1029/JD092iD08p09693

Schertzer, D., Lovejoy, S., 1991. Nonlinear Geodynamical Variability: Multiple Singularities, Universality and Observables. In: Schertzer, D., Lovejoy, S. (Eds.), Non-Linear Variability in Geophysics: Scaling and Fractals. Springer Netherlands, Dordrecht, pp. 41-82. DOI:10.1007/978-94-009-2147-4_4

Schertzer, D., Tchiguirinskaia, I., Lovejoy, S., Hubert, P., 2010. No monsters, no miracles: in nonlinear sciences hydrology is not an outlier! Hydrol. Sci. J., 55(6): 965-979. DOI:10.1080/02626667.2010.505173

Shephard, M.W. et al., 2014. Trends in Canadian Short-Duration Extreme Rainfall: Including an Intensity–Duration–Frequency Perspective. Atmosphere-Ocean, 52(5): 398-417. DOI:10.1080/07055900.2014.969677

Simonovic, S.P., Schardong, A., Sandink, D., Srivastav, R., 2016. A web-based tool for the development of Intensity Duration Frequency curves under changing climate. Environmental Modelling & Software, 81: 136-153. DOI: http://dx.doi.org/10.1016/j.envsoft.2016.03.016

Singh, V.P., 1998. Entropy-based parameter estimation in hydrology. Kluwer Academic Publishers, Dordrecht, xv + 365 pp. pp.

Sivakumar, B., Sorooshian, S., Gupta, H.V., Gao, X., 2001. A chaotic approach to rainfall disaggregation. Water Resour. Res., 37(1): 61-72. DOI:10.1029/2000wr900196

Smith, J.A., 1992. Representation of basin scale in flood peak distributions. Water Resour. Res., 28(11): 2993-2999. DOI:10.1029/92WR01718

Smith, R.L., 2003. Statistics of extremes, with applications in environment, insurance and finance. Department of Statistics, University of North Carolina, Chapel Hill, North Carolina, USA.

Soltani, S., Helfi, R., Almasi, P., Modarres, R., 2017. Regionalization of Rainfall Intensity-Duration-Frequency using a Simple Scaling Model. Water Resources Management, 31(13): 4253-4273. DOI:10.1007/s11269-017-1744-0

Sposito, G., 1998. Scale Dependence and Scale Invariance in Hydrology. Cambridge University Press, Cambridge. DOI:10.1017/CBO9780511551864

Stedinger, J.R., 1980. Fitting Log Normal Distributions to Hydrologic Data. Water Resour. Res., 16(3): 481-490.

Stedinger, J.R., Griffis, V.W., 2008. Flood Frequency Analysis in the United States: Time to Update. J. Hydrol. Eng., 13(4): 199-204. DOI: 10.1061/(ASCE)1084-0699(2008)13:4(199)

Stedinger, J.R., Vogel, R.M., Foufoula-Georgiou, E., 1993. Frequency Analysis of Extreme Events, chapter 18 in Handbook of Hydrology edited by D. A. Maidment. McGraw-Hill, New York, USA.

Teutschbein, C., Wetterhall, F., Seibert, J., 2011. Evaluation of different downscaling techniques for hydrological climate-change impact studies at the catchment scale. Climate Dynamics, 37(9): 2087-2105. DOI:10.1007/s00382-010-0979-8

Thorndahl, S. et al., 2017. Weather radar rainfall data in urban hydrology. Hydrol. Earth Syst. Sci., 21(3): 1359-1380. DOI:10.5194/hess-21-1359-2017

Thrasher, B., Maurer, E.P., McKellar, C., Duffy, P.B., 2012. Technical Note: Bias correcting climate model simulated daily temperature extremes with quantile mapping. Hydrol. Earth Syst. Sci., 16(9): 3309-3314. DOI:10.5194/hess-16-3309-2012

Van de Vyver, H., 2018. A multiscaling-based intensity–duration–frequency model for extreme precipitation. Hydrol. Processes, 32(11): 1635-1647. DOI: 10.1002/hyp.11516

Veneziano, D., Furcolo, P., 2002. Multifractality of rainfall and scaling of intensity-duration-frequency curves. Water Resour. Res., 38(12): 42-1-42-12. DOI:10.1029/2001wr000372

Veneziano, D., Langousis, A., Furcolo, P., 2006. Multifractality and rainfall extremes: A review. Water Resour. Res., 42(6): n/a-n/a. DOI:10.1029/2005WR004716

Veneziano, D., Lepore, C., 2012. The scaling of temporal rainfall. Water Resour. Res., 48(8): n/a-n/a. DOI:10.1029/2012wr012105

Vogel, R.M., 1995. Recent advances and themes in hydrology. Rev. Geophys., 33(S2): 933. DOI:10.1029/95rg00935

Vogel, R.M., Sankarasubramanian, A., 2000. Spatial scaling properties of annual streamflow in the United States. Hydrol. Sci. J., 45(3): 465-476. DOI:10.1080/02626660009492342

Vu, M.T., Raghavan, V.S., Liong, S.Y., 2016. Deriving short-duration rainfall IDF curves from a regional climate model. Natural Hazards. DOI:10.1007/s11069-016-2670-9

Werner, A.T., Cannon, A.J., 2016. Hydrologic extremes -- an intercomparison of multiple gridded statistical downscaling methods. Hydrol. Earth Syst. Sci., 20(4): 1483-1508. DOI:10.5194/hess-20-1483-2016

Wilby, R.L., Dawson, C.W., 2013. The Statistical DownScaling Model: insights from one decade of application. Int. J. Climatol., 33(7): 1707-1719. DOI:10.1002/joc.3544

Wilby, R.L., Dawson, C.W., Barrow, E.M., 2002. SDSM - A decision support tool for the assessment of regional climate change impacts. Environ. Model. Softw., 17(2): 147-159.

Wilks, D.S., 1993. Comparison of three-parameter probability distributions for representing annual extreme and partial duration precipitation series. Water Resour. Res., 29(10): 3543-3549. DOI:10.1029/93wr01710

Willems, P. et al., 2012. Impacts of climate change on rainfall extremes and urban drainage systems. IWA Publishing, London, UK, 238 pp.

WMO, 2008. Guide to Hydrological Practices. Volume 1. Hydrology - From Measurement to Hydrological Information World Meteorological Organization, 296 pp.

WMO, 2009a. Guide to hydrological practices, volume 2: Management of water resources and application of hydrological practices, 6th edition, WMO-No. 168. World Meteorological Organization, Geneva, Switzerland, 302 pp.

WMO, 2009b. Guidelines on analysis of extremes in a changing climate in support of informed decisions for adaptation, WMO-TD No. 1500. World Meteorological Organization, Geneva, Switzerland, 55 pp.

Xu, Z., Han, Y., Yang, Z., 2019. Dynamical downscaling of regional climate: A review of methods and limitations. Science China Earth Sciences, 62(2): 365-375. DOI:10.1007/s11430-018-9261-5

Xue, Y., Janjic, Z., Dudhia, J., Vasic, R., De Sales, F., 2014. A review on regional dynamical downscaling in intraseasonal to seasonal simulation/prediction and major factors that affect downscaling ability. Atmos. Res., 147-148: 68-85. DOI: https://doi.org/10.1016/j.atmosres.2014.05.001

Ye, L., Hanson, L.S., Ding, P., Wang, D., Vogel, R.M., 2018. The probability distribution of daily precipitation at the point and catchment scales in the United States. Hydrol. Earth Syst. Sci., 22(12): 6519-6531. DOI:10.5194/hess-22-6519-2018

Yu, F.X., Naghavi, B., Singh, V.P., Wang, G.-T., 1994. MMO: An improved estimator for log-Pearson type-3 distribution. Stochastic Hydrol Hydraul, 8(3): 219-231.

Yu, P.-S., Yang, T.-C., Lin, C.-S., 2004. Regional rainfall intensity formulas based on scaling property of rainfall. J. Hydrol., 295(1-4): 108-123. DOI:10.1016/j.jhydrol.2004.03.003

Yue, S., Gan, T.Y., 2009. Scaling properties of Canadian flood flows. Hydrol. Processes, 23(2): 245-258. DOI:10.1002/hyp.7135

Yue, S., Yew Gan, T., 2004. Simple scaling properties of Canadian annual average streamflow. Adv. Water Resour., 27(5): 481-495. DOI: http://dx.doi.org/10.1016/j.advwatres.2004.02.019

Zhang, X. et al., 2019. Changes in Temperature and Precipitation Across Canada; Chapter 4 in Bush, E. and Lemmen, D.S. (Eds.) Canada's Changing Climate Report. , Government of Canada, Ottawa, Ontario, .

Zhang, X., Zwiers, F.W., Li, G., Wan, H., Cannon, A.J., 2017. Complexity in estimating past and future extreme short-duration rainfall. Nature Geosci, advance online publication. DOI:10.1038/ngeo2911

Appendix A: Supplementary Materials for Chapter 2

(A Systematic Approach to Selecting the Best Probability Models for Annual Maximum Rainfalls – A case study using data in Ontario, Canada)

Table A-1. Values of the L-skewness (Lskew) and L-kurtosis (Lkurt) of the 5-minute, 1-hour, and 24-hour AMS from the 21 study stations

No	Station ID	5-min AMS		1-hour AMS		24-hour AMS	
		Lskew	Lkurt	Lskew	Lkurt	Lskew	Lkurt
1	6012199	0.180	0.113	0.170	0.163	0.237	0.162
2	6016525	0.122	0.096	0.252	0.111	0.248	0.200
3	6034075	0.060	0.093	0.204	0.101	0.272	0.146
4	6042716	0.066	0.109	0.133	0.131	0.299	0.250
5	6048268	0.211	0.115	0.305	0.278	0.368	0.295
6	6057592	0.111	0.102	0.307	0.241	0.284	0.209
7	6078285	0.080	0.107	0.298	0.264	0.329	0.208
8	6085700	0.256	0.159	0.163	0.038	0.230	0.215
9	6104175	0.089	0.147	0.199	0.139	0.262	0.281
10	6105978	0.090	0.138	0.280	0.152	0.293	0.229
11	6127514	0.108	0.263	0.133	0.146	0.120	0.159
12	6131415	0.214	0.149	0.146	0.124	0.148	0.119
13	6131983	0.073	0.062	0.218	0.163	0.270	0.177
14	6137362	0.237	0.236	0.144	0.114	0.223	0.159
15	6139525	0.177	0.087	0.201	0.137	0.168	0.101
16	6143090	-0.045	0.076	0.348	0.310	0.236	0.247
17	6144478	0.239	0.161	0.268	0.195	0.128	0.051
18	6153301	0.118	0.038	0.106	0.126	0.343	0.171
19	6158355	0.290	0.159	0.201	0.134	0.226	0.100
20	6158731	0.149	0.136	0.185	0.207	0.402	0.300
21	6158875	0.342	0.204	0.326	0.204	0.119	0.057

Appendix B: Supplementary Materials for Chapter 3

(A Novel Scale-Invariance Probability-Weighted-Moment-Based Generalized Extreme Value Distribution for Modeling Rainfall Extremes Across A Wide Range of Time Scales)

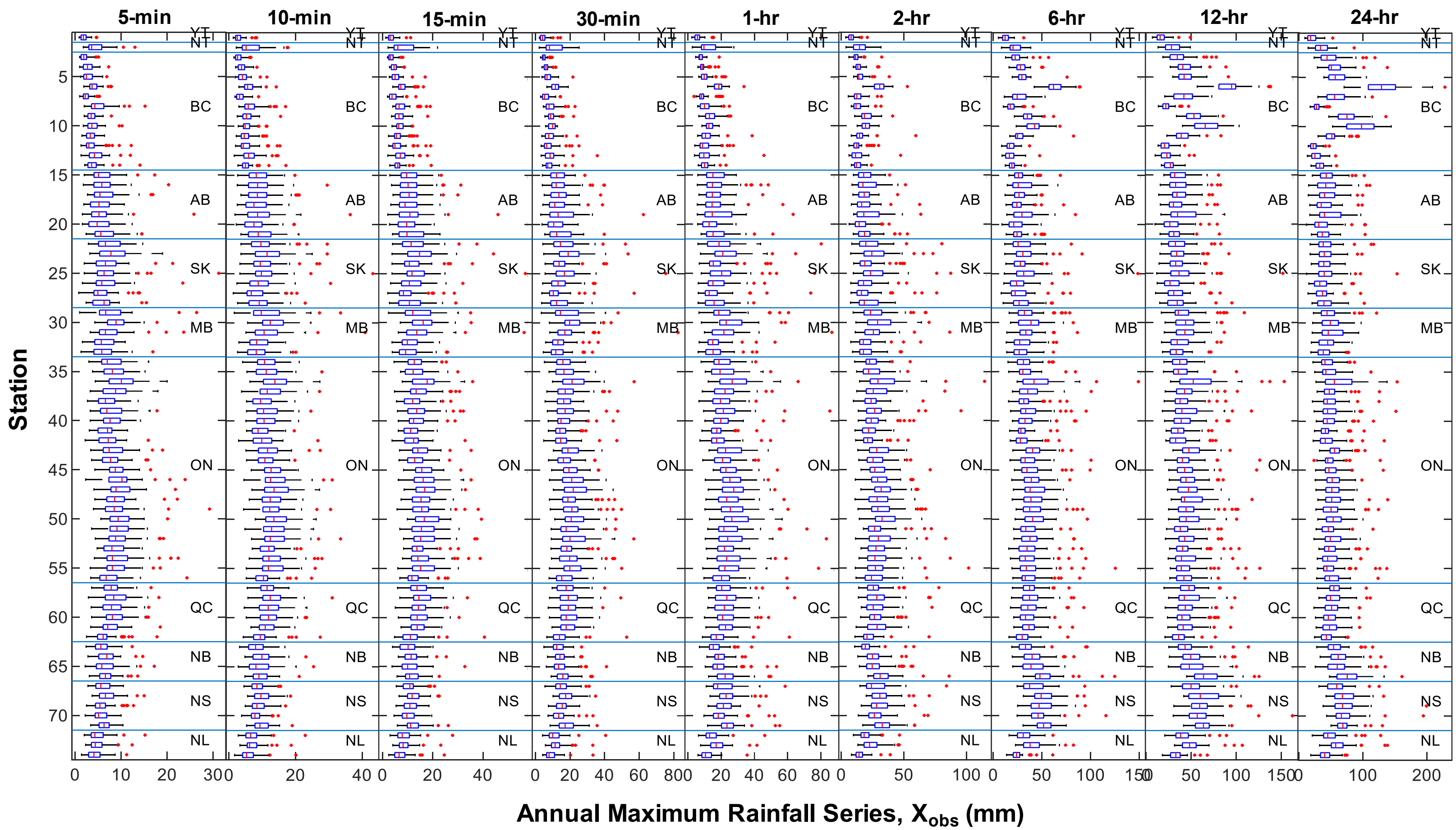

Figure B-1. Observed annual maximum rainfall series (X_{obs}, mm) from 5 to 1440 minutes (24 hours) of the 74 study stations across Canada

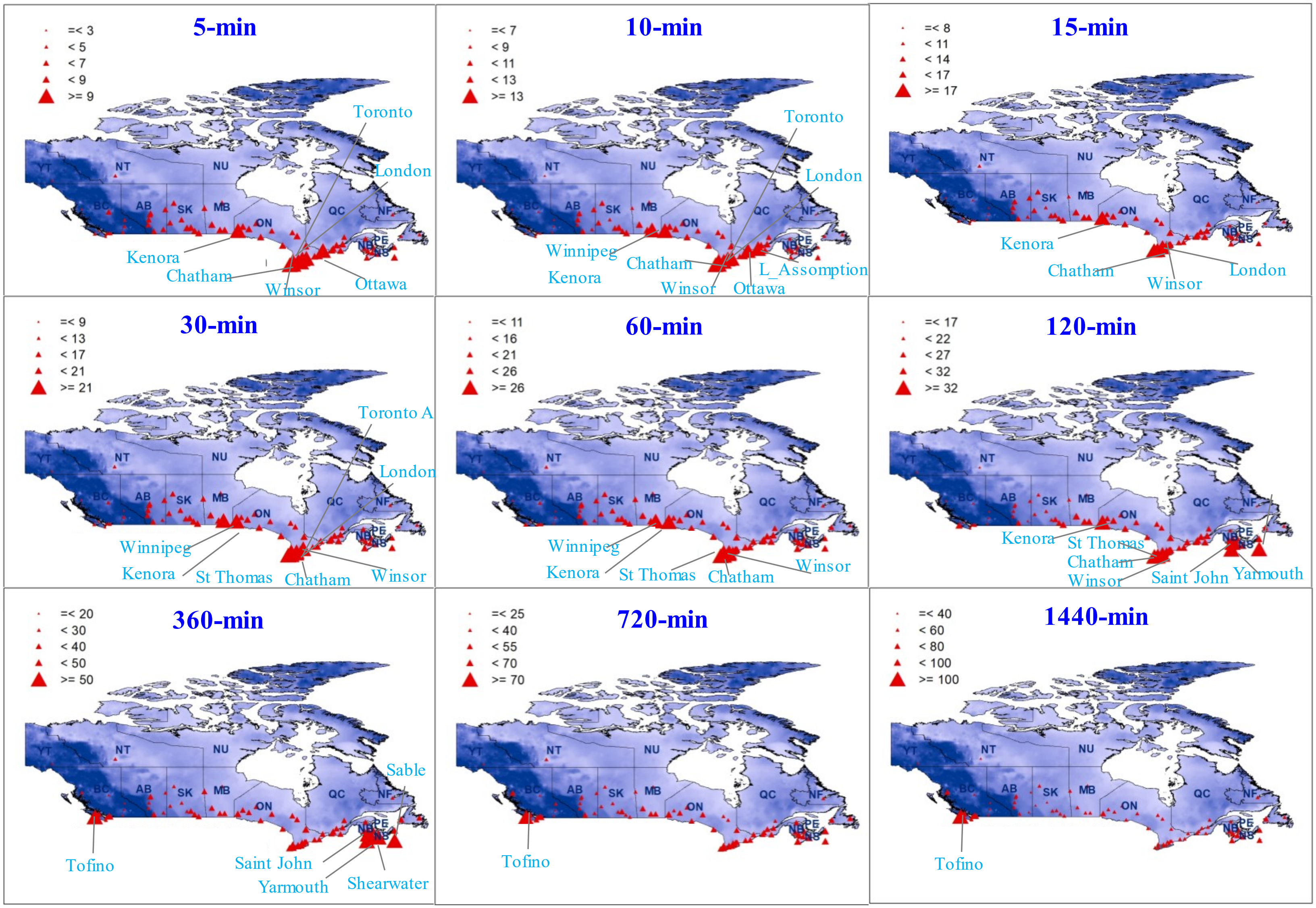

Figure B-2. Spatial representation of the AMS means (triangles with different sizes, mm) of different rainfall durations (from 5 to 1440 minutes) for the study stations across Canada

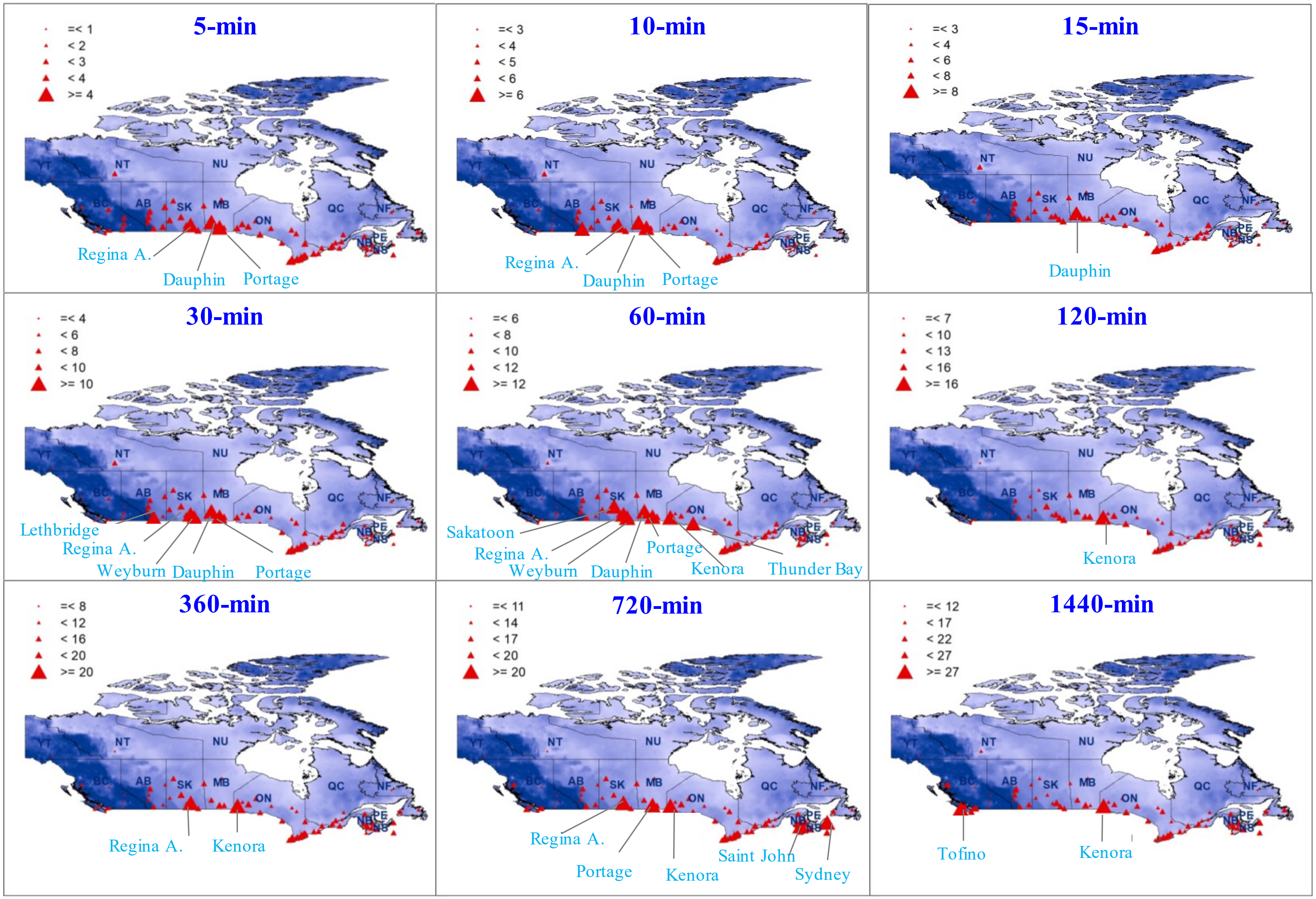

Figure B-3. Spatial representation of the AMS standard deviations (triangles with different sizes, mm) of different rainfall durations (from 5 to 1440 minutes) for the study stations across Canada

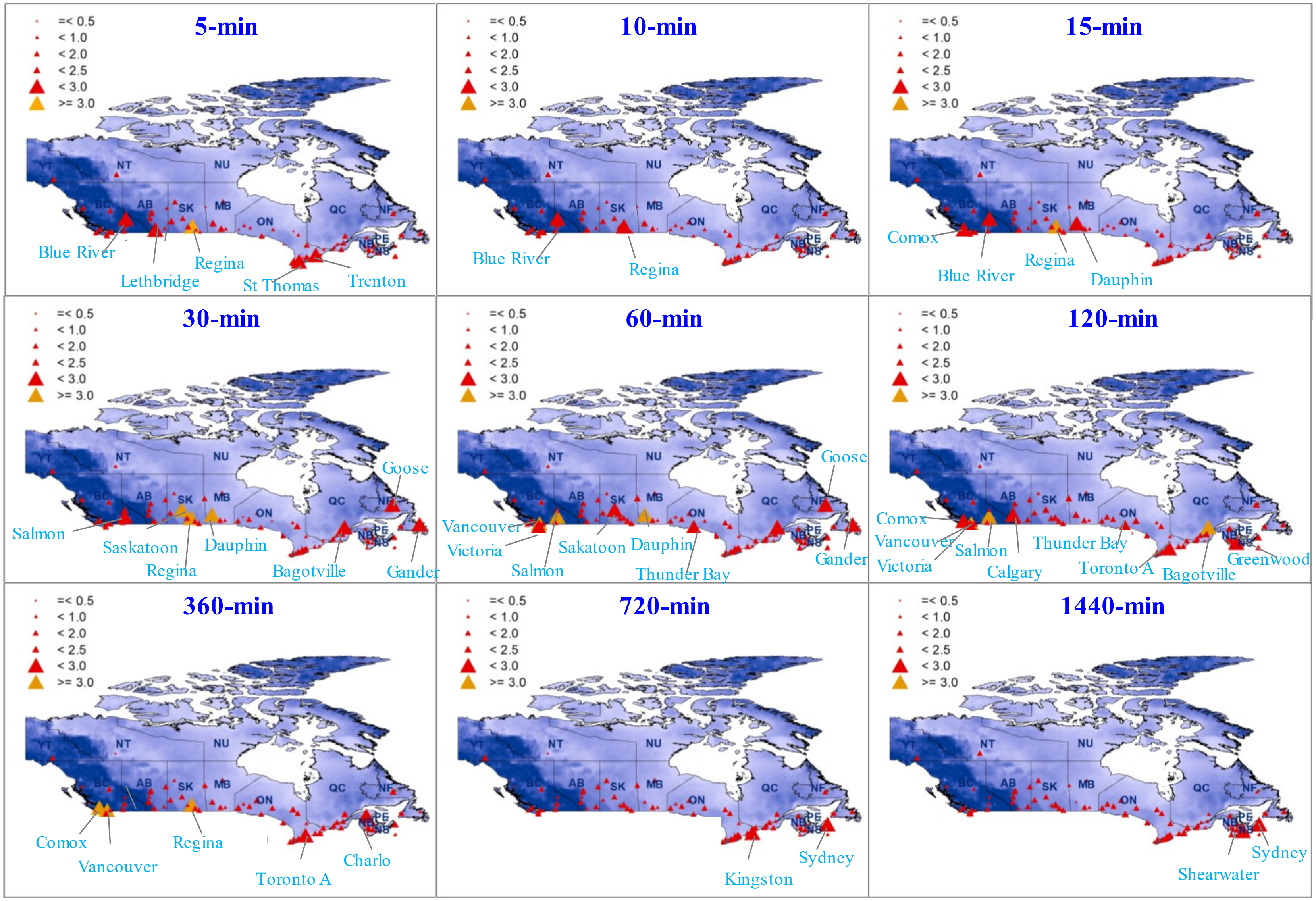

Figure B-4. Spatial representation of the AMS skewness (triangles with different sizes, mm) of different rainfall durations (from 5 to 1440 minutes) for the study stations across Canada

Table B-1. Results of Mann – Kendall trend detection tests. AMS from 74 stations with nine rainfall durations (from 5 to 1440 minutes). Cells highlighted show significant results at 5% significant level.

Stn	Mann–Kendall test for trend detection									Stn	Mann–Kendall test for trend detection								
	5	10	15	30	60	120	360	720	1440		5	10	15	30	60	120	360	720	1440
1	0.64	1.01	0.87	0.72	0.65	0.14	0.65	0.80	1.05	38	0.63	0.72	1.10	1.52	1.70	1.44	1.29	1.74	2.07
2	-0.10	-0.63	-0.68	-0.80	-0.21	0.01	-0.05	0.25	0.37	39	1.28	1.44	1.34	1.55	0.96	0.20	0.79	1.13	1.29
3	0.58	0.44	0.36	1.35	2.86	2.27	1.61	1.13	0.87	40	0.60	1.30	1.55	2.17	1.45	0.54	-1.10	-0.70	-0.18
4	1.48	1.68	1.36	0.04	0.42	0.79	1.14	0.58	0.82	41	0.43	0.06	0.22	0.87	0.25	-0.75	-0.92	-0.88	0.03
5	-0.43	-0.54	-0.24	-0.33	0.33	1.50	0.82	0.39	0.00	42	0.52	0.80	1.02	0.92	0.97	0.29	-0.49	-0.43	-1.12
6	0.70	0.11	0.13	-0.98	-0.12	0.97	1.64	2.35	0.67	43	-1.10	-1.64	-1.38	-1.49	-0.77	-0.89	0.08	0.14	0.77
7	1.35	0.75	0.61	0.63	1.31	1.38	1.78	1.60	2.09	44	0.48	-0.16	-0.37	-0.34	-0.38	-0.80	-0.42	-0.15	-0.67
8	-1.34	-0.57	-0.16	-0.06	-0.03	-1.11	-1.89	-1.64	-1.48	45	-0.77	-0.76	-0.90	-0.72	-1.38	-0.79	0.45	1.05	2.28
9	0.82	0.96	1.19	-0.41	-1.16	-0.78	-0.71	0.28	0.18	46	-0.99	-0.91	-0.97	-0.29	0.67	1.05	0.18	-0.41	-0.29
10	1.00	0.90	0.53	0.68	0.26	0.75	-0.66	-0.69	-0.51	47	0.47	0.48	-0.14	-0.05	0.49	-0.20	-0.47	-0.62	-0.88
11	1.30	0.49	0.56	0.94	0.57	1.05	-0.40	-0.69	-1.67	48	0.07	1.62	1.61	1.38	1.61	0.82	-0.60	-0.66	-0.99
12	2.48	1.21	0.61	1.55	2.11	1.86	1.39	2.11	2.10	49	-0.12	-0.56	-0.98	0.06	0.16	0.11	-0.44	0.08	0.10
13	2.55	2.08	2.58	2.25	1.60	0.42	0.25	0.32	1.17	50	-1.68	-1.90	-1.06	-1.34	-2.24	-2.17	-2.15	-2.47	-0.97
14	2.02	1.55	1.72	2.08	2.21	1.85	1.59	1.67	2.01	51	-0.02	0.59	0.71	0.84	1.14	0.47	-0.90	-1.74	-2.66
15	0.68	0.57	0.16	0.49	0.74	0.75	0.06	0.21	0.39	52	-0.20	1.26	1.09	0.57	-0.05	-0.28	-0.94	-1.12	-1.22
16	-0.38	-0.74	-0.81	-0.94	-1.12	-1.07	-0.59	0.15	0.36	53	-0.32	-0.13	0.14	-0.49	-0.61	-1.14	-0.24	-0.46	0.20
17	1.87	1.80	1.52	1.12	0.77	0.64	0.15	-0.02	-0.32	54	-1.26	-0.87	-0.94	-0.52	-0.90	-1.39	-1.78	-1.99	-2.30
18	-0.93	-0.55	-0.13	0.49	1.04	1.17	0.00	0.91	0.98	55	-0.97	-0.50	-0.77	-0.79	-0.19	-0.70	-1.33	-0.98	-0.66
19	0.33	0.16	0.26	1.16	0.71	0.67	0.49	0.29	0.28	56	-1.45	-0.83	-0.21	0.27	1.80	2.08	1.48	2.07	2.18
20	-2.11	-1.46	-0.63	-0.12	0.46	0.19	-0.85	-0.92	-1.09	57	1.43	1.50	1.48	1.05	-0.20	0.47	0.05	0.79	-0.14
21	-0.51	-0.55	-0.51	0.16	0.21	0.26	-0.72	-0.75	-1.06	58	1.06	2.07	3.20	3.55	2.91	2.23	1.47	0.51	1.74
22	-1.03	-0.79	-0.65	-0.45	-0.44	-0.22	0.00	0.30	0.24	59	1.09	0.73	0.62	1.47	1.53	1.69	2.46	2.20	1.67
23	1.11	0.54	0.36	0.29	0.13	-0.37	-0.02	-0.01	0.52	60	-2.59	-0.80	-0.45	0.30	-0.03	0.79	1.01	-0.25	-1.18
24	1.69	1.94	2.25	1.77	1.18	1.53	1.13	-0.53	-1.07	61	0.16	-0.47	-0.73	-0.29	-0.01	-1.15	-0.56	-0.14	0.88
25	-0.79	-1.48	-1.20	-1.32	-1.04	-1.09	-0.69	-1.00	-0.66	62	0.46	0.00	0.67	0.67	0.44	-0.07	1.09	1.03	0.64
26	1.29	1.76	1.57	1.52	1.34	0.85	1.62	1.24	1.36	63	0.62	1.15	1.09	0.95	0.55	0.82	0.43	0.71	0.60
27	-1.32	-1.17	-1.19	-1.31	-1.20	-0.99	-1.93	-1.76	-1.77	64	-2.87	-1.59	-1.34	-0.74	-0.50	0.58	1.15	1.37	0.91
28	0.78	0.21	0.25	-0.13	0.00	0.61	0.47	0.11	-0.25	65	0.86	0.96	0.55	0.95	1.57	1.26	2.15	2.68	2.80
29	-2.48	-2.55	-2.44	-2.48	-2.09	-1.35	-1.91	-1.49	-0.71	66	-1.01	-1.85	-1.04	-1.24	-1.10	-0.14	-1.29	-1.99	-1.98
30	-0.16	0.52	0.10	0.20	0.31	0.14	-0.15	0.00	-0.03	67	-0.56	-1.21	-0.57	-0.20	-1.27	-0.93	-0.37	0.52	0.99
31	0.47	0.64	0.41	0.43	-0.02	0.20	0.22	0.28	0.52	68	0.23	0.87	1.01	1.57	1.09	0.55	-0.02	-0.04	-0.20
32	-0.20	-0.74	-0.93	-0.87	-1.21	-0.84	-0.48	-0.32	-1.20	69	-0.94	-0.66	0.06	1.33	1.36	0.98	0.63	1.30	1.59
33	0.41	0.08	0.12	-0.01	0.00	-0.12	-0.42	0.11	0.42	70	0.02	1.08	1.13	1.34	0.44	0.59	0.33	-0.63	-0.12
34	0.55	1.16	1.61	1.19	0.25	-0.59	0.49	0.51	0.87	71	-0.35	-1.74	-1.67	-1.86	-0.62	1.46	1.17	0.81	0.15
35	0.34	0.26	0.47	0.21	0.67	0.80	0.22	-0.43	0.11	72	1.39	1.00	0.95	1.16	1.68	2.56	3.32	3.58	3.65
36	-0.38	0.68	0.62	0.63	0.07	0.12	0.70	0.72	0.96	73	2.48	1.06	1.81	2.37	1.96	2.55	1.77	1.63	1.22
37	-0.09	-0.07	0.33	1.07	1.05	1.17	0.90	1.47	0.76	74	0.78	0.56	0.44	0.42	0.70	1.10	-0.13	-0.42	-0.06

Table B-2. Results of Mann-Whitney homogeneity and stationarity tests. AMS from 74 stations with nine rainfall durations (from 5 to 1440 minutes). Cells highlighted show significant results at 5% significant level.

Stn	Mann-Whitney test for homogeneity and stationarity									Stn	Mann-Whitney test for homogeneity and stationarity								
	5	10	15	30	60	120	360	720	1440		5	10	15	30	60	120	360	720	1440
1	-1.24	-0.96	-0.96	-0.82	-0.35	-0.21	-0.80	-0.89	-1.36	38	-0.09	-0.22	-0.55	-1.15	-1.58	-1.58	-2.11	-2.45	-1.99
2	-0.21	-0.47	-0.82	-0.67	-0.11	-0.09	-0.06	-0.74	-1.27	39	-0.43	-0.80	-0.84	-1.49	-1.05	-0.48	-0.44	-0.71	-1.12
3	-0.60	-0.66	-0.13	-0.63	-1.54	-1.38	-0.84	-0.16	-0.09	40	-0.14	-0.43	-0.47	-1.07	-1.13	-0.32	-1.13	-0.87	-0.03
4	-1.29	-1.39	-1.29	-0.57	-0.65	-1.39	-1.85	-0.79	-1.29	41	-0.77	-0.57	-0.59	-1.02	-0.54	-0.24	-0.29	-0.44	-0.44
5	-0.24	-0.27	-0.22	-0.11	-0.57	-1.14	-1.19	-1.03	-0.08	42	-1.34	-1.22	-1.53	-0.39	-0.29	-0.16	-0.23	-0.02	-0.72
6	-0.59	-0.32	-0.30	-0.05	-0.82	-2.11	-2.41	-2.88	-0.77	43	-1.17	-1.36	-1.43	-1.64	-1.30	-0.57	-0.18	-0.29	-0.63
7	-0.19	-0.02	-0.49	-0.36	-0.45	-0.62	-0.83	-0.96	-1.40	44	-0.60	-0.25	-0.08	-0.16	-0.07	-0.08	-1.31	-1.02	-0.56
8	-0.63	-0.34	-0.10	-0.18	-0.13	-0.42	-1.36	-0.52	-0.63	45	-1.41	-1.20	-1.27	-0.98	-1.48	-0.80	-0.58	-0.99	-2.26
9	-1.39	-1.22	-0.91	-0.58	-1.44	-1.31	-1.08	-0.58	-0.35	46	-0.80	-0.62	-0.42	-0.34	-0.94	-1.28	-0.80	-0.60	-0.72
10	-0.89	-0.62	-0.81	-1.00	-0.65	-0.43	-1.16	-1.54	-1.46	47	-1.38	-1.27	-1.00	-0.92	-1.08	-0.08	-0.03	-0.24	-0.81
11	-1.58	-1.13	-0.95	-1.47	-1.29	-1.95	-0.01	-0.65	-1.78	48	-0.36	-1.27	-1.83	-1.70	-1.85	-1.50	-0.26	-0.01	-0.30
12	-2.98	-1.53	-0.92	-1.03	-1.69	-1.90	-1.27	-2.11	-2.79	49	-0.05	-0.88	-1.00	-0.46	-0.41	-0.47	-0.44	-0.73	-0.48
13	-2.10	-1.67	-1.85	-1.70	-1.22	-0.49	-1.12	-1.45	-2.25	50	-2.29	-2.76	-1.67	-1.74	-2.06	-1.69	-1.83	-1.89	-0.33
14	-1.88	-2.02	-2.11	-2.58	-2.32	-1.95	-1.31	-1.74	-2.04	51	-0.62	-1.36	-1.36	-1.81	-2.05	-1.24	-0.21	-0.87	-1.60
15	-0.73	-0.17	-0.13	-0.21	-0.55	-0.60	-0.06	0.00	-0.40	52	-0.25	-0.98	-0.89	-0.87	-0.42	-0.39	-0.22	-0.33	-0.01
16	-0.26	-0.38	-0.58	-1.00	-1.27	-0.88	-0.25	-0.83	-1.14	53	-0.40	-0.49	-0.40	-0.40	-0.66	-1.04	-0.15	-0.02	-0.08
17	-1.53	-1.24	-0.95	-0.70	-0.70	-0.66	-0.54	-0.31	-0.19	54	-0.89	-0.35	-0.64	-0.46	-0.85	-1.63	-2.16	-2.35	-2.57
18	-1.49	-1.23	-0.59	-0.17	-0.36	-1.15	-0.47	-1.11	-0.89	55	-0.71	-0.44	-0.77	-1.03	-0.55	-0.77	-1.34	-1.02	-0.59
19	-0.02	-0.19	-0.15	-0.32	-0.11	-0.19	-0.06	-0.28	-0.36	56	-1.99	-1.66	-1.13	-0.34	-1.44	-1.46	-0.91	-1.50	-1.68
20	-1.30	-0.70	-0.10	-0.37	-0.60	-0.47	-0.63	-0.65	-0.44	57	-0.30	-1.26	-1.66	-1.53	-0.03	-0.08	-0.63	-0.32	-0.43
21	-0.35	-0.16	-0.12	-0.23	-0.06	-0.06	-0.74	-0.87	-0.99	58	-0.36	-1.61	-2.52	-2.88	-2.13	-1.14	-0.86	-0.14	-1.36
22	-0.60	-0.31	-0.13	-0.16	-0.21	-0.68	-0.39	-1.17	-1.12	59	-1.70	-1.75	-1.49	-2.43	-2.48	-2.06	-2.45	-1.72	-1.56
23	-0.59	-0.11	-0.18	-0.33	-0.15	-0.13	-0.38	-0.68	-1.19	60	-2.19	-0.89	-0.75	-0.27	-0.61	-0.38	-1.17	-0.17	-0.84
24	-1.30	-1.14	-1.62	-1.38	-1.20	-1.42	-0.48	-0.92	-1.44	61	-1.34	-0.75	-0.27	-0.59	-1.09	-0.48	-0.52	-0.77	-1.50
25	-0.04	-0.60	-0.26	-0.66	-0.64	-0.51	-0.66	-0.95	-0.57	62	-0.41	-0.18	-0.82	-1.02	-0.79	-0.25	-1.34	-1.50	-0.68
26	-0.68	-1.10	-1.48	-1.46	-1.12	-1.26	-1.84	-1.20	-1.14	63	-1.55	-1.96	-1.75	-1.26	-0.85	-0.75	-0.17	-0.19	-0.06
27	-1.22	-1.08	-1.30	-1.19	-1.30	-0.87	-0.89	-0.84	-0.78	64	-2.43	-1.43	-1.13	-0.70	-0.32	-0.28	-0.60	-0.47	-0.02
28	-0.18	-0.16	0.00	-0.08	-0.10	-0.39	-0.42	-0.26	-0.10	65	-0.44	-0.58	-0.43	-0.97	-1.38	-0.77	-1.08	-1.40	-1.94
29	-1.41	-1.62	-1.43	-1.51	-1.22	-0.35	-1.00	-0.60	-0.11	66	-0.30	-1.41	-0.92	-0.81	-0.70	-0.14	-1.35	-1.87	-1.84
30	-0.30	-0.53	-0.03	-0.11	-0.19	-0.24	-0.29	-0.21	-0.18	67	-0.36	-0.75	-0.05	-0.05	-1.21	-1.29	-0.61	-0.27	-0.51
31	-0.08	-0.30	-0.41	-0.54	-0.32	-0.30	-0.41	-0.54	-0.49	68	-0.60	-0.87	-0.72	-0.90	-0.73	-0.23	-0.11	-0.38	-0.30
32	-0.65	-1.04	-1.20	-0.97	-1.15	-0.94	-1.25	-0.70	-1.43	69	-0.39	-0.30	-0.62	-1.08	-0.42	-0.14	-0.38	-0.18	-0.74
33	-1.00	-0.95	-0.95	-0.83	-0.73	-0.90	-0.78	-0.83	-0.61	70	-0.43	-0.59	-0.87	-0.75	-0.28	-0.53	-0.04	-0.46	-0.28
34	-0.49	-0.90	-1.23	-0.84	-0.13	-0.82	-0.34	-0.69	-1.23	71	-0.02	-1.04	-1.48	-1.46	-0.80	-1.17	-0.92	-0.58	-0.02
35	-0.23	-0.37	0.00	-0.37	-0.23	-0.42	0.00	-0.44	-0.29	72	-1.12	-1.13	-1.11	-1.27	-1.87	-2.57	-3.32	-3.51	-4.26
36	-0.35	-1.15	-1.13	-1.20	-0.66	-0.47	-1.36	-1.74	-2.00	73	-2.41	-1.09	-1.73	-2.45	-2.06	-2.12	-1.28	-1.46	-1.01
37	-0.60	-0.19	-0.24	-1.35	-1.76	-2.19	-2.00	-2.14	-1.38	74	-1.17	-1.09	-1.07	-1.32	-1.42	-1.09	-0.60	-0.28	-0.44

Table B-3. Results of Wald-Wolfowitz independence and stationarity tests. AMS from 74 stations with nine rainfall durations (from 5 to 1440 minutes). Cells highlighted show significant results at 5% significant level.

Stn	Wald-Wolfowitz test for independence and stationarity								Stn	Wald-Wolfowitz test for independence and stationarity							
	5	10	15	30	60	120	360	720	1440		5	10	15	30	60	120	360	720	1440
1	0.08	-0.24	-0.32	-0.86	-1.17	-0.79	0.83	0.53	0.52	38	0.00	0.02	0.89	0.13	0.10	0.10	1.32	0.17	0.75
2	-1.79	-1.94	-1.94	-1.89	-1.58	-1.22	1.04	1.58	1.04	39	-0.94	-0.84	-0.78	-0.34	-0.25	-0.56	-1.35	-1.02	-1.54
3	0.59	0.90	0.84	0.89	0.19	0.29	0.61	0.33	0.20	40	0.50	1.54	1.35	0.52	-0.18	0.18	0.77	0.49	1.16
4	0.52	0.32	-0.44	-0.15	0.09	-0.13	-1.20	-0.18	0.35	41	-0.73	0.53	0.82	0.34	0.42	0.97	-0.53	-0.25	-0.32
5	0.03	-0.32	-0.55	-0.50	0.33	1.39	0.24	0.11	-0.50	42	0.38	1.29	1.04	-0.69	-1.54	-1.10	-0.79	-0.07	-0.01
6	0.79	0.67	0.73	0.46	-0.11	-0.39	-0.79	1.03	1.11	43	-1.10	-0.41	-0.74	-0.51	-1.09	-0.75	-0.58	0.17	0.08
7	0.45	0.71	0.39	0.66	-0.07	-0.13	1.92	2.45	2.21	44	-0.09	-0.43	-1.16	-0.79	0.49	0.84	1.06	0.12	0.28
8	0.36	0.14	-0.14	0.22	0.63	0.32	2.11	2.05	1.61	45	1.08	-0.06	0.04	-0.27	-0.80	-0.26	0.79	0.84	0.30
9	-1.83	-1.56	-1.68	-1.55	-1.26	-0.19	0.62	0.34	0.57	46	-0.83	-0.91	-0.60	-1.06	-1.77	0.12	-0.18	0.25	-0.09
10	0.08	-0.20	0.92	1.43	-1.17	-1.25	-0.23	0.89	-0.05	47	0.10	0.16	-0.35	0.74	0.84	1.16	0.64	-0.47	-1.03
11	3.06	2.49	2.55	2.14	1.11	0.02	0.04	0.25	0.45	48	0.42	-0.65	-1.34	-1.73	-1.26	-1.57	-0.19	0.98	0.96
12	0.80	-0.46	-0.90	-1.13	-1.24	-0.43	1.58	2.41	2.91	49	0.11	0.22	0.05	-0.70	-0.59	-1.04	0.97	1.78	1.48
13	0.58	-0.83	-0.28	-0.18	-0.09	-0.27	0.39	0.70	0.91	50	-0.11	0.89	1.09	0.27	0.84	0.27	-0.48	0.00	-0.83
14	0.87	0.55	0.39	-0.07	-0.52	-1.22	-0.37	1.38	1.15	51	-1.97	-2.11	-1.75	-1.31	-1.20	-0.63	0.74	-0.36	-0.67
15	-0.86	-0.35	-0.37	-0.69	-0.92	-0.97	-0.89	-0.68	-0.86	52	-0.25	0.39	0.96	1.44	0.52	-0.03	-0.04	-0.18	0.22
16	-1.30	0.41	0.80	0.15	-0.42	-1.17	0.45	1.33	1.03	53	-0.99	-0.40	-0.61	-0.06	0.49	-0.47	-1.30	-1.09	-0.55
17	0.77	1.31	2.09	2.27	1.98	2.59	0.08	1.05	0.78	54	-1.39	-1.26	-0.86	-0.48	-0.30	-0.83	-0.43	-0.47	0.30
18	1.17	0.96	1.41	1.22	1.31	1.27	-0.36	-0.23	-0.52	55	0.57	1.60	2.25	1.85	1.21	1.63	0.37	0.28	-0.17
19	-1.53	-1.81	-1.78	-1.39	-1.43	-1.37	-0.44	-0.12	-0.09	56	2.15	1.73	1.47	-0.30	0.31	-0.19	0.04	-0.26	-0.53
20	-0.27	-0.17	0.46	0.92	1.41	1.77	0.53	0.53	-0.01	57	0.78	1.34	0.74	0.35	1.77	2.82	1.53	0.75	0.69
21	-1.19	-1.46	-0.96	-0.37	-0.31	-0.32	1.41	1.95	0.86	58	1.79	3.40	3.79	2.92	1.81	0.93	1.26	0.70	2.20
22	-2.05	-1.01	-1.24	-0.78	-0.41	-0.21	-0.02	0.63	0.63	59	0.85	1.14	0.99	1.79	2.11	0.61	-0.21	-0.44	-1.36
23	-0.15	-0.29	-0.18	-0.10	-0.24	-0.66	-0.49	-0.33	-0.52	60	1.38	0.93	1.39	1.14	0.56	-0.29	-1.38	-1.57	-0.64
24	1.43	1.27	1.55	1.64	1.61	0.88	0.87	0.46	-0.07	61	0.38	-0.39	-0.71	-0.15	-0.58	-0.64	-0.96	-0.82	-0.80
25	1.77	1.66	1.34	1.05	0.37	0.72	0.24	0.12	0.61	62	1.24	1.30	1.11	0.44	1.05	1.52	1.12	1.80	0.25
26	-0.63	-0.14	-0.35	-1.10	-0.92	-1.01	-0.86	-0.64	-0.62	63	0.46	1.26	1.41	0.65	0.87	0.44	-0.92	-0.94	-0.61
27	0.39	-0.40	-0.15	-0.15	-0.23	0.05	0.71	0.67	0.31	64	-0.49	-1.08	-1.53	-1.16	-1.94	-1.40	-0.81	1.21	1.60
28	1.84	1.22	1.19	2.46	2.59	2.61	1.44	0.94	1.03	65	0.87	0.31	-0.24	-0.41	-0.91	-1.52	-0.62	0.44	0.59
29	-0.39	-0.42	-0.16	0.47	0.63	0.31	-0.09	-0.24	0.30	66	0.48	0.59	1.22	0.74	0.60	-0.35	0.87	0.96	0.16
30	-0.24	-0.23	-0.33	-0.69	-0.72	0.25	-0.22	0.56	0.28	67	-1.76	-1.72	-1.24	-2.15	-1.34	-0.56	-0.42	-0.95	-0.51
31	1.53	0.84	1.01	0.72	0.62	1.03	0.44	0.15	1.07	68	0.11	0.81	0.84	0.80	0.01	-0.88	-0.76	-0.33	0.44
32	0.01	-1.24	-1.27	-0.83	-0.59	-0.56	-0.13	-0.56	0.36	69	0.42	1.05	0.46	0.30	0.71	1.92	0.80	0.41	0.22
33	-0.62	-0.89	-0.78	-0.32	-0.51	-0.70	-1.37	-1.66	-1.45	70	-0.46	0.86	1.12	0.83	0.14	-0.35	-1.04	-1.28	-1.13
34	1.24	1.05	1.46	1.28	0.13	0.03	1.16	0.58	-1.04	71	0.27	0.22	0.30	0.30	-0.25	0.68	0.80	0.77	0.52
35	-0.39	0.47	-0.27	0.35	-0.36	-0.44	-0.58	-0.53	-0.77	72	0.60	1.47	1.58	1.57	2.04	1.67	1.57	0.63	0.57
36	-0.49	0.47	0.40	0.47	0.15	-0.26	0.23	0.24	0.53	73	-0.26	-0.19	-0.45	-0.08	0.32	0.63	-0.70	0.27	0.81
37	1.39	0.81	0.65	1.45	1.50	0.96	0.53	2.12	1.65	74	1.17	1.51	1.03	0.39	-0.15	-1.04	-0.95	-0.93	-1.50

Appendix C: Supplementary Materials for Chapter 4

(Linking Climate Change to Urban Storm Drainage System Design: An Innovative Approach to Modeling of Extreme Rainfall Processes Over Different Spatiotemporal Scales)

D.1. One factor analysis of variance (ANOVA)

- **Data and situation:**

There are k groups of data are to be compared, to determine if their means are significantly different. Each group is assumed to have a normal distribution around its mean. All groups have the same variance. Note that when ANOVA is performed on the ranks rather than the original data, an average rank is used in case of tied data.

- **Null and alternate hypotheses:**

H_0: the k group means are identical $\mu_1 = \mu_2 = \cdots = \mu_k$
H_a: at least one mean is different

- **Computation:**

The treatment mean square (MST) and error mean square (MSE) are computed as their sum of squares divided by their degrees of freedom (df). When the treatment mean square is larger than the error mean square as measured by an F-test, the group means are significantly different.

$$MST = \frac{\sum_{j=1}^{k} n_j\left(\bar{y}_j - \bar{y}\right)}{k-1} \tag{D-1}$$

$$MSE = \frac{\sum_{j=1}^{k}\sum_{i=1}^{n_j}\left(y_{ij} - \bar{y}_j\right)}{\sum_{j=1}^{k}(n_j - 1)} = \frac{\sum_{j=1}^{k}\sum_{i=1}^{n_j}\left(y_{ij} - \bar{y}_j\right)}{N-k} \tag{D-2}$$

where $(k-1)$ = treatment degrees of freedom; and $(N-k)$ = error degrees of freedom

- **F statistic:**

$$F = \frac{MST}{MSE} \tag{D-3}$$

- **Decision rule:**

Reject H_0 if $F \geq F^{*}_{(1-\alpha),(k-1),(N-k)}$ the $(1-\alpha)$ quantile of an F distribution with $(k-1)$ and $(N-k)$ degrees of freedom; otherwise do not reject H_0

D.2. Tukey's HSD test

Two group means μ_i and μ_j can be considered different taking into account that all possible comparisons of k treatments if:

$$\left|\bar{y}_i - \bar{y}_j\right| > q_{(1-\alpha),k,N-k} \cdot \sqrt{MSE \cdot \frac{n_i + n_j}{2n_i n_j}} \tag{D-4}$$

where q is the upper significance level of the studentized range statistic for k means and $(N-k)$ degrees of freedom. The value of q could be found in Harter (1960); α is the overall significant level, k is the number of treatment group means compared $(N-k)$ are the degrees of freedom for the MSE; and n is the sample size per group.

D.3. Magnitude of differences between two groups

- **Non-parametric approach:**

In the situation where each group of data is non-normal distribution, the Hodges-Lehmann estimator can be used to calculate the absolute and relative difference between the two groups of data. It is computed by taking the median of all possible pairwise differences between the x and y groups:

$$\hat{\Delta} = median(x_i - y_j) \tag{D-5}$$

$$\widehat{\Delta_r} = median\left(\frac{x_i - y_j}{x_i}\right) \tag{D-6}$$

where $x_i = 1\ to\ n$; $y_j = 1\ to\ m$; and there will be $N = n \cdot m$ pairwise differences.

Confidence interval for $\hat{\Delta}$ and $\widehat{\Delta_r}$:

$$R_l = \frac{N - z_{\frac{\alpha}{2}} \cdot \sqrt{\frac{N(n+m+1)}{3}}}{2} \tag{D-7}$$

$$R_u = \frac{N + z_{\frac{\alpha}{2}} \cdot \sqrt{\frac{N(n+m+1)}{3}}}{2} + 1 = N - R_l + 1 \tag{D-8}$$

where R_l and R_u are the lower and upper ranks respectively; and $Z_{\frac{\alpha}{2}}$ is from a table of standard normal quantiles.

- **Parametric approach:**

In the situation where each group of data closely follow a normal distribution (i.e. the t-test is appropriate), the difference between the two groups of data is computed as:

$$\bar{\Delta} = (\bar{x} - \bar{y}) \tag{D-9}$$

$$\overline{\Delta_r} = \left(\frac{\bar{x} - \bar{y}}{\bar{x}}\right) \tag{D-10}$$

Confidence interval for $\bar{\Delta}$:

$$CI = \bar{x} - \bar{y} \pm t_{\alpha/2,(df)} \cdot \sqrt{s_x^2/n + s_y^2/m} \tag{D-11}$$

$$df = \frac{\left({s_X^2}/{n} + {s_Y^2}/{m} \right)^2}{\frac{\left({s_X^2}/{n} \right)^2}{(n-1)} + \frac{\left({s_Y^2}/{m} \right)^2}{(m-1)}} \tag{D-12}$$

where s_X^2 and s_Y^2 is the sample variance of the first and second group respectively; df is the approximate degrees of freedom; $t_{\alpha/2,(df)}$ is from a table of the t-distribution.

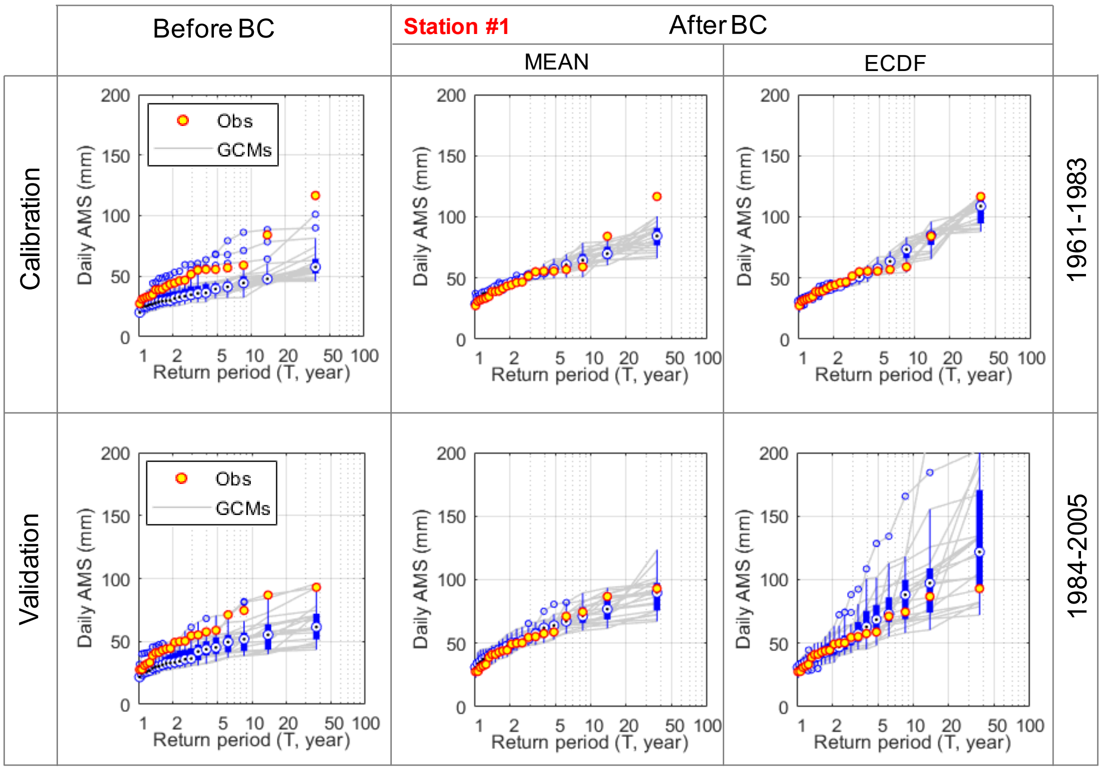

Figure D-1. Similar to Figure 4-4 but Station #1 – Sault Ste Marie Airport Station

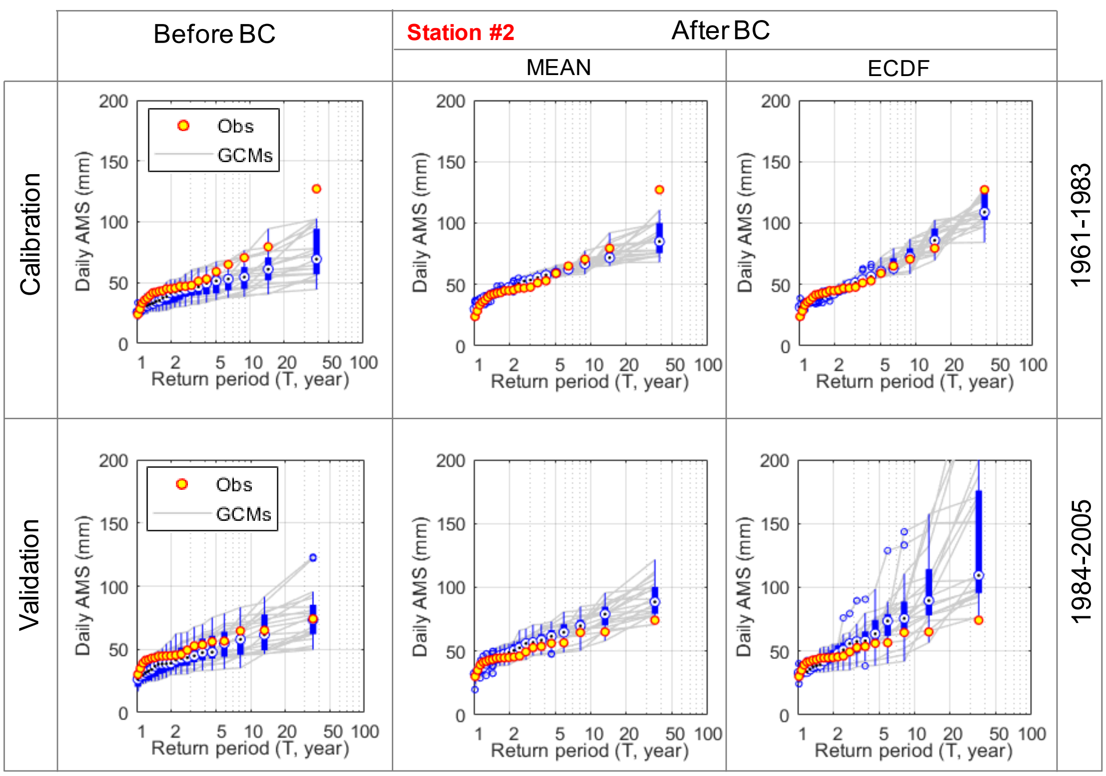

Figure D-2. Similar to Figure 4-4 but for Station #2 – Kingston pumping station

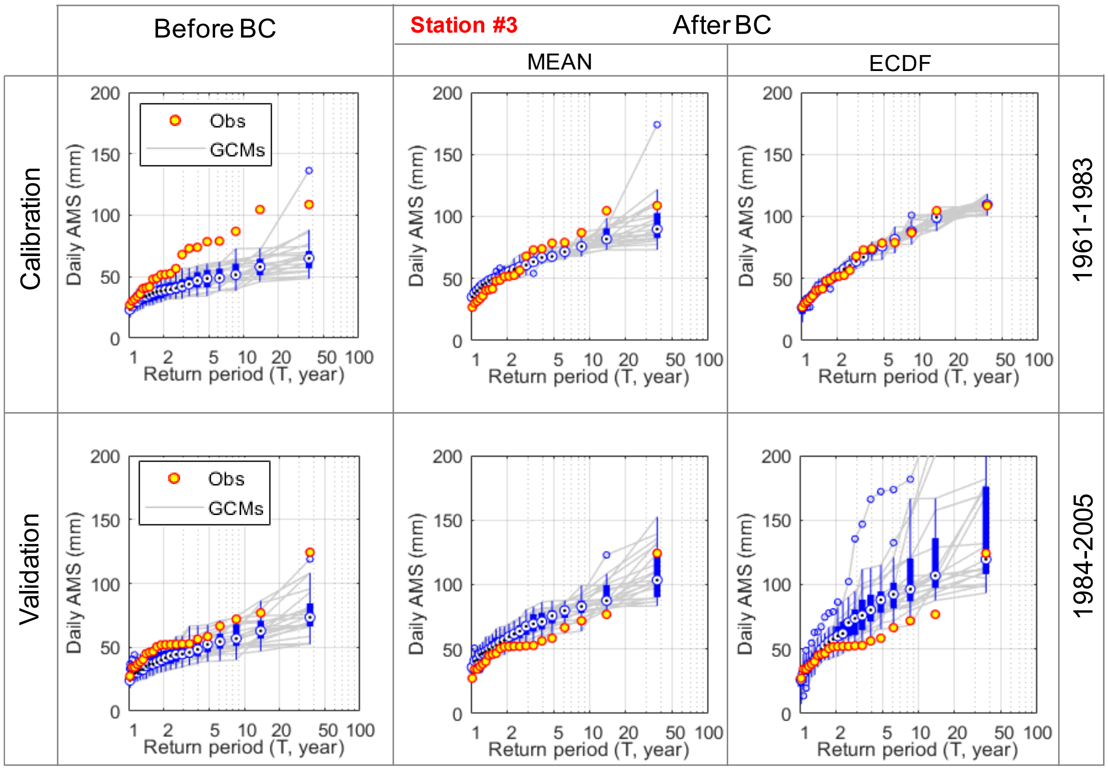

Figure D-3. Similar to Figure 4-4 but for Station #3 – St Thomas WPCP Station

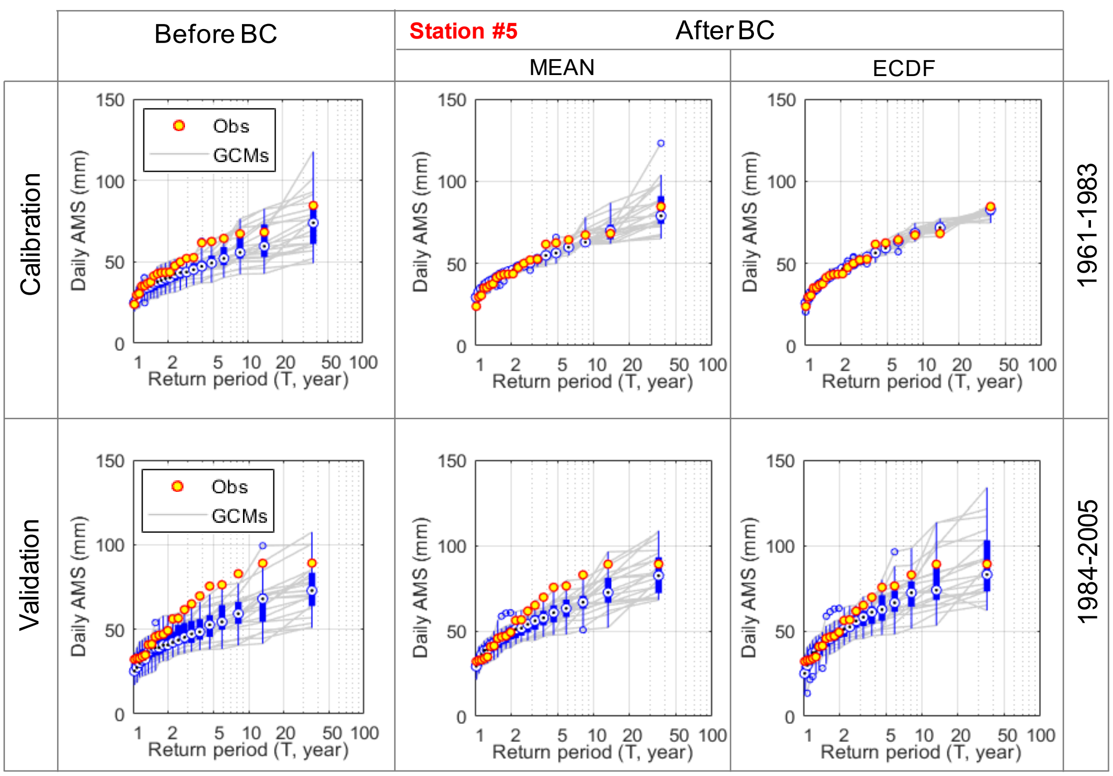

Figure D-4. Similar to Figure 4-4 but for Station #5 – London CS Station

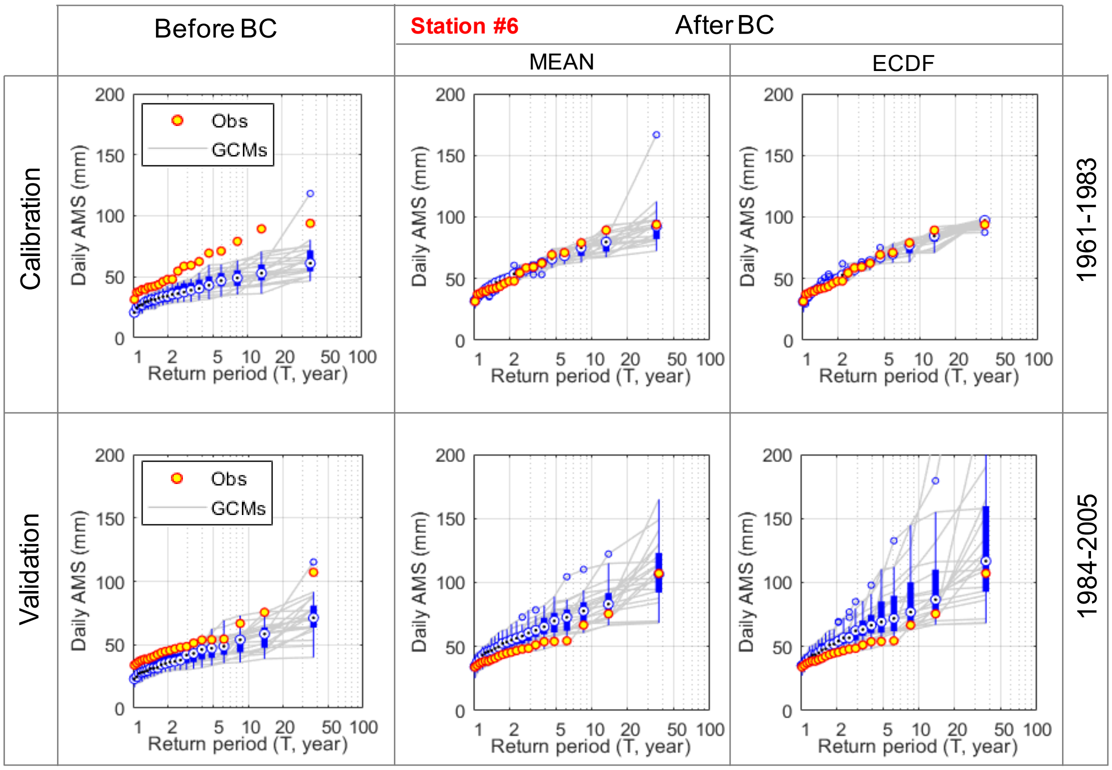

Figure D-5. Similar to Figure 4-4 but for Station #6 – Hamilton RBG CS Station

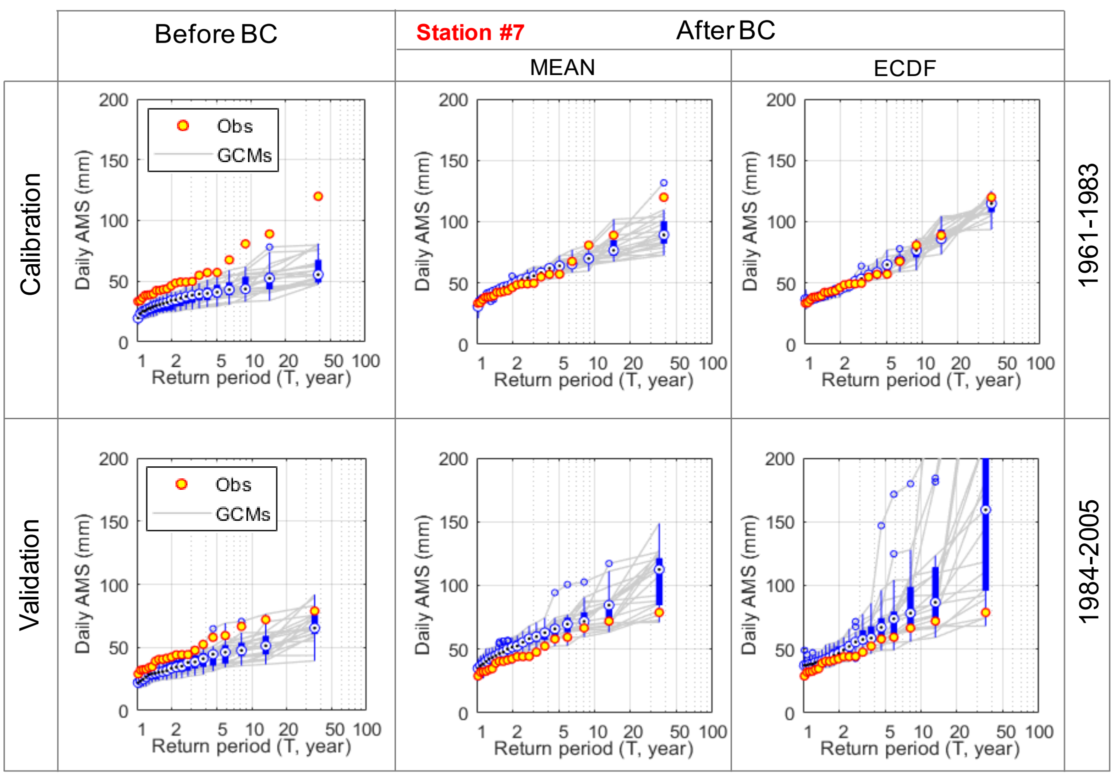

Figure D-6. Similar to Figure 4-4 but for Station #7 – Toronto International Airport Station

(a) PPCC test

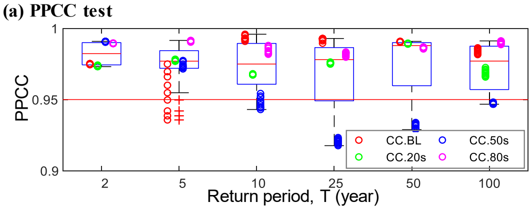

Station #1 Sault Ste Marie A ID: 6057592

Data:
Group 1 = Baseline = 1961-1990
Group 2 = 2020s = 2011-2040
Group 3 = 2050s = 2041-2070
Group 4 = 2080s = 2071-2100

Critical values
Significant level:
$\alpha = 0.05$
PPCC test: r*=0.95
ANOVA: F*=2.73
Tukey test: q*=3.71

(b) ANOVA F-test on the data

D \ T	2	5	10	25	50	100
1440	13.42	14.47	14.05	10.89	7.84	5.43
720	13.34	14.53	14.04	10.80	7.84	5.52
360	13.26	14.59	14.02	10.73	7.85	5.62
120	13.24	14.65	13.94	10.60	7.85	5.73
60	13.22	14.69	13.88	10.53	7.87	5.82
30	13.21	14.72	13.82	10.48	7.90	5.93
15	13.20	14.75	13.76	10.43	7.95	6.04
10	13.20	14.76	13.72	10.41	7.98	6.11
5	13.20	14.78	13.66	10.39	8.04	6.25

(c) ANOVA F-test on the ranks

D \ T	2	5	10	25	50	100
1440	17.63	19.62	17.60	13.21	9.78	6.94
720	17.40	19.58	17.41	13.20	9.84	7.06
360	17.12	19.88	17.40	13.12	9.89	6.98
120	17.07	19.75	16.86	12.97	9.89	7.10
60	16.89	19.49	16.91	12.88	9.90	7.32
30	16.97	19.59	16.94	12.81	9.90	7.37
15	16.93	19.75	16.73	12.80	9.78	7.71
10	16.91	19.73	16.71	12.73	9.78	7.75
5	16.97	19.64	16.52	12.65	9.79	7.80

(d) Tukey's HSD test on the data

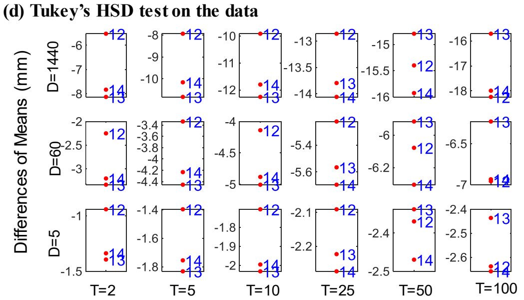

(e) Tukey's HSD test on the ranks

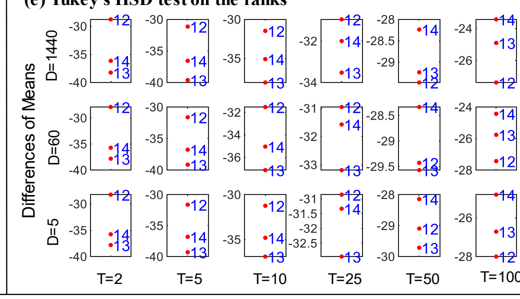

Figure D-7. Similar to Figure 4-11 but for Station #1 – Sault Ste Marie Airport Station;

(a) PPCC test

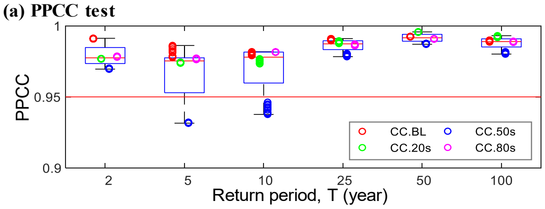

Station #2 Kingston Pumping Stn ID: 6104175

Data:
Group 1 = Baseline = 1961-1990
Group 2 = 2020s = 2011-2040
Group 3 = 2050s = 2041-2070
Group 4 = 2080s = 2071-2100

Critical values
Significant level:
$\alpha = 0.05$
PPCC test: r*=0.95
ANOVA: F*=2.73
Tukey test: q*=3.71

(b) ANOVA F-test on the data

D \ T	2	5	10	25	50	100
1440	17.76	13.98	10.24	5.64	3.21	1.70
720	17.76	13.97	10.20	5.62	3.21	1.72
360	17.76	13.96	10.16	5.60	3.22	1.74
120	17.74	13.87	10.00	5.51	3.21	1.79
60	17.73	13.80	9.90	5.46	3.22	1.83
30	17.72	13.74	9.80	5.41	3.23	1.87
15	17.71	13.67	9.70	5.37	3.24	1.91
10	17.71	13.62	9.65	5.35	3.25	1.94
5	17.70	13.55	9.55	5.32	3.27	1.99

(c) ANOVA F-test on the ranks

D \ T	2	5	10	25	50	100
1440	24.71	22.51	17.66	7.65	3.73	1.83
720	24.71	22.33	17.62	7.62	3.73	1.88
360	24.74	22.38	17.49	7.62	3.75	1.92
120	24.87	21.92	16.89	7.58	3.77	1.90
60	24.87	21.98	16.32	7.58	3.75	1.93
30	24.84	22.15	15.78	7.53	3.77	2.02
15	24.84	22.15	15.68	7.49	3.79	2.14
10	24.84	22.17	15.60	7.42	3.79	2.20
5	24.84	22.13	15.44	7.42	3.78	2.24

(d) Tukey's HSD test on the data

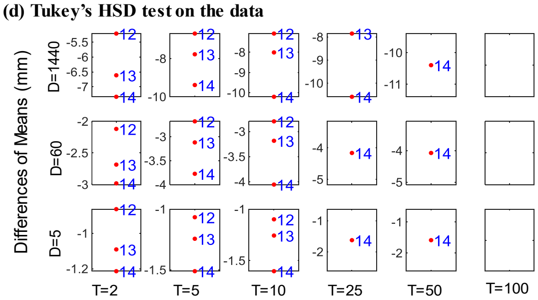

(e) Tukey's HSD test on the ranks

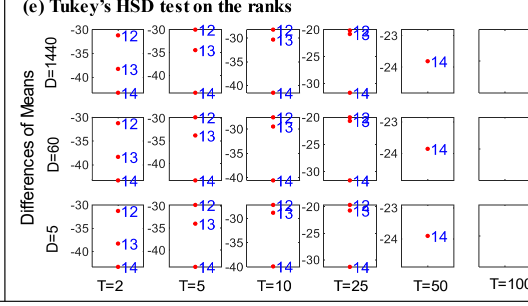

Figure D-8. Similar to Figure 4-11 but for Station #2 – Kingston pumping Station

(a) PPCC test

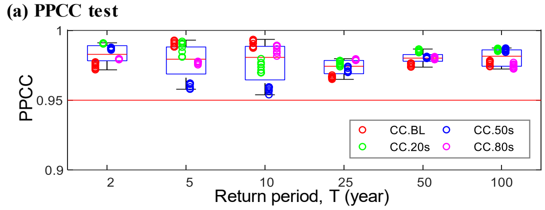

Station #3 St Thomas WPCP ID: 6137362

Data:
Group 1 = Baseline = 1961-1990
Group 2 = 2020s = 2011-2040
Group 3 = 2050s = 2041-2070
Group 4 = 2080s = 2071-2100

Critical values
Significant level:
α = 0.05
PPCC test: r*=0.95
ANOVA: F*=2.73
Tukey test: q*=3.71

(b) ANOVA F-test on the data

D \ T	2	5	10	25	50	100
1440	14.45	13.96	11.13	5.89	3.29	1.84
720	14.43	13.97	11.14	5.90	3.30	1.85
360	14.41	13.98	11.16	5.91	3.31	1.87
120	14.37	14.00	11.18	5.92	3.32	1.88
60	14.40	13.97	11.49	6.21	3.43	1.90
30	14.43	13.90	11.77	6.55	3.59	1.94
15	14.47	13.81	12.00	6.92	3.78	2.01
10	14.50	13.74	12.10	7.16	3.92	2.07
5	14.55	13.60	12.23	7.58	4.20	2.19

(c) ANOVA F-test on the ranks

D \ T	2	5	10	25	50	100
1440	16.55	13.50	11.50	6.96	3.84	2.07
720	16.58	13.61	11.63	6.95	3.86	2.09
360	16.61	13.60	11.69	6.95	3.88	2.12
120	16.71	13.77	11.77	7.00	3.91	2.17
60	16.48	13.69	11.95	7.36	3.95	2.11
30	16.58	13.69	12.01	7.59	4.06	2.18
15	16.65	13.79	12.35	8.02	4.25	2.23
10	16.68	13.91	12.29	8.29	4.40	2.28
5	16.82	14.04	12.31	8.62	4.58	2.47

(d) Tukey's HSD test on the data

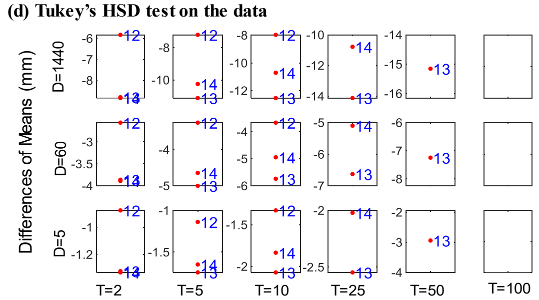

(e) Tukey's HSD test on the ranks

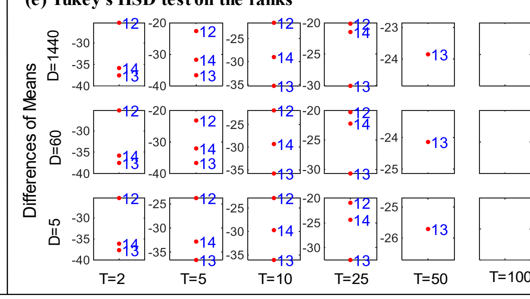

Figure D-9. Similar to Figure 4-11 but for Station #3 – St Thomas WPCP Station

(a) PPCC test

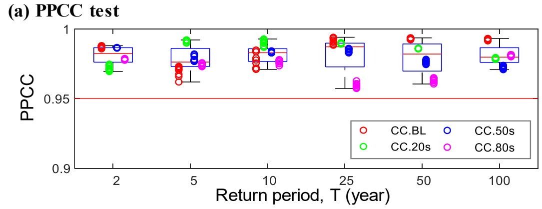

Station #5 London CS ID: 6144478

Data:
Group 1 = Baseline = 1961-1990
Group 2 = 2020s = 2011-2040
Group 3 = 2050s = 2041-2070
Group 4 = 2080s = 2071-2100

Critical values
Significant level:
α = 0.05
PPCC test: r*=0.95
ANOVA: F*=2.73
Tukey test: q*=3.71

(b) ANOVA F-test on the data

D \ T	2	5	10	25	50	100
1440	10.98	9.05	6.34	3.44	2.20	1.51
720	10.99	9.17	6.53	3.55	2.24	1.52
360	10.99	9.29	6.71	3.67	2.30	1.54
120	10.98	9.46	7.00	3.87	2.40	1.58
60	10.98	9.56	7.17	4.00	2.48	1.62
30	10.97	9.65	7.35	4.15	2.56	1.66
15	10.96	9.74	7.52	4.30	2.65	1.71
10	10.97	9.66	7.36	4.16	2.57	1.66
5	10.98	9.51	7.07	3.93	2.43	1.59

(c) ANOVA F-test on the ranks

D \ T	2	5	10	25	50	100
1440	12.06	11.58	7.87	3.61	2.09	1.58
720	12.29	11.63	8.13	3.82	2.12	1.57
360	12.32	11.81	8.32	4.06	2.21	1.57
120	12.25	11.97	8.68	4.33	2.43	1.59
60	12.30	11.39	9.15	4.49	2.48	1.65
30	12.32	11.45	9.42	4.64	2.52	1.69
15	12.30	11.57	9.73	4.83	2.54	1.80
10	12.32	11.39	9.43	4.65	2.53	1.69
5	12.19	11.62	8.74	4.39	2.44	1.63

(d) Tukey's HSD test on the data

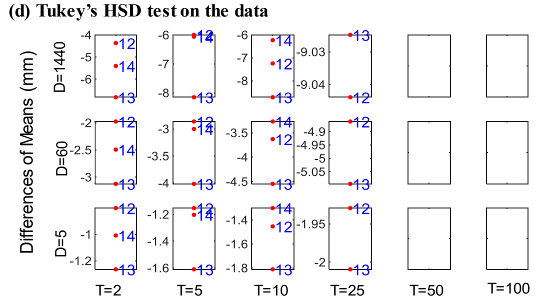

(e) Tukey's HSD test on the ranks

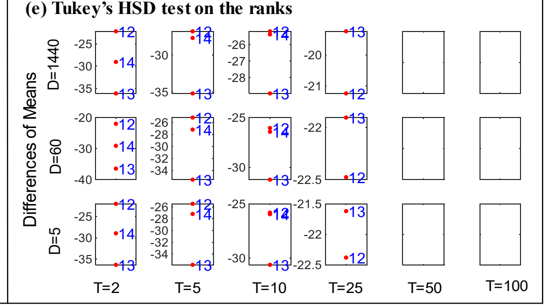

Figure D-10. Similar to Figure 4-11 but for Station #5 – London CS Station

(a) PPCC test

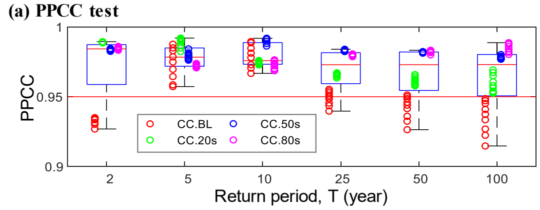

Station #6 Hamilton RBG CS ID: 6153301

Data:
Group 1 = Baseline = 1961-1990
Group 2 = 2020s = 2011-2040
Group 3 = 2050s = 2041-2070
Group 4 = 2080s = 2071-2100

Critical values
Significant level:
α = 0.05
PPCC test: r*=0.95
ANOVA: F*=2.73
Tukey test: q*=3.71

(b) ANOVA F-test on the data

D \ T	2	5	10	25	50	100
1440	12.05	8.04	5.33	2.71	1.59	0.99
720	11.99	7.92	5.17	2.62	1.57	1.00
360	11.94	7.77	5.00	2.55	1.56	1.03
120	11.86	7.52	4.74	2.47	1.57	1.09
60	11.81	7.35	4.59	2.43	1.60	1.14
30	11.77	7.16	4.45	2.42	1.64	1.21
15	11.71	6.83	4.23	2.43	1.75	1.35
10	11.68	6.63	4.13	2.46	1.83	1.46
5	11.60	6.29	4.01	2.56	2.00	1.67

(c) ANOVA F-test on the ranks

D \ T	2	5	10	25	50	100
1440	18.86	12.92	7.17	2.87	1.54	0.73
720	18.97	13.20	7.05	2.76	1.53	0.75
360	18.80	12.95	6.96	2.70	1.50	0.79
120	18.53	12.90	6.58	2.63	1.50	0.84
60	18.53	12.74	6.45	2.64	1.58	0.85
30	18.40	12.56	6.20	2.63	1.64	0.99
15	18.36	12.33	6.01	2.73	1.73	1.35
10	18.10	11.66	5.76	2.76	1.94	1.46
5	17.92	10.20	5.52	2.96	2.27	1.91

(d) Tukey's HSD test on the data

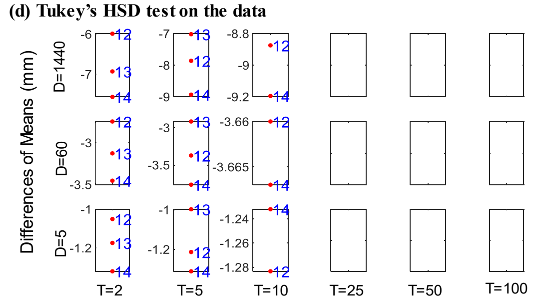

(e) Tukey's HSD test on the ranks

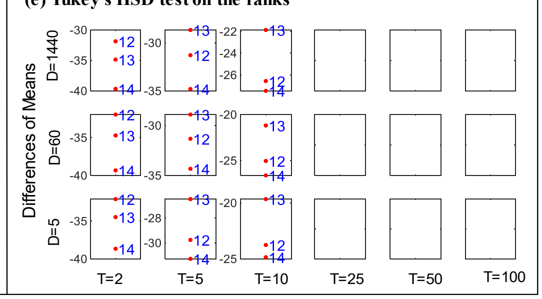

Figure D-11. Similar to Figure 4-11 but for Station #6 – Hamilton RBG CS Station

(a) PPCC test

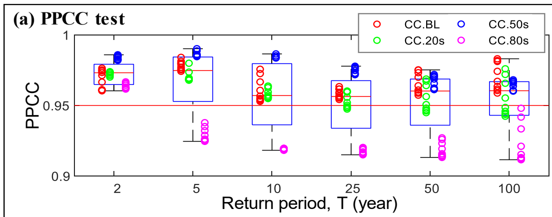

Station #7 Toronto Intl A ID: 6158731

Data:
Group 1 = Baseline = 1961-1990
Group 2 = 2020s = 2011-2040
Group 3 = 2050s = 2041-2070
Group 4 = 2080s = 2071-2100

Critical values
Significant level:
α = 0.05
PPCC test: r*=0.95
ANOVA: F*=2.73
Tukey test: q*=3.71

(b) ANOVA F-test on the data

D \ T	2	5	10	25	50	100
1440	15.30	10.32	6.60	3.04	1.52	0.72
720	15.23	9.92	6.07	2.80	1.50	0.80
360	15.19	9.43	5.59	2.68	1.57	0.95
120	15.18	8.54	5.03	2.72	1.85	1.35
60	15.17	7.98	4.81	2.86	2.13	1.70
30	15.10	7.48	4.71	3.08	2.49	2.13
15	15.13	7.59	4.72	3.03	2.40	2.03
10	15.14	7.65	4.73	3.00	2.35	1.97
5	15.16	7.76	4.76	2.95	2.28	1.88

(c) ANOVA F-test on the ranks

D \ T	2	5	10	25	50	100
1440	21.77	19.40	11.93	4.30	2.04	0.60
720	21.28	19.87	10.27	3.93	1.98	0.69
360	21.53	18.94	9.10	3.66	2.03	0.99
120	21.85	16.47	7.96	3.62	2.43	1.79
60	21.90	15.29	7.28	3.79	2.98	2.35
30	22.49	14.14	7.26	4.19	3.23	2.98
15	22.48	14.36	7.22	4.14	3.15	2.92
10	22.59	14.52	7.26	4.07	3.17	2.80
5	22.34	14.59	7.28	3.94	3.07	2.66

(d) Tukey's HSD test on the data

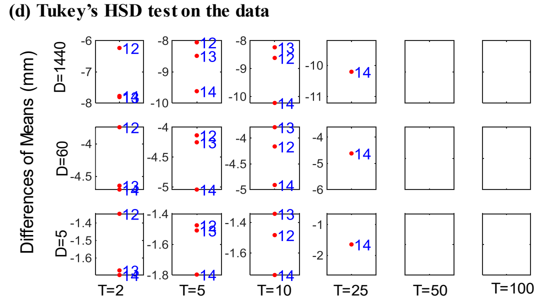

(e) Tukey's HSD test on the ranks

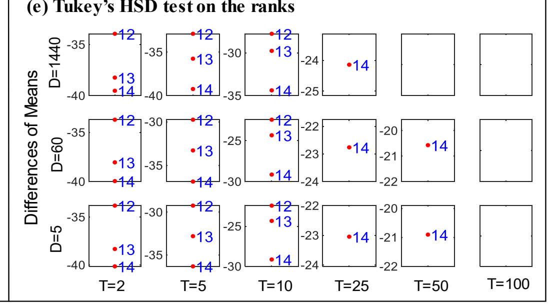

Figure D-12. Similar to Figure 4-11 but for Station #7 – Toronto International Airport Station

Appendix D: Supplementary Materials for Chapter 5

(*Mathematical Frameworks and Scaling Properties of Several Probability Distribution Models Commonly Used in Hydrologic Frequency Analysis*)

Table D-1. Coefficients of the approximations $A_i (i = 0\ to\ 3)$ and $B_j (j = 1\ to\ 3)$ used in Eqn. (5-39). These values are extracted from Table A.1 of Hosking and Wallis (1997)

$A_0 = 4.8860251 \times 10^{-1}$	$B_1 = 6.4662924 \times 10^{-2}$
$A_1 = 4.4493076 \times 10^{-3}$	$B_2 = 3.3090406 \times 10^{-2}$
$A_2 = 8.8027039 \times 10^{-4}$	$B_3 = 7.4290680 \times 10^{-5}$
$A_3 = 1.1507084 \times 10^{-6}$	

Table D-2. Coefficients of the approximations $A_i (i = 0\ to\ 3)$, $B_j (j = 1\ to\ 2)$, $E_k\ (k = 1\ to\ 3)$, and F_k used in Eqn. (5-59). These values are extracted from Table A.2 of Hosking and Wallis (1997)

$A_0 = 3.2573501 \times 10^{-1}$	$E_1 = 2.3807576$
$A_1 = 1.6869150 \times 10^{-1}$	$E_2 = 1.5931792$
$A_2 = 7.8327243 \times 10^{-2}$	$E_3 = 1.1618371 \times 10^{-1}$
$A_3 = -2.9120539 \times 10^{-3}$	
	$F_1 = 5.1533299$
$B_1 = 4.6697102 \times 10^{-1}$	$F_2 = 7.1425260$
$B_2 = 2.4255406 \times 10^{-1}$	$F_3 = 1.9745056$

Appendix E: Supplementary Materials for Chapter 6

(Decision-Support Tool for Constructing Robust Rainfall IDF Relations in Consideration of Model Uncertainty and Climate Change Information for The Design and Management of Urban Water Systems)

Table E-1. List of stations used in the study and their record lengths (RCL, years)

No	Station name	RCL	No	Station name	RCL	No	Station name	RCL
1	Big Trout Lake	25	29	Picton	27	57	Waterloo Wel. A.	33
2	Lansdowne Hou.	21	30	Toronto Booth	26	58	Belleville	37
3	Red Lake A.	25	31	Toronto Ellesm.	25	59	Bowmanville M.	31
4	Atikokan (AUT)	24	32	Toronto Island A.	24	60	Burketon Mclag.	31
5	Rawson Lake (A.)	26	33	Toronto Nor. Y.	29	61	Hamilton A.	33
6	Caribou Island	22	34	Toronto Old W. R	22	62	Oshawa WPCP	32
7	Pukaskwa Natl.	20	35	Toronto Butt. A.	20	63	Peterborough A.	33
8	Slate Island	20	36	Lindsay Filt. P.	24	64	Ear Falls (AUT)	49
9	Mississagi On. H.	22	37	Peterborough S.	28	65	Pickle Lake (AUT)	41
10	White River	21	38	Sioux Lookout A.	39	66	Kenora A.	40
11	Wawa (AUT)	21	39	Sudbury A.	35	67	Geraldton A.	48
12	Chapleau A.	26	40	Kapuskasing CDA	36	68	Thunder Bay CS	47
13	Kirkland Lake C.	26	41	Moosonee RCS	30	69	Sault St. Marie A.	45
14	Pinard	24	42	Brockville PCC	35	70	Timmins Victor P.	47
15	Combermere	20	43	Cornwall Ont H.	33	71	North Bay A.	41
16	Smiths Falls TS	21	44	Kemptville CS	34	72	Kingston Pump. Stn	63
17	Barrie WPCC	26	45	Otta. M.-C. Int'l A.	39	73	Ottawa Cda RCS	50
18	Beausoleil	24	46	Petawawa Nat F.	33	74	Sarnia Airport	40
19	Goderich	22	47	Orillia Brain	35	75	Chatham WPCP	40
20	Harrow CDA A.	28	48	Owen Sound Moe	37	76	Delhi CS	42
21	Niagara Falls	26	49	Wiarton A.	33	77	St Thomas WPCP	75
22	Simcoe	23	50	Port Colborne	37	78	Windsor A.	60
23	Vineland Sta. R.	26	51	Ridgetown RCS	30	79	Guelph Turfgra.	42
24	Point Pelee Cs	22	52	St Catharines A.	33	80	London CS	57
25	Preston WPCP	22	53	Brantford Moe	36	81	Hamilton RBG CS	44
26	Elora RCS	29	54	Fergus Shand D.	37	82	Toronto City	59
27	Campbellford	24	55	Mount Forest (A.)	30	83	Toronto Intl. A.	60
28	Main Duck Isl.	21	56	Stratford WWTP	36	84	Trenton A.	41

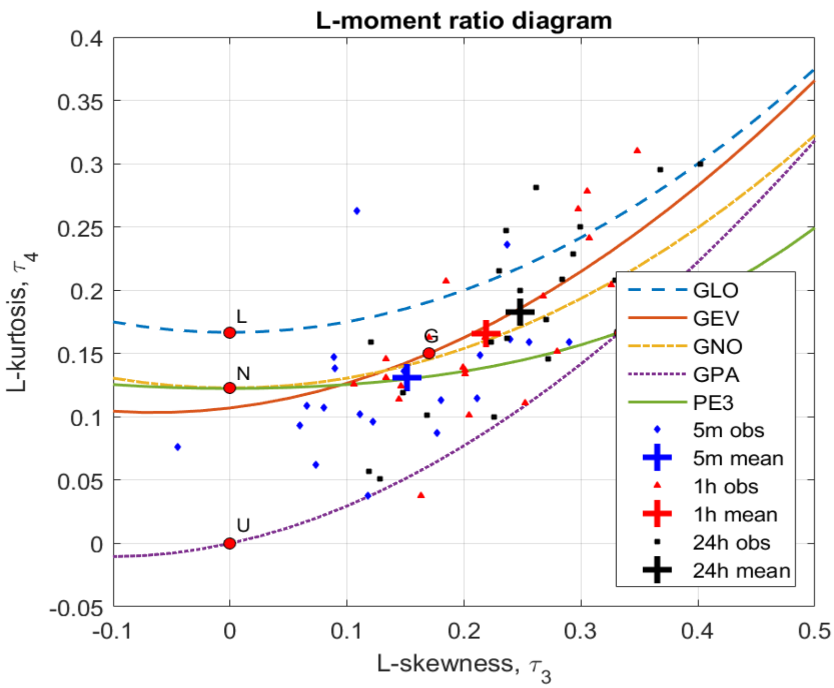

Figure E-1. L-moment ratio diagram of 63 AMS from 21 rain-gauges containing at least 40-year records.

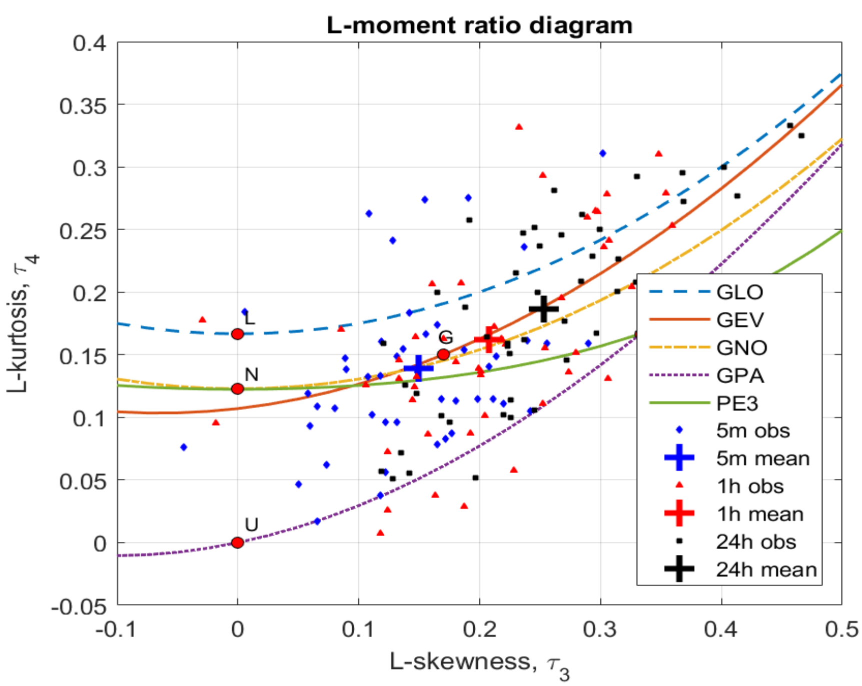

Figure E-2. L-moment ratio diagram of 141 AMS from 47 rain-gauges containing at least 30-year records.

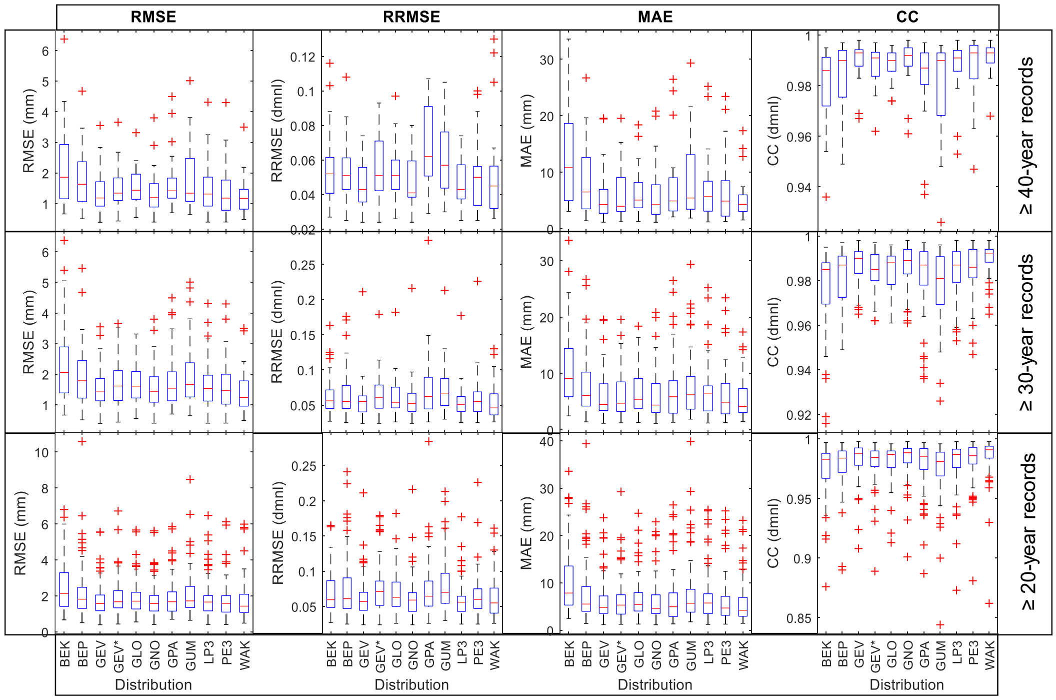

Figure E-3. Comparing boxplots of RMSE, RRMSE, MAE, and CC results of 11 selected candidates using 1-hour AMS of stations containing at least 40-year, 30-year, and 20-year records respectively

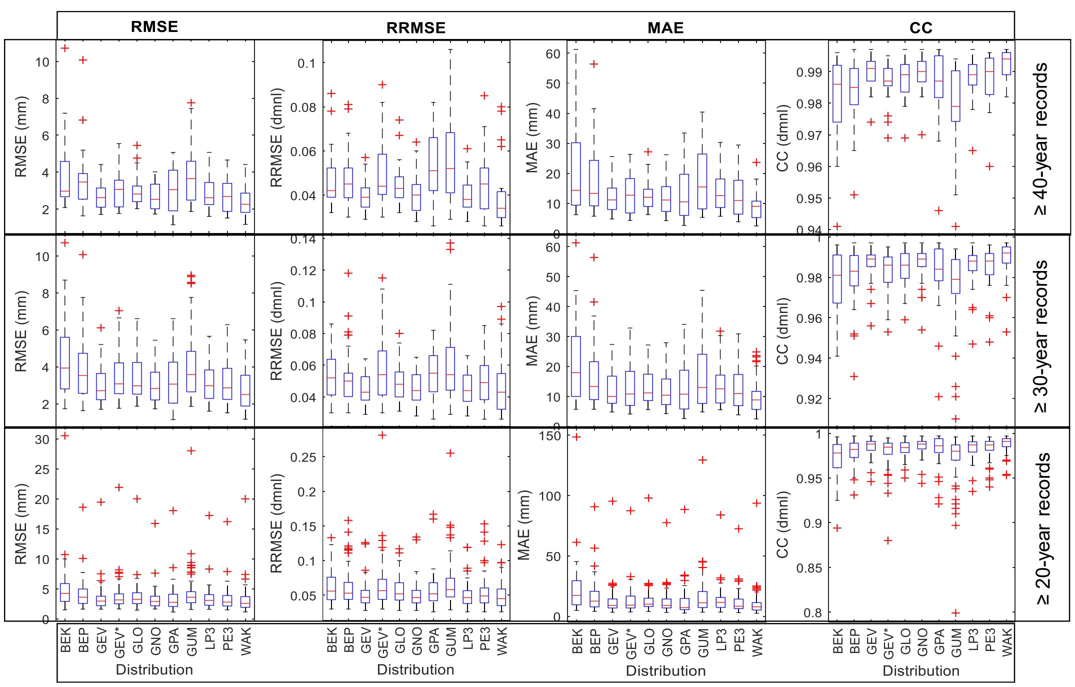

Figure E-4. Comparing boxplots of RMSE, RRMSE, MAE, and CC results of 11 selected candidates using 24-hour AMS of stations containing at least 40-year, 30-year, and 20-year records respectively

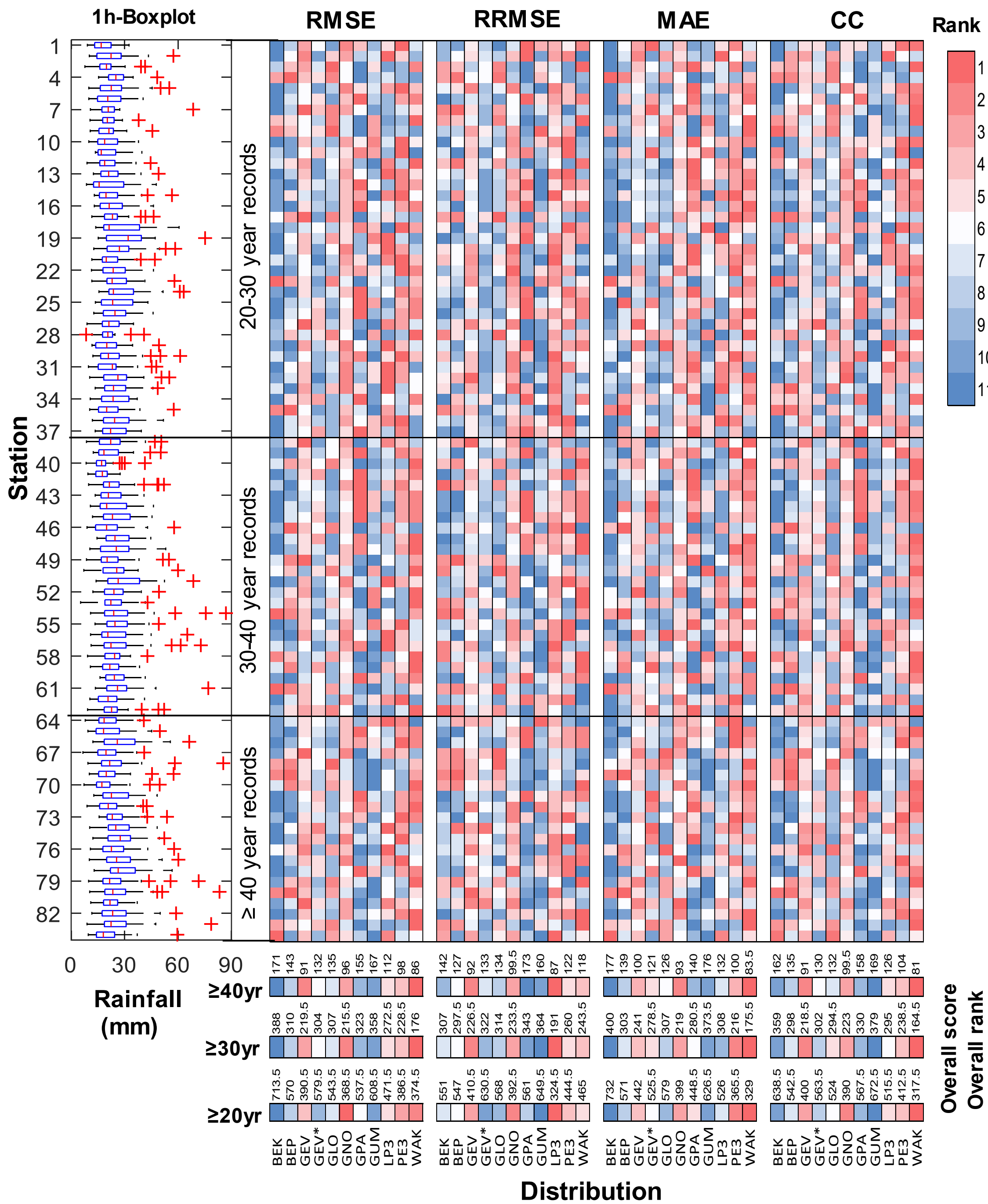

Fig. 1. The ranking of 11 distributions for 1-hour AMS for each station individually and the overall rank for 84 stations based on the four statistical criteria. Rank = 1 (or close to 1) indicates the best distribution and rank = 11 (or close to 11) indicates the worst distribution. Boxplots of the 1-hour data of all 84 stations are shown on the left

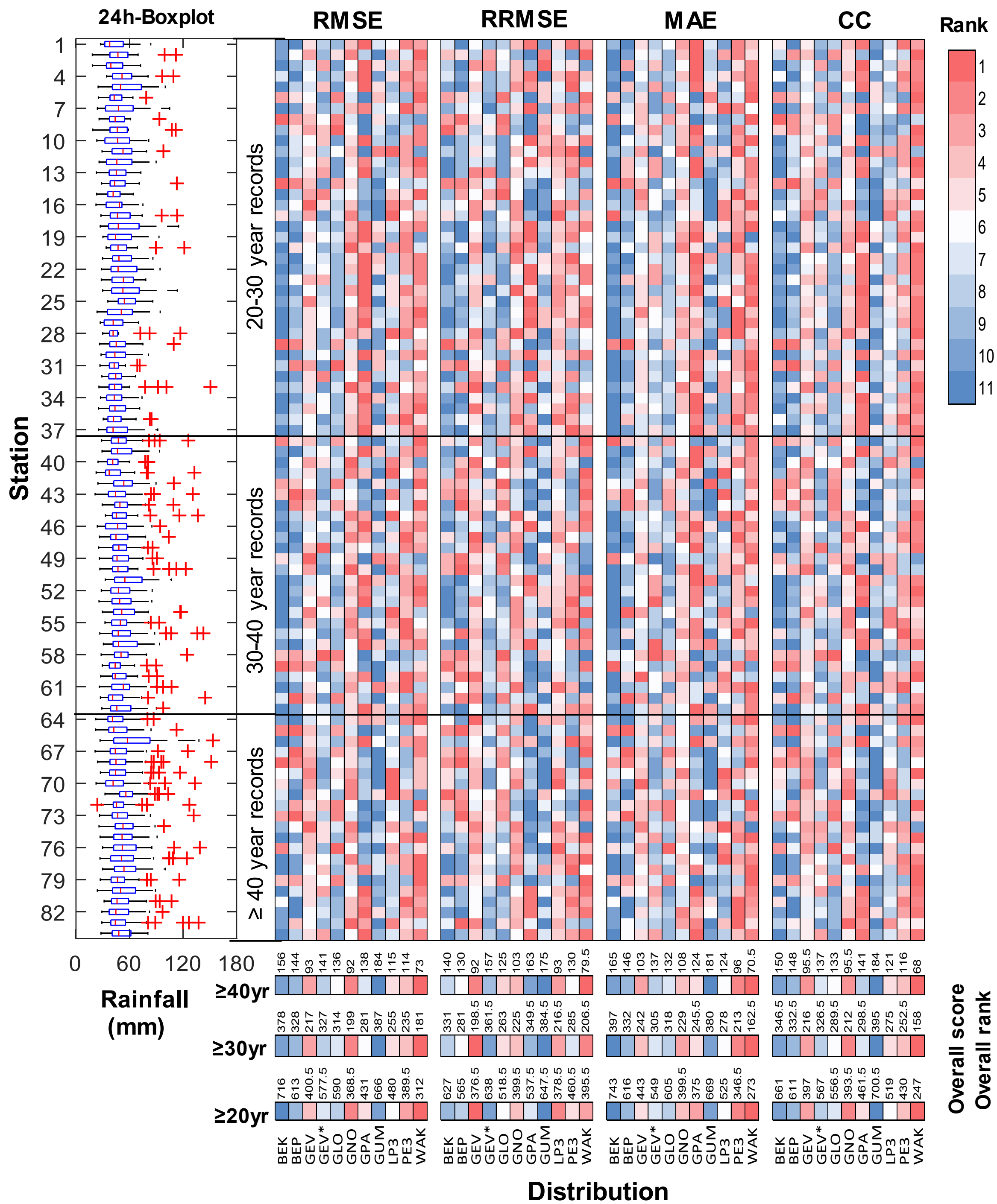

Fig. 2. The ranking of 11 distributions for 24-hour AMS for each station individually and the overall rank for 84 stations based on the four statistical criteria. Rank = 1 (or close to 1) indicates the best distribution and rank = 11 (or close to 11) indicates the worst distribution. Boxplots of the 24-hour data of all 84 stations are shown on the left

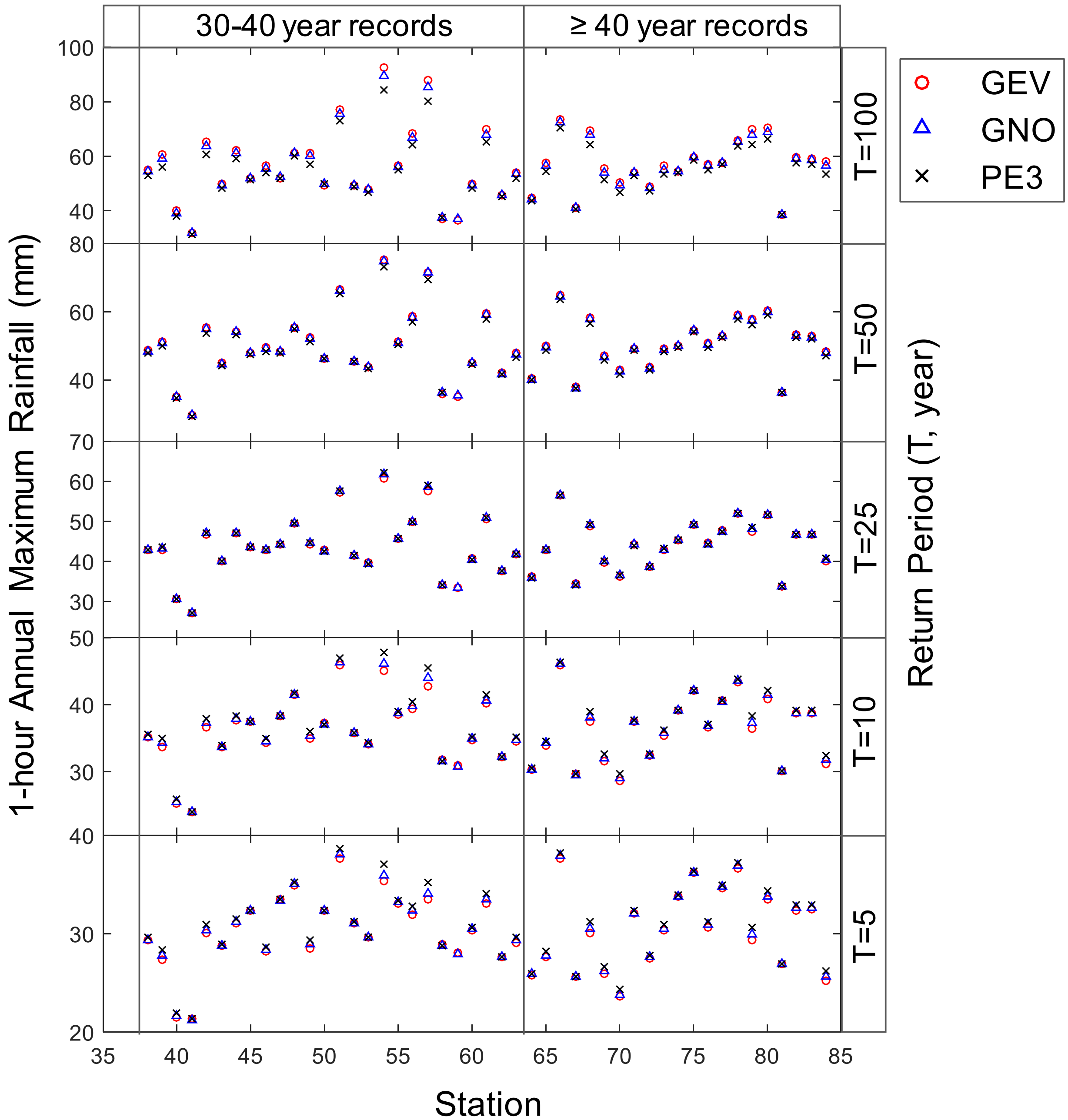

Fig. 3. Comparing extreme design rainfalls estimates for different return periods (T=5, 10, 25, 50, 100 years) using 1-hour AMS of all stations containing at least 30 years of records and the top three distributions GEV, GNO, and PE3

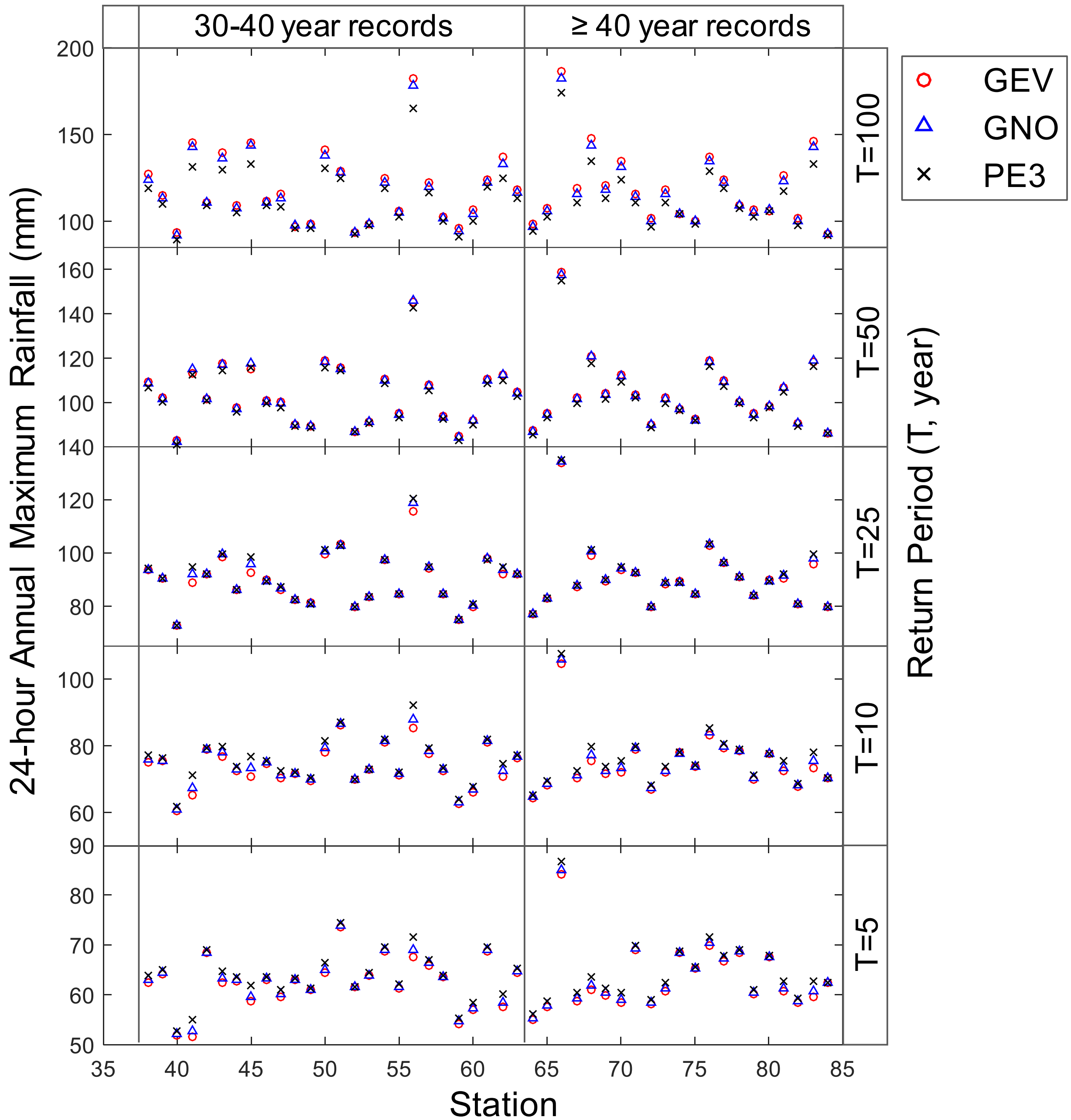

Fig. 4. Comparing extreme design rainfalls estimates for different return periods (T=5, 10, 25, 50, 100 years) using 24-hour AMS of all stations containing at least 30 years of records and the top three distributions GEV, GNO, and PE3